Epidemiology and Evolution of Vector Borne Disease

Harrison, Eleanor

Award date:
2013

Awarding institution:
University of Bath

Epidemiology and Evolution of Vector Borne Disease

submitted by

Eleanor Margaret Harrison

for the degree of Doctor of Philosophy

of the

University of Bath

Department of Mathematical Sciences

December 2013

Acknowledgements

Foremost, I would like to thank my supervisor Dr. Ben Adams for his time and help during my PhD. I would also like to thank Prof. Nick Britton and Dr. Merrilee Hurn for their comments on early work, and my examiners Dr. Jane White and Dr. Christina Cobbold for their comments, corrections and advice. Furthermore, I would like to thank all those in the CMB and in my office who have offered help, criticism and conversation throughout the last four years. I must also express my gratitude to Prof. Alastair Spence who convinced me to stick at it before I'd even started.

Finally I thank my family and friends, without whose support this wouldn't have been possible. Mum, Dad, Nan, Christian, I couldn't have done this without you. Despite everything that's been thrown at us in the last few years, I got there in the end.

Summary

In recent years the incidence of many vector borne-diseases has increased worldwide. We investigate the epidemiology and evolution of vector-borne disease, focussing on the neglected tropical disease leishmaniasis to determine suitable strategies for control and prevention. We develop a compartmental mathematical model for leishmaniasis, and examine the dependence of disease spread on model parameters. We perform an elasticity analysis to establish the relative impact of disease parameters and pathways on infection spread and prevalence. We then use optimal control theory to determine optimal vaccination and spraying strategies for leishmaniasis, and assess the dependence of control on disease relapse. We investigate the evolution of virulence in vector-borne disease using adaptive dynamics and both non-spatial and metapopulation models for disease spread. Using our metapopulation model we also determine the impact of land-use change such as urbanisation and deforestation on disease spread and prevalence.

We find that in the absence of evolution, control techniques which directly reduce the rate of vector transmission lead to the greatest reduction in potential disease spread. Although the spraying of insecticide can reduce the basic reproductive number R_0, we find that vaccination is more effective. Disease relapse is the driving force behind infection at endemic equilibrium and greatly increases the level of control required to prevent a disease epidemic.

When a trade-off is in place between transmission and virulence we find that control techniques which reduce the duration of transmission lead to the fixation of pathogen strains with heightened virulence. Control techniques such as spraying can therefore be counterproductive, as increasing virulence increases human infection prevalence. This holds true when virulence is in either the host or vector and suggests that virulence within the vector should not be ignored. Urbanisation and deforestation can also lead to increases in both transmission and virulence, as reducing the distance between urban settlements and the vector natural habitat alters disease incidence.

Contents

List of Figures

List of Tables

Chapter 1

Introduction and Literature Review

1.1 Introduction and Thesis Outline

Neglected tropical diseases, or NTDs, are a group of 17 diseases which now affect over one billion people worldwide [79]. Named for their lack of prominence in public health policy, NTDs are most commonly diagnosed in the poorest countries in the world. Diseases such as schistosomiasis, trypanosomiasis and leprosy can be chronic, disabling, and contribute to the perpetuation of poverty, yet have not been extensively studied. As our world develops and environmental conditions change, the incidence of neglected tropical diseases is increasing worldwide. For this reason, many neglected tropical diseases are termed emergent diseases, as they infect more people in more countries than ever before [79]. One such disease is leishmaniasis, a vector-borne NTD caused by Leishmania protozoa transmitted between humans by female sandflies. Previously associated with the impoverished in Africa, leishmaniasis has now spread to South America and the Mediterranean Basin, with global incidence at an all time high. The increased prevalence of leishmaniasis means that more information about its epidemiology has become available in recent years, but there is still much more to understand [45].

The aim of this thesis is to investigate the epidemiology and evolution of vector-borne diseases such as leishmaniasis. In order to better inform public health policy we use mathematical modelling techniques to assess the advantages and disadvantages of a range of strategies for disease control and prevention. In Chapter 2 we use the information gathered in a literature review to develop a compartmental differential equation model for the spread of leishmaniasis. We consider both anthroponotic and

zoonotic disease, and investigate the dependence of disease spread on model parameters. In Chapter 3 we further this investigation by carrying out an elasticity analysis to establish the relative impact of model parameters on infection spread and prevalence. In Chapter 4 we determine optimal control strategies for Leishmania infection when a cost constraint is introduced. In Chapter 5 we use Adaptive Dynamics to explore the evolution of virulence in vector-borne diseases when different control techniques are applied. This investigation is extended in Chapter 6 to consider the evolution of virulence when disease spread has a spatial component. Our conclusions are contained within Chapter 7.

Novel work includes:

- The adaptation of vector-borne disease models to capture the dynamics of relapsing leishmaniasis.
- The subsequent use of our leishmaniasis model in optimal control and metapopulation frameworks.
- The application of elasticity analysis at endemic equilibrium.
- The investigation of virulence evolution in the vector and its consequences for human infection prevalence.

We begin by reviewing the literature on leishmaniasis epidemiology and the modelling of vector-borne disease.

1.2 Leishmaniasis

1.2.1 Background

Leishmaniasis covers a range of diseases caused by the protozoan Leishmania. Currently endemic in 88 countries, leishmaniasis is thought to threaten over 350 million people worldwide and cause over 30,000 deaths every year [20, 26, 79]. Leishmaniasis incidence is at an all time high, with over 1.3 million new cases diagnosed annually [73, 79]. This number may not represent the true burden of the infection however, as cases are often misdiagnosed or unreported.

Traditionally leishmaniasis is split into two groups, Old World and New World, depending on the geographic region in which the infection is obtained. Old World refers to infection acquired in the Mediterranean Basin, Asia, the Middle East or Africa, whereas New World refers to infection acquired in the Americas [26, 79]. Figure (1-1) shows the countries in which leishmaniasis is endemic. Infection by the Leishmania

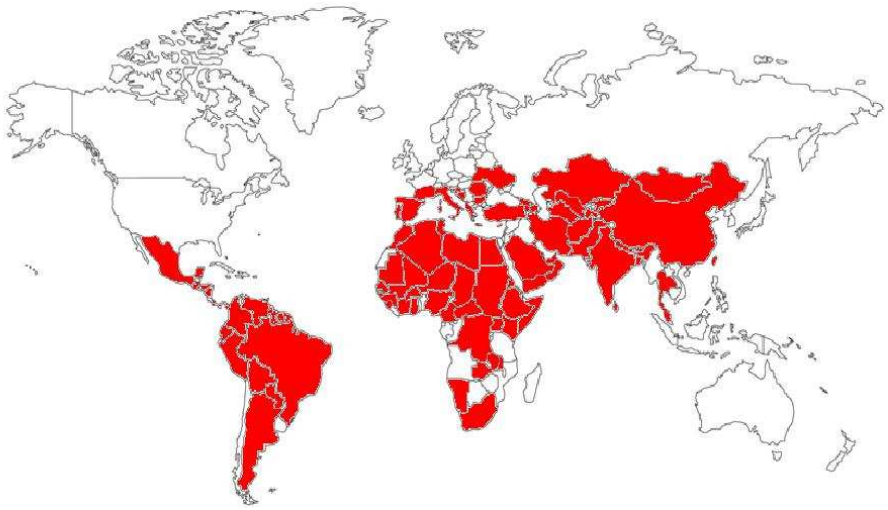

Figure 1-1: Map showing countries where leishmaniasis is present. Based on map 10.1, http://www.who.int/csr/resources/publications/CSR_ISR_2000_1leish/en/

protozoa is primarily acquired when a susceptible individual is bitten by an infected female sandfly. Sandflies usually feed on sugary substances such as sap; however female sandflies take a blood meal in order to obtain proteins needed to mature eggs [53]. Males do not carry infection since they have no need to bite. Although infection may also be obtained through other means, such as blood transfusion, venereal, congenital and needle transmission, this is rare, more easily prevented and not often considered [53].

There are many strains of Leishmania protozoa, transmitted by two genera of sandflies. In the Old World the sandfly vector is of the genus Phlebotomus, whereas in the New World it is of the genus Lutzomyia [53]. Of these two genera, over 30 species of sandfly are able to support the development of Leishmania in their guts and pass the pathogen to humans [22]. During the day sandflies rest in cool places, but disperse several hundred metres at night in search of mates and blood [53, 76, 79]. With a flight speed in the order of 1m/s, sandflies remain close to the ground as they are unable to fly in the increased wind speeds of greater heights. Breeding sites are at or close to ground level, where sandflies lay their eggs in moist soil and organic matter, rich in the nutrients required to support their larvae. The greatest period of sandfly biting activity tends to be between June and August, leading to seasonal patterns of infection in some cases [79].

Leishmaniasis can also be categorised by the host species involved in transmission. When humans are the preferred host, disease is anthroponotic. In India for instance,

transmission is solely between humans; however in other countries humans are not the only blood source for female sandflies. When other animals also act as reservoirs for leishmaniasis infection, disease is often zoonotic. In this case humans are a dead-end host, as the concentration of Leishmania found in human blood is not sufficiently high to be transmitted. An example of zoonotic leishmaniasis can be found in Brazil, where both dogs and rodents have been implicated as Leishmania reservoirs [79].

1.2.2 Leishmania Life Cycle

Leishmaniasis is a Trypanosomal disease, meaning it is caused by a protozoan with only a single flagellum. The life cycle of a Leishmania protozoan is complex as it consists of two forms which are varied between host and vector. When an uninfected sandfly takes a blood meal from an infected mammal it ingests Leishmania amastigotes. These amastigotes are imbibed and transform in the midgut of the fly to form promastigotes, each of which has a single flagellum to propel the Leishmania onwards. The promastigotes multiply, divide and migrate to the pharyngeal valve, where they can be regurgitated at a subsequent blood meal and infect a mammalian host [20, 22]. Before the pathogen can be transmitted, both amastigotes and promastigotes must therefore cling to the epithelial cells to avoid being digested by enzymes or excreted from a vector [53].

Once a mammalian host has become infected the promastigotes invade the immune system cells. Those which survive transform back into amastigotes and replicate within phagocytic cells, causing cell lysis and putting strain on the immune system. Attacking the immune system is beneficial for the parasite since it reduces the development of memory cells. The destruction of immune cells such as macrophage through disease replication also means that further immune cells are recruited to the area, providing more cells in which the Leishmania may reproduce.

Leishmaniasis is an example of a disease which exhibits concomitant immunity, i.e. the long term persistence of the parasite within the host provides immunity by allowing the host to maintain resistance to reinfection. This is somewhat paradoxical since it means that resistance to reinfection only occurs because of the persistence of the original infection. The persistence of small amounts of Leishmania makes leishmaniasis hard to treat, and can lead to relapse. This presents a particular problem for those suffering from HIV/AIDS [41]. A weakened immune system can no longer maintain the infection at low levels, thus the infection can re-emerge.

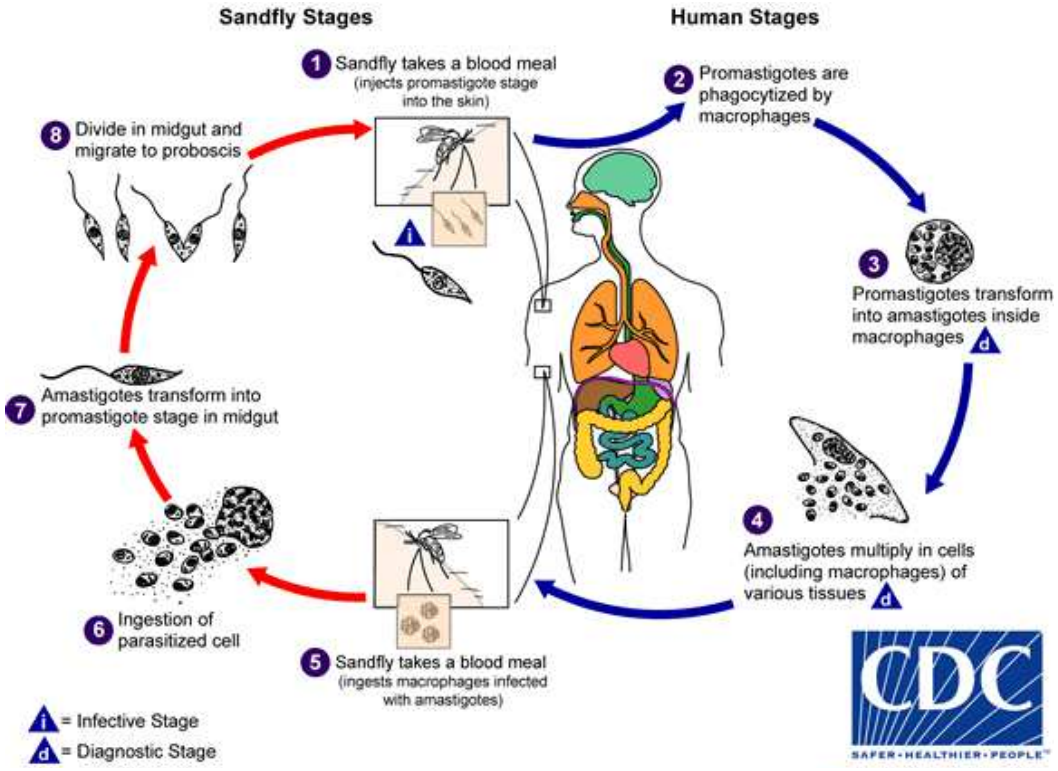

Figure 1-2: Diagram illustrating the life cycle of Leishmania.
Copyright www.dpd.cdc.gov/dpdx/html/leishmaniasis.htm.

1.2.3 Human Leishmaniasis

At least 21 strains of Leishmania are known to cause disease in humans [26]. The symptoms exhibited by infected hosts depend upon the particular strain with which they are infected and the immune response mounted against the disease. Although no two strains are completely identical, there are only three main types of leishmaniasis disease: visceral, cutaneous and mucocutaneous [79].

Cutaneous Leishmaniasis (CL)

Cutaneous leishmaniasis (CL), also known as 'Baghdad Boil', 'Oriental Sore' or 'Uta', is the most common form of leishmaniasis. Once infected with Leishmania protozoa, a person enters an incubation period lasting between a week and several months during which no physical symptoms are presented [26]. When the incubation period is complete, multiple lesions form on the skin, often in exposed areas which have been targeted by sandflies. Although lesions are often self curing, disfiguring scars can be left

behind. Parasites also persist at the original site of infection for many years, leading to concomitant immunity, but also relapse. In the past the immunity acquired from CL has been exploited by some tribal societies, such as the Bedouin, who encouraged sandflies to bite babies' bottoms so that they would gain protection from further infection without having to suffer disfiguring lesions on the face [41].

Ninety percent of cutaneous leishmaniasis cases occur in Afghanistan, Algeria, Brazil, Pakistan, Peru, Saudi Arabia and Syria [26], but the local epidemiology can be very different. The principal reservoir host for Leishmania infection can vary depending upon the strain of Leishmania in question, the species of the sandfly vectoring the infection and the geographic region in which it spreads. Cutaneous leishmaniasis may be either anthroponotic, and have humans as a sole host, or zoonotic and have its primary reservoir in another species. In areas of the Middle East and North Africa cutaneous leishmaniasis caused by *Leishmania major* is zoonotic and has its primary reservoir in rodents, such as the Great Gerbil, *Rhombomys opimus* and the Fat Sand Rat, *Psammomys obesus* [69]. Leishmaniasis caused by *Leishmania braziliensis* in Brazil is also zoonotic, and principally infects either rodents or dogs bitten by the sandfly *Lutzomyia whitmani*. Human case numbers are particularly high in drier areas in the north east, where the absence of dense vegetation seems to increase sandfly prevalence. Anthroponotic cutaneous leishmaniasis is found in the drier western parts of India [58], and in Afghanistan, where disease is commonly caused by *Leishmania tropica* spread by the sandfly *Phlebotomus sergenti* [79]. In general, the infections of the Old World tend to be of lower virulence and heal more rapidly than those of the New World [26].

Mucocutaneous Leishmaniasis (MCL)

Cutaneous leishmaniasis can sometimes turn into mucocutaneous leishmaniasis, where lesions destroy the mucous membranes. Unlike CL, MCL can be life threatening and must be treated. Sometimes occurring years after the first bout of cutaneous leishmaniasis, it is caused by Leishmania protozoa colonising macrophages in the enasooraphary ngeal mucosa [22]. Similar to other forms of leishmaniasis, clinical progression is dependent on the immune response of the host and on the strain of Leishmania with which they are infected.

Visceral Leishmaniasis (VL)

Visceral leishmaniasis, also known as Kala-Azar, affects the internal organs (the viscera), with symptoms including: hepatosplenology, cachexia and anaemia. Although

more strains of Leishmania seem to cause cutaneous leishmaniasis than visceral, the latter is more severe as left untreated it will lead to death [59]. The average incubation period for visceral leishmaniasis is 2-6 months, but can range from 10 days to many years [77]. If left untreated, active infections will kill a human host within two years [79]. Even after successful treatment parasites are not eradicated completely and remain in small amounts [59]. In some cases this leads to protection from reinfection, but it can also precipitate disease relapse.

Overall, 500,000 new human cases of VL are diagnosed worldwide every year [22, 12], 90% of which occur in Bangladesh, Brazil, India, Ethiopia, Nepal and Sudan. The disease is also emerging in the Mediterranean Basin and can be either anthroponotic or zoonotic. Dogs are the principal reservoir for Leishmania species causing zoonotic visceral leishmaniasis (ZVL) in both the Old and New Worlds, with dog reservoirs found in countries throughout South America and the Mediterranean Basin [79]. Infections caused by *Leishmania infantum*, carried by *Lutzomyia Longipalpis* in the New World and *Phlebotomus ariasi* and *P. orientalis* in the Old World are the most common source of ZVL. Anthroponotic visceral leishmaniasis is commonly caused by *Leishmania donovani* spread by the sandfly *P. argentipes* and is prevalent in north-east Africa and eastern states of India in areas with a hot, humid climate [58, 79].

1.2.4 Controlling Leishmaniasis

Medications used to treat leishmaniasis are often expensive, toxic and difficult to obtain. This had led to many practitioners opting not to treat self-healing forms of the disease [77, 78]. The main treatment for leishmaniasis is the administration of pentevalent antimony, a poison which in small doses will kill the Leishmania protozoa [26, 59]. Antimony is not always effective however, and resistance to the drug has been reported in up to 15% of CL patients. Other drugs such as Miltefosine, Pentamidine, Amphotericin B and Paromomycin, have been introduced to treat the complaint, but all are known to have detrimental side effects [59].

The lack of available and efficient treatment means control techniques which target disease prevention are commonly employed. Some general control methods for leishmaniasis include: the application of insecticides and insect repellents, covering exposed skin, and avoiding contact with known disease reservoirs [79]. Culling dogs has been trialled as a control in Brazil, but was only effective when incorporated with other control techniques. In some regions new dogs replaced those culled so quickly that the effect of culling alone was small and the reservoir was soon replenished [65]. One of the current focal points for leishmaniasis research is the engineering of suitable vaccines for both cutaneous and visceral strains. The antigenic variety of the different strains cou-

pled with the complex life cycle of the Leishmania protozoa makes the development of a vaccine complicated, and results obtained so far have not yet proven 100% successful [41].

1.2.5 Leishmaniasis in the Military

Leishmaniasis has been a problem for those serving in the armed forces for many years. During World Wars One and Two it is estimated that thousands of troops contracted the disease, with cases noted all over the world [25]. Cases were also reported after the Gulf War, and at the US Army Jungle Training Operating Center in Panama. The high prevalence of leishmaniasis infected sandflies in Iraq and Afghanistan led to an outbreak within the US armed forces in 2003-2004, with more than 600 people affected in 2004 [77] and approximately 1300 overall. Although it was warned in 2002 that leishmaniasis could prove a problem to troops, control methods were not widely available and an epidemic ensued. Since this time the number of cases has dropped due to better preventative measures being put into place, however cases were still identified as recently as October 2009 [9]. The additional pressure on armed forces to reduce the burden of leishmaniasis on troops has led to the US government, amongst others, to provide funding for research on how best to control the spread of the disease. Currently, troops are banned from donating blood for a time after returning from a tour of duty to prevent spread through blood transfusions, with veterans of the Gulf War banned from giving blood between 1991 and 1993 [46]. The US military has also contributed research into the understanding of disease transmission and vector biology, as well as funding drugs trials in order to try and halt the spread of the disease [25].

1.3 Mathematical Models for Vector-Borne Disease

1.3.1 Malaria Models

Since leishmaniasis research has been neglected in the past, the body of mathematical literature available for review is small. We therefore consider the modelling of malaria, a vector-borne protozoan transmitted in the bite of a female *Anopheles* mosquito. Since malaria transmission is comparable to that of leishmaniasis, similar modelling approaches will be applicable. Unlike leishmaniasis there is a plethora of research into the spread of malaria, since half of the world's population is thought to be at risk from the disease [79].

A comprehensive review of malaria models can be found in [7]. The first model introduced is that of Ross, which has been used as a basis for many epidemiological

studies focusing on malaria since the early twentieth century. Although relatively simple, the model incorporates basic features of disease epidemiology and host-vector interactions. The set of ODEs (1.1)-(1.2) is used to describe disease dynamics in both the host and vector. Variables and parameters are defined in Table (1.1).

$$\frac{dx}{dt} = \frac{abM}{N}y(1-x) - rx \tag{1.1}$$

$$\frac{dy}{dt} = ax(1-y) - \mu y \tag{1.2}$$

Symbol	Definition
x	The proportion of the human population which is infected.
y	The proportion of the female mosquito population which is infected.
N	The total size of the human population.
M	The total size of the female mosquito population.
a	The number of bites on humans a single mosquito makes per unit time.
b	The proportion of infected bites that actually lead to infection.
r	The per capita recovery rate of humans.
μ	The per capita mortality rate of mosquitoes.

Table 1.1: Table listing the variables and parameters used in the initial Ross malarial model (1.1)-(1.2) from [7].

Vectors take blood meals from hosts at random. Hosts then become infected at a rate $\frac{abMy(1-x)}{N}$, which depends on the proportion of susceptible hosts $(1-x)$, the bites per person per unit time $\frac{a}{N}$, the proportion of bites which lead to infection b, and the number of infected female vectors yM. Since the rate at which humans recover from infection is much faster than the natural mortality rate, no death rate is incorporated for the host, and they recover from infection at rate r. Vectors are infected at rate $x\,(1-y)$ and stay infectious for the rest of their lives, dying at rate μ.

Although this model provides a good set of basic assumptions and a straightforward way of looking at the interactions between the two species it does have its shortcomings. The model is highly simplified, and ignores some of the more complex population and disease dynamics. For example, neither the incubation period before new infections emerge or the immunity conferred by infection is considered. Although these factors will have an impact on the transmission of the disease and would be required to produce more biologically realistic results, the model does provide a good starting point to build on.

The first adaptation of the Ross model considered in [7], is the inclusion of an incubation period in the vector. The equation for infected hosts remains (1.1), however

an additional class of vectors is added in order to take into account the time taken between initial infection, and parasites multiplying sufficiently for an individual to become infectious. Introducing z to represent the proportion of infected, but not yet infectious vectors and setting the latent period to be fixed and of duration τ, the model equation for the vector is split into two to become:

$$\frac{dz}{dt} = ax(1-y-z) - a\hat{x}\,(1-\hat{y}-\hat{z})\,e^{-\mu\tau} - \mu z \tag{1.3}$$

$$\frac{dy}{dt} = a\hat{x}\,(1-\hat{y}-\hat{z})\,e^{-\mu\tau} - \mu y \tag{1.4}$$

where the notation $\hat{p} = p(t-\tau)$ represents the proportion of individuals in some class p at time τ in the past, and $(1-y-z)$ is the number of uninfected, susceptible mosquitoes at current time t. Mosquitoes are infected at the same rate as before, now written $ax(1-y-z)$, but enter the latent class z instead of going straight into the infected class y. Latent individuals are lost through natural death $(-\mu z)$ and through the transition to the infected class y, where $a\hat{x}\,(1-\hat{y}-\hat{z})\,e^{-\mu\tau}$ is the rate at which individuals initially infected by a bite at time τ survive the latent class to become infectious. The proportion of infected individuals increases as individuals are recruited from the latent class, and are lost through natural death.

The most important model adaptation considered, and the main stumbling block when turning models towards use in leishmaniasis epidemiology, is the inclusion of an immune response in human hosts. Although necessary for a more biologically realistic outcome, the differences in immune response between the two diseases means that specific aspects of malaria models may not be adapted. Unlike leishmaniasis, malaria exhibits waning immunity. Concurrent reinfections with the same or different strains, known as superinfections, play an important role in the maintenance of an immune response. Persistent reinfection with the disease in areas where it is endemic provides longer lasting immunity through the persistence of antibodies, with a degree of heterologous immunity meaning some strains also help to protect against others. Immune response is often positively correlated with age, since children have naive immune systems that have not yet built up any protection against the disease [7].

One way of including immunity which can be used for both malaria and leishmaniasis is the use of an SIR compartmental model. An example of such a system of

equations for malaria is:

$$\frac{dS}{dt} = \gamma R - \beta S \tag{1.5}$$

$$\frac{dI}{dt} = \beta S - \nu I \tag{1.6}$$

$$\frac{dR}{dt} = \nu I - \gamma R \tag{1.7}$$

Where S, I and R represent susceptible, infected and immune individuals respectively, β is the infection rate, γ is loss of immunity, and ν is the recovery rate. The introduction of an immune class makes disease dynamics more realistic, but it is still not sufficient to provide a comprehensive representation of the most complex behaviour exhibited by the immune response. It is suggested that incorporating some techniques aimed at macroparasitic diseases, such as parasite load, could be used to produce more accurate results [7]. Although current models can be used to provide forecasts for disease spread, the authors of [7] believe that the constant evolution of parasites adapting to changes in environment presents a challenge when trying to accurately capture dynamics.

The malaria models presented in [7] provide some basic techniques which can be used or adapted to describe the spread of leishmaniasis. The basic assumptions used to create the models are useful building blocks, which can be fitted to different disease dynamics. The transmission term created by Ross, with the inclusion of biting rates and infection probabilities, can be directly used for leishmaniasis owing to the similarity in disease vectors and the circumstances under which they feed. The inclusion of a latent period will also fit the disease dynamics exhibited by leishmaniasis, however the fixed latent periods presented in [7] are not necessarily the best choice as the latent period in leishmaniasis is more variable.

1.3.2 Existing models for Leishmaniasis

Although much of the existing body of work on leishmaniasis is focussed upon the immunology of the disease, there are some examples of mathematical models being used to describe disease spread. In [23] the authors state that models for leishmaniasis have been poorly developed compared to those for other diseases. They therefore consider a general model for the spread of American cutaneous leishmaniasis. A basic set of compartmental differential equations is provided to describe disease transmission between an incidental host, reservoir host and vector. Using model assumptions drawn

from the Ross malaria model, the following system of equations is obtained:

$$\frac{dH(t)}{dt} = \beta_H V(t)(A(t) - H(t)) - \gamma_H H(t) \quad (1.8)$$

$$\frac{dR(t)}{dt} = \beta_R V(t)(B(t) - R(t)) - \gamma_R R(t) \quad (1.9)$$

$$\frac{dV(t)}{dt} = \beta_R R(t)(C(t) - V(t)) - \mu V(t) \quad (1.10)$$

the variables and parameters of which are defined in Table (1.2). A schematic for the model is shown in Figure (1-3).

Symbol	Definition
$H(t)$	Number of infected incidental hosts at time t.
$R(t)$	Number of infected reservoir hosts at time t.
$V(t)$	Number of infected vectors at time t.
$A(t)$	Total population size of incidental hosts at time t.
$B(t)$	Total population size of reservoir hosts at time t.
$C(t)$	Total population size of vectors at time t.
β_H	Contact rate of infection for incidental hosts.
β_R	Contact rate of infection for reservoir hosts.
γ_H	Recovery rate of incidental hosts.
γ_R	Recovery rate of reservoir hosts.
μ	Mortality rate of vectors.

Table 1.2: Table listing the variables and parameters used in the model from [23].

The rate of host infection is dependent on the contact rate, number of infected vectors, and number of susceptible hosts. Hosts recover at rate γ_H or γ_R, dependent on their type. Infection in vectors is dependent on the contact between susceptible vectors and infected reservoir hosts. Once again it is assumed that the vector does not survive to recover, and dies at rate μ. The model is used to derive threshold conditions for disease spread, such as the basic reproductive number R_0. Arguably the most important quantity in epidemiology, R_0 is defined as the number of secondary infections arising from one primary infection introduced into a wholly susceptible population. The basic reproductive number can be used as a measure of potential disease spread since an epidemic may only occur if $R_0 > 1$ [8]. A main result in [23] is that R_0 is not dependent on incidental hosts.

Although [23] presents a good basis for a leishmaniasis model, the simplicity of the chosen equations means the system is not particularly biologically realistic. This issue has been raised by the authors themselves, who suggest a number of possible

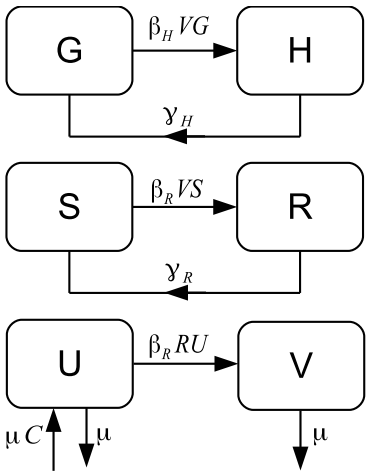

Figure 1-3: Schematic of model (1.8)-(1.10) from [23]. $G = A - H$, $S = B - R$ and $U = C - V$ are the numbers of susceptible incidental hosts, reservoir hosts and vectors respectively.

improvements aimed at either increasing generality, precision or realism. For example, the model assumes that the rates of infection β_H and β_R are independent. In reality this independence does not hold, as each fly will bite either an incidental or reservoir host at each blood meal, and not both. This therefore means that transmission rates could be made more realistic if they were to depend on one another, as every bite on an incidental host means one less bite to a reservoir host. Other suggested improvements include introducing climatic variables to investigate how global warming impacts upon the spread of the disease, introducing a spatial aspect to the model or including disease relapse to better represent the immunity conferred by the disease.

Compartmental differential equation models are also used to describe the spread of leishmaniasis in [35] and [43]. In [43] a model is constructed for the spread of canine leishmaniasis, in cases of both heterogeneous and homogeneous transmission. When transmission is homogeneous the vector has no preferential blood source. When transmission is heterogeneous vectors have a preferred blood source. A heterogeneous model is considered since it is claimed some working dogs are bitten on average more frequently than pet dogs. In both cases, infection dynamics are modeled for two types of dogs, labelled type-A and type-B, and a sandfly vector. After receiving an infected bite type-A dogs go through a latent period before becoming symptomatic. Type-B dogs also enter a latent period, but they do not become symptomatic, and are not infectious to sandflies. This means type-B dogs are dead-end hosts, as described in

[23]. The model in [43] is given by the system of equations:

$$\frac{dS_A(t)}{dt} = B_A - \beta_{FA} I_F(t) \frac{S_A(t)}{N_D(t)} - \delta_D S_A(t) \tag{1.11}$$

$$\frac{dE_A(t)}{dt} = \beta_{FA} I_F(t) \frac{S_A(t)}{N_D(t)} - (\sigma_A + \delta_D) E_A(t) \tag{1.12}$$

$$\frac{dI_A(t)}{dt} = \sigma_A E_A(t) - \delta_A I_A(t) \tag{1.13}$$

$$\frac{dS_B(t)}{dt} = B_B - \beta_{FB} I_F(t) \frac{S_B(t)}{N_D(t)} + \sigma_B E_B(t) - \delta_D S_B(t) \tag{1.14}$$

$$\frac{dE_B(t)}{dt} = \beta_{FB} I_F(t) \frac{S_B(t)}{N_D(t)} - (\sigma_B + \delta_D) E_B(t) \tag{1.15}$$

$$\frac{dI_F(t)}{dt} = \beta_{AF} \left[N_F e^{-\delta_F L_F} - I_F(t) \right] \frac{I_A(t - L_F)}{N_D(t)} - \delta_F I_F(t) \tag{1.16}$$

where variables and parameters are defined in Table (1.3). A schematic representing the model can be found in Figure (1-4).

Symbol	Definition
$S_A(t)$	Number of susceptible type-A dogs.
$E_A(t)$	Number of latently infected type-A dogs.
$I_A(t)$	Number of infectious type-A dogs.
$S_B(t)$	Number of susceptible type-B dogs.
$E_B(t)$	Number of latently infected type-B dogs.
$I_F(t)$	Number of infectious sandflies.
$N_A(t)$	Total number of type-A dogs. $N_A(t) = S_A(t) + E_A(t) + I_A(t)$.
$N_B(t)$	Total number of type-B dogs. $N_B(t) = S_B(t) + E_B(t)$.
$N_D(t)$	Total number of dogs. $N_D = N_A(t) + N_B(t)$
$N_F(t)$	Total number of sandflies.
t	Time (unit is one day).
B_A	Number of new-born type-A dogs per day.
B_B	Number of new-born type-B dogs per day.
L_F	Latent period of the parasite in sandflies, in days.
β_{FA}	Transmission rate to type-A dogs, per infectious sandfly per day.
β_{AF}	Transmission rate per infectious type-A dog to sandflies, per day.
β_{FB}	Transmission rate to type-B dogs, per infectious sandfly per day.
δ_D	Death rate of asymptomatic type-A dogs and of type-B dogs.
δ_A	Death rate of infectious dogs.
δ_F	Death rate of sandflies.
σ_A	Rate at which latent type-A dogs become infectious.
σ_B	Rate at which latent type-B dogs become susceptible again.

Table 1.3: Table listing the variables and parameters used in the model in [43].

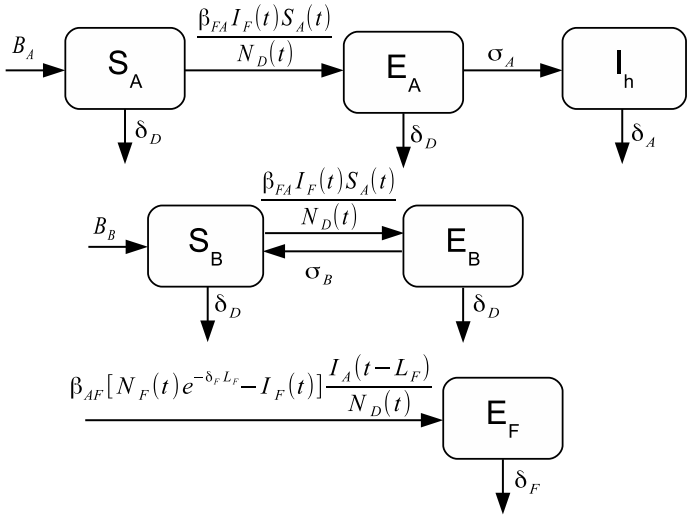

Figure 1-4: Schematic representing model (1.11)-(1.16) in [43].

Type-A dogs can be susceptible, latently infected or infectious. Since the life expectancy of dogs is on the same scale as the infection dynamics, a natural mortality rate δ_D is incorporated in all host compartments. A disease related death term is also incorporated in the mortality of infectious type-A dogs, due to the high virulence of infection in this group. Type-B dogs are either susceptible or latently infected and do not suffer from disease related death. The disease dynamics for the vector are summarised in one equation. As in the Ross malaria model, transmission is governed by a rate dependent on the bite rate of the vector, and proportion of susceptible and infected hosts and vectors. After becoming infected, vectors must survive a latent period of duration L_F before they become infectious. The latent period is included through the product of the number of sandflies which become infected at time $t - L_F$ and the number which survive the latent period $\exp(-\delta_F L_F)$. The number of susceptible sandflies at time $t - L_F$, the transmission rate from infectious type A dogs to sandflies β_{AF} and the proportion of dogs which are actually are infectious at time $t - L_F$, $\frac{I_A(t-L_F)}{N_D(t)}$, are also considered. Vectors do not recover from infection, and die at rate δ_F.

Once infection has been introduced to a system the numbers of individuals in the susceptible compartments will deplete, meaning that R_0 which is based on a wholly susceptible population, becomes an overestimate of the number of secondary infections per infected individual as we move away from disease free equilibrium. In order to enable the investigation of potential disease spread as time progresses, both R_0 and an effective reproductive number are derived in [43]. The effective reproductive number,

often denoted $R_e(t)$, is defined as the expected number of secondary infections arising from the introduction of one infected individual at time t to a population containing $S(t)$ susceptibles, and thus takes into account any reduction in the susceptible population. The effective reproduction number is used to estimate R_0 from prevalence data and a few additional model components. R_0 is not used to discuss the efficacy of different disease control techniques in this paper, and the main focus is on how R_0 can be calculated.

The compartmental model given for heterogeneous transmission is similar to that of the homogeneous case. In order to take into account the more complex transmission the dog population is divided between a finite number of groups i. It is assumed all dogs within each group are equally attractive to sandflies, and that the number of dogs in each group remains constant. Infection dynamics for each group of dogs i is governed by a set of equations similar to (1.11)-(1.16). For example, equation (1.11) for type-A susceptible dogs becomes:

$$\frac{dS_{Ai}(t)}{dt} = B_{Ai}(t) - \beta_{FA}\gamma_i I_F(t)\frac{S_{Ai}(t)}{N_{Di}(t)} - \delta_D S_{Ai}(t) \tag{1.17}$$

where γ_i represents the proportion of blood meals vectors take from group i. Each γ_i is non-negative, and $\sum_{i\in G}\gamma_i = 1$, where G is the set of indexes i which refer to individual dog groups. The adapted model is used to calculate R_0 and R_e.

The model presented in [43] is more detailed than that in [23] and provides an interesting insight into how leishmaniasis can be modelled in dogs. Transmission has been made more biologically realistic than in [23] through the inclusion of infection probabilities in transmission rates β_{AF}, β_{FA} and β_{FB}, and through the inclusion of a latent period in the host and vector species. Asymptomatic and symptomatic hosts are also considered; however asymptomatic hosts are not infectious to vectors. Literature such as [11] and [63] suggest that asymptomatic dogs are still infectious to sandflies, albeit at a reduced level. The absence of disease related death in type-B dogs means $\delta_A > \delta_B$ and so these asymptomatic dogs will live longer and have the potential to infect sandflies over a greater period of time. This would impact upon disease forecasts, and any control methods suggested.

In [35] a compartmental differential equation model is used to describe visceral leishmaniasis in humans, vectors and an animal reservoir when a host vaccination schedule is implemented. A proportion of infected humans also develop Post Kala-Azar Dermal leishmaniasis (PKDL), a rare complication of visceral leishmaniasis caused by *Leishmania donovani* which leads to a nodular rash on the skin. Disease dynamics are modelled using system (1.18)-(1.26). Variables and parameters are given in Table

(1.4). Subscript v represents the sandfly vectors, subscript r represents the animal reservoir population and subscript h represents the human hosts. A schematic of the model structure used in [35] is shown in Figure (1-5).

$$\frac{dS_h}{dt} = \Gamma_h + (1-\epsilon)\,A - \frac{acI_v(t)S_h(t)}{N_h(t)} - (\alpha_1 + \mu_h)\,S_h(t) \tag{1.18}$$

$$\frac{dV_h}{dt} = \alpha_1 S_h(t) - \frac{\rho acI_v(t)V_h(t)}{N_h(t)} - \mu_h V_h(t) \tag{1.19}$$

$$\frac{dI_h}{dt} = \epsilon A + \frac{acI_v(t)\,(S_h(t) + \rho V_h(t))}{N_h(t)} - (\gamma_1 + \delta + \mu_h)\,I_h(t) \tag{1.20}$$

$$\frac{dP_h}{dt} = (1-\sigma)\,\gamma_1 I_h(t) - (\gamma_2 + \beta\mu_h)\,P_h(t) \tag{1.21}$$

$$\frac{dR_h}{dt} = \sigma\gamma_1 I_h(t) + (\gamma_2 + \beta)\,P_h(t) - \mu_h R_h(t) \tag{1.22}$$

$$\frac{dS_r}{dt} = \Gamma_r - \frac{abI_v(t)S_r(t)}{N_r(t)} - \mu_r S_r(t) \tag{1.23}$$

$$\frac{dI_r}{dt} = \frac{abI_v(t)S_r(t)}{N_r(t)} - \mu_r I_r(t) \tag{1.24}$$

$$\frac{dS_v}{dt} = \Gamma_v - acS_v(t)\left(\frac{I_h(t) + P_h(t)}{N_h(t)} + \frac{I_r(t)}{N_r(t)}\right) - \mu_v S_v(t) \tag{1.25}$$

$$\frac{dI_v}{dt} = acS_v(t)\left(\frac{I_h(t) + P_h(t)}{N_h(t)} + \frac{I_r(t)}{N_r(t)}\right) - \mu_v I_v(t) \tag{1.26}$$

In [35], humans enter the system via births or immigration. Immigrants can be either susceptible or infected. As in [23] and [43] transmission is based on the assumptions of Ross [7]. Humans either become immune after infection, or can develop PKDL. The system of equations governing disease dynamics is used to calculate R_0, and investigate the ability of vaccination to prevent an epidemic. It is found that vaccination is only a viable control strategy when the immigration rate is low. The vaccination rate is constant however, and transient solutions are not considered. Although the model for human leishmaniasis in [35] is more detailed than that in [23], asymptomatic reservoirs are not included in model equations, and recovered individuals do not relapse.

The models presented in [7], [23], [35] and [43] form a set of building blocks that can be used to develop a more biologically realistic model for leishmaniasis. Information is provided for modelling both human and canine infections, and can be tailored to look at different scenarios. In Chapter 2 we use the information collected in this literature review in order to develop a mathematical model for leishmaniasis.

Symbol	Definition
S_z	Susceptible individual of type z
V_z	Vaccinated individual of type z
I_z	Infected individual of type z
P_z	PKDL infected individual of type z
R_z	Recovered individual of type z
Γ_z	Recruitment rate of type z individuals per day
A	Human immigration rate per day
ϵ	Proportion of immigrants infected with leishmaniasis
μ_z	Mortality rate of type z individuals per day
a	Sandfly bite rate per day
b	Progression rate of VL in sandflies per day
c	Progression rate of VL in humans and animals per day
α_1	Human vaccination rate per day
$1-\rho$	Vaccination efficiency
δ	Disease induced mortality rate in humans, per day
γ_1	Human treatment rate, per day
γ_2	Rate of PKDL recovery without treatment, per day
σ	Fraction of treated individuals that contract PKDL
β	Natural recovery rate

Table 1.4: Table listing the variables and parameters used in the model (1.18)-(1.26) in [35].

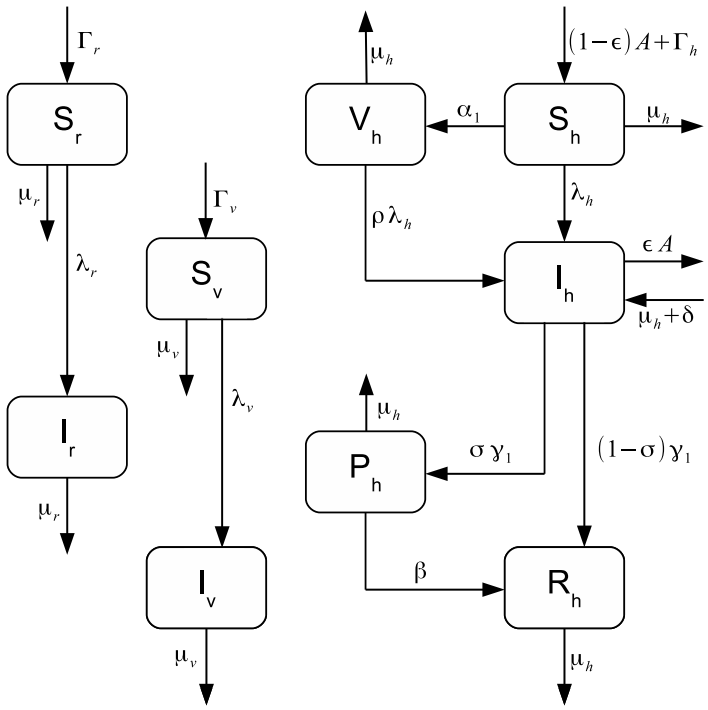

Figure 1-5: Schematic representing the model (1.18)-(1.26) used in [35].

Chapter 2

Model Formulation and Basic Analysis

We now use the information gathered in Chapter 1 to develop a mathematical model for the spread of leishmaniasis. We begin by introducing a base host-vector model for an anthroponotic leishmaniasis with only one host and one vector species. We build upon the models presented in the literature review in order to describe both host and vector disease dynamics with a compartmental differential equation model. Using our model we derive expressions for the basic reproductive number R_0 and endemic infection prevalence I^*. A suitable numerical parameterisation will then be considered and used in conjunction with R_0 and I^* to investigate the dependence of these key quantities on individual disease parameters. Results will be used to identify key aspects of the transmission process and ensure a comprehensive understanding of the base model. We then extend the base model to consider the transmission of a zoonotic leishmaniasis with one competent host and one dead-end host.

2.1 One Host Model

Our base model contains two populations, one representing the host and one the vector. The two populations are divided between the compartments listed in Table (2.1) dependent on their disease status. Throughout this thesis parameters and variables with subscript h are associated to the host population and parameters with subscript v are associated to the vector population.

Individuals move between compartments at rates dependent on species and disease status. The complete demographic and epidemiological dynamics are represented in the schematic in Figure (2-1). Time t is measured in months, and parameters are

defined in Table (2.2).

Compartment	Definition
$S_h(t)$	Total number of susceptible hosts at time t
$E_h(t)$	Total number of hosts in the latent state at time t
$I_h(t)$	Total number of infectious hosts at time t
$R_h(t)$	Total number of recovered hosts at time t
$S_v(t)$	Total number of susceptible female vectors at time t
$E_v(t)$	Total number of female vectors in the latent state at time t
$I_v(t)$	Total number of infectious female vectors at time t

Table 2.1: Table listing the compartments used in the basic one-host, one-vector model (2.1)-(2.7).

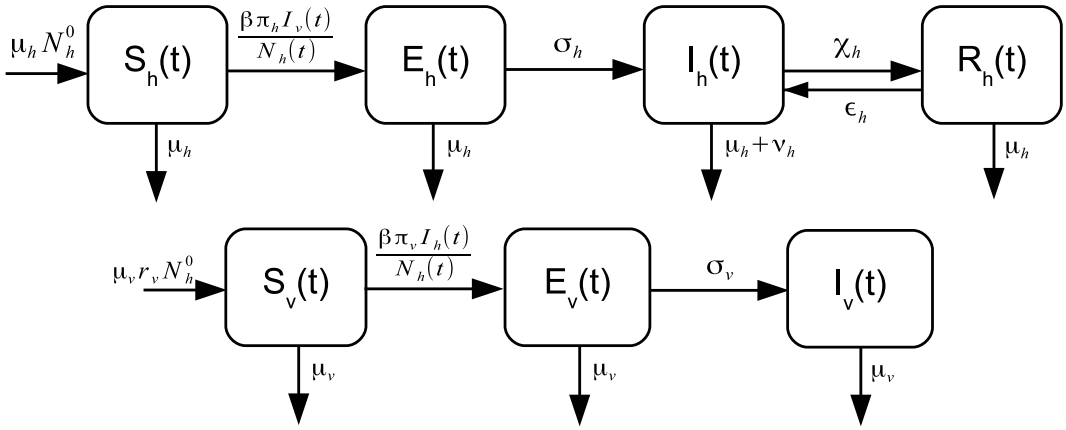

Figure 2-1: Schematic for the one-host one-vector model (2.1)-(2.7). Disease compartments are defined in Table (2.1), parameters are defined in Table (2.2).

In our base model all individuals are assumed to be susceptible to infection at birth. The host population is closed and the total population is given by $N_h(t) = S_h(t) + E_h(t) + I_h(t) + R_h(t)$. Unlike the models presented in Chapter 1, we include the host demographics of birth and death. Hosts are born at a constant rate $\mu_h N_h^0$ and have life expectancy $\frac{1}{\mu_h}$. Including host demography allows the existence of an endemic equilibrium, which can be used to investigate leishmaniasis dynamics in countries such as India where the disease is established. A Ross transmission term is used, where vectors bite hosts at random and transmission from an infected vector to a susceptible host occurs with probability π_h. Susceptible hosts enter a latent class at a rate $\frac{\beta \pi_h I_v}{N_h}$, where β is the bite rate per vector per month. Infected hosts either die of natural causes at rate μ_h or leave the latent class and become infectious at rate σ_h. Infectious individuals recover at rate χ_h, or die due to natural mortality at rate μ_h or disease

Parameter	Definition
μ_h	Natural birth/death rate of the host species per month
N_h^0	Total host population at disease free equilibrium
β	Bite rate per vector per month
π_h	Probability a bite from an infectious vector leads to infection
σ_h	Transfer rate from E_h to I_h per month
χ_h	Host recovery rate per month
ν_h	Rate of disease related death in the host per month
ϵ_h	Host relapse rate per month
μ_v	Natural birth/death rate of the vector per month
r_v	Ratio of vectors to hosts
π_v	Probability a vector becomes infected after biting an infectious host
σ_v	Transfer rate from E_v to I_v per month

Table 2.2: Table listing the parameters used in Figure (2-1) for the one-host, one-vector model (2.1)-(2.7).

induced mortality at rate ν_h. In the case of cutaneous leishmaniasis the infection is self healing, $\nu_h = 0$ and $N_h(t) = N_h^0 \; \forall \, t$. Hosts who survive the infectious period to recover either remain in the recovered class for the remainder of their lifespan, or relapse into the infectious class at rate ϵ_h. The inclusion of host demography is also important when investigating the impact of relapse on disease dynamics, as the rates of host relapse and mortality are of a similar order of magnitude.

The total female vector population is both closed and constant, and is given by $N_v(t) = r_v N_h^0 = S_v(t) + E_v(t) + I_v(t)$. Vectors are born at a constant rate $\mu_v r_v N_h^0$ and have life expectancy $\frac{1}{\mu_v}$. We express the vector birth rate as a function of the total host population in order to focus on the ratio of vectors to hosts r_v rather than explicit population sizes. Note that $\mu_v \gg \mu_h$ since the lifespan of a vector is much less than that of a host. The transmission term is again based on that of Ross, and is dependent on the bite rate β and the transmission probability π_v. Susceptible vectors enter a latent class at rate $\dfrac{\beta \pi_v I_h}{N_h}$, or die due to natural mortality at rate μ_v. Infected vectors die due to natural mortality at rate μ_v or leave the latent class and become infectious at rate σ_v. Note that the duration of the host latent period $\frac{1}{\sigma_h}$ is far greater than that of vectors so $\sigma_v \gg \sigma_h$. Female vectors do not recover from infection and remain in the infectious class until death. To simplify the model we ignore any disease related mortality in the vector population at this time.

Expressing the rates of change of each compartment as differential equations, we obtain the model system (2.1)-(2.7). The system has not been rescaled to allow easier biological interpretation of parameters.

$$\frac{dS_h}{dt} = \mu_h N_h^0 - \beta \pi_h I_v(t) \frac{S_h(t)}{N_h(t)} - \mu_h S_h(t) \tag{2.1}$$

$$\frac{dE_h}{dt} = \beta \pi_h I_v(t) \frac{S_h(t)}{N_h(t)} - (\sigma_h + \mu_h) E_h(t) \tag{2.2}$$

$$\frac{dI_h}{dt} = \sigma_h E_h(t) - (\mu_h + \chi_h + \nu_h) I_h(t) + \epsilon_h R_h(t) \tag{2.3}$$

$$\frac{dR_h}{dt} = \chi_h I_h(t) - (\mu_h + \epsilon_h) R_h(t) \tag{2.4}$$

$$\frac{dS_v}{dt} = \mu_v r_v N_h^0 - \beta \pi_v S_v(t) \frac{I_h(t)}{N_h(t)} - \mu_v S_v(t) \tag{2.5}$$

$$\frac{dE_v}{dt} = \beta \pi_v S_v(t) \frac{I_h(t)}{N_h(t)} - (\mu_v + \sigma_v) E_v(t) \tag{2.6}$$

$$\frac{dI_v}{dt} = \sigma_v E_v(t) - \mu_v I_v(t) \tag{2.7}$$

2.1.1 R_0: Intuitive Method

We now use our base model to analyse the epidemiological characteristics of an anthroponotic leishmaniasis. One measure of the potential disease spread is to consider the basic reproductive number R_0. If $R_0 > 1$ a disease will spread and an epidemic may occur. If $R_0 < 1$ there will not be a sustained epidemic. By studying the model equations it is possible to obtain R_0 intuitively for the system (2.1)-(2.7). In the case of leishmaniasis we consider the total number of secondary infections over a complete infection cycle i.e. host-vector-host or vector-host-vector. Firstly, when one latently infected host is introduced into an otherwise susceptible system they will initially infect:

$$R_{lv} = \left(\frac{\sigma_h}{\sigma_h + \mu_h} \right) \left(\frac{\beta \pi_v}{\chi_h + \mu_h + \nu_h} \right) \frac{N_v^0}{N_h^0} \tag{2.8}$$

vectors, where $\dfrac{\sigma_h}{\sigma_h + \mu_h}$ is the probability a host survives the latent period to become infectious, and $\dfrac{\beta \pi_v r_v}{\chi_h + \mu_h + \nu_h}$ is the total number of transmission events before death or recovery of the host. One latently infected sandfly infects:

$$R_{vl} = \left(\frac{\sigma_v}{\sigma_v + \mu_v} \right) \left(\frac{\beta \pi_h}{\mu_v} \right) \tag{2.9}$$

hosts, where $\dfrac{\sigma_v}{\sigma_v + \mu_v}$ is the probability a vector will survive the latent period to become infectious and $\dfrac{\beta \pi_h}{\mu_v}$ is the total number of transmission events before the death of the vector. If there is no relapse R_0^2 is obtained after two generations by taking the product

of R_{lv} and R_{vl}, however this is not the case in our model. Instead, a proportion

$$\frac{\chi_h}{\chi_h + \mu_h + \nu_h}$$

of infectious hosts recover rather than dying whilst infectious, and a proportion of recovered hosts

$$\frac{\epsilon_h}{\epsilon_h + \mu_h}$$

relapse rather than dying in the recovered state. Let

$$R_{iv} = \left(\frac{\beta \pi_v r_v}{\chi_h + \mu_h + \nu_h} \right)$$

be the number of latently infected vectors from one actively infected host, and

$$R_{vh} = \left(\frac{\sigma_h}{\mu_h + \sigma_h} \right) R_{vl}$$

be the number for actively infectious hosts from one latently infected vector. Each infectious host causes a further

$$R_{iv} \frac{\chi_h \epsilon_h}{(\chi_h + \mu_h + \nu_h)(\epsilon_h + \mu_h)}$$

infections due to a relapse after their first infection. However,

$$\left(\frac{\chi_h \epsilon_h}{(\chi_h + \mu_h + \nu_h)(\epsilon_h + \mu_h)} \right)^2$$

hosts recover and relapse twice and

$$\left(\frac{\chi_h \epsilon_h}{(\chi_h + \mu_h + \nu_h)(\epsilon_h + \mu_h)} \right)^k$$

hosts recover and relapse k times. Using the sum of an infinite geometric progression we find that the total number of infections caused by one latently infected host is in fact:

$$\begin{aligned} R_{hv} &= \sum_{k=0}^{\infty} R_{iv} \left(\frac{\chi_h \epsilon_h}{(\chi_h + \mu_h + \nu_h)(\epsilon_h + \mu_h)} \right)^k \\ &= \frac{R_{iv}}{1 - \frac{\chi_h \epsilon_h}{(\chi_h + \mu_h + \nu_h)(\epsilon_h + \mu_h)}} \\ &= \frac{(\epsilon_h + \mu_h)\beta \pi_v r_v}{\mu_h (\chi_h + \epsilon_h + \mu_h + \nu_h) + \nu_h \epsilon_h} \end{aligned}$$

In order to obtain R_0 we then take the product of R_{hv} and R_{vh}.

$$R_0^2 = \frac{\beta^2 \pi_h \pi_v \sigma_h \sigma_v r_v \left(\epsilon_h + \mu_h\right)}{\mu_v \left(\sigma_v + \mu_v\right)\left(\sigma_h + \mu_h\right)\left(\left(\chi_h + \mu_h + \nu_h\right)\left(\epsilon_h + \mu_h\right) - \chi_h \epsilon_h\right)}$$

so that

$$R_0 = \sqrt{\frac{\beta^2 \pi_h \pi_v \sigma_h \sigma_v r_v \left(\epsilon_h + \mu_h\right)}{\mu_v \left(\sigma_v + \mu_v\right)\left(\sigma_h + \mu_h\right)\left(\left(\chi_h + \mu_h + \nu_h\right)\left(\epsilon_h + \mu_h\right) - \chi_h \epsilon_h\right)}} \tag{2.10}$$

2.1.2 R_0: The Next Generation Matrix Method

For more complex systems of equations it is not always possible to construct R_0 intuitively. The next generation matrix is an alternative method to derive the basic reproductive number. In the case of equations (2.1)-(2.7) it can be used to verify the intuitive construction.

The next-generation matrix (NGM) can be used to calculate R_0 when there are multiple classes of infected individual. In order to compute the next-generation matrix the set of ODEs describing the disease dynamics is linearised about the disease-free equilibrium (DFE) by constructing a Jacobian matrix. We use the DFE since R_0 considers the initial spread of an infection in a wholly susceptible population, and assumes any change in the susceptible population due to disease is negligible.

Once the Jacobian has been obtained it is split into two components, T and Σ. The matrix T represents transmission; the production of new infections. The matrix Σ represents transition; the movement of individuals between classes by all other means e.g. death, recovery, relapse.

The matrix $-\Sigma$ is inverted and multiplied by T to produce the NGM $\left(-T\Sigma^{-1}\right)$. The $(i,j)^{th}$ element of T is the rate at which infected individuals in compartment j produce infections in compartment i, and the $(j,k)^{th}$ entry of $-\Sigma^{-1}$ is the average length of time an infected individual introduced in compartment k spends in compartment j during its lifetime. The $(i,k)^{th}$ element of the NGM therefore gives the expected number of new infections in compartment i produced by an infective individual initially introduced in compartment k. We find R_0 by calculating $\rho\left(-T\Sigma^{-1}\right)$, where $\rho(A)$ represents the dominant eigenvalue, or spectral radius, of the matrix A. A more detailed explanation of the theory behind the next-generation matrix method can be found in [28], [32] and [33].

We now use the next-generation matrix method to compute R_0 for the system of equations (2.1)-(2.7) presented in Section (2.1). To account for the transmission

and transition of infection we include the latent, infected and recovered classes in our calculations. We use the disease free equilibrium $(S_h, E_h, I_h, R_h, S_v, E_v, I_v) = (N_h^0, 0, 0, 0, r_v N_h^0, 0, 0)$ to produce our Jacobian matrix. Although there are seven classes in the model only five need to be used when calculating the basic reproductive number, since we require only the infection subsystem and the linearisation assumption implies S_h and S_v are constant. Let

$$T = \begin{pmatrix} 0 & 0 & 0 & 0 & \beta\pi_h \\ 0 & 0 & 0 & 0 & 0 \\ 0 & 0 & 0 & 0 & 0 \\ 0 & \beta\pi_v r_v & 0 & 0 & 0 \\ 0 & 0 & 0 & 0 & 0 \end{pmatrix}$$

and

$$\Sigma = \begin{pmatrix} -(\mu_h + \sigma_h) & 0 & 0 & 0 & 0 \\ \sigma_h & -(\chi_h + \mu_h + \nu_h) & \epsilon_h & 0 & 0 \\ 0 & \chi_h & -(\epsilon_h + \mu_h) & 0 & 0 \\ 0 & 0 & 0 & -(\mu_v + \sigma_v) & 0 \\ 0 & 0 & 0 & \sigma_v & -\mu_v \end{pmatrix}$$

so that the infection subsystem of equations (2.1)-(2.7) is given by

$$\frac{d\mathbf{x}}{dt} = (T + \Sigma)\,\mathbf{x}$$

where $\mathbf{x} = [E_h, I_h, R_h, E_v, I_v]^T$. The next generation matrix is therefore given by:

$$-T\Sigma^{-1} = \begin{pmatrix} 0 & 0 & 0 & \frac{\beta\pi_h\sigma_v}{\mu_v(\mu_v+\sigma_v)} & \frac{\beta\pi_h}{\mu_v} \\ 0 & 0 & 0 & 0 & 0 \\ 0 & 0 & 0 & 0 & 0 \\ \frac{f\sigma_h(\epsilon_h+\mu_h)}{(\mu_h+\sigma_h)g} & \frac{f(\epsilon_h+\mu_h)}{g} & \frac{f\epsilon_h}{g} & 0 & 0 \\ 0 & 0 & 0 & 0 & 0 \end{pmatrix} \tag{2.11}$$

where $f = r_v\beta\pi_v$ and $g = (\chi_h + \mu_h + \nu_h)(\epsilon_h + \mu_h) - \chi_h\epsilon_h$.

The matrix (2.1.2) takes into account not only new infections but also the transitional changes of those previously infected. The basic reproductive number R_0 is only concerned with potential disease spread arising from newly infected individuals, so any information about the rest of the infection subsystem is often left unused. In [33], Diekmann et al. argue that next generation matrices such as (2.11) containing infor-

mation about all stages of infection are unnecessarily large, and can often be reduced to a lower dimension to make R_0 easier to compute.

Let subscript L denote the NGM of large domain K_L given by (2.11). The NGM of reduced domain is obtained by pre- and post- multiplying K_L by an auxiliary matrix E. The auxiliary matrix consists of unit column vectors that remove all compartments an individual cannot enter immediately after infection. The NGM of reduced domain K can be obtained using equation (2.12), the details of which can be found in [33].

$$K = E'K_LE = -E'T\Sigma^{-1}E \tag{2.12}$$

In order to obtain the reduced form of the NGM (2.11) we use the auxiliary matrix (2.13).

$$E = \begin{pmatrix} 1 & 0 \\ 0 & 0 \\ 0 & 0 \\ 0 & 1 \\ 0 & 0 \end{pmatrix} \tag{2.13}$$

The NGM of reduced domain is then

$$K = \begin{pmatrix} 0 & \frac{\beta\pi_h\sigma_v}{\mu_v(\mu_v+\sigma_v)} \\ \frac{r_v\beta\pi_v(\mu_h+\epsilon_h)\sigma_h}{(\mu_h+\sigma_h)(\mu_h(\epsilon_h+\mu_h+\chi_h+\nu_h)+\nu_h\epsilon_h)} & 0 \end{pmatrix}. \tag{2.14}$$

This matrix has spectral radius:

$$\sqrt{\frac{\beta^2\pi_h\pi_v\sigma_h\sigma_v r_v\left(\epsilon_h+\mu_h\right)}{\mu_v\left(\sigma_v+\mu_v\right)\left(\sigma_h+\mu_h\right)\left(\left(\chi_h+\mu_h+\nu_h\right)\left(\epsilon_h+\mu_h\right)-\chi_h\epsilon_h\right)}} = R_0 \tag{2.15}$$

which matches the intuitive expression for R_0 (2.10). Further information regarding the simplification of the next-generation matrix can be found in [33].

2.1.3 Type Reproductive Numbers

The use of R_0 as a measure of the effort required for epidemic prevention is of particular benefit when considering a population with only one homogeneous population, however it may not be appropriate when considering a system with multiple subpopulations. In systems containing multiple subpopulations control techniques may be targeted at a subset of population groups. It may be preferable to calculate the control effort required to eliminate infection when only a particular group is targeted.

Type reproductive numbers T are a threshold quantity, useful when estimating the

control effort required to prevent disease spread when the control technique is applied only to a subpopulation of those involved in the transmission dynamics. According to [44], the type reproductive number is defined as:

> *'The expected number of cases in individuals of type i caused by one infected individual of type i in a completely susceptible population; either directly or through chains of infection passing through any sequence of other types.'*

Each subpopulation has its own type reproductive number which accounts for the fact that infections may have to pass through other subpopulations before any secondary infections can occur. In a homogeneous system $T_1 = R_0$ for the unique subpopulation of type 1 individuals. In a heterogeneous population with a finite number of subpopulations the two quantities only share a threshold at $T_1 = R_0 = 1$ and $T_1 > 1 \iff R_0 > 1$. Further details can be found in [70].

In the case of the model (2.1)-(2.7) presented in Section (2.1) there are two subpopulations, host and vector. The type reproductive number for hosts is the number of secondary infections in hosts arising from the introduction of one infected host. The type reproductive number for vectors is the number of secondary infections in vectors arising from the introduction of one infected vector. By working through the infection cycle it can be seen that no matter where infection originates, it must pass through every class in both hosts and vectors before it returns to its starting point. Letting T_h and T_v be the type reproductive numbers for hosts and vectors respectively, we obtain:

$$T_h = T_v = \frac{\beta^2 \pi_h \pi_v \sigma_h \sigma_v r_v N_h^0 \left(\epsilon_h + \mu_h\right)}{n_h \mu_v \left(\sigma_v + \mu_v\right)\left(\sigma_h + \mu_h\right)\left(\mu_h\left(\chi_h + \epsilon_h + \mu_h + \nu_h\right) + \nu_h \epsilon_h\right)} = R_0^2 \qquad (2.16)$$

This result implies that the same control effort must be applied to either the host or vector population to prevent an epidemic.

The type reproductive number may also be derived using linear algebra techniques to manipulate information from the next generation matrix [44, 70]. T_1 can be derived using equation (2.17):

$$T_1 = e' K \left(I - \left(I - P\right) K\right)^{-1} e \qquad (2.17)$$

where I is the identity matrix, e is the first unit vector and P is a projection matrix with $p_{11} = 1$ and $p_{ij} = 0 \ \forall \ i, j \neq 1$. Applying this technique to the model (2.1)-(2.7) presented in Section (2.1), using matrix (2.14) for K and setting

$$P = \begin{pmatrix} 1 & 0 \\ 0 & 0 \end{pmatrix} \qquad I = \begin{pmatrix} 1 & 0 \\ 0 & 1 \end{pmatrix} \quad \text{and} \quad e = \begin{pmatrix} 1 \\ 0 \end{pmatrix},$$

yields the type reproduction numbers given by equation (2.16).

2.1.4 Parameterisation

In Sections (2.1.9) and (2.1.10) we use the value of R_0 derived in Section (2.1.1) to investigate the key parameters involved in the ignition of an epidemic. This analysis is then extended to look at an endemic equilibrium to see if the same parameters control both disease spread and maintenance. The results for the R_0 analysis can also be used to infer results for the type reproductive numbers T_h and T_v since they are functions of R_0. Before this analysis can take place however, we must first establish a baseline parameterisation. We have chosen to parameterise the model for an anthroponotic leishmaniasis where humans are the sole host species, and female sandflies are the vector species. It is also be possible to tailor parameter values to transmission in different host species such as dogs.

Although assorted parameter values can be drawn from previous research, there is a high degree of uncertainty in some parameters due to the difficulty in obtaining data. For instance, trapping flies to work out the true number of flies is inexact, people do not report all cases of the disease and the number of sandfly bites acquired is highly variable and difficult to measure. Some parameters will also vary depending on the geographical location of the infection and the strain of leishmaniasis in question. Reasonable parameter ranges have been obtained from the literature and are listed in Table (2.3).

Parameter Range	**Source Information**
$1 < \beta < 8$ bite rate per female sandfly per month	Taking the entire vector population into account, estimates for β range from 20-50 bites per night [64] to 10-400 per month [68], to 1-259 landings per man per hour [40].
$0 < \pi_h < 1$ probability a bite from an infectious sandfly leads to infection	π_h is a probability. When $\pi_h = 0$ an infected bite never leads to infection. When $\pi_h = 1$ infection is certain.
$0 < \pi_v < 1$ probability a bite to an infectious host leads to infection	π_v is a probability. When $\pi_v = 0$ an infected bite never leads to infection. When $\pi_v = 1$ infection is certain.

$\frac{1}{15} < \chi_h < \frac{1}{2}$ host recovery rate per month	Without treatment, recovery takes between 2-15 months to occur [26].
$\frac{1}{841} < \epsilon_h < \frac{1}{36}$ relapse rate per host per month	The rate at which relapse occurs is highly dependent on the strain of leishmaniasis and the immune system of the infected individual. The expected minimum time before relapse occurs is 3 years.
$\frac{1}{540} < \mu_h < \frac{1}{840}$ human natural birth/death rate per month	$\frac{1}{\mu_h}$ is human life expectancy. Human life expectancy in Sub-Saharan Africa is approximately 45-50 years. In Brazil/North Africa it is 70 years [21]. A range of 45-70 years has been assigned to incorporate this information.
$\frac{15}{13} < \mu_v < \frac{15}{2}$ female sandfly natural birth/death rate per month	$\frac{1}{\mu_v}$ is vector life expectancy. Female sandfly life expectancy estimates range from 4-15 days [37] to an average 12-26 days [49]. A range of 4-26 days has been assigned to incorporate this information.
$\frac{1}{12} < \sigma_h < 1$ rate of transference from E_h to I_h per month	$\frac{1}{\sigma_h}$ is the incubation period in the host. σ_h can be from 2-6 months for visceral leishmaniasis [22] and anything between 1 week and several months for cutaneous leishmaniasis [73]. A range of 1-12 months has been chosen for σ_h in order to include this variation.
$\frac{6}{5} < \sigma_v < \frac{15}{2}$ rate of transference from E_v to I_v per month	$\frac{1}{\sigma_v}$ is the incubation period in the vector. The latent period in sandflies is between 4 and 25 days [79].
$\frac{1}{3} < r_v < 3$ ratio of vectors to hosts at DFE	The ratio of hosts to vectors is unknown. We assume there are between $\frac{1}{3}$ and 3 times as many vectors as hosts.
$\frac{1}{36} < \nu_h < \frac{1}{24}$ virulence in hosts per month	If visceral leishmaniasis is left untreated the fatality rate can be as high as 100% in 2 years [79].

Table 2.3: Ranges of values for parameters used in the one-host one-vector model (2.1)-(2.7). Information about the source from which these ranges were obtained is provided where available.

2.1.5 Latin Hypercube Sampling

Sanchez and Blower suggest that if there is uncertainty in parameter estimates it may be more appropriate to assign probability density functions (pdf) to parameter values and treat them as random variables [72]. These pdfs can then be sampled to obtain a frequency distribution for a particular quantity of interest. In this study the quantity of interest depends on the epidemiological context. At disease free equilibrium the basic reproductive number R_0 is an important quantity, since it provides insight into how variation in individual parameters can alter the potential for an epidemic to occur. At endemic equilibrium the infection prevalence I^* is an important quantity.

With suitable probability density functions in place the parameter space is then sampled. The sampling technique we will use is Latin Hypercube Sampling; a method which ensures a sample parameter value is taken from each of a finite number of intervals of the parameter space. Latin Hypercube Sampling is a type of stratified Monte Carlo Sampling first described by McKay in 1979 [61]. The technique is a generalisation of Latin Square sampling and is often used in uncertainty analysis as it produces a sample representative of the whole sample space and its variability. The following procedure is undertaken to obtain a Latin Hypercube Sample:

- For a model with M parameters a pdf is assigned to each individual parameter and then split into a number N of equally probable intervals.
- A sample is taken at random from each of the N intervals to produce an N-dimensional vector of possible values for each of the M parameters.
- Each entry of the vector is assigned an index, according to its position within the vector. The M vectors are then combined to form an M dimensional sample space over all parameters from which N parameter sets can be obtained. No two parameters within a parameter set share the same index and each parameter value appears only once. This can perhaps be most easily visualised in two dimensions, when $M = 2$ and we use a Latin Square. Letting $N = 3$, we have a 2-dimensional square sample space with 3 rows and 3 columns, see Figure (2-2). Only one sample is taken from each row and each column of the square, thus producing 3 unique parameter sets.

It has been shown that Latin Hypercube Sampling is more efficient than simple, random and fractional stratified sampling for large sample sizes when estimating means and cumulative distribution functions [15]. The technique allows us to obtain a sample across our entire parameter space and can be applied to multiple variables.

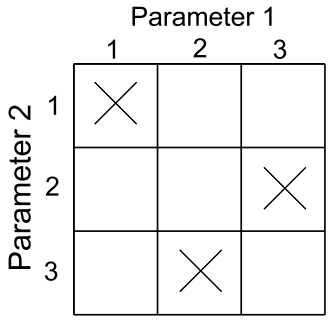

Figure 2-2: An example of Latin Square sampling on a 3×3 grid.

Latin Hypercube Sampling was used to choose representative sets of parameters with which numerical values of R_0 and I^* could be calculated. In the absence of evidence supporting a particular pdf, uniform distributions were assigned to input parameters for simplicity. Figure (2-3) shows the distribution of R_0 values obtained when the 1000 parameter sets obtained using Latin Hypercube Sampling were input into equation (2.10). Figure (2-4) shows the distribution of I^* values obtained for both the cutaneous and visceral cases of leishmaniasis. The endemic infection prevalence $I^* = I_h^* + I_v^*$ was calculated using the endemic equilibrium for equations (2.1)-(2.7) found in Appendix (A). The infection prevalence is displayed as the proportion of the total human and vector population.

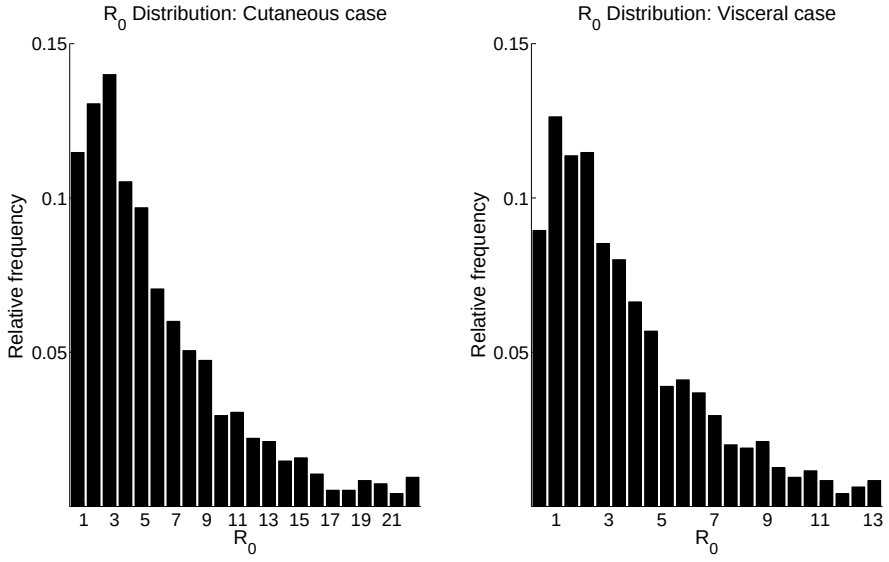

Figure 2-3: Distribution of R_0 values obtained when a full Latin Hypercube Sample is substituted into equation (2.10) for the one-host one-vector model (2.1)-(2.7). All parameter values vary. 1000 parameter sets were used.

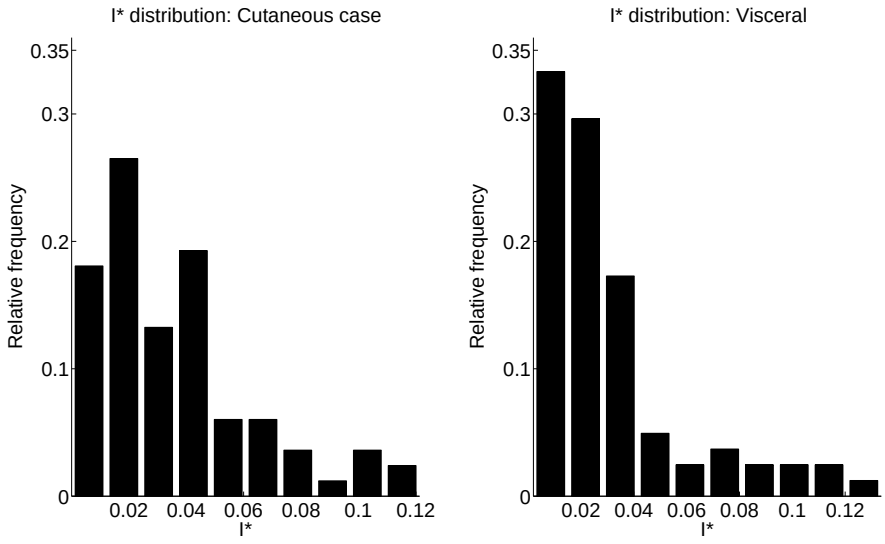

Figure 2-4: Distribution of I^* values obtained when a full Latin Hypercube Sample is substituted into I^* for the one-host one-vector model (2.1)-(2.7). All parameter values vary. 1000 parameter sets were used.

2.1.6 Latin Hypercube Distributions

The left hand panel of Figure (2-3) plots the R_0 values obtained for cutaneous leishmaniasis with $\nu_h = 0$. Results ranged from 0.08 to 81, with over 95% of values falling below 22. The distribution of $R_0 \leq 22$ was highly skewed, and 84% of R_0 values were below 10. The median R_0 value was 4.7. $R_0 > 1$ in 903 out of the 1000 parameter sets, meaning an epidemic occurs with non-zero probability in 90.3% of cases.

The right hand panel of Figure (2-3) plots the R_0 values obtained for visceral leishmaniasis. In general, the R_0 values for visceral leishmaniasis are lower than their cutaneous counterparts. Disease related death decreases the duration of transmission and leads to a reduction in the number of infections. Results ranged from 0.06 to 43.96, with over 95% of values falling below 13. The distribution of $R_0 \leq 13$ was skewed, and 76% of R_0 values obtained were below 5. The median R_0 value was 3.1. $R_0 > 1$ in 847 out of the 1000 parameter sets, meaning an epidemic occurs with non-zero probability in 84.7% of cases.

Figure (2-4) displays the I^* distributions for both cutaneous and visceral disease. The distributions are constructed by substituting the 847 Latin Hypercube parameter sets which led to an endemic equilibrium for both types of leishmaniasis into the expression $I^* = \frac{I_h^* + I_v^*}{N_h^* + N_v^*}$. In the case of cutaneous leishmaniasis the distribution of I^* values is skewed, with 95% of values below 0.0379. In the case of visceral leishmaniasis the distribution of I^* values is also skewed, with 95% of values below 0.0282. Table

(2.4) compares statistics such as the median, mean and range of I^* values. We find that the presence of disease related death in visceral leishmaniasis leads to a reduction in the average proportion of infectious individuals present at endemic equilibrium when compared to the cutaneous case.

Statistic	Cutaneous case	Visceral case
mean I^*	0.0359	0.0309
median I^*	0.0274	0.0186
minimum I^*	0.0002	0.0002
maximum I^*	0.1336	0.1212
range of I^* (max-min)	0.1334	0.1210

Table 2.4: Statistics for the I^* values obtained using Latin Hypercube parameter sets. Statistics are obtained from the same data set used to produce the histograms in Figure (2-4).

2.1.7 Confidence Intervals

Confidence intervals for the mean values of R_0 and I^* were obtained using the frequency distributions created with our full Latin Hypercube parameter sample. The inbuilt Matlab command expfit was first used to fit exponential distributions to the data sets used to create Figures (2-3) and (2-4). 95% confidence intervals for the mean were then extracted using the same command. Results are shown in Table (2.5). Again we find that the presence of disease related death in visceral leishmaniasis leads to a reduction in the average proportion of infectious individuals when compared to the cutaneous case.

Case	Lower bound, 95% CI	Upper bound, 95% CI
Cutaneous R_0	4.5598	5.1784
Visceral R_0	2.9172	3.3129
Cutaneous I^*	0.0292	0.0450
Visceral I^*	0.0251	0.0389

Table 2.5: 95% Confidence intervals for the mean value of R_0 and I^*, obtained using the full Latin Hypercube frequency distributions (2-3) and (2-4).

2.1.8 Time Dependent Infection Prevalence: One host model

Figure (2-5) shows how the combined infection prevalence I^*, human infection prevalence $\frac{I_h^*}{N_h^*}$ and vector infection prevalence $\frac{I_v^*}{N_h^*}$ vary over time. Using the base parameter set given in Table (C.1) we find that in both cutaneous and visceral cases the epidemic

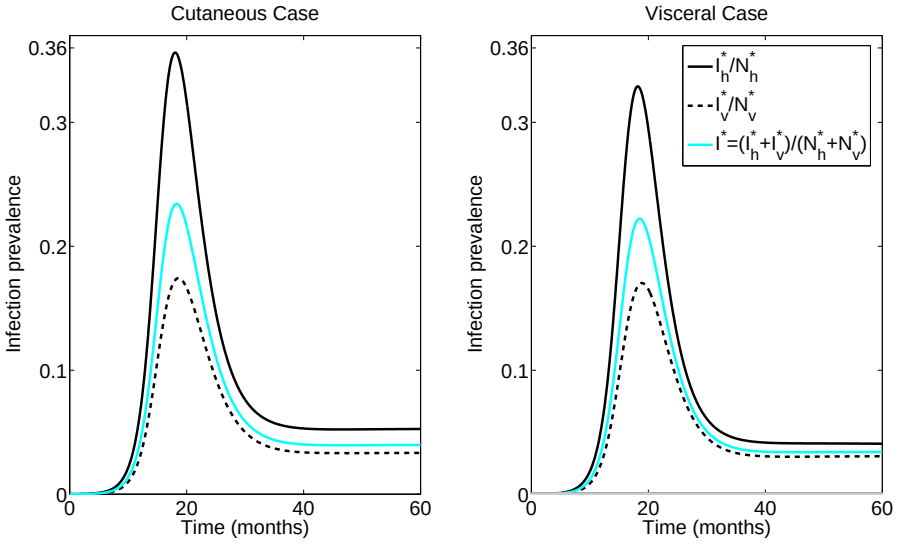

Figure 2-5: Plots of time dependent infection prevalence for the one-host one-vector model (2.1)-(2.7). Parameters are fixed at the values given in Table (C.1).

peaks at approximately 18 months. In the cutaneous case approximately 36% of humans and 17.5% of vectors are infected at the height of the epidemic. This corresponds to a combined infection prevalence of $I^* = 23\%$. In the visceral case approximatly 33% of humans and 17% of vectors are infected, so that the combined infection prevalence is $I^* = 22\%$. As in Figure (2-4), infection prevalence is lower in visceral leishmaniasis than in the cutaneous case due to the reduction in both the number of infectives and the duration of transmission caused by disease related death. In both cutaneous and visceral cases vectors have the lowest infection prevalence and humans have the highest. Since vector life expectancy is short, epidemic turnover in vectors is fast and infection prevalence is low. Including the total vector population in I^* therefore causes a dilution effect which reduces the combined infection prevalence below that of the human infection prevalence.

2.1.9 R_0 and Individual Parameters

We now investigate the relationship between individual parameters and potential disease spread. For each parameter we construct a vector of equally spaced values and substitute these into equation (2.10) for R_0. All other parameters are held fixed at the values given in Table (C.1). The vector of R_0 values obtained by varying one parameter can be used to produce a basic measure of how potential disease spread is related to a particular parameter. If R_0 has a large range when a parameter is varied, potential disease spread is sensitive to this parameter. There is no measure by which to quan-

tify a large parameter sensitivity; it is only possible to compare results relative to one another. In order to make line plots more easily comparable the R_0 values obtained have been scaled by dividing through by a quantity $R0_{base}$. $R0_{base}$ is the value of R_0 when all parameters are fixed at the values given in Table (C.1). Dividing through by $R0_{base}$ means line plots show the proportional deviation in R_0.

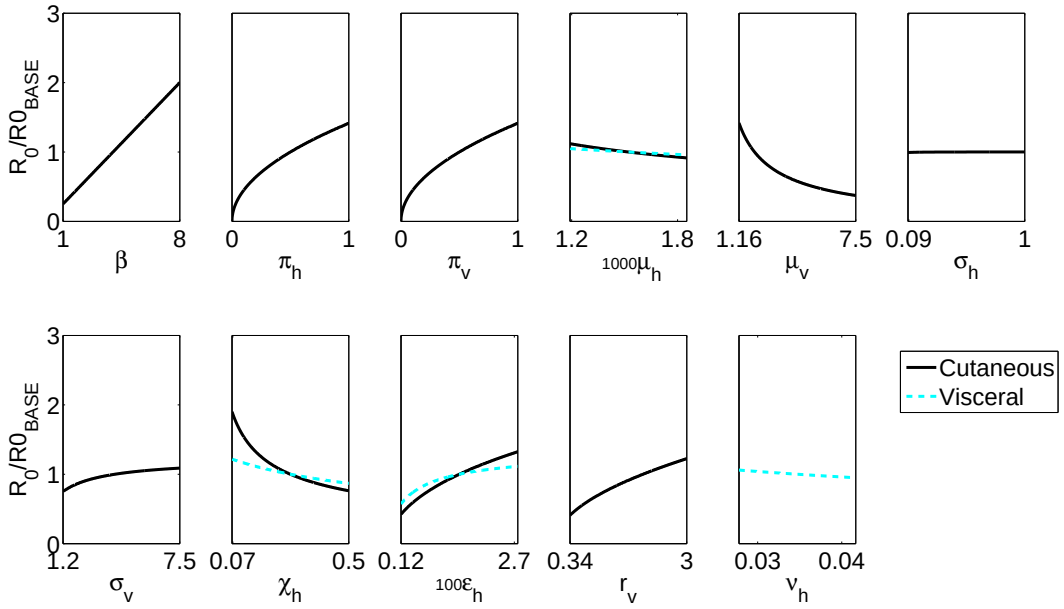

Figure 2-6: Relationships between R_0 (2.10) for the one-host one-vector model (2.1)-(2.7) and lower level parameters. In each subplot one parameter was varied across its range and input into (2.10). All other parameters were fixed at the values given in Table (C.1).

2.1.10 R_0: Results of Single Parameter Variation

Figure (2-6) shows how R_0 depends on each individual parameter in the one-host one-vector model (2.1)-(2.7). The results for both a cutaneous and a visceral leishmaniasis are displayed. In the case of cutaneous leishmaniasis there is no disease related death, $\nu_h = 0$ and $N_h(t) = N_h^0 \, \forall \, t$. Increasing β, π_h, π_v, σ_v, ϵ_h or r_v increases R_0, whereas increasing μ_h, μ_v, χ_h or ν_h decreases R_0. Increasing the bite rate β increases R_0 linearly, whereas increasing all other parameters leads to a non-linear change in R_0. Doubling β will quadruple the parameters contribution to R_0^2 since it appears in both fly-human and human-fly transmission pathways. All other parameters are involved in only one of the two transmission pathways and enter R_0 under a square root. Since $T_v = T_h = R_0^2$, parameters that increase the basic reproductive number will also increase the type reproductive number.

The value of R_0 is dependent upon both the rate and duration of transmission. Increasing the rate of transmission by increasing either the bite rate β or the transmission probabilities π_h and π_v increases the potential for disease spread and hence R_0. Increasing the ratio of vectors to hosts r_v also increases the potential disease spread by increasing the average number of bites per person and hence the likelihood an infectious contact occurs.

Increasing the duration of the infectious period also leads to an increase in the value of R_0 obtained. The duration of the infectious period governs the time in which transmission can occur, and is controlled by a number of parameters. Increasing either the rate of recovery χ_h, host mortality rate μ_h, vector mortality rate μ_v or disease induced death rate ν_h leads to a reduction in the duration of transmission and decreases the value of R_0. Increasing the relapse rate ϵ_h increases the average time spent in the infectious class, thus increasing both the duration of transmission and R_0. In the case of visceral leishmaniasis, the presence of disease induced mortality dilutes the impact host parameters μ_h, ϵ_h and χ_h have on the duration of transmission and R_0. When disease induced mortality is present there is a greater likelihood humans die before they recover and the average duration of the infectious period is reduced.

2.1.11 I^* and Individual Parameters

We now consider the model equations (2.1)-(2.7) at endemic equilibrium and investigate the relationship between individual parameters and infection prevalence $I^* = I_h^* + I_v^*$. In Figure (2-7) the y-axis has been rescaled by dividing through by I_{base}^*, the value of I^* obtained when all parameters are at the fixed values given in Table (C.1). This allows the Figures to be more easily compared. The value of $\frac{I^*}{I_{base}^*}$ can be interpreted as the deviation from the base value obtained by varying an individual parameter. The value of the base infection prevalence is $I_{base} = 158$ for cutaneous leishmaniasis, and $I_{base} = 71$ for visceral leishmaniasis.

Comparing Figure (2-7) to Figure (2-6) we see that the relationships between I^* and lower level parameters are similar to those that R_0 has with the same parameters. With the exception of the human death rate μ_h, parameters which when increased lead to an increase in R_0 also increase the value of I^* obtained. Although the rate and duration of transmission once again influence results, the impact parameters have at endemic equilibrium is also governed by the distribution of individuals between the different disease compartments. At disease free equilibrium the population is wholly susceptible to infection and there is a large pool of individuals available for novel disease transmission. At endemic equilibrium the majority of humans reside in the recovered class R_h and a smaller proportion of new infections arise from direct contacts with

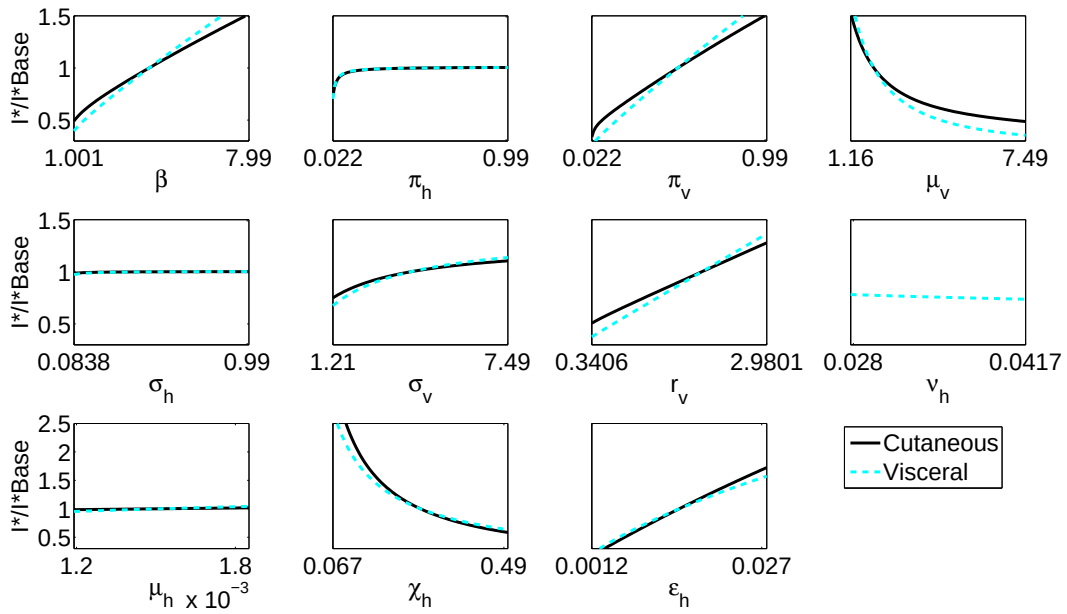

Figure 2-7: Relationships between I^* and lower level parameters for the one-host one-vector model represented by system (2.1)-(2.7). In each subplot one parameter was varied across its range and input into I^*. All other parameters were fixed at the values given in Table (C.1).

infected sandflies. Relapse becomes the driving force behind infection. The larger the proportion of recovered individuals the smaller the likelihood an infectious vector will make contact with a susceptible host, thus reducing the impact of β, π_h, π_v and r_v.

2.2 Two Host Model

In many areas where leishmaniasis is prevalent, humans are not the primary host species. Although a number of species have been implicated in the spread of leishmaniasis, dogs are the most important [11]. When dogs are the main reservoir of infection the transmission of leishmaniasis is zoonotic. Humans may become infected but are dead-end hosts and do not infect sandflies [65]. Some evidence suggests that amphixenotic transmission, where both humans and lower animals such as dogs transmit infection, may exist or evolve in some areas; however the data supporting the existence of amphixenotic leishmaniasis is weak at present ([79]).

In this Section a two host model for zoonotic leishmaniasis will be considered. The set of model equations (2.1)-(2.7) presented in Section (2.1) will be adjusted to incorporate disease dynamics in dogs and to take into account the fact that sandflies may now feed on more than one species. Introducing the subscript d to denote a second host such as a dog, the additional compartments required for the two host model are

listed in Table (2.6). A schematic representing the additional disease compartments is shown in Figure (2-8). Parameter definitions can be found in Table (2.7).

Compartment	Definition
$S_d(t)$	Total number of susceptible dogs at time t
$E_d(t)$	Total number of dogs in the latent period at time t
$A_d(t)$	Total number of asymptomatic infectious dogs at time t
$I_d(t)$	Total number of symptomatic infectious dogs at time t
$R_d(t)$	Total number of recovered dogs at time t

Table 2.6: Table listing the compartments used in our basic two-host, one-vector model.

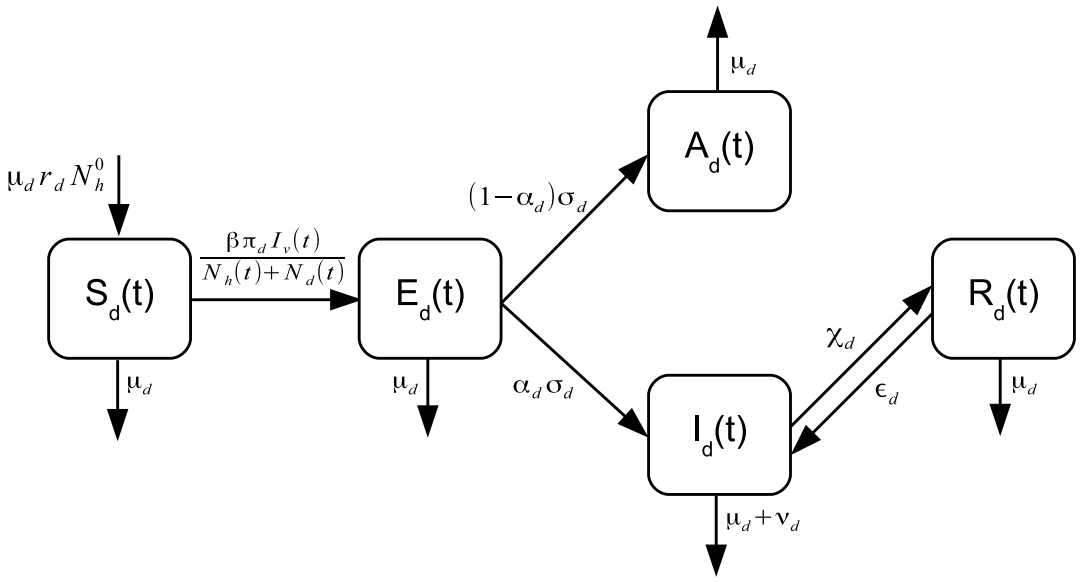

Figure 2-8: Schematic for the dog compartments of a two-host one-vector model.

The total dog population is closed and given by $N_d(t) = S_d(t) + E_d(t) + A_d(t) + I_d(t) + R_d(t)$. As well as the previously considered susceptible, latent, infectious and recovered classes, dogs can also reside in an asymptomatic class A. The asymptomatic class represents dogs that have become infected, but due to genetic immunity do not show obvious signs of infection [11]. The compartments have been chosen to incorporate aspects of disease dynamics shown in a flow chart in [63], and information from [11, 34, 65]. Such information includes: the presence of asymptomatic dogs, the ability of asymptomatic dogs to infect sandflies - albeit at a reduced rate, and the presence of disease related death in dogs. To simplify model equations we assume asymptomatic dogs never recover, and remain infectious until they die of natural causes. Immunity to canine leishmaniasis is concomitant, and the Leishmania parasite is never cleared from

Parameter	Definition
μ_d	Dog natural birth/death rate per month
r_d	Ratio of dogs to the number of humans at DFE
π_d	Probability a bite from a sandfly on a dog leads to infection
σ_d	Rate of progression to infectious class in dogs per month
α_d	Proportion of dogs that become symptomatic
ν_d	Rate of disease related death in dogs per month
χ_d	Dog recovery rate per month
ϵ_d	Dog relapse rate per month
ω_d	Proportional reduction in infectiousness of asymptomatic dogs

Table 2.7: Table defining the additional parameters used in the two-host, one-vector leishmaniasis model shown schematically in Figures (2-8), (2-9) and (2-10).

the host. The continued persistence of the pathogen causes asymptomatic individuals to be infectious, and prevents full recovery. We also assume genetic immunity cannot be compromised and asymptomatic dogs do not relapse.

All dogs are assumed susceptible to infection at birth, and enter the population at a constant rate $\mu_d r_d N_h^0$. Susceptible individuals leave the system through natural mortality at a rate μ_d or are infected at rate $\frac{\beta \pi_d I_v(t)}{N_h(t) + N_d(t)}$. As in the one host model of Section (2.1), we also assume that vectors have no host preference and bite at random. The fly bite rate β remains constant, and is independent of the number of humans and dogs. We therefore set the denominator of the transmission rate to be $N_h(t) + N_d(t)$ to account for the increased number of blood sources.

Upon infection, dogs enter a latent period. Infected individuals then become infectious at rate σ_d. A proportion α_d of those who become infectious show symptoms and enter the infectious class I_d. The remaining $(1 - \alpha_d)$ remain asymptomatic and enter the A_d class. Asymptomatic dogs are still infectious to sandflies, but transmit with a lower probability than dogs residing in the infectious I_d class [11, 63]. They do not suffer disease related mortality as parasite level is maintained at a low level by the immune system. Individuals that become infectious are lost at an increased rate due to disease related death ν_d. They may recover at a rate χ_d, however recovery need not be lifelong as relapse occurs at rate ϵ_d.

Figure (2-9) provides a schematic of the human disease compartments for the two host model. The human disease dynamics match those of the one host model in Figure (2-1),with the exception of the transmission term, which now incorporates the larger pool of blood sources.

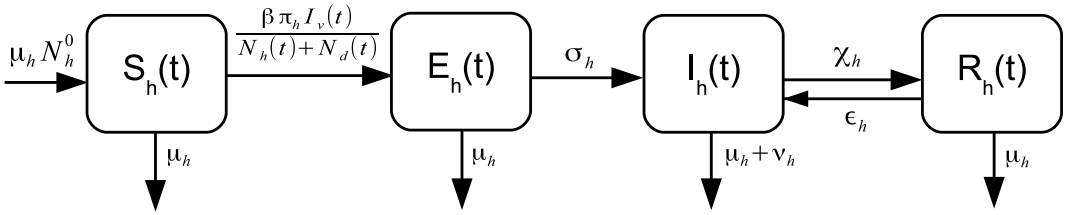

Figure 2-9: Schematic for the human compartments, two-host one-vector model.

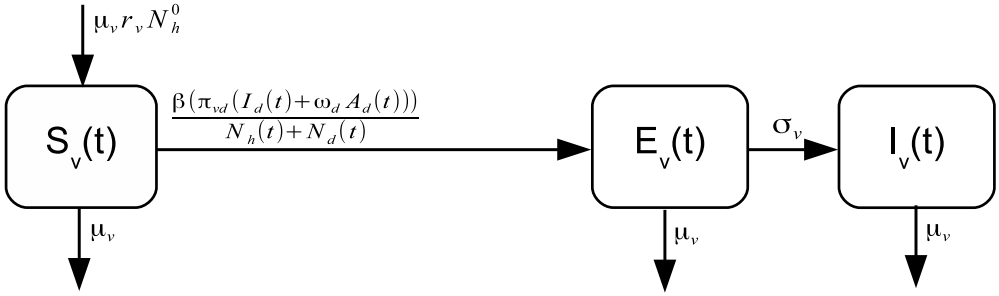

Figure 2-10: Schematic for the vector compartments, two-host one-vector model.

Figure (2-10) provides a schematic of the vector disease compartments for the two host model. With the exception of the transmission term:
$\frac{\beta(\pi_{vd}(I_d+\omega_d A_d))}{N_h(t)+N_d(t)}$, disease dynamics match those of the one host model. In the two host model bites still occur at the same rate β, and on the same total population $N_h(t)+N_d(t)$ as in the human transmission term, but vector infection can either come from infected humans I_h, infected dogs I_d or asymptomatic dogs A_d. In the case of infection obtained from asymptomatic dogs there is also an additional parameter ω_d which takes into account the fact that infections arising from bites to asymptomatic dogs do so at a lower probability than those arising from symptomatic dogs.

Incorporating all of the information shown in Figures (2-8), (2-9) and (2-10) the system of ODEs (2.18)-(2.29) describes the basic two host model for leishmaniasis.

$$\frac{dS_h}{dt} = \mu_h N_h^0 - \frac{\beta \pi_h S_h(t) I_v(t)}{N_h(t) + N_d(t)} - \mu_h S_h(t) \tag{2.18}$$

$$\frac{dE_h}{dt} = \frac{\beta \pi_h S_h(t) I_v(t)}{N_h(t) + N_d(t)} - (\mu_h + \sigma_h) E_h(t) \tag{2.19}$$

$$\frac{dI_h}{dt} = \sigma_h E_h(t) - (\mu_h + \chi_h + \nu_h) I_h(t) \tag{2.20}$$

$$\frac{dR_h}{dt} = \chi_h I_h(t) - (\mu_h + \epsilon_h) R_h(t) \tag{2.21}$$

$$\frac{dS_d}{dt} = \mu_d r_d N_h^0 - \frac{\beta \pi_d I_v(t) S_d(t)}{N_h(t) + N_d(t)} - \mu_d S_d(t) \tag{2.22}$$

$$\frac{dE_d}{dt} = \frac{\beta \pi_d I_v(t) S_d(t)}{N_h(t) + N_d(t)} - (\sigma_d + \mu_d) E_d(t) \tag{2.23}$$

$$\frac{dA_d}{dt} = (1 - \alpha_d) \sigma_d E_d(t) - \mu_d A_d(t) \tag{2.24}$$

$$\frac{dI_d}{dt} = \alpha_d \sigma_d E_d(t) + \epsilon_d R_d(t) - (\chi_d + \mu_d + \nu_d) I_d(t) \tag{2.25}$$

$$\frac{dR_d}{dt} = \chi_d I_d(t) - (\mu_d + \epsilon_d) R_d(t) \tag{2.26}$$

$$\frac{dS_v}{dt} = \mu_v r_v N_h^0 - \frac{\beta S_v(t) \pi_d \left(I_d(t) + \omega_d A_d(t)\right)}{N_h(t) + N_d(t)} - \mu_v S_v(t) \tag{2.27}$$

$$\frac{dE_v}{dt} = \frac{\beta S_v(t) \pi_d \left(I_d(t) + \omega_d A_d(t)\right)}{N_h(t) + N_d(t)} - (\mu_v + \sigma_v) E_v(t) \tag{2.28}$$

$$\frac{dI_v}{dt} = \sigma_v E_v(t) - \mu_v I_v(t) \tag{2.29}$$

For simplicity we assume the transference of the disease from dog-vector is equally likely in both directions. The parameter π_v has been removed and a probability π_d is used for dog-fly and fly-dog transmission.

2.2.1 R_0 and T_1

We derive the basic reproductive number R_0 for the two host model using the next generation matrix method. The reduced next generation matrix for the system (2.18)-(2.29) is given by:

$$K = \begin{pmatrix} 0 & 0 & k_{13} \\ 0 & 0 & k_{23} \\ 0 & k_{32} & 0 \end{pmatrix} \tag{2.30}$$

where

$$
\begin{aligned}
k_{13} &= \frac{\beta N_h^0 \pi_h \sigma_v}{\mu_v \left(N_h(t) + N_d(t)\right)\left(\mu_v + \sigma_v\right)} \\
k_{23} &= \frac{\beta r_d N_h^0 \pi_d \sigma_v}{\mu_v \left(N_h(t) + N_d(t)\right)\left(\mu_v + \sigma_v\right)} \\
k_{32} &= \frac{\beta r_v N_h^0 \pi_d \sigma_d \left(\mu_d \alpha_d \left(\epsilon_d + \mu_d\right) - \omega_d \left(\alpha_d - 1\right)\left(\mu_d \left(\chi_d + \nu_d + \epsilon_d + \mu_d\right) + \epsilon_d \nu_d\right)\right)}{\mu_d \left(N_h(t) + N_d(t)\right)\left(\mu_d + \sigma_d\right)\left(\mu_d \left(\chi_d + \epsilon_d + \nu_d + \mu d\right) + \epsilon_d \nu_d\right)},
\end{aligned}
$$

hence

$$R_0 = \sqrt{k_{23} k_{32}}. \tag{2.31}$$

Type reproductive numbers for the two host model can be constructed intuitively. Infection that originates in either a dog or sandfly must pass through both dog and fly disease compartments before returning to the species in which it originates. The type reproduction numbers for dogs and sandflies are therefore $T_d = R_0^2$ and $T_v = R_0^2$ respectively. Since humans are dead-end hosts and do not contribute to transmission the type reproduction number for humans is $T_h = 0$. Although human hosts do not contribute directly to transmission, they do play an important role by introducing a dilution effect. Increasing the size of the host population on which sandflies can take blood meals decreases the likelihood an individual is bitten more than once, hence reducing transmission. The presence of a dead-end host further decreases transmission, as infection that enters the human population cannot be further transmitted in the future.

2.2.2 Parameter Values: Two-Host Model

Table (2.8) details the ranges obtained for the parameters introduced in the two host model. Unless otherwise stated, ranges for parameters used in the one host model will remain the same as those listed in Table (2.3).

Parameter Range	Source Information
$\frac{1}{216} < \mu_d < \frac{1}{84}$ dog natural birth/death rate per month	Dog life expectancy is approximately 7 to 13 years on average [62].
$0 < \pi_d < 1$ probability a bite to a dog leads to infection	π_d is a probability. When $\pi_d = 0$ an infected bite never leads to infection. When $\pi_d = 1$ infection is certain.
$\frac{1}{8} < \sigma_d < \frac{1}{2}$ rate of transference from E_d to I_d per month	$\frac{1}{\sigma_d}$ is the incubation period in dogs. σ_d can be from 2-4 months [63], or up to 12 months [12]. A range of 2-8 months has been chosen.
$0 < \alpha_d < 1$ the proportion of latently infected dogs that become symptomatically infectious	Since α_d is a proportion it ranges between 0 and 1.
$\frac{1}{60} < \chi_d < \frac{1}{12}$ dog recovery rate per month	Without treatment, recovery takes between 1 and 5 years [57].
$\frac{217}{7811} < \nu_d < \frac{84}{2015}$ disease related death rate in dogs per month	The life expectancy of an infected dog is between 2 and 3 years [63]. Calculated using $24 < \frac{1}{\mu_d + \nu_d} < 36$.
$\frac{1}{217} < \epsilon_d < \frac{1}{12}$ relapse rate per dog per month	According to [63] the majority of relapses occur after one year, although relapse may not occur at all.

$0 < \omega_d < 1$ proportional reduction in the infectiousness of asymptomatic dogs	Since ω_d is a proportion it varies between 0 and 1.
$\frac{1}{3} < r_d < 3$ ratio of dogs to humans at DFE	The ratio of dogs to humans is unknown. We assume there are between $\frac{1}{3}$ and 3 times as many dogs as humans.

Table 2.8: Table listing parameter ranges for new parameters introduced for the two host model (2.18)-(2.29).

2.2.3 Latin Hypercube Distributions

As in Section (2.1.6), R_0 and I^* distributions were calculated using Latin Hypercube parameter sets which span the entire parameter space. Figure (2-11) shows the distribution of R_0 values obtained when 1000 parameter sets obtained using Latin Hypercube Sampling were input into equation (2.31). Figure (2-12) shows the distribution of I^* values obtained. In the case of the two host model the endemic infection prevalence I^* is defined as the sum of the individuals residing in the I_h, I_d, I_v and A_d classes, i.e. $I^* = I_h + I_d + I_v + A_d$. The asymptomatic class is now included in the infection prevalence in order to make results more comparable with those obtained at disease free equilibrium. Since no explicit analytic solution could be obtained for the endemic equilibrium, I^* results were calculated for the system (2.18)-(2.29) numerically. Parameter sets with $R_0 > 1$ were used in order to ensure an endemic equilibrium was feasible.

2.2.4 R_0 and I^* Distributions

Figure (2-11) shows the distribution of R_0 results obtained when 1000 parameter sets obtained using Latin Hypercube Sampling were input into equation (2.31). The R_0 values ranged from 10^{-4} to 55, with over 95% of values falling below 10.62. The distribution of $R_0 \leq 10.6$ is highly skewed, as 77% of R_0 values obtained are below 5. The median R_0 value is 1.88 and $R0_{base} = 9.67$. $R_0 > 1$ and an epidemic occurs in 68.3% of cases. The values of R_0 obtained for the zoonotic model are on average smaller than those obtained for the anthropontoic model. A larger number of viable hosts reduces the likelihood the same individuals is bitten twice, and therefore the

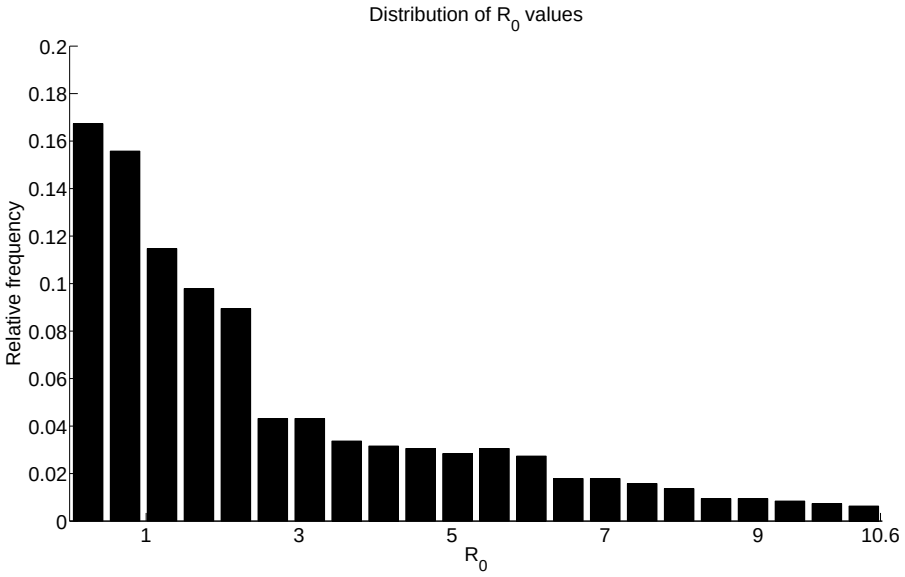

Figure 2-11: Distribution of R_0 values obtained when a full Latin Hypercube Sample is substituted into equation (2.31) for the two-host one-vector model (2.18)-(2.29). All parameter values vary. 1000 parameter sets were used. Cutaneous case.

chance transmission can occur.

Figure (2-12) shows the distribution of I^* values obtained for both the cutaneous and visceral forms of the zoonotic two-host one-vector model. Results are displayed as proportions of the total host population. In the case of cutaneous leishmaniasis the distribution of I^* values was skewed, with 95% of values below 0.16. In the case of visceral leishmaniasis the distribution of I^* values was also skewed, with 95% of values below 0.2. Table (2.9) compares statistics such as the median, mean and range of I^* values. We find that the proportion of infectious individuals of all types at endemic equilibrium was lower for cutaneous leishmaniasis than visceral leishmaniasis. In the latter case, disease related death in humans increases the number of bites to viable dog hosts and hence overall prevalence.

Statistic	Cutaneous case	Visceral case
mean	0.0746	0.0910
median	0.0659	0.0777
minimum	0.000026429	0.00001731
maximum	0.2742	0.3526
range	0.2741	0.3526

Table 2.9: Statistics for the I^* values obtained using Latin Hypercube parameter sets. Statistics are obtained from the same data set used to produce the histograms in Figure (2-12).

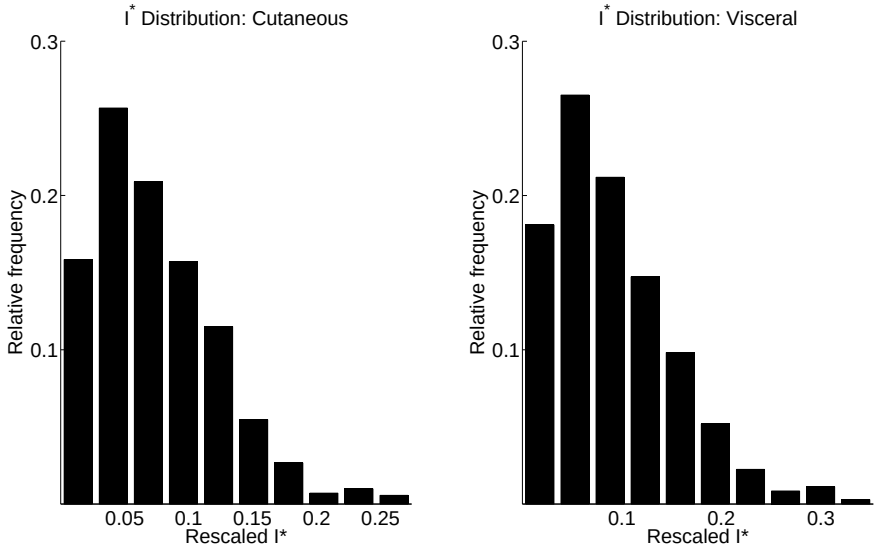

Figure 2-12: Distribution of I^* values for the two-host one-vector model. All parameter values vary. 683 Latin hypercube parameter sets with $R_0 > 1$ were used in order to ensure an endemic equilibrium was feasible.

2.2.5 Confidence Intervals

Confidence intervals for the mean values of R_0 and I^* were also obtained using the frequency distributions created with our full Latin Hypercube parameter sample. The inbuilt Matlab command expfit was first used to fit exponential distributions to the data sets used to create Figures (2-3) and (2-4). 95% confidence intervals for the mean were then extracted using the same command. Results are shown in Table (2.10). Since disease related death in humans increases the number of bites to viable dog hosts, the average overall prevalence is increased in the visceral case.

Case	Lower bound, 95% CI	Upper bound, 95% CI
Cutaneous/Visceral R_0	2.4611	2.7950
Cutaneous I^*	0.0694	0.0804
Visceral I^*	0.0847	0.0980

Table 2.10: 95% Confidence intervals for the mean value of R_0 and I^*, obtained using the full Latin Hypercube frequency distributions (2-11) and (2-12).

2.2.6 Time Dependent Infection Prevalence: Two-host model

Figure (2-13) shows how the combined infection prevalence I^*, human infection prevalence $\frac{I_h^*}{N_h^*}$, canine infection prevalence $\frac{A_d^* + I_d^*}{N_d^*}$ and vector infection prevalence $\frac{I_v^*}{N_h^*}$

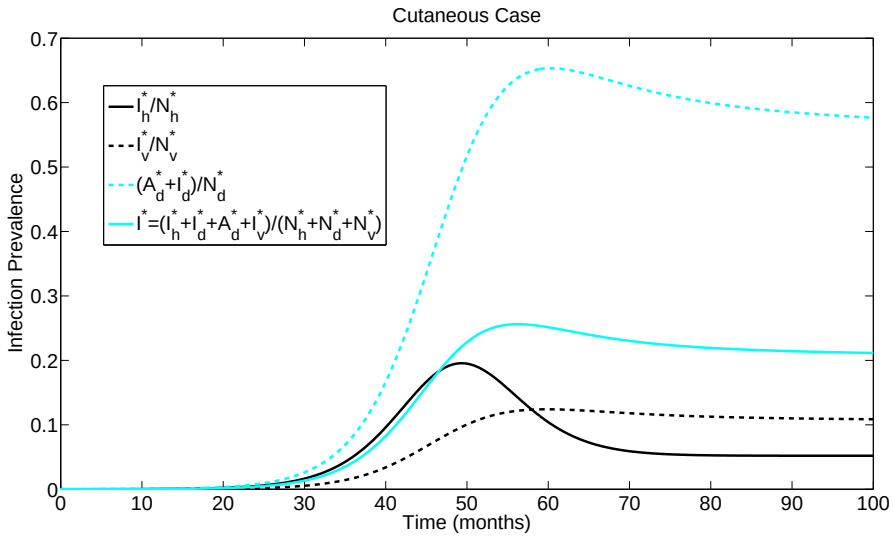

Figure 2-13: Plots of time dependent infection prevalence for the two-host one-vector model (2.18)-(2.29). Cutaneous case. Parameters are fixed at the values given in Table (C.1).

vary over time. Results are displayed for a cutaneous leishmaniasis parameterised using $\nu_h = 0$ and values given in Table (C.1). In Figure (2-13) we find that the canine and vector epidemics peak after 60 months, when approximately 65% of dogs and 12% of vectors are infected. The human epidemic peak occurs after 49 months, when approximately 19.6% of the human population are infected. Since humans are dead-end hosts, only dogs can transmit infection to the sandfly vector. This leads to the canine and vector epidemics peaking at the same time. The human epidemic peak occurs when the transmission rate to humans $\dfrac{\beta\pi_h S_h I_v}{N_h + N_d}$ is at a maximum. Since humans have a longer life expectancy than either dogs or sandflies, the epidemic turnover in humans is slower. The susceptible human population therefore depletes at a faster rate and the human epidemic peaks earlier. Reducing the number of susceptible humans reduces the likelihood a novel infection can occur, hence reducing the transmission rate and the number of infected humans. Since the combined infection prevalence I^* takes into account all infection prevalences it peaks after 56 months when $I^* = 25.6\%$.

Comparing the individual infection prevalences in Figure (2-13) we find that the vector infection prevalence is the lowest. This is due to the fact that vectors have the shortest life expectancy and fastest epidemic turnover, and is consistent with findings for the one host model. The canine infection prevalence is highest due to the asymptomatic dogs which do not suffer disease related death yet remain infectious for the duration of their lives. The combined infection prevalence I^* is lower than the canine infection prevalence, due to the dilution effect caused by considering multiple hosts; however I^* is higher than the human infection prevalence at endemic equilibrium. This

is due to the large number of infectious asymptomatic dogs which skew the combined result. Since humans are dead-end hosts and do not contribute to either canine or vector infection prevalences, similar results can be obtained for the visceral case. The presence of disease related death in the visceral case does reduce the human infection prevalence by 0.6% however, as individuals are directly removed from the infectious class.

2.2.7 R_0 and Individual Parameters

We now investigate the effect of varying individual parameters at disease free equilibrium. One parameter was varied across its range to obtain numerical values of R_0 when all other parameters were fixed at the values given in Table (C.1). As in Section (2.1.9), both cutaneous and visceral forms of Leishmania infection will be considered. When disease is cutaneous, the human disease related mortality rate $\nu_h = 0$, but the disease related death rate in dogs $\nu_d \neq 0$. When disease is visceral we set $\nu_h \neq 0$ and $\nu_d \neq 0$. The expression (2.31) will be used for R_0.

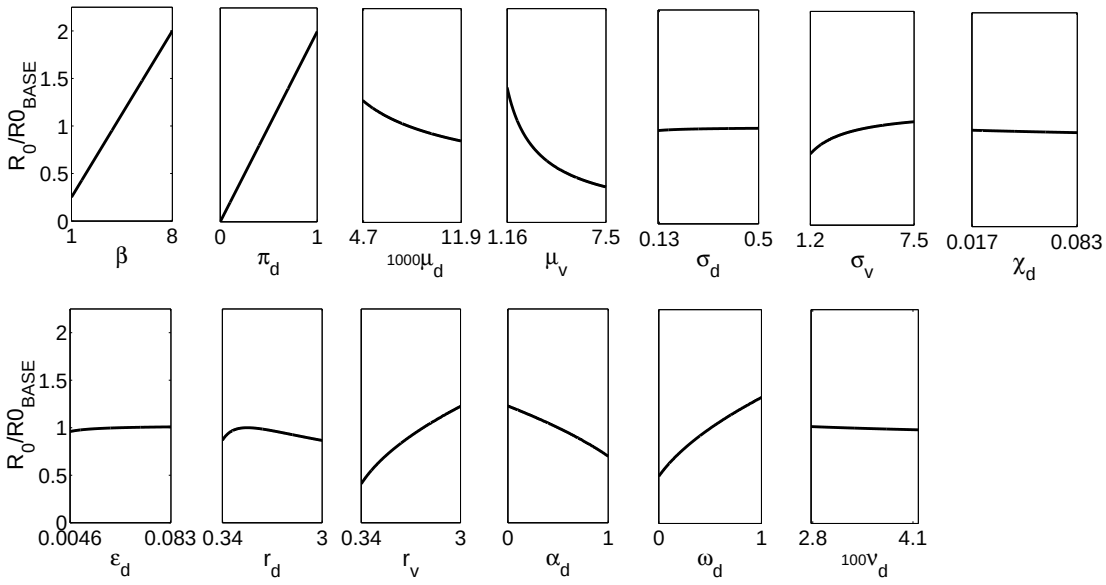

Figure 2-14: Relationships between R_0 and lower level parameters for the zoonotic two-host one-vector model represented by system (2.18)-(2.29). One parameter was varied across its range and input into equation (2.31) for R_0. All other parameters were fixed at the values given in Table (C.1).

Figure (2-14) shows the results of varying individual parameters for the zoonotic two-host one-vector model at DFE. Lineplots have been rescaled using base values

in order to make plots more easily comparable. R_0 values are the same for both cutaneous and visceral leishmaniasis since there is no disease related death at disease free equilibrium and humans do not contribute to transmission.

Since humans do not transmit infection, the R_0 results for the zoonotic model are similar to the one host model, but with dogs as the sole host. The relationship between R_0 and dog parameters such as death rate μ_d, recovery rate χ_d, relapse rate ϵ_d and disease related death ν_d in Figure (2-14) are similar to their human counterparts in Figure (2-6). Increasing either the rate or duration of transmission leads to an increase in the basic reproductive number. Parameters appearing in only one of the transmission terms have non-linear relationships with R_0, whereas the bite rate β which appears in both transmission pathways has a linear relationship with R_0. Since we assume that transmission is equally likely in both directions the transmission probability π_d also appears in both transmission pathways and has a linear relationship with R_0.

There are also additional disease parameters to consider. Increasing ω_d, the proportional reduction in the infectiousness of asymptomatic dogs, increases R_0 non-linearly. Increasing the infectiousness of asymptomatic dogs increases the likelihood of transmission from this class hence increasing R_0. Increasing the proportion α_d of dogs that enter the infectious state upon leaving the latent period decreases R_0. This is due to an interesting trade-off between the level of infectiousness and the duration of the infectious period. Although asymptomatic dogs are less infectious than those residing in the symptomatic infectious class, they remain infectious for a longer period of time. This allows the asymptomatic dogs to contribute more to the expected overall number of new infections per generation. Disease related death reduces the time period over which symptomatic infectious individuals can transmit disease, therefore reducing transmission from this class of individuals.

The final parameter for consideration is the ratio of dogs to humans r_d. When $r_d < 1$ humans are the predominant host species, and a vector is more likely to take a blood meal from a dead-end human host than from a dog. In this case increasing the number of dogs in the system increases the likelihood a blood meal is taken from a competent canine host, thus increasing the likelihood of transmission and R_0. Once $r_d > 1$ dogs become the predominant host species. Although it is more likely that a vector takes a blood meal from a competent host, increasing the total host population causes a dilution effect which reduces R_0. There is a reduction in the likelihood that the same host is bitten twice, and the likelihood of transmission occurring reduces as host population size increases. The dilution effect only becomes apparent once the competent host is the predominant host.

2.2.8 I^* and Individual Parameters

We now investigate the impact changing parameter values has on the endemic equilibrium. Results are shown in Figure (2-15).

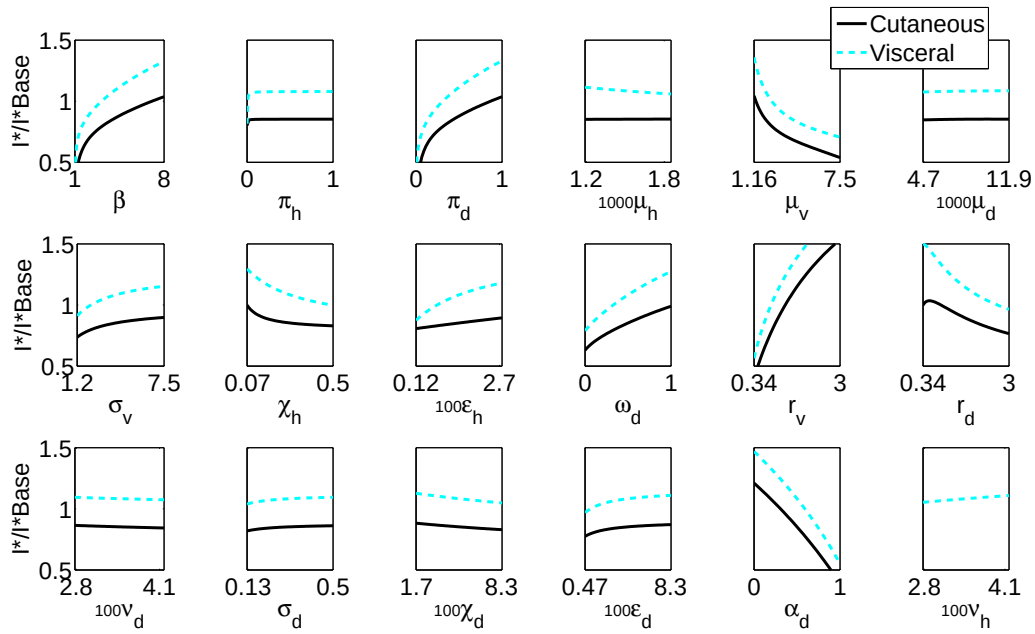

Figure 2-15: Relationships between I^* and lower level parameters for the zoonotic two-host one-vector model represented by system (2.18)-(2.29). One parameter was varied across its range and input into I^*. All other parameters were fixed at the values given in Table (C.1).

With the exception of μ_d, r_d and r_v, in Figure (2-15) we see that the relationships between I^* and lower level parameters are similar to those in Figure (2-14) for R_0. Increasing the duration or rate of transmission allows a greater number of infections to arise, hence increasing infection prevalence I^*. As in the one-host one-vector model of Section (2.1), the distribution of individuals between compartments differs at disease free and endemic equilibrium. The impact of novel transmission is reduced at endemic equilibrium due to the presence of asymptomatic and recovered hosts; however the saturating change in parameters such as the bite rate β and transmission probability π_d is less pronounced. The ability of asymptomatic dogs to transmit infection to susceptible sandflies increases the impact of β and π_d relative to the one host model.

At disease free equilibrium human parameters contribute to R_0 only via N_h, causing a dilution effect that reduces the potential spread of infection. At endemic equilibrium humans have a greater impact, contributing directly to infection prevalence I^* via the number of infected humans I_h^*. The impact of varying human parameters is relatively low however, as they still act as a dead-end host. Increasing relapse via ϵ_h increases the

input to the infectious class I_h^* and hence increases I^*. Although disease related death in humans ν_h also decreases the time humans spend in the infectious class, increasing ν_h leads to an increase in the infection prevalence I^*. When disease related death in humans is increased, the total human population is decreased. The smaller the number of humans, the greater the likelihood a sandfly feeds on a dog. This in turn increases the likelihood transmission is to a viable, and not dead-end host and so transmission and infection prevalence are increased.

Using the base parameter set given in Table (C.1) we find that a greater number of dogs reside in the asymptomatic rather than infectious class. This highlights their importance in the maintenance of infection. In fact there are approximately 631 dogs residing in A_d at endemic equilibrium and only 104 residing in I_d. This means that roughly 59.6% of the total dog population contributes to I^*. This is much higher than the contribution of sandflies of 9% and humans 3%. The importance of the asymptomatic class of dogs at endemic equilibrium can be also seen when considering the lineplot for α_d. Increasing the proportion of individuals that move into the symptomatic infectious class reduces $(1 - \alpha_d)$, the proportion that become asymptomatic. Symptomatic infectious dogs suffer from disease related death, so increasing the proportion of symptomatic dogs reduces the lifespan of a greater number of dogs. This in turn reduces the time and number available for new transmission and decreases infection prevalence. Decreasing the infectiousness of asymptomatic dogs via ω_d also reduces prevalence I^* by decreasing transmission to sandflies and thus reducing the number in I_v^*. Parameters which reduce numbers in I_v^* and I_d^* will also have a knock on effect on all infections as there will be a reduced number of infectious individuals to cause further transmission.

2.3 Conclusions

The results in Sections (2.1) and (2.2) give us basic information about potential disease spread, the infection prevalence I^* and their relationships with the lower level parameters from which they are constructed. We have found that the rate and duration of transmission are the key factors in deciding the ease with which disease spreads or the prevalence at which it is maintained. This holds true for both anthroponotic and zoonotic models. In the anthroponotic model the high proportion of recovered individuals at endemic equilibrium reduces the relative impact of novel infections, and the maintenance of infection is highly dependent on the relapse of previously infected individuals. In the zoonotic model, asymptomatic dogs are the driving force behind infection. Although the rate of transmission from asymptomatic dogs is lower than that

of infectious dogs, asymptomatic individuals do not suffer from disease related death therefore enabling them to transmit infection for a longer period of time. The presence of a dead-end human host reduces infection spread and prevalence by increasing the number of blood meal sources and causing a dilution effect.

For both the anthroponotic and zoonotic models we now know the form of the relationship between R_0, I^* and each individual parameter. We can identify the key parameters for disease spread at disease free equilibrium and disease prevalence at endemic equilibrium. However, there is a high level of uncertainty in the parameter ranges from which the results were obtained. In the next Chapter, we will therefore undertake a sensitivity analysis. A sensitivity analysis will enable us to quantify the magnitude of the impact individual parameters have on a quantity of interest such as R_0 and I^*. Making use of Latin Hypercube Sampling to conduct this analysis across the entire parameter space, the most influential parameters can then be identified and compared to identify the best targets for disease control.

Chapter 3

Sensitivity and Elasticity Analysis

For many models accurate parameter estimates for numerical calculations are difficult to obtain from the literature. Sensitivity analysis is a form of perturbation analysis which provides a measure of how variation in individual parameters can affect model results. Sensitivity analysis aids model development by providing a better understanding of the relationships between different parameters, and by quantifying uncertainty in model outcomes. The uniformity of model behaviour can be checked across a high dimensional parameter space and influential parameters can be identified for further investigation. Traditionally associated with economics, the technique has recently been discussed in the context of ecological models [19] and compartmental models for tick borne disease [42] and [60]. In this chapter we use sensitivity and elasticity analysis techniques to better understand and develop the models for anthroponotic and zoonotic vector-borne disease presented in Chapter 2.

3.1 Sensitivity Analysis

A sensitivity analysis considers the absolute and proportional responses of a dependent variable to changes in parameters. The absolute response is termed the sensitivity and the proportional response is termed the elasticity [60]. In the case of epidemic models the basic reproductive number R_0 is an informative dependent variable upon which a sensitivity analysis can be undertaken. A sensitivity analysis on R_0 will identify the parameters or disease pathways that have the greatest impact on the potential for an epidemic to occur, and so require the most accuracy in their estimation. This information can also be used to inform possible disease prevention strategies.

In order to find the sensitivity of R_0 to lower level parameters, we use the Next Generation Matrix,

$$K = \begin{pmatrix} k_{11} & k_{12} & \dots \\ k_{21} & k_{22} & \dots \\ \vdots & \vdots & k_{ij} \end{pmatrix}.$$

Each element k_{ij} of the NGM represents the expected number of infections of type i caused by individuals of type j, and represents a particular transmission pathway. The response of the basic reproductive number to a change in a particular transmission pathway is therefore given by the sensitivity:

$$s_{ij} = \frac{\partial R_0}{\partial k_{ij}}, \tag{3.1}$$

provided that the matrix elements k_{ij} are independent [19]. The sensitivity can be calculated for any element of the NGM, even those for which $k_{ij} = 0$. In the case of our NGM, the sensitivities of zero matrix elements provide information as to how R_0 would change if disease is no longer strictly vector-borne, and spread between members of the same species becomes possible.

Multiple transmission pathways k_{ij} may change simultaneously. In this scenario the net effect of a perturbation dk_{ij} on R_0 is given by:

$$dR_0 = \sum_{i,j} \frac{\partial R_0}{\partial k_{ij}} dk_{ij} \tag{3.2}$$

where dR_0 represents the sum of the changes in R_0 with respect to the perturbed matrix elements. This equation can be used to find sensitivities for a lower level parameter θ by considering:

$$dk_{ij} = \frac{\partial k_{ij}}{\partial \theta} d\theta \tag{3.3}$$

i.e. how a matrix element changes with respect to a particular parameter when the parameter value is changed. Substituting (3.3) into equation (3.2) gives:

$$\frac{dR_0}{d\theta} = \sum_{ij} \frac{\partial R_0}{\partial k_{ij}} \frac{\partial k_{ij}}{\partial \theta} \tag{3.4}$$

Equation (3.4) is the net change in R_0 when parameter θ varies in every element in the matrix K in which it is present. Note that we recover (3.1) when θ only appears in one element, so the k_{ij} are independent with respect to θ. The general formulae for the sensitivities of a 2 by 2 matrix are given in Appendix B.

3.2 Elasticity Analysis

The parameterisations of many models depend on rates at a variety of scales. In this situation it may not be appropriate to measure absolute changes in quantities, and instead the proportional change is considered. A commonly used quantity in economics, the proportional response to a proportional perturbation is known as the elasticity. For a Next Generation Matrix with independent elements, the elasticity e_{ij} of R_0 to a matrix element k_{ij} is given by:

$$e_{ij} = \frac{k_{ij}}{R_0}\frac{\partial R_0}{\partial k_{ij}} = \frac{\partial \log R_0}{\partial \log (k_{ij})} = \frac{k_{ij}}{R_0}s_{ij}, \tag{3.5}$$

where s_{ij} is the sensitivity of R_0 to the matrix element k_{ij} given by equation 3.4. When the matrix elements k_{ij} are independent, the elasticity of R_0 to an element k_{ij} can be interpreted as the proportion of infections contributed to R_0 by transmission from type j to type i. In this case the elasticity enables us to quantify the relative importance of each transmission pathway, and arises due to the fact that eigenvalues are homogeneous of degree one. The sum of all matrix elements is one and the equality:

$$\sum_{i,j} e_{ij} = \sum_{i,j} \frac{k_{ij}}{\lambda}\frac{\partial \lambda}{\partial k_{ij}} = 1$$

holds. See [27] for further information.

Assuming the matrix elements k_{ij} are not longer independent, the elasticity of a lower level parameter θ is given by:

$$e_\theta = \frac{\theta}{R_0}\frac{dR_0}{d\theta} = \frac{\theta}{R_0}\sum_{i,j}\frac{\partial k_{ij}}{\partial \theta}\frac{\partial R_0}{\partial k_{ij}}. \tag{3.6}$$

This equation represents the proportional change in R_0 when there is a proportional change in some parameter θ, in every element k_{ij} in which θ is present. The loss of independence means that the interpretation of elasticities as contributions to R_0 no longer holds and the sum of elasticities will not necessarily be constant.

3.3 Elasticity Analysis: One Host Model

3.3.1 Elasticity of R_0 to Lower Level Parameters

In order to investigate the sensitivity of the models in Chapter 2, we perform an elasticity analysis. Elasticity analysis is the most appropriate technique for our vector-borne disease model since the lifespans of hosts and vectors differ by several orders

of magnitude. By undertaking an elasticity analysis on R_0 we aim to identify the parameters, pathways and compartments which have the most influence on potential disease spread so that the most effective control techniques can be determined.

We now undertake an elasticity analysis for both the cutaneous and visceral interpretations of the leishmaniasis model (2.1)-(2.7). These analyses will enable us to compare the important transmission pathways and parameters for the two types of infection, and allow us to investigate whether both disease forms can be controlled using the same methods. We begin by calculating the elasticities of the transmission pathways represented by the elements of the Next Generation Matrix. If the elements of the NGM are independent, their elasticities can be interpreted as the proportional contribution to R_0, see Section (3.2). The element with the greatest elasticity will contribute the greatest proportion of infections to R_0, and the associated transmission pathway may be a good target for control techniques. Once the elasticities have been obtained for NGM elements, the elasticities of lower level parameters will be determined. Parameters with a large elasticity value have a greater potential to alter model results, so it is important to estimate these parameters accurately to reduce uncertainty in model output. The relative sizes of lower level elasticities will also provide insight into which parameters make good targets to reduce disease spread.

We derive the elasticities of Next Generation Matrix elements k_{12} and k_{21} from the NGM (2.14) using equation (3.5). Since there is no direct transmission e_{11}, representing host-host transmission, and e_{22}, representing vector-vector transmission are zero. The elasticities e_{12} and e_{21} representing host-vector and vector-host transmission are equal, and $e_{12} = e_{21} = \frac{1}{2}$. This holds true for both cutaneous and visceral disease. As in the one host model, both transmission pathways are equally important and contribute the same proportion of infections to R_0. Since there is no direct transmission within species, both the fly-human and human-fly transmission pathways must be present in order for disease to persist. Although humans are subject to relapse, this does not increase the proportion of novel infections contributed by the host. Relapsing infections are not novel, and can only occur after a host has already been infected by a vector.

We derive the elasticities of the lower level parameters using formula (3.6) from Section (3.2). Results are displayed in Table (3.1). Since lower level parameters can appear in either or both transmission pathways, results need not be constant and can no longer be interpreted as proportional contributions to R_0. Parameters which describe the durations of latency and transmission cannot be separated from one another, and have elasticities which depend on the parameters with which they are coupled. The elasticity of the human death rate μ_h is dependent upon human latency, recovery, relapse and disease related death for example. In the case of cutaneous leishmaniasis

$\nu_h = 0$ since there is no disease related death. Elasticities which depend on ν_h are therefore different for cutaneous and visceral models.

Parameter	Elasticity
β	1
π_h	$\frac{1}{2}$
π_v	$\frac{1}{2}$
μ_h	$\frac{-\mu_h}{2(\mu_h+\sigma_h)} - \frac{\mu_h\left(\epsilon_h^2+2\epsilon_h\mu_h+\chi_h\epsilon_h+\mu_h^2\right)}{2(\epsilon_h+\mu_h)\left(\mu_h^2+\chi_h\mu_h+\epsilon_h\mu_h+\epsilon_h\nu_h+\mu_h\nu_h\right)}$
μ_v	$\frac{-1}{2}\frac{2\mu_v+\sigma_v}{(\mu_v+\sigma_v)}$
σ_h	$\frac{1}{2}\frac{\mu_h}{\mu_h+\sigma_h}$
σ_v	$\frac{1}{2}\frac{\mu_v}{\mu_v+\sigma_v}$
χ_h	$-\frac{1}{2}\frac{\chi_h\mu_h}{(\mu_h(\epsilon_h+\mu_h+\chi_h+\nu_h)+\epsilon_h\nu_h)}$
ϵ_h	$\frac{1}{2}\frac{\epsilon_h\chi_h\mu_h}{(\epsilon_h+\mu_h)\left(\mu_h^2+\chi_h\mu_h+\epsilon_h\mu_h+\epsilon_h\nu_h+\mu_h\nu_h\right)}$
N	$\frac{1}{2}$
ν_h	$\frac{-\nu_h(\epsilon_h+\mu_h)}{2(\mu_h(\chi_h+\epsilon_h+\nu_h+\mu_h)+\epsilon_h\nu_h)}$

Table 3.1: Table listing the elasticities calculated using formula (3.6) from Section (3.2) for lower level parameters in the one-host one-vector model (2.1)-(2.7). When infection is cutaneous $\nu_h = 0$.

Using the elasticity formulae in table (3.1) and the parameter sets obtained in Chapter 2 using Latin Hypercube Sampling, we now obtain numerical values for lower level elasticities. For each parameter θ we calculated $\frac{dR_0}{d\theta}$ for the 1000 parameter sets obtained using Latin Hypercube Sampling. Outliers were removed in order to produce clearer and more representative results. Using our numerical elasticities we are able to investigate which parameters have the most influence on R_0, and how consistent the model behaviour is across the entire parameter space. Results are displayed in Figure (3-1).

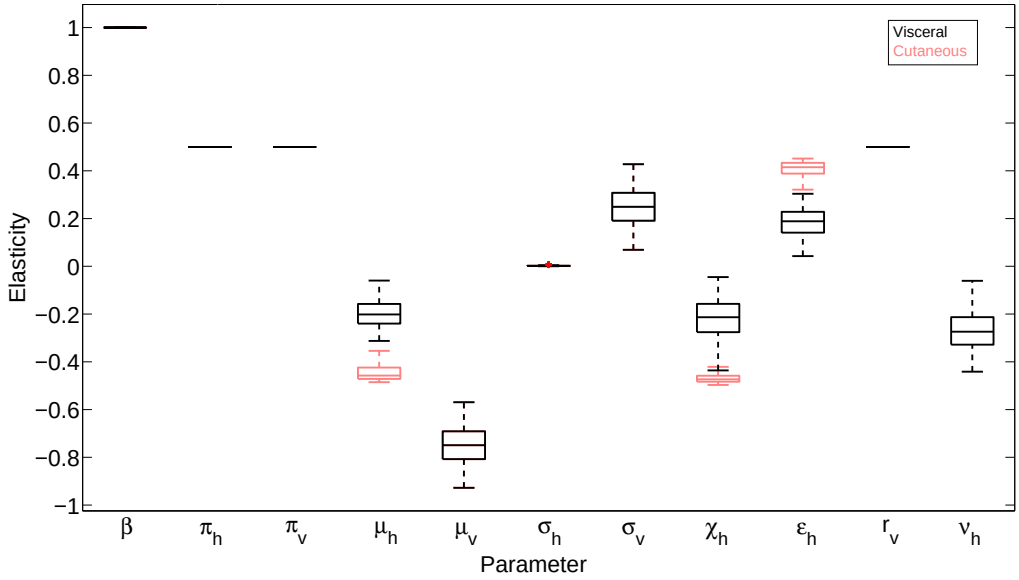

Figure 3-1: Boxplots representing the elasticity of R_0 to lower level parameters for the one-host one-vector model (2.1)-(2.7) when 1000 Latin Hypercube parameter sets were input into the formulae given in Table (3.1). Outliers have been removed.

3.3.2 Results of Elasticity Analysis on R_0

Figure (3-1) shows the range of elasticity results obtained for a Latin Hypercube Sample of our parameter space. When the elasticity of R_0 to a lower level parameter θ is positive, increasing θ increases either the duration or rate of transmission and hence R_0. When the elasticity of R_0 to θ is negative, increasing θ decreases R_0. The elasticity of R_0 to parameters which can be decoupled in the equation for R_0 are constant, whereas coupled parameters give rise to a range of elasticity values which are represented by boxplots. For each boxplot the the central line represents the median, the box contains data points within the 25th and 75th percentiles, and the whiskers extend to the most extreme data points. Outliers have been removed to produce clearer and more representative plots.

In both cutaneous and visceral cases the elasticity of R_0 to the bite rate β has the highest mean value. An elasticity of 1 means that if β were to change by 10% then R_0 would also change by 10%. This result is consistent across all parameter sets. The bite rate β has the greatest impact on the potential spread of infection as it is the only parameter to appear in both vector-human and human-vector transmission pathways. The elasticities of R_0 to the ratio of vectors to hosts r_v and the transmission probabilities π_h and π_v are also constant in both cutaneous and visceral cases. These

three parameters give rise to the second highest positive elasticites, and have the third greatest potential impact on R_0 overall. Since the transmission probabilities and ratio of vectors to hosts each effect only one of two pathogen generations they have half the impact of the bite rate β.

The parameter with the second greatest potential impact on R_0 is the sandfly mortality rate μ_v. This is due to the fact that the mortality rate μ_v and the parameter σ_v, which governs the duration of the latent period, are of a similar order of magnitude. Increasing the mortality rate μ_v increases the likelihood that infected vectors die before they become infectious. The smaller the difference between σ_v and μ_v the smaller the likelihood vectors survive to become infectious, and the smaller the value of R_0. Although the elasticity of R_0 to the human mortality rate μ_h is also negative, its impact on R_0 is less than its vector counterpart. This is due to the fact that human life expectancy is of a greater order of magnitude than latency, so individuals almost always survive to become infectious. This leads to σ_h, which governs the duration of latency in the host, having the smallest impact on R_0.

When infection is visceral, the presence of disease related death reduces the magnitude and range of R_0 elasticities obtained for the human death rate μ_h, recovery rate χ_h and relapse rate ϵ_h. Disease induced mortality decreases the likelihood that individuals recover, relapse or die of natural causes and so the impact of these parameters is reduced.

3.3.3 Interpreting Results - R_0

The results of Sections (2.1.10) and (3.3) will now be used to suggest control strategies for vector-borne diseases such as leishmaniasis. Our aim is to find strategies for which $R_0 < 1$ and an epidemic can be prevented. We begin by considering the elasticity analysis in Section (3.3). For both cutaneous and visceral infection we find that the bite rate β has the largest and most consistent impact on R_0. No matter what value the bite rate takes, a 1% change in its value always leads to a 1% change in R_0. The impact of varying the bite rate is also independent of the values of other parameters, making it an efficient and reliable parameter for control. In order to reduce R_0 the bite rate β must be reduced. This can be achieved via the use of bed nets, a control aid which is already available. The results of the elasticity analysis also show that the transmission probabilities π_h and π_v have constant and relatively high elasticities. Targeting these parameters is unlikely to be practical however, as the factors which determine the probability with which disease is transmitted are poorly known. Prophylactic drugs to prevent the spread of leishmaniasis are rare, and expensive.

The parameter with the second greatest mean influence on R_0 is the sandfly death

rate μ_v. The reduction in R_0 associated with increasing μ_v is not constant however, and depends on the duration of the sandfly latent period $\frac{1}{\sigma_v}$. This means that the spraying of insecticide to reduce fly life-expectancy will reduce R_0; however its effectiveness will depend to some extent on the the duration of latency in the vector. The longer the duration of the latent period, the higher the likelihood a sandfly dies before they become infectious. If fewer sandflies survive to become infectious the duration of the infectious period $\frac{1}{\mu_v}$ has less impact on R_0, the elasticity of μ_v decreases and control aimed at reducing the sandfly death rate become less efficient.

3.3.4 Independence Assumption in Elasticity Analysis

One flaw in the use of elasticity analysis in epidemiology is touched upon in [60]. In order for the elasticities of transmission pathways to be interpreted as proportional contributions to R_0, we must first assume that all elements of the Next Generation Matrix are independent. This is not necessarily the case. An example can be seen in the NGM (2.14), where the parameter β is present in both $k_{12} = \dfrac{\beta\pi_h\sigma_v}{\mu_v\left(\mu_v+\sigma_v\right)}$ and $k_{21} = \dfrac{r_v N_h^0 \beta\pi_v\sigma_h\left(\mu_h+\epsilon_h\right)}{\left(\mu_h+\sigma_h\right)\left(\left(\chi_h+\mu_h+\nu_h\right)\left(\epsilon_h+\mu_h\right)-\chi_h\epsilon_h\right)}$. If we drop the assumption that k_{12} and k_{21} are independent, the sensitivity for the element k_{12} is:

$$s_{12} = \frac{\partial R_0}{\partial k_{12}} + \frac{\partial R_0}{\partial k_{21}}\frac{dk_{21}}{dk_{12}}. \tag{3.7}$$

When the elements of the NGM are independent, $\frac{dk_{21}}{dk_{12}} = 0$ and $s_{12} = \frac{\partial R_0}{\partial k_{12}} = \frac{1}{2}\sqrt{\frac{k_{21}}{k_{12}}}$ as before; however, if the parameter β is changing and k_{12} and k_{21} are dependent, we can rewrite k_{21} in terms of $\beta = \frac{\mu_v(\mu_v+\sigma_v)k_{12}}{\pi_h\sigma_v}$ to give:

$$s_{12} = \frac{1}{2}\sqrt{\frac{k_{21}}{k_{12}}} + \sqrt{\frac{r_v N_h^0\mu_v\left(\mu_v+\sigma_v\right)\pi_v\sigma_h\left(\mu_h+\epsilon_h\right)}{4\pi_h\sigma_v\left(\mu_h+\sigma_h\right)\left(\mu_h\left(\epsilon_h+\mu_h+\nu_h\right)+\nu_h\epsilon_h\right)}}.$$

Assuming k_{12} and k_{21} are independent leads to an error term equalling:

$$\sqrt{\frac{r_v N_h^0\mu_v\left(\mu_v+\sigma_v\right)\pi_v\sigma_h\left(\mu_h+\epsilon_h\right)}{4\pi_h\sigma_v\left(\mu_h+\sigma_h\right)\left(\mu_h\left(\epsilon_h+\mu_h+\nu_h\right)+\nu_h\epsilon_h\right)}}$$

Similarly for s_{21} there is an error term:

$$\frac{\partial R_0}{\partial k_{12}}\frac{dk_{12}}{dk_{21}} = \sqrt{\frac{\left(\mu_h+\sigma_h\right)\left(\left(\mu_h+\chi_h+\nu_h\right)\left(\epsilon_h+\mu_h\right)-\chi_h\epsilon_h\right)\pi_h\sigma_v}{r_v N_h^0\pi_v\left(\mu_h+\epsilon_h\right)\sigma_h\mu_v\left(\mu_v+\sigma_v\right)}}$$

The next generation matrix element elasticities when k_{12} and k_{21} are not independent are therefore given by:

$$e_{12} = \frac{k_{12}}{R_0} s_{12} = \frac{k_{12}}{R_0} \left(\frac{\partial R_0}{\partial k_{12}} + \frac{\partial R_0}{\partial k_{21}} \frac{dk_{21}}{dk_{12}} \right) \tag{3.8}$$

$$e_{21} = \frac{k_{21}}{R_0} s_{21} = \frac{k_{21}}{R_0} \left(\frac{\partial R_0}{\partial k_{21}} + \frac{\partial R_0}{\partial k_{12}} \frac{dk_{12}}{dk_{21}} \right) \tag{3.9}$$

If k_{12} and k_{21} are perturbed independently by any parameter other than β, the elasticity of either transmission pathway is $e_{12} = e_{21} = \frac{1}{2}$. If the perturbation is due to a change in the value of β then k_{12} and k_{21} are not independent, and we use equations (3.8) and (3.9) to find that $e_{12} = e_{21} = 1$. The interpretation as proportions is lost.

In the case of system (2.1)-(2.7), only β appears in multiple terms and hence sensitivities based on the assumption of independence can be used for the vast majority of transmission terms. In more complex systems this may not be the case however and multiple parameters may appear in several elements of the NGM. The effect of co-dependence in matrix elements on sensitivity analysis is something that cannot necessarily be ignored and may warrant further investigation. The relative importance of different species in maintaining transmission can perhaps instead be identified by considering the relative differences between the elasticities with respect to their corresponding lower level parameters.

3.4 Elasticity at Endemic Equilibrium

Although leishmaniasis is an emerging vector-borne disease in some countries, in others such as Brazil and India it is already established. Information about control techniques based on the analysis of R_0 is less helpful when disease is endemic, as emphasis shifts from epidemic prevention to reducing disease prevalence. In order to find out more information about important disease parameters and possible disease control techniques when away from the disease free equilibrium, the use of elasticity analysis at an endemic equilibrium will be investigated. The analyses for endemic and disease free equilibria will then be compared in order to see if the same parameters are influential, and the same control methods can be applied.

We consider the elasticity of the endemic infection prevalence $I^* = I_h^* + I_v^*$, to lower level disease parameters for the one-host one-vector model (2.1)-(2.7). Since the NGM is parameterised about DFE, we are unable to derive elasticities for the transmission pathways represented by k_{ij}, and instead focus on the elasticities of lower level parameters.

The elasticity of I^* with respect to a lower level parameter θ is:

$$e_\theta = \frac{\theta}{I^*}\frac{\partial I^*}{\partial \theta} \tag{3.10}$$

and is the proportional response in I^* given a proportional change in θ. Using the analytic expressions for I_h^* and I_v^* given in Appendix A, an analytic expression for the elasticity $e_\theta = \frac{\theta}{I^*}\frac{dI^*}{d\theta}$ was constructed for each lower level parameter θ. 1000 parameter sets constructed using Latin Hypercube Sampling were then input into the analytic expression for elasticity and plotted. Results are shown in Figure (3-2).

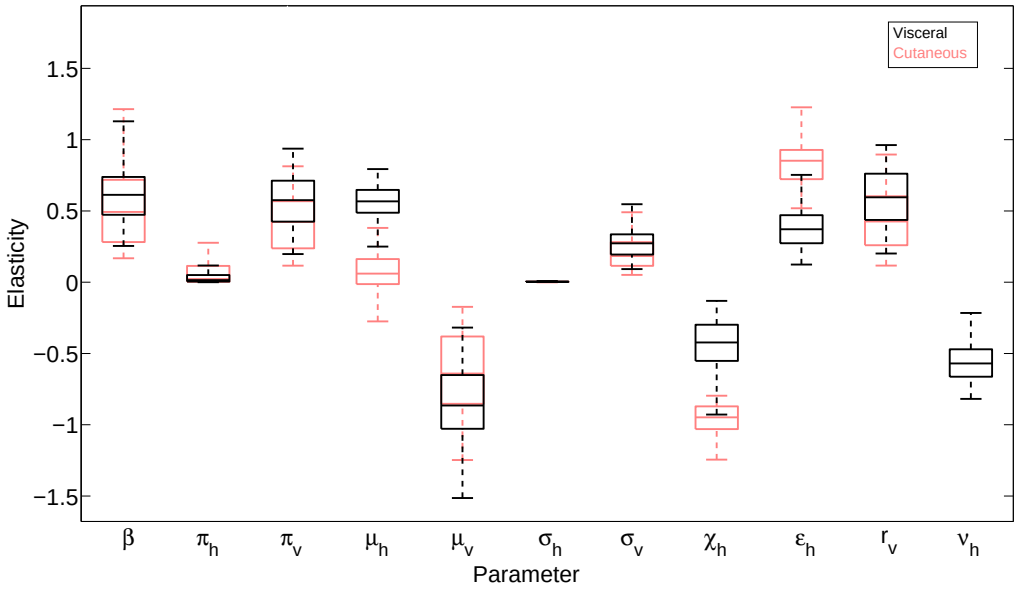

Figure 3-2: Boxplots representing the elasticity of I^* to lower level parameters for the one-host one-vector model (2.1)-(2.7). 1000 Latin Hypercube parameter sets were used. Outliers have been removed.

3.4.1 Results of Elasticity Analysis on I^*

With the exception of the human mortality rate μ_h, the elasticity of I^* to each parameter retains the positive or negative sign it had in the R_0 case. The range of all elasticities is greater than zero. The most influential parameters differ depending on whether infection is cutaneous or visceral; however σ_h which governs the duration of latency in the host has the least impact in both cases.

In the case of cutaneous leishmaniasis, the host relapse rate ϵ_h and recovery rate χ_h have the greatest impact on I^*. As described in Chapter 2, the impact parameters have

at endemic equilibrium is not only governed by the rate and duration of transmission, but also by the distribution of individuals between the different disease compartments. At endemic equilibrium the majority of humans reside in the recovered class R_h. The relapse of recovered hosts becomes the driving force behind infection, and so the parameters χ_h and ϵ_h which govern the duration of recovery have greater impact. In the case of visceral leishmaniasis, the elasticities of I^* to the bite rate β, ratio of vectors to hosts r_v and vector death rate μ_v have the greatest absolute mean value. The introduction of disease related death has decreased the number of individuals that survive to recover, and so relapse is less important.

In both cutaneous and visceral cases the elasticity of I^* with respect to the host mortality rate μ_h attains positive elasticities. A positive elasticity indicates that increasing μ_h, and hence decreasing host life expectancy, will increase endemic prevalence. Previously, μ_h led only to negative elasticities. Increasing the mortality rate increases demographic turnover. Less time is spent in the recovered class and a greater number of novel infections occur.

When comparing the elasticity analysis for R_0 and I^* a further difference can be seen when considering the results for the transmission probabilities. The parameter π_h has a greatly reduced impact, and has less impact on I^* than the analogous π_v. At disease free equilibrium both of these parameters had the same elasticity value. The increase in I^* due to π_h is moderated by the size of the susceptible host population. The reduction in the human susceptible population also explains why the elasticity of I^* to β and r_v is not constant. These parameters are no longer independent of population and other disease dynamics, as the effect they can have becomes constrained by the number of individuals in each compartment. The elasticity of I^* to the transmission probability π_v retains a higher value, as the proportion of susceptible vectors remains high and novel transmission from host to vector occurs at a higher rate.

3.4.2 Interpreting results - I^*

Results suggest that when infection is endemic, the most effective control technique depends on the form of Leishmania infection. When infection is cutaneous, infection is driven by host relapse. Control techniques aimed at the host population should therefore lead to the greatest reduction in endemic prevalence. In this case, the administration of medication to increase immune system function and reduce the chance of relapse would be an effective and practical way to reduce endemic infection prevalence. Administering drugs to increase the rate of recovery may also be effective, providing the rate of relapse is low. Drugs used to treat leishmaniasis are expensive however. The vector death rate μ_v and bite rate β also have a significant impact at endemic

equilibrium, so controls aimed at the vector population will also be efficient, and may be more cost effective. When infection is visceral, relapse contributes less to the endemic prevalence than in the cutaneous case. Consequently, control techniques aimed at reducing the number of novel infections, such as the use of bed-nets or insecticides, will be most effective.

3.5 Elasticity Analysis: Two Host Model

3.5.1 Elasticity of R_0 to Lower Level Parameters

Using the methodology outlined in Section (3.2) we now perform an elasticity analysis for the zoonotic two host model (2.18)-(2.29) presented in Section (2.2). Once again we begin by calculating the elasticity of R_0 with respect to Next Generation Matrix elements. Using formula (3.5) and NGM (2.30) we find that the matrix element representing fly-human transmission has an elasticity $e_{13} = 0$, whereas the elements representing dog-fly and fly-dog transmission have elasticities $e_{23} = e_{32} = \frac{1}{2}$. Humans are dead-end hosts and do not contribute to transmission. As in the case of the one-host model, the competent host and vector contribute the same proportion of infections to R_0. Since R_0 does not explicitly depend upon human disease parameters these results hold true for both cutaneous and visceral cases.

We now consider the elasticity of R_0 to lower level parameters. Using expression (2.31) for R_0, and the Latin Hypercube parameter sample obtained in Chapter 2, we calculate sets of numerical elasticities. Results are shown in Figure (3-3). Since R_0 does not explicitly depend upon human disease parameters results are again the same for both visceral and cutaneous cases.

3.5.2 Results of Elasticity Analysis on R_0

The results of the R_0 elasticity analysis for the two host model are similar to those of the one host model presented in Figure (3-1), Section (3.3). The elasticity of R_0 to the bite rate β is joint highest, as β is present in both of the disease pathways that contribute to R_0. In the zoonotic model the transmission probability π_d also appears in both fly-dog and dog-fly transmission pathways, thus sharing the same elasticity value as the bite rate. The elasticity of R_0 to the population ratios r_v and r_d are also constant. We find that $e_{r_v} = e_{r_d} = \frac{1}{2}$, as both population ratios are uncoupled in the equation for R_0 and appear in only one transmission pathway.

The parameter which leads to the largest mean negative elasticity is once again the fly death rate μ_v. The duration of latency in the competent host, now governed by σ_d,

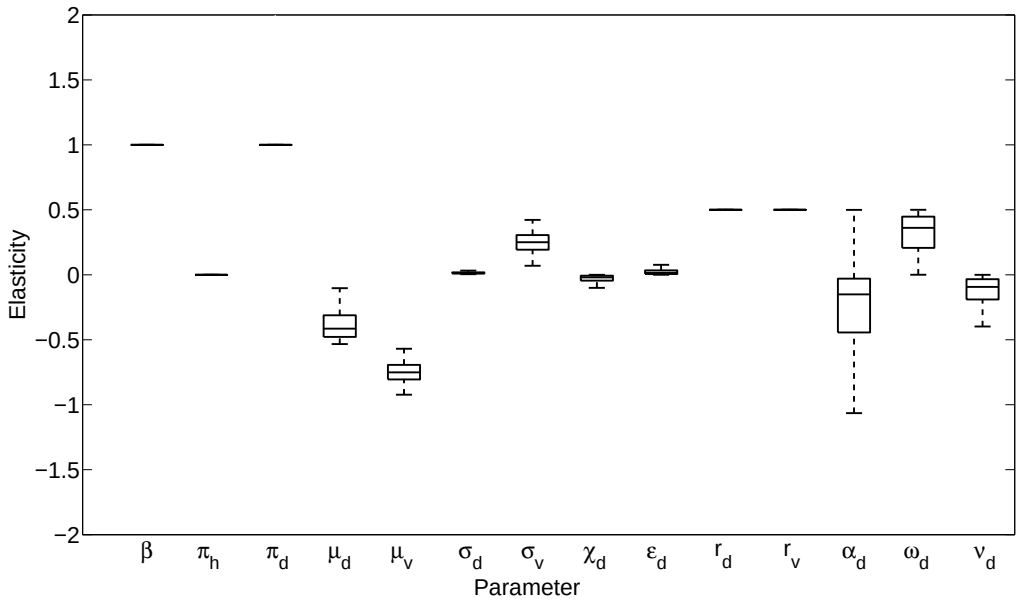

Figure 3-3: Boxplots representing the elasticity of R_0 to lower level parameters for the two-host one-vector model (2.18)-(2.29). 1000 Latin Hypercube parameter sets were used. Outliers have been removed.

has the smallest impact of all the parameters appearing in R_0. This is due to the fact that the duration of latency is short in relation to host lifespan, and latent individuals almost always survive to become infectious. Human parameters such as π_h which do not appear explicitly in the equation for R_0 lead to zero elasticity.

In Figure (3-3) we see that the elasticity of R_0 to α_d, the proportion of symptomatically infectious dogs, has the largest range of values. Depending on other parameter values in the sample, the elasticity of R_0 with respect to α_d can either be positive or negative, although most are below zero. Increasing the proportion of symptomatically infectious dogs decreases the proportion of asymptomatic dogs $(1 - \alpha_d)$ which are also able to transmit infection. Although asymptomatic dogs tend to transmit infection at a lower rate than their symptomatic counterparts, the absence of disease related death increases the duration of time over which they can transmit. This makes asymptomatic dogs important in the spread of infection. Positive elasticities are obtained with respect to α_d in parameter sets where the infectiousness of asymptomatic dogs $\omega_d\pi_d$ is close to zero. In this case increasing the number of symptomatic dogs will be beneficial to overall transmission and increase R_0.

3.5.3 Interpreting Results - R_0

We use the results of sections (2.2.7) and (3.5) to suggest control techniques for epidemic prevention. Overall, control techniques targeting sandflies are likely to be most effective for both cutaneous and visceral leishmaniasis. The results of the elasticity analysis in Section (3.5) suggest targeting the bite rate β as this parameter has a large and consistent elasticity. The bite rate can also be practically controlled using existing measures such as bed nets, and insecticide impregnated dog collars. The use of insecticides to increase fly death rate μ_v is also a feasible control.

Although the transmission probability π_d and the ratio of dogs to humans r_d also have high and consistent elasticity values, scientific and moral implications make these parameters more difficult to control. The main control technique available to reduce r_d is the culling of dogs. The ethical implications of killing dogs, and the ability of feral dog populations to replenish quickly [65] reduces the efficacy and the ability to employ this technique. Since the factors governing the transmission probabilities are poorly understood at this time, control targeting the parameter π_d is also not feasible.

Employing control techniques aimed at humans, the proportion of asymptomatic dogs α_d or the duration of the latent period $\frac{1}{\sigma_d}$ in dogs will be least effective. Targeting the human population will not be effective since humans are dead end hosts and do not transmit infection. Unless the proportion of asymptomatic dogs which transmit infection is known to be low, decreasing the proportion of symptomatic dogs is also not effective. The elasticity of R_0 to α_d can be either positive or negative and without being certain of all other parameter values we cannot be sure if control will reduce or increase R_0. The result for σ_d, matches that of σ_h in the one-host one-vector model.

3.5.4 Elasticity of I^* to Lower Level Parameters

We now calculate the elasticity of infection prevalence $I^* = I_h^* + A_d^* + I_d^* + I_v^*$ to lower level parameters. Although no full explicit analytic endemic equilibrium could be obtained, expressions for individual disease compartments could be found in terms of lower level parameters and the total population sizes $N_h(t)$ and $N_d(t)$. The population size $N_h^* + N_d^*$ at endemic equilibrium was obtained for each of our parameter sets by solving the ODE system numerically. These solutions were then substituted into the elasticity expressions given by Formula (3.10). Since humans contribute to the number of actual infections I^* via I_h^* the elasticity of I^* to human parameters was considered. Elasticities were only calculated for parameter sets with $R_0 > 1$, ensuring an endemic was feasible.

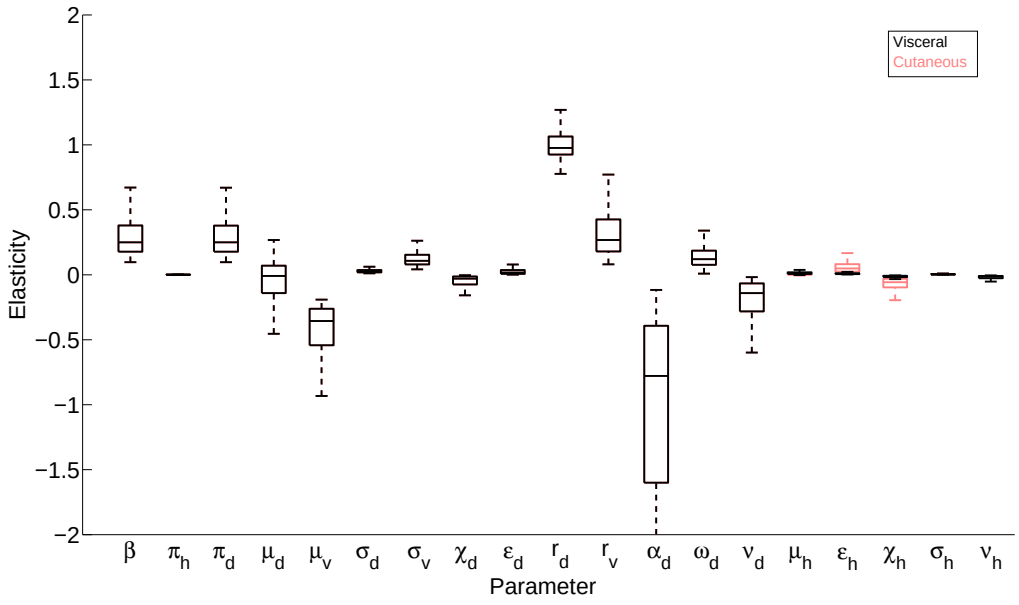

Figure 3-4: Boxplots representing the elasticity of I^* to lower level parameters for the two-host one-vector model (2.18)-(2.29). 1000 Latin Hypercube parameter sets were used. Outliers have been removed.

3.5.5 Results of Elasticity Analysis on I^*

With the exception of the fly death rate μ_d and the proportion of symptomatically infectious dogs α_d, the elasticities of I^* to lower level parameters have the same positive or negative sign they had for R_0. The most influential parameters differ however. As in the one host model, the impact of any parameter is constrained by complex non-linear disease dynamics. At endemic equilibrium the majority of the host population resides in either a recovered or asymptomatic class, and the impact of novel transmission is reduced. The elasticity of I^* to parameters such as the bite rate β, and transmission probabilities are reduced, while the elasticity of I^* to the relapse rates ϵ_h and ϵ_d increases in mean value.

In the case of the zoonotic two host model at endemic equilibrium, the ratio of dogs to humans r_d is one of the most influential parameters. The proportion of infected dogs that show symptoms α_d also has a large potential impact on infection prevalence. The elasticity of I^* to α_d is strictly negative, but has the widest range of values. This shows that the endemic prevalence is highly dependent on the transmission of infection from asymptomatic dogs. The parameters σ_h and σ_d governing the duration of host latency have the smallest impact on I^*.

For both cutaneous and visceral infection, increasing the disease related death rate

in dogs reduces the endemic prevalence. This leads to a reduction in the impact of recovery and relapse as fewer infectious individuals survive to recover. The absence of human disease related death in the cutaneous case does not greatly alter the elasticity results for any other parameters, and as such we only highlight the difference in the plots for χ_h and ϵ_h. The impact of disease related death in humans is low, as humans are dead-end hosts and do not contribute to transmission.

3.5.6 Interpreting Results - I^*

The results presented in Sections (2.2.8) and (3.5.4) can be used to suggest control techniques aimed at reducing the endemic prevalence of zoonotic leishmaniasis. As in the one-host one-vector model, the application of controls aimed at the competent host should prove to be most effective. We find that reducing the ratio of dogs to humans r_d is likely to cause the largest reduction in endemic prevalence. At endemic equilibrium, dogs contribute 80% of the infections counted in I^*. Although reducing r_d reduces the overall size of the host population, it increases the likelihood that a sandfly will take a blood meal from a human host rather than a dog. This means that the disease is more likely to enter a dead-end host and cease to be transmitted. Reductions in r_d may be achieved by the culling of the dog population, however this has ethical implications and may not be feasible.

The infection prevalence I^* may also be decreased by increasing the proportion of infected dogs α_d that become symptomatically infectious. This may seem counterintuitive, however increasing α_d decreases $1 - \alpha_d$, the proportion of dogs that enter the asymptomatic class. Asymptomatic dogs are key in the maintenance of infection, as they cause a higher expected number of transmission events over a life time. The identification of asymptomatic dogs and their subsequent treatment, or culling if accepted, may reduce infection prevalence. The very nature of the infection in asymptomatic dogs will make these dogs difficult to identify, and as such it may be more efficient to employ other means of control.

In the situation where disease in the dog population is hard to control via parameters such as r_d and α_d, results suggest targeting the sandfly vectors. We revert to the control techniques suggested for R_0 as the elasticities of I^* to the sandfly natural death rate μ_v, bite rate β and ratio of sandflies to humans r_v have some of the largest mean values. This would once again suggest the spraying of insecticide to reduce the lifespan and population size of sandflies, and the use of insecticide impregnated dog collars to prevent bites to the competent hosts. The use of bed nets as a control technique for a model where humans are a dead end host would need to be further investigated. Although the use of bed nets will directly reduce incidence in humans, it will increase

the likelihood dogs are bitten instead. The infection will therefore enter a competent, not dead-end host and can be further transmitted.

3.6 Conclusions

Results suggest that the most effective controls for both the one host and two host models are those directly aimed at reducing the rate at which vectors transmit disease. This holds true when leishmaniasis infection is either emergent or endemic, cutaneous or visceral. Although there is some benefit in reducing the rate of host relapse when visceral infection is anthroponotic, control techniques aimed at reducing sandfly transmission are both easier to implement, and effective in a wider range of situations. When infection is zoonotic, reducing the number of dogs is also likely to be an effective control. This is particularly true when the number of asymptomatic infectious dogs is reduced; however the ethical and practical implications of culling, coupled with the difficulties of identifying asymptomatic dogs means that this control option may not be feasible. In areas such as Brazil or Iran where leishmaniasis is primarily zoonotic, the spraying of insecticide to reduce sandfly life expectancy and the use of insecticide impregnated collars to prevent sandflies biting dogs could reduce the prevalence of the disease. In Afghanistan where anthroponotic leishmaniasis is an emerging vector-borne disease, our results suggest the spraying of insecticide and the use of bed-nets to reduce the rate of sandfly transmission in both cutaneous and visceral cases.

In contrast to initial belief, we found that the latent period of the host is not an important aspect of disease dynamics in either dogs or humans. The parameters σ_h and σ_d and latent classes E_h and E_d may be removed from disease dynamics to simplify equations without greatly altering model outcomes. This will be taken into account in further work building on the one and two host models. Equations will be altered in such a way that susceptible hosts move straight into the asymptotic or infectious class upon infection. If tailoring the model to a zoonotic host other than a dog the elasticity analysis would need to be repeated however. Hosts such as the Great Gerbil *R. opimus* have a shorter life expectancy than dogs and removing the latent period may no longer be appropriate.

Chapter 4

Optimal Control of Leishmaniasis

In Chapter 3 we used an elasticity analysis to identify the key parameters and processes behind the spread and persistence of Leishmania infection in our baseline models. Our results indicated how parameters could be altered to reduce the epidemic risk in disease-free populations, and the infection prevalence in disease-endemic populations. In reality the most suitable control technique is not only chosen for its ability to reduce infection prevalence, but also for its affordability. In this chapter we therefore use an optimal control framework to assess the best control strategies to implement in the event of an epidemic, given the costs of treatment and infection.

The implementation of two possible controls will be investigated for the one-host one-vector model given in Chapter 2. The first control considered is vaccination targetted at the host population. We then investigate control aimed at the vector population, before considering the impact of applying both vector and host control simultaneously. Optimal control strategies are calculated for both relapsing and non-relapsing infection in order to better understand how relapse may change our approach to infection management.

4.1 Optimal Control: Theory

Optimal control theory is a mathematical optimisation technique which allows us to find the most economically viable disease control strategy, given the disease dynamics and a set of cost constraints. A number of biological applications for optimal control theory are given in the book by Lenhart and Workman [54]. An example of particular relevance can be found in Chapter 13, where optimal control theory is applied to an SEIR epidemic model. Further examples of optimal epidemic controls can be found in [13], [18] and [47]. We are not aware of any literature where the theory has been

specifically applied to an epidemic model for leishmaniasis; however the optimal control of malaria is considered in [3] and [14].

In [14], two controls representing prevention and treatment are assumed. It is found that prevention methods such as the use of bednets lead to the greatest reduction in disease incidence. In [3], combinations of three controls representing prevention, treatment and insecticide spraying are considered. The authors suggest that the application of both treatment and prevention, or spraying and prevention will lead to the greatest reduction in disease incidence. Since the epidemiology of malaria differs from that of leishmaniasis, neither paper investigates the impact of disease relapse on the optimal control. We hypothesise that the relapse of infection that occurs in leishmaniasis will have a significant impact on the control effort required to stop the spread of infection.

In order to formulate our optimal control problem, we adopt the notation set out in Lenhart and Workman [54]. Let $u_i(t)$ be the control variable(s), and $x_i(t)$ be the state variable(s) for $i \in (1, N)$, $N \in \mathbb{N}$. The state equation(s) describing the state of the system at time t, when under control $u(t)$ is given by:

$$x_i'(t) = g_i(t, x(t), u(t)). \tag{4.1}$$

Dependent on the control problem under consideration, the aim is to find the optimal values of control u^* and state variable(s) x^* that minimise or maximise an objective functional of the form:

$$J(u) = \int_{t_0}^{t_1} f(t, x(t), u(t))\, dt \tag{4.2}$$

subject to the state equation(s) (4.1), with boundary conditions $x(0) = x_0$ and $x(t_1)$ free and the control set:

$$U = \{u_i(t) \mid u_i(t), \text{piecewise continuous on } [0, t_1] \text{ with } a_i \le u_i(t) \le b_i, \\ a_i, b_i \in \mathbb{R},\ i \in (1, N)\}. \tag{4.3}$$

This is achieved by using Pontryagin's maximum principle, a version of which is given in [54], and stated below:

The Maximum Principle: *If $u^*(t)$ and $x^*(t)$ are optimal for (4.2), then there exists a piecewise differentiable adjoint variable $\lambda(t)$ such that*
$H(t, x^*(t), u(t), \lambda(t)) \le H(t, x^*(t), u^*(t), \lambda(t))$
for all controls u at each time t, where the Hamiltonian H is $H = f(t, x(t), u(t)) + \lambda(t) g(t, x(t), u(t))$ and $\lambda'(t) = -\dfrac{\partial H(t, x^*(t), u^*(t), \lambda(t))}{\partial x}$, with transversality condition $\lambda(t_1)$=0.

The optimality system is produced via the coupling of the state and adjoint systems along with their corresponding initial and transversality conditions. An expression for u^* can be obtained by solving $\frac{\partial H}{\partial u} = 0$ for $u(t) = u^*$; however this solution often depends on the value of the adjoint variables. The maximum principle allows us to obtain the adjoint equations, and thus u^*. Once u^* has been obtained it can be substituted into the state equation(s) (4.1) to find the optimal state of the system $x^*(t)$.

Pontryagin's maximum principle provides us with the necessary conditions for a control to be optimal; however the existence and uniqueness of an optimal control must also be considered to fully describe the optimal control problem. In order to ensure there exists a unique optimal control $u^* \in U$ such that $min_u J(u) = J(u^*)$, the following conditions must be satisfied [38]:

1. The set of controls and corresponding state variables must be non-empty.
2. The control set U must be closed and convex.
3. The right hand side of the state system must be bounded by a linear function in the state and control variables.
4. The integrand of the objective functional must be convex on U.
5. The integrand of the objective functional must be bounded below by $c_1 |u|^\beta - c_2$ where $c_1, c_2 > 0$, $\beta > 1$ are constants.

4.2 Optimal Control Applied to the One-Host One-Vector Model

We now present a version of the one-host one-vector model for leishmaniasis introduced in Chapter 2 which allows for the vaccination of susceptible hosts. Although an effective vaccine for leishmaniasis is not yet available, there is much research into the area and a number of trials have been carried out [79]. One study led to the protection of mice against *L. major* infection using DNA constructs encoding some Leishmania antigens [79]. The fact that recovery from cutaneous leishmaniasis infection offers protection from further new CL infections also suggests there may be a vaccine available in the future [79].

We construct an optimal control problem to find a vaccination schedule for the one-host one-vector model (2.1)-(2.7) from Chapter 2. Taking into account the results of the elasticity analysis in Chapter 3, the set of model equations (2.1)-(2.7) has been

modified and the latent class of humans has been removed. Susceptible humans now move straight to the I_h class upon infection, at a rate $\frac{\pi_h \beta S_h I_v}{N_h}$.

The objective functional we wish to minimise incorporates the total cost associated with Leishmania infection, as well as the cost of undertaking a vaccination programme. We introduce the control variable $u(t)$, which represents the rate at which susceptible individuals are vaccinated per unit time. We assume that the vaccine is 100% effective and its effects are lifelong. Incorporating vaccination $u(t)$, the system of state equations is:

$$\frac{dS_h}{dt} = \mu_h N_h^0 - \frac{\beta \pi_h S_h(t) I_v(t)}{N_h(t)} - \mu_h S_h(t) - u(t) S_h(t) \tag{4.4}$$

$$\frac{dI_h}{dt} = \frac{\beta \pi_h S_h(t) I_v(t)}{N_h(t)} - (\mu_h + \chi_h) I_h(t) + \epsilon_h R_h(t) \tag{4.5}$$

$$\frac{dR_h}{dt} = \chi_h I_h(t) - (\epsilon_h + \mu_h) R_h(t) \tag{4.6}$$

$$\frac{dV_h}{dt} = u(t) S_h(t) - \mu_h V_h(t) \tag{4.7}$$

$$\frac{dS_v}{dt} = \mu_v r_v N_h^0 - \mu_v S_v(t) - \frac{\beta \pi_v S_v(t) I_h(t)}{N_h(t)} - \mu_v S_h(t) \tag{4.8}$$

$$\frac{dE_v}{dt} = \frac{\beta \pi_v S_v(t) I_h(t)}{N_h(t)} - (\mu_v + \sigma_v) E_v(t) \tag{4.9}$$

$$\frac{dI_v}{dt} = \sigma_v E_v(t) - \mu_v I_v(t) \tag{4.10}$$

where $V_h(t)$ represents the number of vaccinated humans at time t, $N_h(t) = S_h(t) + I_h(t) + R_h(t) + V_h(t) \; \forall \, t$ and N_h^0 is the total number of humans at disease free equilibrium. $S_h(0) = N_h^0, I_h(0) = 0, R_h(0) = 0, V_h(0) = 0, S_v(0) = r_v N_h^0 - 1, E_v(0) = 0$ and $I_v(0) = 1$. This initial condition allows us to consider the control of an epidemic in an area where disease is emerging. To better understand the behaviour of $u(t)$ before adding additional complexity we consider the simplest case of disease spread, with only one host and no disease related death. The basic reproductive number R_0 for the system of equations (4.4)-(4.10) is:

$$R_0^2 = \frac{\beta^2 \pi_h \pi_v r_v \sigma_v (\epsilon_h + \mu_h)}{\mu_v (\mu_v + \sigma_v)(\mu_h + u_0)(\chi_h + \epsilon_h + \mu_h)} \tag{4.11}$$

where u_0 is a constant vaccination rate which can be used to calculate the threshold at which $R_0 = 1$. Setting $R_0 = 1$ and solving for u_0 we find the minimum vaccination rate, which if applied constantly, will ensure the disease free equilibrium is stable:

$$u_0 = \frac{r_v \sigma_v (\epsilon_h + \mu_h) \beta^2 \pi_h \pi_v}{\mu_v (\mu_v + \sigma_v)(\chi_h + \epsilon_h + \mu_h)} - \mu_h. \tag{4.12}$$

We can use equation (4.12) to obtain a measure of how relapse impacts upon the vaccination rate. For the parameter set given in Appendix C we find that when there is no relapse, a constant vaccination rate of $u(t) > 0.0127$ is required to reduce $R_0 < 1$. A constant vaccination rate $u(t) > 0.1411$ is required to keep $R_0 < 1$ when relapse is present. The vaccination rate must therefore be an order of magnitude higher when relapse is present.

Physical, financial and behavioural constraints make it impossible to vaccinate the entire susceptible population. We therefore set an upper bound for $u(t)$ that corresponds to vaccination coverage of 90% in one year. As described in [18], the maximum value of control that corresponds to z% coverage in one year can be determined from:

$$\frac{dS_h}{dt} = -uS_h, \text{ given } S(12) = (1 - \frac{z}{100})S_h(0) \tag{4.13}$$

where S_h is the total number of susceptible individuals eligible for vaccination, and $\frac{z}{100}$ is the proportion of susceptible individuals remaining after one year. Since our time unit is one month, $t = 12$. For 90% coverage after 12 months $e^{-12u} = 0.1$ and so $u_{max} \approx 0.19$. We therefore constrain $u(t)$ such that $0 \leq u\,(t) \leq 0.19$.
With a control now in place, we introduce the objective functional:

$$J\,(u) = \int_0^T A_1 I_h\,(t) + A_2 u^2\,(t)\,dt = A_1 \int_0^T I_h(t) + Au^2(t)dt \tag{4.14}$$

where $A = \frac{A_2}{A_1}$. We wish to find

$$\min_u J(u) = J(u^*) \tag{4.15}$$

under the control set $U = \{u\,(t) : 0 \leq u\,(t) \leq 0.19, 0 \leq t \leq T\}$. Constants $A_1 \geq 0$ and $A_2 \geq 0$ are weights per unit time for the costs of infection and vaccination respectively. The weighting A_1 represents the cost per unit time of an infection burden I_h. This corresponds to factors such as the cost of treatment and the loss of productivity in the workplace caused by illness. The weighting A_2 represents the cost per unit time of a vaccination effort $v(t) = u^2(t)$, where the vaccination effort $v(t)$ corresponds to the effort required to vaccinate at a rate $u(t)$. The weighting A therefore represents the cost of the vaccination programme per unit time relative to the cost of a single infection. We assume the vaccination effort is independent of the population size we wish to vaccinate, so the objective functional does not depend on $S_h(t)$. We also assume there is a non-linear relationship between the vaccination rate $u(t)$ and the cost of the vaccination effort. The greater the number of individuals to be vaccinated, the harder and more costly it is to locate them all. This is a conventional approach, leading to an

objective functional which is quadratic in u. Examples of this can also be found in [3], [13], [14], [18], [47], and [54].

We first prove the existence of a unique optimal control u^* using the five conditions stated in Section (4.1). Since $S_h + I_h + R_h + V_h + S_v + E_v + I_v + u \leq (1 + r_v)N_h^0 + 0.19$, the system of state equations under control (4.4)-(4.10) is bounded above by a linear function of state and control variables so condition (3) is satisfied. Applying Theorem 9.2.1. from page 182 of [55], the boundedness of the system guarantees the existence of a solution. The set of controls and corresponding state variables is therefore non-empty and condition (1) is fulfilled.

We now prove that condition (2) is also satisfied i.e. the control set U is both closed and convex. We first prove the control set U is convex. U is convex if given elements x and y in U the element $ky + (1-k)x$ is also in U for every $0 \leq k \leq 1$. So, pick $x \in U$, $y \in U$. Let $x_k = x + k(y - x) = (1-k)x + ky$. Then $x_k \leq (1-k)0.19 + 0.19k = 0.19 \Rightarrow x_k \leq 0.19$ and $x_k \geq (1-k)0 - k0 = 0 \Rightarrow x_k \geq 0$ hence $0 \leq x_k \leq 0.19$ and $x_k \in U$ Since the limit points $u = 0$ and $u = 0.19$ are in the set, U is also closed and condition (2) is satisfied. Condition (4) requires the objective functional to be convex on U. Since the second derivative with respect to $u(t)$ is clearly $A \geq 0$ condition (4) is fulfilled.

Finally we need to show that $c_1 |u|^\beta - c_2 \leq I_h + Au^2$. Pick $\beta = 2$. We need to show $c_1 u^2 - c_2 \leq I_h + Au^2$. Since $0 \leq I_h \leq N_h^0$, $0 \leq u \leq 0.19$ and $A \geq 0$ by construction we know that $I_h + Au^2 \geq 0$. A solution can be found by picking c_1, c_2 such that $c_1 u^2 - c_2 < 0$. Since $\max_u u^2 = 0.361$, we can therefore choose $c_1 = 1$ and $c_2 = 1$ to obtain $c_1 |u|^\beta - c_2 \leq I_h + Au^2$, and condition (5) is satisfied. All five conditions have therefore been satisfied, and a unique optimal control exists.

In order to find the optimal control strategy we require the Hamiltonian:

$$
\begin{aligned}
H &= f\left(t, x\left(t\right), u\left(t\right)\right) + \lambda\left(t\right) g\left(t, x\left(t\right), u\left(t\right)\right) \\
&= I_h(t) + Au^2(t) + \lambda_1(t)\left(\mu_h N_h^0 - \frac{\beta \pi_h S_h(t) I_v(t)}{N_h(t)} - \mu_h S_h(t) - u(t) S_h(t)\right) \\
&\quad + \lambda_2(t)\left(\frac{\beta \pi_h S_h(t) I_v(t)}{N_h(t)} - (\mu_h + \chi_h) + \epsilon_h R_h(t)\right) \\
&\quad + \lambda_3(t)\left(\chi_h I_h(t) - (\epsilon_h + \mu_h) R_h(t)\right) + \lambda_4(t)\left(u(t) S_h(t) - \mu_h V_h(t)\right) \\
&\quad + \lambda_5(t)\left(\mu_v r_v N_h^0 - \mu_v S_v(t) - \frac{\beta \pi_v S_v(t) I_h(t)}{N_h(t)} - \mu_v S_h(t)\right) \\
&\quad + \lambda_6(t)\left(\frac{\beta \pi_v S_v(t) I_h(t)}{N_h(t)} - (\mu v + \sigma_v)\right) + \lambda_7(t)\left(\sigma_v E_v(t) - \mu_v I_v(t)\right)
\end{aligned}
$$

Differentiating the Hamiltonian H with respect to u and solving $\frac{\partial H}{\partial u} = 0$ for u^* gives:

$$u^* = \frac{S_h^*(t)\left(\lambda_1^*(t) - \lambda_4^*(t)\right)}{2A}. \tag{4.16}$$

To complete the optimality conditions we have the following system of adjoint equations:

$$\begin{aligned}
\frac{d\lambda_1}{dt} = -\frac{\partial H}{\partial S_h} &= \lambda_1(t)\left(\mu_h + u(t) + \frac{\beta\pi_h I_v(t)}{N_h(t)}\left(1 - \frac{\lambda_2(t)}{\lambda_1(t)}\right)\right) - \lambda_4(t)u(t) && (4.17)\\
\frac{d\lambda_2}{dt} = -\frac{\partial H}{\partial I_h} &= \lambda_2(t)(\chi_h + \mu_h) - \chi_h\lambda_3(t) - A + (\lambda_5(t) - \lambda_6(t))\frac{\beta\pi_v S_v(t)}{N_h(t)} && (4.18)\\
\frac{d\lambda_3}{dt} = -\frac{\partial H}{\partial R_h} &= \lambda_3(t)\left(\epsilon_h + \mu_h\right) - \epsilon_h\lambda_2(t) && (4.19)\\
\frac{d\lambda_4}{dt} = -\frac{\partial H}{\partial V_h} &= \lambda_4(t)\mu_h && (4.20)\\
\frac{d\lambda_5}{dt} = -\frac{\partial H}{\partial S_v} &= \lambda_5(t)\left(\mu_v + \frac{\beta\pi_v I_h(t)}{N_h(t)}\right) - \frac{\beta\pi_v I_h(t)\lambda_6(t)}{N_h(t)} && (4.21)\\
\frac{d\lambda_6}{dt} = -\frac{\partial H}{\partial E_v} &= \lambda_6(t)\left(\mu_v + \sigma_v\right) - \lambda_7(t)\sigma_v && (4.22)\\
\frac{d\lambda_7}{dt} = -\frac{\partial H}{\partial I_v} &= \lambda_7(t)\mu_v + \frac{\beta\pi_h\lambda_1(t)S_h(t)}{N_h(t)} - \frac{\beta\pi_h\lambda_2(t)S_h(t)}{N_h(t)} && (4.23)
\end{aligned}$$

coupled with the transversality conditions $\lambda_i(T) = 0$, $i \in (1, .., 7)$.

Taking the upper and lower bounds for u into account, the optimal control u^* is therefore:

$$u^* = \begin{cases} 0 & \text{if } \frac{S_h^*(t)\left(\lambda_1^*(t) - \lambda_4^*(t)\right)}{2A} < 0 \\ \frac{S_h^*\left(\lambda_1^*(t) - \lambda_4^*(t)\right)}{2A} & \text{if } 0 < \frac{S_h^*(t)\left(\lambda_1^*(t) - \lambda_4^*(t)\right)}{2A} < 0.19 \\ 0.19 & \text{if } \frac{S_h^*(t)\left(\lambda_1^*(t) - \lambda_4^*(t)\right)}{2A} > 0.19 \end{cases}$$

which can be written in compact notation as:

$$u^* = \min\left\{\max\left\{0, \frac{S_h^*(t)\left(\lambda_1^*(t) - \lambda_4^*(t)\right)}{2A}\right\}, 0.19\right\}. \tag{4.24}$$

4.2.1 A Numerical Method for Finding the Optimal Control

We determine the optimal control strategy by solving the optimality system (4.14), (4.4)-(4.10), (4.17)-(4.23) numerically. We use a forward-backward sweep fourth order Runge-Kutta method. An initial guess is made for the control variable $u(t)$ which is used to solve the state equations forward in time. The solution to the state equations is then used to solve the adjoint equations backwards in time using the transversality

conditions. The optimal control $u^*(t)$ is calculated using the solutions for the adjoint and state variables.

The left hand column of Figure (4-1) shows the human disease dynamics for the one-host one-vector model in the absence of control, both with and without disease relapse. The right hand column of Figure (4-1) shows the human disease dynamics and optimal control strategy for the one-host one-vector model with optimal vaccination, both with and without disease relapse.

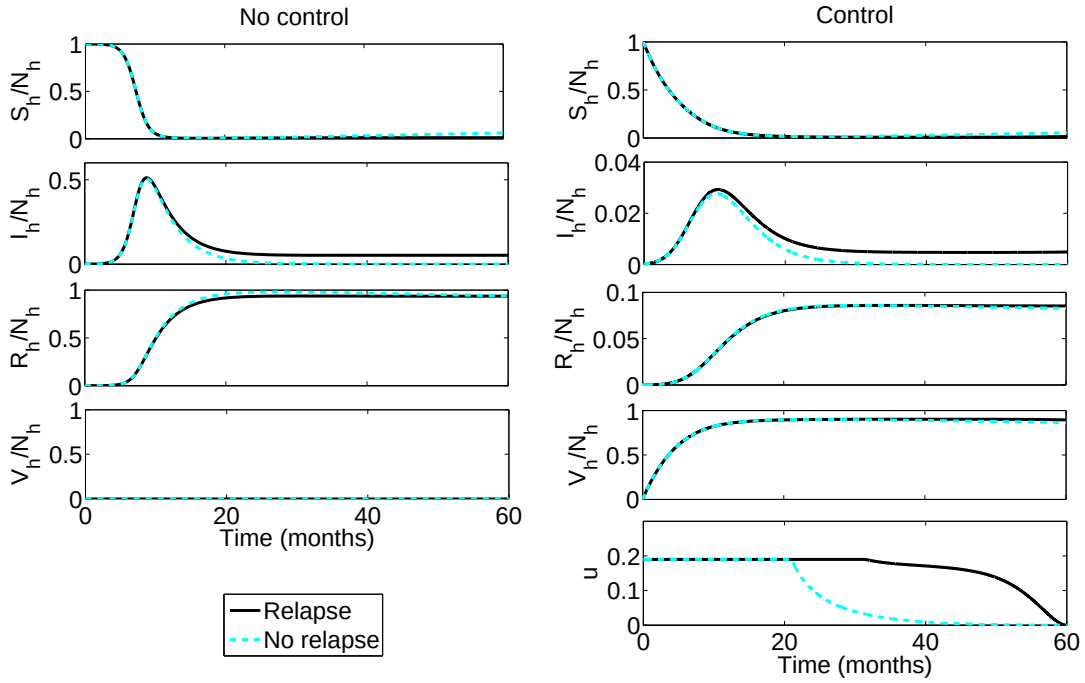

Figure 4-1: Left hand column: Human disease dynamics for the one-host one-vector model (4.4)-(4.10) in the absence of control. Right hand column: Human disease dynamics under optimal control by vaccination with $u_{max} = 0.19$, $A = 20$ and objective function (4.14). Non-control parameters are fixed at the values in Table (C.1).

4.2.2 Optimal Vaccination Strategy

In the absence of disease control, the epidemic peak for the example in Figure (4-1) occurs after approximately 9 months when roughly 50% of the human population are simultaneously infected. The presence of disease relapse does not alter the timing and size of the epidemic peak; however it does affect the proportion of the human population $\frac{I_h}{N_h}$ that is infected after the epidemic peak has subsided. When relapse is present and no control is applied, the infection prevalence is approximately 6%, compared to 1% when relapse is absent.

Comparing the left- and right-hand columns of Figure (4-1), we find that the application of control greatly reduces the size of the epidemic. When control is present the peak number of infections again occurs at 9 months, however the percentage of simultaneously infected humans does not increase above 3%. After $t = 30$, roughly 90% of individuals have been vaccinated and only 8% are in the recovered class. When infection is non-relapsing, the epidemic is brought almost entirely under control within 30 months. Vaccination is implemented at its highest rate until the epidemic peak subsides, before decreasing to zero due to the boundary conditions and the reduction in infection prevalence. The relapse of recovered individuals leads to a non-negligable proportion of the human population remaining infectious after the epidemic has passed. Control is applied at its maximum level for a longer period, and only decreases close to $t = 60$ due to the boundary conditions.

In the example shown in Figure (4-1) control is applied at the maximum rate because the cost of control is low relative to the cost of infection. In general however, the optimal control depends on the relative cost of control and the maximum rate at which it can be implemented. Figures (4-2) and (4-4) show how disease dynamics and the optimal vaccination strategy change when either the cost of vaccination or the maximum vaccination rate is altered.

We obtain Figure (4-2) by fixing the maximum vaccination rate $u_{max} = 0.19$ and varying A, the cost of vaccination relative to the cost of infection. Four metrics are used to measure how increasing the cost of vaccination impacts upon the disease dynamics and the level of control applied. In panel 1 we investigate the relationship between the size of the epidemic peak $max\left(\frac{I_h}{N_h}\right)$ and the cost of vaccination relative to the cost of infection. In panel 2 we consider how the timing of the epidemic peak varies with the relative vaccination cost A. In panel 3 we plot the relationship between the average rate of control $\bar{u} = \frac{\sum_{t=0}^{t=T} u(t)}{T}$ and cost A. In panel 4 we investigate the relationship between the cost of vaccination and the proportion of the total human population that suffers from a novel infection over the 5 year period.

In panel 1 we find that when $A < 2000$ varying the cost of vaccination has little impact on the size of the epidemic peak. As the cost of vaccination increases above 2000 however, the size of the epidemic peak increases rapidly. The cheaper the relative cost of vaccination, the longer the time period over which the maximum control is applied. When $A < 2000$ control is applied at its maximum level for the entire duration of the epidemic, and so the size of the peak does not change with A. When $A > 2000$ the rate at which control is applied drops below its maximum before the epidemic peak has fully subsided and so the number of infections increases with A. The relationship between the optimal control strategy and cost A is shown in Figure (4-3).

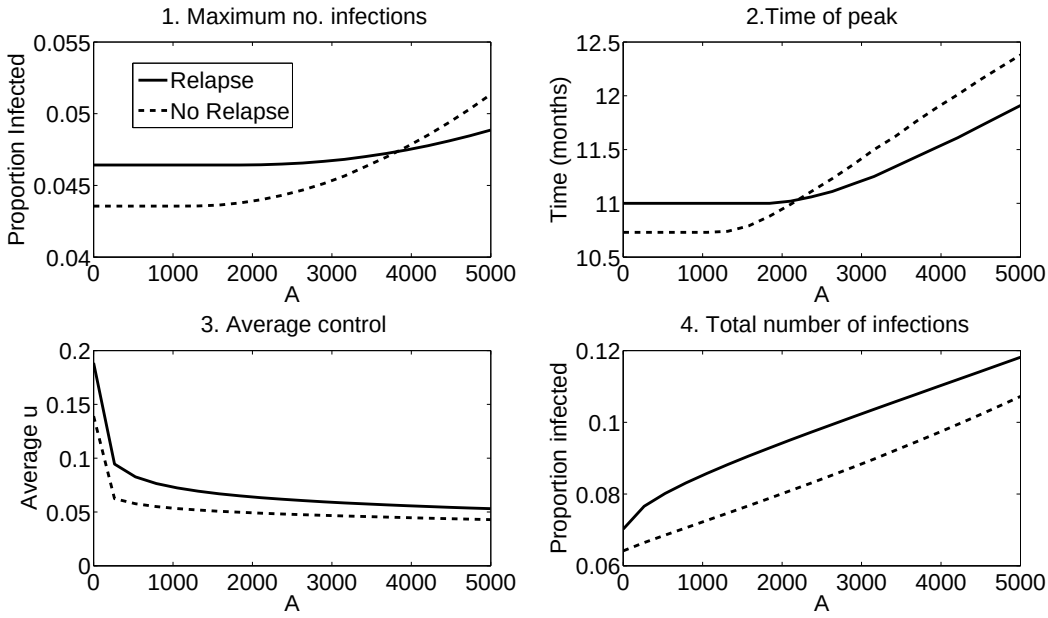

Figure 4-2: Relationship between the relative cost of vaccination A and: 1. The proportion of the human population infected at the epidemic peak. 2. Timing of the epidemic peak. 3. Average rate of control. 4. Total proportion of the human population infected over a five year period. One-host one-vector model (4.4)-(4.10) with vaccination. We use optimality condition (4.14) and $u_{max} = 0.19$. Other parameters are fixed at the values given in Table (C.1).

In panel 1 of Figure (4-2) we also find that when $A < 4000$, the epidemic peak is higher when there is relapse; however as A increases above 4000 the peak is higher when there is no disease relapse. When $A < 2000$ control is applied at its maximum level throughout the epidemic peak for both $\epsilon_h = 0$ and $\epsilon_h > 0$. Despite the application of the same control regime, the relapse of recovered individuals leads to a higher epidemic peak. As the cost of control increases, we see from Figure (4-3) that control is applied at a higher level for longer when relapse is present. The epidemic peak becomes smaller when relapse is present as control is reduced at a slower rate. Less infection is tolerated, since the recurrence of infection and additional transmission associated to relapse increase the cost of infection.

In panel 2 of Figure (4-2) we find that when $A < 2000$ the timing of the epidemic peak is constant. This is due to the fact that control is applied at its maximum level throughout the initial outbreak. When the cost of control increases above $A = 2000$, the epidemic peak occurs later. Increasing the cost A leads to a reduction in the time period over which control is applied at its maximum level. The higher the level of control applied, the faster the rate at which humans leave the susceptible class. When

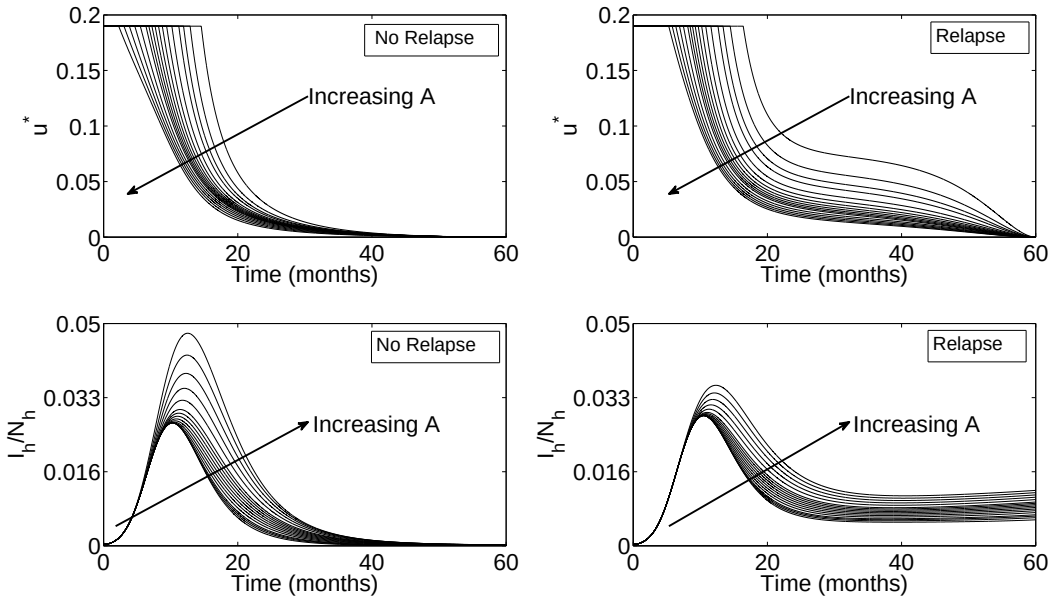

Figure 4-3: Relationship between optimal control u^*, state variable I_h under optimal control and cost weighting A for the one-host one-vector model (4.4)-(4.10) with vaccination. $u_{max} = 0.19$, $20 \leq A \leq 10000$. All other parameters are fixed at the values given in Table (C.1).

$A > 2000$ the rate of control drops below its maximum before the epidemic peaks. The remaining susceptibles then further fuel the epidemic. The earlier maximum control finishes, the larger the remaining susceptible population and the longer it takes for the epidemic to peak.

In panel 3 of Figure (4-2) we see that the average level of control decreases as the cost of control increases. The presence of disease relapse increased the average level of control applied. The higher cost of infection associated with relapsing disease increases the advantage of control. For a fixed cost A more vaccinations are therefore carried out when relapse is present than when it is not. Unlike in panels 1 and 2 the lines for relapse and no relapse never cross in panel 3. No matter when the vaccination rate drops below its maximum the cost of an infection will always be higher when relapse is present, and so the average control remains higher.

In panel 4 of Figure (4-2) we find that increasing the cost of vaccination linearly increases the total number of human infections. The higher the cost of vaccination relative to the cost of infection, the more infection is tolerated and the higher the number of infected individuals. The total proportion of infections is higher when $\epsilon_h > 0$ and relapse is present due to the new and repeated infections caused by relapsing individuals.

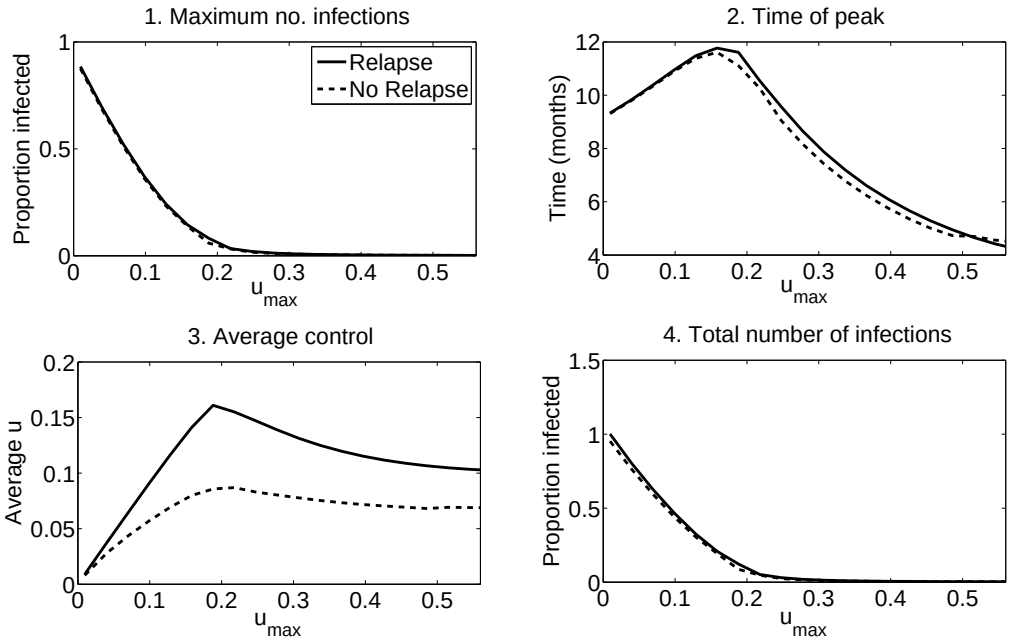

Figure 4-4: Relationship between the maximum attainable rate of vaccination u_{max} and: 1. The proportion of the human population infected at the epidemic peak. 2. Timing of the epidemic peak. 3. Average rate of control. 4. Total proportion of the human population infected over a five year period. One-host one-vector model (4.4)-(4.10) with vaccination. $A = 20$, Objective function 4.14. Non-control parameters are fixed at the values in Table (C.1).

We obtain Figure (4-4) by fixing cost A and varying u_{max}, the maximum attainable vaccination rate. We set an interval of $0.0096 < u_{max} < 0.575$ to represent 90% vaccine coverage taking from 4 months to 10 years to achieve. The same metrics are used as in Figure (4-2).

Panel 1 of Figure (4-4) shows that increasing the maximum rate at which vaccination can occur decreases the size of the epidemic peak. Since control is inexpensive, it begins at its maximum level. Increasing the maximum rate at which vaccination can occur therefore increases the initial rate at which humans leave the susceptible class. This leads to a faster reduction in the number of susceptibles available for infection and so the size of the epidemic peak is reduced.

Panel 2 of Figure (4-4) shows us that when $u_{max} < 0.15$ increasing the maximum level of control increases the time before the epidemic peak occurs, but when $u_{max} > 0.15$ the epidemic peaks earlier. The timing of the epidemic peak is dependent on the number of susceptible humans present and hence their removal rate via vaccination. When $u_{max} > 0.15$ the number of susceptible humans follows a purely convex curve, see Figure (4-5) for an example. Since control is initially applied at its maximum level, the

higher the value of $u(t) = u_{max}$, the faster the depletion of the susceptible population and the quicker the epidemic peaks. We see in panel (3) that this in turn leads to a reduction in the average control effort required over time. Since the cost of control is low it is applied at its maximum level initially, before reducing after the epidemic peak occurs. The faster the epidemic peak occurs, the sooner the treatment levels drop and the lower the average vaccination rate.

When $u_{max} < 0.15$, the epidemic is slowed but not controlled as $R_0 > 1$. The curve representing the proportion of susceptible humans over time is first concave, before becoming convex. An example of this can be seen in Figure (4-5). The delay in the reduction of the proportion of susceptible individuals means that it takes longer for $\frac{dI_h}{dt}$ to equal zero and an epidemic peak to occur. When $u_{max} < 0.15$ increasing u_{max} increases the number of susceptibles after $t = 10$ months and further delays the epidemic peak, see Figure (4-6).

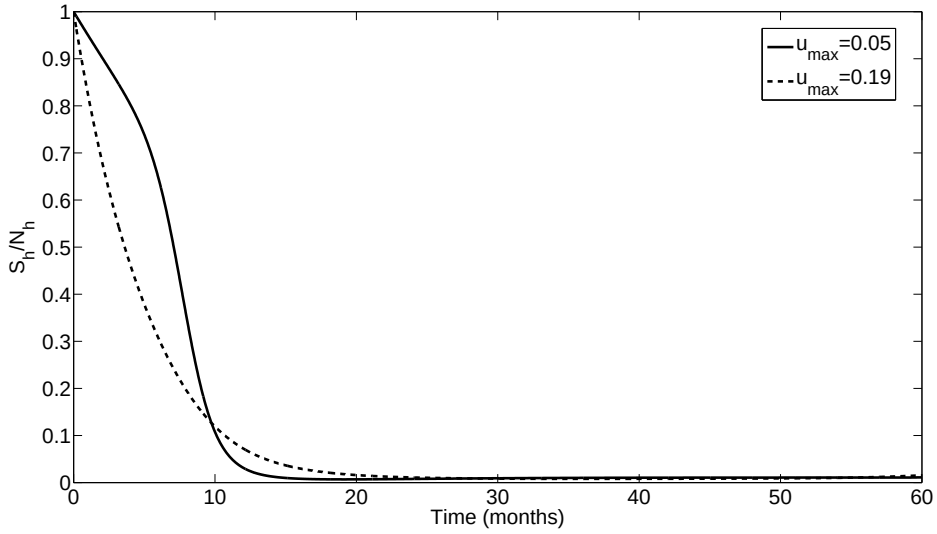

Figure 4-5: An example of how the shape of the S_h plot differs for u_{max} above and below 0.15 for the one-host one-vector model (4.4)-(4.10) with vaccination and relapse. $A = 20$. Non-control parameters are fixed at the values given in Table (C.1).

Panel 4 of Figure (4-4) shows us that increasing the maximum attainable rate of control decreases the total number of infected humans. Once again the increase in control $u(t)$ decreases the number of susceptible humans available for infection, therefore reducing the number which can become infected.

Overall, the presence of disease relapse has a smaller impact on results when u_{max} is varied than when cost A is varied. When u_{max} is varied the relative cost of treatment to

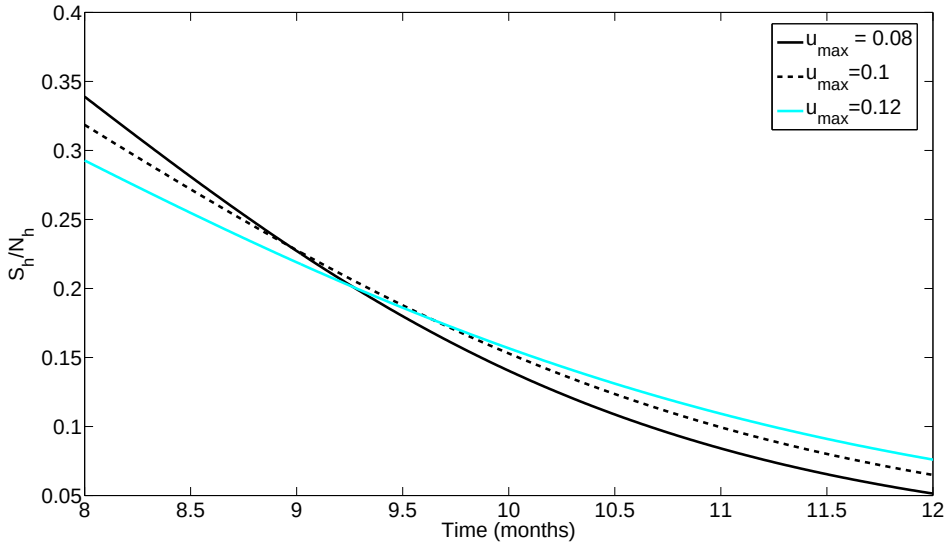

Figure 4-6: An example of how the shape of the S_h plot differs for u_{max} below 0.15 for the one-host one-vector model (4.4)-(4.10) with vaccination and relapse. $A = 20$. Parameters fixed at the values in Table (C.1).

infection remains constant, and only the rate of treatment may change. As previously mentioned, the low cost of control leads to its maximum application at the start of the control period and during the epidemic peak. During this initial time period both relapse and non-relapse cases are undergoing the same vaccination schedule so the difference between the size and time of the epidemic peak is negligible. The relapse of recovered individuals slightly increases the average rate of control, but this maintained control helps to reduce the total number of human infections to a level similar to that of the non-relapse case.

4.2.3 Optimal Vaccination: Summary

Our results show that the presence of disease relapse greatly increases the control effort required to prevent a leishmaniasis epidemic. A control strategy that may be used to control an epidemic of non-relapsing leishmaniasis may not be sufficient to control an outbreak where relapse is present. We also found that the impact of a control is dependent on its relationship with the threshold at $\frac{dI_h}{dt} = 0$. In the case of vaccination, the proportion of susceptible humans plays a key role in determining the size and timing of a disease epidemic. Increasing the rate at which individuals leave the susceptible class reduces both the time it takes for the epidemic peak to occur, and the size of the

epidemic peak.

We have found that increasing the relative cost of vaccination increases the size of the epidemic. More infection is tolerated as the cost of infection becomes smaller than the cost of treatment. When the cost of treatment is sufficiently low, increasing the maximum rate of control reduces the size of the epidemic. For all vaccination costs considered the optimal control strategy begins by vaccinating at the maximum attainable level.

4.3 S_h in the Optimality Condition

In Section (4.2) we considered an optimal vaccination strategy for leishmaniasis, where the control effort u^2 and the cost of infection were minimised by applying Pontryagin's maximum principle to the system of ODEs (4.4)-(4.10), with an objective functional of the form:

$$J(u) = A_1 \int_0^T I_h(t) + Au^2(t)dt. \tag{4.25}$$

In this case the vaccination effort was independent of the population size we wished to vaccinate, and the emphasis was on minimising the running costs of a vaccination programme. Realistically the vaccination effort may also be dependent on the number of susceptible individuals to be targetted. The larger the number of susceptibles, the higher the unit cost of vaccination per unit time as the greater the number of nurses, vaccines and clinics required. We now wish to investigate how the optimal control strategy differs when the objective functional is dependent on the size of the population we wish to vaccinate. We use the state equations (4.4)-(4.10) and an objective functional of the form:

$$J(u) = A_1 \int_0^T I_h(t) + \hat{A}S_h(t)u^2(t)dt. \tag{4.26}$$

We once again wish to find

$$\min_u J(u) = J(u^*) \tag{4.27}$$

under the control set $U = \{u(t) : 0 \leq u(t) \leq 0.19, 0 \leq t \leq T\}$ where $\hat{A}$ is the cost of vaccinating at unit rate per person to be vaccinated. We set $\hat{A}S_h(0) = 0$ to align the initial conditions of the models both with and without S_h in the objective functional.

In order to prove that an optimal control exists, the five conditions laid out in Section (4.1) must be satisfied. The fulfillment of conditions (1)-(4) follows from the results given in Section (4.2). Condition (5) can be satisfied by setting $\beta = 2$, $c_1 = 1$ and $c_2 = 100$. An optimal control exists, and the maximum principle can be applied.

With the exception of $\frac{d\lambda_1}{dt} = \lambda_1\left(\mu_h + u + \frac{\beta\pi_h I_v}{n_h}\right) - \lambda_4 u - \hat{A}u^2 - \frac{(\beta\pi_h I_v \lambda_2)}{n_h}$, the costate equations and transversality conditions are identical to those in Section (4.2) for the optimal control problem without S_h in the objective functional. Setting $\frac{\partial H}{\partial u} = 0$ and solving for the optimal control u^* we obtain:

$$u^* = \frac{\lambda_1 - \lambda_4}{2\hat{A}}. \tag{4.28}$$

Taking the upper and lower bounds into account, the optimal control u^* is therefore:

$$u^* = \begin{cases} 0 & \text{if } \frac{\lambda_1-\lambda_4}{2\hat{A}} < 0 \\ \frac{\lambda_1-\lambda_4}{2\hat{A}} & \text{if } 0 < \frac{\lambda_1-\lambda_4}{2\hat{A}} < 0.19 \\ 0.19 & \text{if } \frac{\lambda_1-\lambda_4}{2\hat{A}} > 0.19 \end{cases}$$

which can be written in compact notation as:

$$u^* = \min\left\{\max\left\{0, \frac{\lambda_1 - \lambda_4}{2\hat{A}}\right\}, 0.19\right\}. \tag{4.29}$$

4.3.1 Optimal Vaccination Strategy

Numerical results can again be obtained using the method detailed in Section (4.2.1). Figures (4-7) and (4-8) compare the optimal state solution and optimal control for the two different objective functionals (4.14) and (4.26).

In Figure (4-7) we see that the optimal solution to the state equations is almost identical for objective functionals (4.25) and (4.26). The optimal vaccination rate differs however, and is held at a higher level for longer when S_h is present in the objective functional. When the objective functional is dependent only on $u(t)$ and $I_h(t)$, the level of control drops after the epidemic peak starts to subside. When S_h is added to the objective function, control is maintained until $I_h \approx 0$. In the absence of disease relapse, vaccination is employed at its maximum rate for 18 additional months when the objective function is dependent on S_h. When disease relapse is present, vaccination is applied at its maximum rate for approximately 28 additional months when the objective function is dependent on S_h. In fact, the additional infections caused by relapse leads to the maintenance of control, and the rate of vaccination only decreases to zero at $t = 60$ due to the boundary conditions.

As in Section (4.2.2), the optimal control is also dependent upon the cost of control, and the maximum attainable control rate. Figure (4-8) shows how varying the cost of vaccination relative to the cost of infection $A = \hat{A}S_h(0)$ affects the optimal control solution and corresponding state variables. Once again we consider four metrics, namely

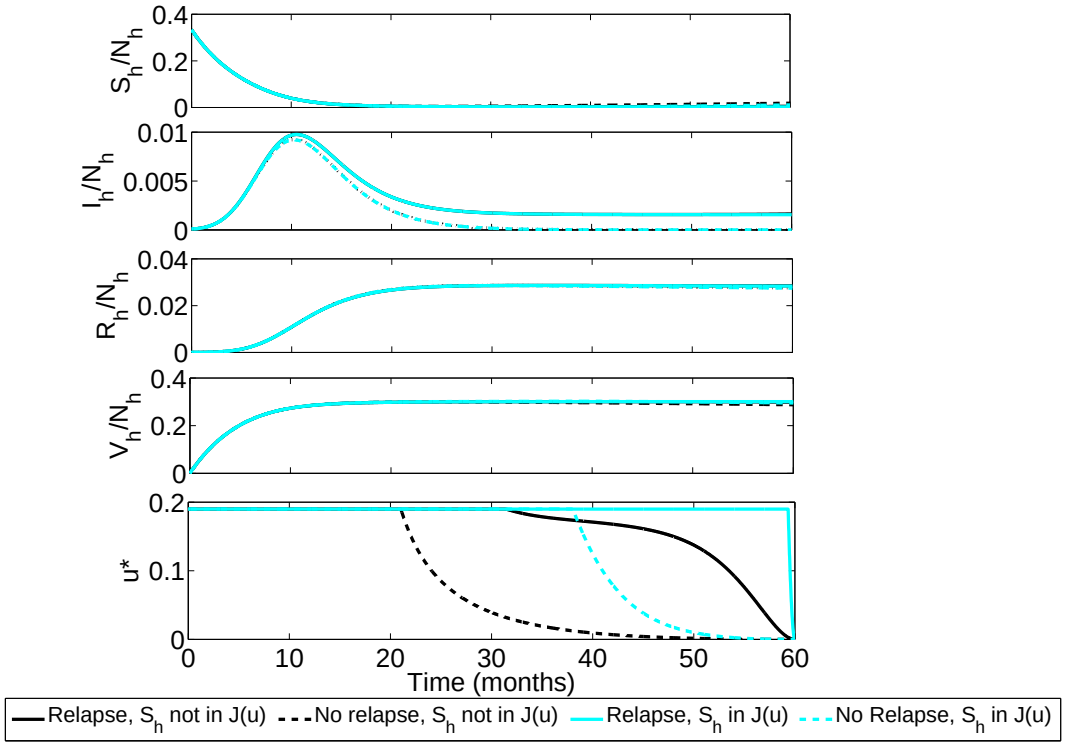

Figure 4-7: Comparing the optimal state solution for (4.4)-(4.10) with vaccination under objective functionals (4.14) and (4.26). $u_{max} = 0.19$ and $A = \hat{A}S_h = 20$. Parameters fixed at the values in Table (C.1).

the size and timing of the epidemic peak, the average rate of control and the total number of novel human infections.

In panels 1 and 2 of Figure (4-8), both objective functionals yield the same results for $A < 2500$. For $A > 2500$ the size and timing of the epidemic does not change when S_h is present in the objective functional. This is due to the fact that a higher average control is applied when S_h is in the objective function, see panel 3. Since the proportion of hosts residing in the susceptible class S_h is small after the epidemic peak subsides, it is cheap to continue vaccination. When the number of susceptible hosts is not included in the objective function, it is cheaper to stop vaccinating earlier thus allowing some of the epidemic to escape. The constant size of the epidemic peak, and high level of control applied when S_h is included in the objective function also lead to a constant, and reduced number of novel infections in panel 4. The additional infections incurred due to relapse increase the control applied in all cases, hence reducing the size and timing of the epidemic.

When varying the maximum attainable control rate u_{max}, results for objective function (4.26) including S_h were similar to those in Figure (4-4) for objective function

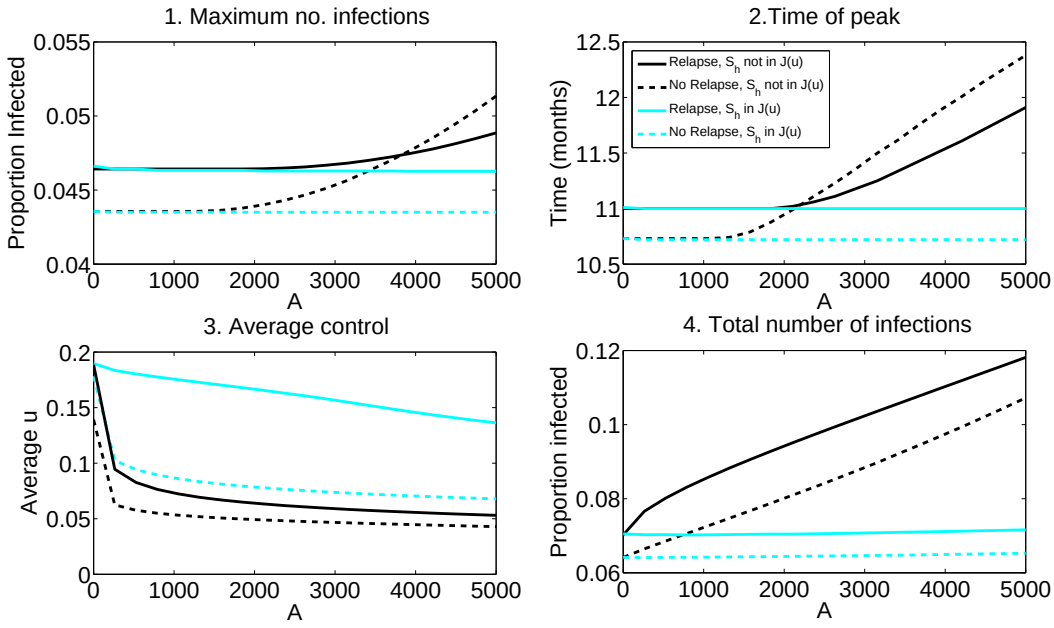

Figure 4-8: Relationship between the relative cost of vaccination A and: 1. The human epidemic peak. 2. Timing of the epidemic peak. 3. Average rate of control. 4. Total proportion of infected humans over the five year period. One-host one-vector model (4.4)-(4.10) with vaccination, objective function (4.26).$u_{max} = 0.19$. Disease parameters fixed at the values in Table (C.1).

(4.25) without S_h. The control applied throughout the epidemic peak was the same for both objective functions considered, and so the timing of the epidemic peak, size of the epidemic peak and total number of infections were unaltered. The average control applied was higher for the objective function including S_h, to minimise potential infectious contacts.

Comparing results for objective functionals (4.14) and (4.26) we find that the overall number of human infections is reduced when the objective function is dependent on the number of susceptibles to be vaccinated. In this case, control is applied at a higher level for longer in order to minimise the number of potential infectious contacts. The larger the population to be vaccinated, the greater the level of control applied and the smaller the epidemic peak. Once again the presence of relapse increases the average rate and duration of control.

4.4 Optimal Spraying

We now consider control targetted at the vector population. One control regularly employed in the fight against vector-borne disease is insecticide spraying. We now use optimal control theory to obtain an optimal spraying regime for a cutaneous leishmaniasis model with one host and one vector. We introduce the control variable $u(t)$, which now represents the increase in the sandfly mortality rate caused by the spraying of insecticide. Incorporating spraying into the system of equations (4.4)-(4.10) we obtain the following set of state equations:

$$\frac{dS_h}{dt} = \mu_h N_h^0 - \frac{\beta \pi_h S_h(t) I_v(t)}{N_h(t)} - \mu_h S_h(t) \tag{4.30}$$

$$\frac{dI_h}{dt} = \frac{\beta \pi_h S_h(t) I_v(t)}{N_h(t)} - (\mu_h + \chi_h) I_h(t) + \epsilon_h R_h(t) \tag{4.31}$$

$$\frac{dR_h}{dt} = \chi_h I_h(t) - (\epsilon_h + \mu_h) R_h(t) \tag{4.32}$$

$$\frac{dS_v}{dt} = \mu_v r_v N_h^0 - \mu_v S_v(t) - \frac{\beta \pi_v S_v(t) I_h(t)}{N_h(t)} - (\mu_v + u(t)) S_h(t) \tag{4.33}$$

$$\frac{dE_v}{dt} = \frac{\beta \pi_v S_v(t) I_h(t)}{N_h(t)} - (\mu_v + \sigma_v + u(t)) E_v(t) \tag{4.34}$$

$$\frac{dI_v}{dt} = \sigma_v E_v(t) - (\mu_v + u(t)) I_v(t) \tag{4.35}$$

with disease free equilibrium given by $\left(S_h^0, I_h^0, R_h^0, S_v^0, E_v^0, I_v^0\right) = \left(N_h^0, 0, 0, \frac{\mu_v r_v N_h^0}{\mu_v + u_0}, 0, 0\right)$ and basic reproductive number:

$$R_0^2 = \frac{\beta^2 \pi_h \pi_v \sigma_v \left(\epsilon_h + \mu_h\right) r_v \mu_v}{\left(\mu_v + u_0\right)^2 \left(\mu_v + \sigma_v + u_0\right) \left(\mu_h \left(\chi_h + \epsilon_h + \mu_h\right)\right)}, \tag{4.36}$$

where u_0 is a constant spraying rate that can be used to calculate the threshold at which $R_0 = 1$. Spraying must remain at a constant level of u_0, or above in order to prevent a leishmaniasis epidemic. Setting $R_0 = 1$ and solving for u_0 we find that when relapse is present $u_0 = 9.89$ and when relapse is not present $u_0 = 3$ for the parameter set in Table (C.1). This suggests that in order to prevent an epidemic the sandflies must have a life expectancy below 2.5 days when relapse is present, and 6 days when relapse is not present.

We now formulate our optimal control problem. Once again we must consider physical and financial constraints which limit the rate of spraying. We introduce the

objective functional:

$$J(u) = \int_0^T A_1 I_h(t) + A_2 u^2(t)\, dt = A_1 \int_0^T I_h(t) + A u^2(t) dt \tag{4.37}$$

where $A = \frac{A_2}{A_1}$, $A \geq 0, A_1 \geq 0, A_2 \geq 0$. We wish to find

$$\min_u J(u) = J(u^*) \tag{4.38}$$

under the control set $U = \{u(t) : 0 \leq u(t) \leq 10, 0 \leq t \leq T\}$. We base our control set on our findings for u_0, and pick an upper bound for $u(t)$ which allows spraying to occur at a rate which prevents an epidemic.

The existence of a unique optimal control can be proven using the method detailed in Section (4.2). Using the maximum principle we obtain the Hamiltonian:

$$H = I_h(t) + Au^2(t) + \lambda_1(t)\frac{dS_h}{dt} + \lambda_2\frac{dI_h}{dt} + \lambda_3\frac{dR_h}{dt} + \lambda_4\frac{dS_v}{dt} + \lambda_5\frac{dE_v}{dt} + \lambda_6\frac{dI_v}{dt} \tag{4.39}$$

and costate equations:

$$\frac{d\lambda_1}{dt} = \lambda_1(t)\left(\mu_h + \frac{\beta\pi_h I_v(t)}{N_h(t)}\right) - \frac{\beta\pi_h I_v(t)\lambda_2}{N_h(t)} \tag{4.40}$$

$$\frac{d\lambda_2}{dt} = \lambda_2(t)(\chi_h + \mu_h) - \chi_h\lambda_3(t) - A_1 + \frac{\beta\lambda_4(t)\pi_h S_v(t)}{N_h(t)} - \frac{\beta\lambda_5(t)\pi_v S_v(t)}{N_h(t)} \tag{4.41}$$

$$\frac{d\lambda_3}{dt} = \lambda_3(t)(\epsilon_h + \mu_h) - \epsilon_h\lambda_2(t)) \tag{4.42}$$

$$\frac{d\lambda_4}{dt} = \lambda_4(t)\left(\mu_v + u(t) + \frac{\beta\pi_v I_h(t)}{N_h(t)}\right) - \frac{\beta\pi_v I_h(t)\lambda_5(t)}{N_h(t)} \tag{4.43}$$

$$\frac{d\lambda_5}{dt} = \lambda_5(t)(\mu_v + \sigma_v + u(t)) - \lambda_6(t)\sigma_v \tag{4.44}$$

$$\frac{d\lambda_6}{dt} = \lambda_6(t)(\mu_v + u(t)) + (\lambda_1(t) - \lambda_2(t))\frac{\beta\pi_h S_h(t)}{N_h(t)} \tag{4.45}$$

with transversality conditions $\lambda_i(T) = 0 \,\forall\, i \in (1, .., 6)$. The optimal control for the optimality system (4.30)-(4.35), (4.39), (4.40)-(4.45) is therefore:

$$u^* = \min\left\{\max\left\{0, \frac{E_v\lambda_5 + I_v\lambda_6 + S_v\lambda_4}{2A}\right\}, 1.5\right\}. \tag{4.46}$$

4.4.1 Optimal Spraying Strategy

Using the numerical method outlined in Section (4.2.1) we now present a numerical solution for the optimality system (4.30)-(4.35), (4.39), (4.40)-(4.45). Figure (4-9)

shows the optimal state solution and optimal control strategy for the one-host one-vector model with and without disease relapse; $u_{max} = 10$, and the cost of control is low ($A = 20$).

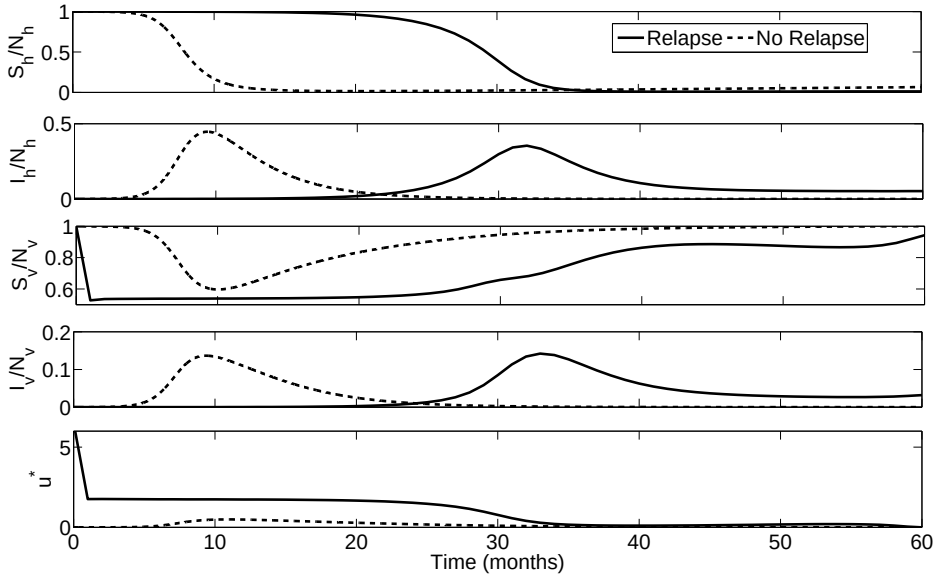

Figure 4-9: An example of an optimal spraying control for the one-host one-vector model (4.30)-(4.35) with optimality condition (4.37), $u_{max} = 10$, $A = 20$. Non-control parameters are fixed at the values given in Table (C.1).

In Figure (4-9) we find that the shape of the optimal control depends on relapse. When relapse is present $u(0) \approx 6$, but then drops to $u(1) \approx 1.76$ after one month. Control is maintained at this level until $t \approx 25$ when control drops steadily towards zero. When there is no disease relapse, there is a delay of five months before control is applied. After five months control increases to $u \approx 0.55$ for the duration of the epidemic peak. Once the epidemic peak subsides, control gradually tails off to zero. Relapse increases the cost of an infection and therefore a greater level of control is applied in this case. Spraying starts earlier to minimise the impact of relapse.

The application of spraying impacts upon all sandfly classes. Since the vector lifespan is short, the majority of the vector population resides in the susceptible class. Increasing the rate of spraying therefore kills more susceptible vectors than vectors of any other type, see Figure (4-9). When relapse is present there is a second peak in control at $t \approx 50$, when the number of susceptible hosts begins to increase. Reducing the proportion of susceptible vectors reduces transmission by decreasing the likelihood a susceptible vector bites an infectious host. A reduced rate of transmission to sandflies will then reduce the transmission back to humans and so on.

Overall, the application of control in Figure (4-9) only leads to a small reduction in the epidemic peak. In non-relapsing infection the epidemic peak still occurs around 10 months, when approximately 48% of humans and 17% of vectors are infected. The epidemic peak in relapsing infection is delayed, occurring at approximately 32 months, when 35% of humans and 14% of vectors are infected. In both cases, the optimal control never reaches its maximum attainable rate of $u_{max} = 10$. When relapse is present $u(t) < 6 \; \forall \, t$ and when relapse is absent $u(t) < 0.55 \; \forall \, t$. Even though the cost of control is low, the large population of sandflies and the inability to target control at infected individuals make spraying inefficient. The benefits of spraying are outweighed by the cost. In further investigations we therefore use a smaller bound on control $u(t)$, to investigate the impact of a sub-optimal control.

In the case of non-relapsing infection, the low number of infections, short vector lifespan and low efficacy of control means no control is applied in the first five months. Control is only applied when the number of infectious individuals increases at the start of the epidemic peak. The impact of varying the delay before control is applied on the number of infections is investigated in Figure (4-10). Control is applied at a constant rate $u(t) = 0.8$ after a time delay of either 0, 2, 5, or 10 months. The corresponding state solutions are obtained, and can be used to assess the reason for the delay before control in non-relapsing disease, and the impact on disease prevalence were the delay to change.

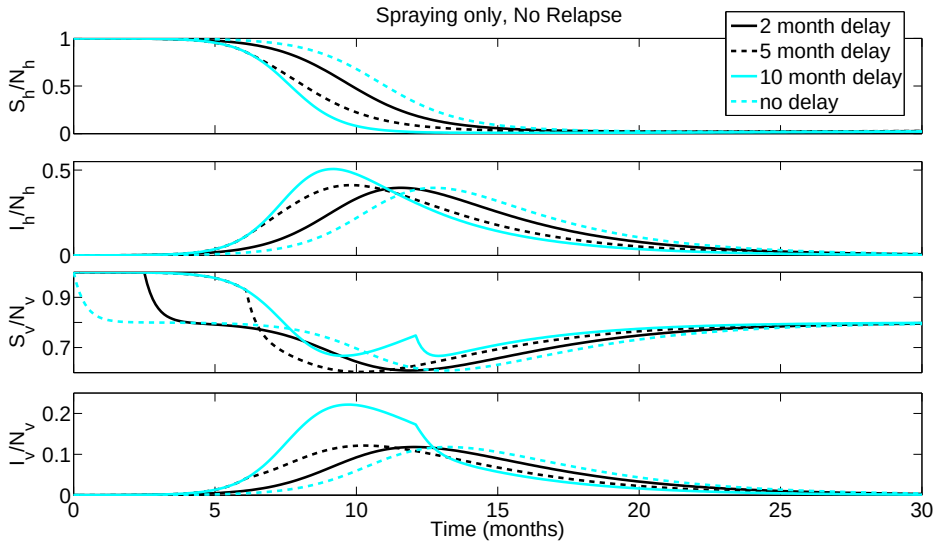

Figure 4-10: State solutions for the one-host one-vector model (4.30)-(4.35) with spraying. The delay before control is applied is varied. When control is applied, it is applied at a constant rate $u = 0.8$. No relapse is present. $A = 20$. Disease and demographic parameters are fixed at the values in Table (C.1).

In Figure (4-10) we see that the size of the human epidemic peak is almost constant when the delay before the application of control is less than approximately 5 months. Delaying the application of control reduces the cost of control without impacting on the number of infections. When the delay before the application of control is greater than 5 months, the size of the epidemic peak and hence the cost of infection increases.

We now investigate how the optimal control strategy depends on the cost and maximum rate of control. Figures (4-11) and (4-13) use the metrics set out in Section (4.2.2) to investigate how the disease dynamics and optimal spraying strategy alter with cost and maximum spray rate respectively.

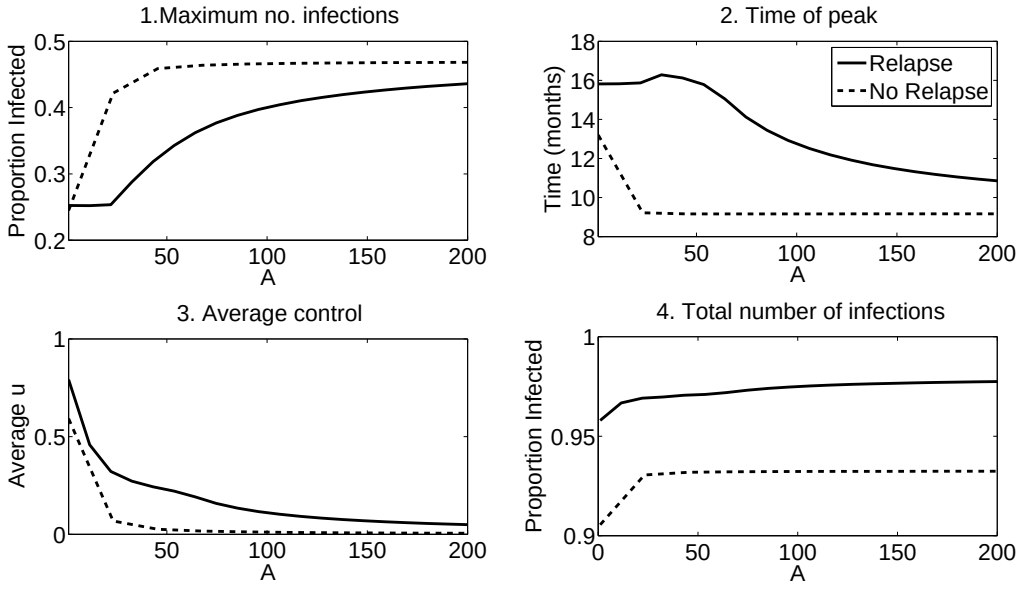

Figure 4-11: Relationship between the relative cost of spraying A and: 1. The proportion of the human population infected at the epidemic peak. 2. Timing of the epidemic peak. 3. Average rate of control. 4. Total proportion of the human population infected over a five year period. One-host one-vector model (4.30)-(4.35) with spraying. We use optimality condition (4.37) and $u_{max} = 0.8$. Other parameters are fixed at the values given in Table (C.1).

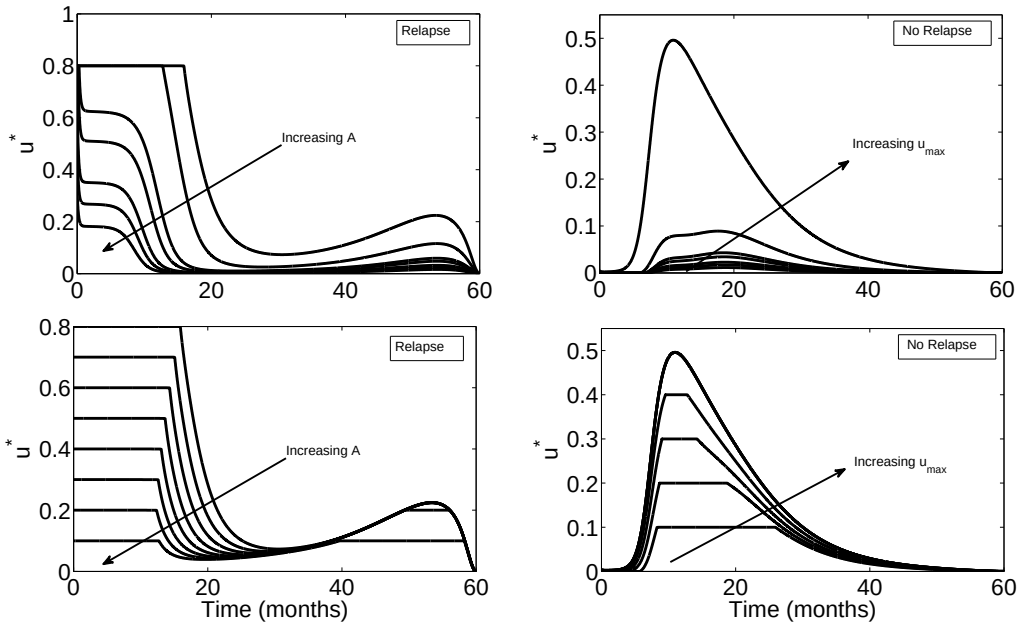

Figure 4-12: Optimal control trajectories for the one-host one-vector model (4.30)-(4.35) with spraying. In the left column each optimal control solution is for a different value of cost A, $u_{max} = 0.8$. In the right column each optimal control solution is for a different maximum spray rate u_{max}, $A = 20$. Other parameters are fixed at the values in Table (C.1).

We obtain Figure (4-11) by fixing the maximum spraying rate $u_{max} = 0.8$ and varying A, the cost of spraying relative to the cost of infection. As A increases, the reduction in infection is outweighed by the price of spraying. This leads to a decrease in the average level of control applied, as seen in panel 3. A reduced level of control leads to an increase in the size of the epidemic peak in panel 1, and increases the total number of human infections in panel 4. The level of control applied depends on whether or not relapse is present however. In panel 3 we find that the average rate of control is always higher when relapse is present. The additional infection cost related to relapse increases the benefit of control, and leads to the application of higher rates of spraying over longer periods of time. See Figure (4-12) for an example. The higher level of control applied in relapsing infection does not stop the epidemic from occurring, but does reduce its size below that of the non-relapsing case. The total number of human infections in panel 4 of Figure (4-12) is still higher when relapse is present however, highlighting the importance of relapsing infections in the persistence of disease.

In panel 2 we see that the relationship between cost A and the timing of the epidemic peak is also dependent on whether relapse is present. When $A < 25$, increasing A decreases the timing of the epidemic peak for non-relapsing infection, but has no impact on the timing of the epidemic peak for relapsing infection. When $A > 25$ the timing

of the epidemic peak is constant for non-relapsing infection, but increasing A first increases then decreases the timing of the epidemic peak for relapsing infection. The timing of the epidemic peak is again dependent on the rate at which susceptible humans are removed from the S_h class. The higher the level of spraying, the smaller the number of susceptible and infectious sandflies. Smaller values of S_v and I_v decrease the transmission rates $\frac{\beta\pi_h S_h I_v}{N_h}$ and $\frac{\beta\pi_v S_v I_h}{N_h}$, thus reducing the rate at which humans are removed from the susceptible class and increasing the time it takes for humans to become infectious.

The timing of the epidemic peak is also dependent on the shape of the optimal control. Examples of optimal control solutions can be found in Figure (4-12). When relapse is absent, we see in Figure (4-12) that control never reaches its maximum level for the costs A considered. When relapse is present and $A < 25$, control is applied at its maximum level throughout the epidemic, which causes the epidemic peak time to be constant. When $25 < A < 45$ maximum control is not applied throughout the epidemic peak, only through part of it. Ceasing to control at a high level throughout the epidemic allows a resurgence in transmission and so delays the peak. When $A > 45$, control does not reach its maximum level at any point during the epidemic. High transmission leads to a larger epidemic that peaks earlier.

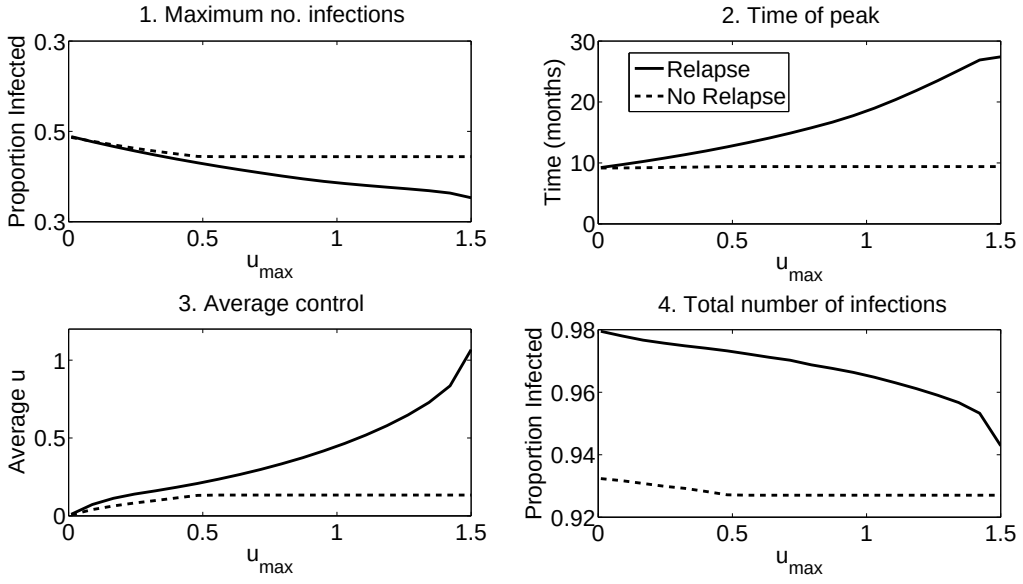

Figure 4-13: Relationship between the maximum attainable spray rate u_{max} and: 1. The proportion of the human population infected at the epidemic peak. 2. Timing of the epidemic peak. 3. Average rate of control. 4. Total proportion of the human population infected over a five year period. One-host one-vector model (4.4)-(4.10) with vaccination. We use optimality condition (4.37) and $A = 20$. Other parameters are fixed at the values given in Table (C.1).

We obtain Figure (4-13) by fixing cost $A = 20$ and varying u_{max}, the maximum attainable spraying rate. The same metrics were used as in Figure (4-11). Once again results are dependent upon the presence of relapse. In panel 1 we find that when relapse is present, increasing the maximum attainable spraying rate decreases the size of the epidemic peak. Increasing the maximum rate of control also decreases the overall proportion of humans infected in panel 4, and delays the epidemic peak in panel 2.

In panel 3 of Figure (4-13) the average level of control applied is highest when relapse is present. When relapse is present, infection is more costly. Increasing the maximum attainable control always increases the average control in the range of values considered. The prevention of novel infections arising from relapsing hosts means that the benefit of increasing control outweighs its cost. When there is no relapse the average control increases until $u_{max} = 0.55$ and then levels out. In this case the optimal control solution for a fixed cost $A = 20$ is the same for all values of $u_{max} > 0.55$. One such example can be seen in Figure (4-9). When $u_{max} > 0.55$ the benefits of control are outweighed by the cost and there is no further increase in the level of control. The constant level of optimal control leads to the size of the epidemic peak, timing of the epidemic peak and total proportion of infected humans becoming constant for $u_{max} > 0.55$.

4.4.2 Optimal Spraying: Summary

In both relapsing and non-relapsing infections, spraying at the rates considered in Section (4.4.1) proves ineffective. For both types of infection we find that over 90% of humans were infected for all costs A, and spraying rates u_{max} considered. Even when the cost of spraying was low, spraying at the rates required for $R_0 < 1$ was not economically viable. The beneficial impact of control is low relative to its cost and so infection is tolerated. Increasing the cost of control decreases the average control rate and leads to a larger epidemic peak. The time spent at the maximum control rate u_{max} drops, and the total number of human infections increases. A higher level of control is employed when relapse is present; however the average rate of control still tends to zero as A increases.

4.5 Two Control Problem: Vaccination and Spraying

We now consider the application of both host and vector control. We introduce the control variables $u_1(t)$ and $u_2(t)$ to represent vaccination and spraying respectively. Incorporating both controls into the system of equations (4.4)-(4.10) we obtain the

following system:

$$\begin{aligned}
\frac{dS_h}{dt} &= \mu_h N_h^0 - \frac{\beta \pi_h S_h(t) I_v(t)}{N_h(t)} - \mu_h S_h(t) - u_1(t) S_h(t) && (4.47)\\
\frac{dI_h}{dt} &= \frac{\beta \pi_h S_h(t) I_v(t)}{N_h(t)} - (\mu_h + \chi_h) I_h(t) + \epsilon_h R_h(t) && (4.48)\\
\frac{dR_h}{dt} &= \chi_h I_h(t) - (\epsilon_h + \mu_h) R_h(t) && (4.49)\\
\frac{dV_h}{dt} &= u_1(t) S_h(t) - \mu_h V_h(t) && (4.50)\\
\frac{dS_v}{dt} &= \mu_v r_v N_h^0 - \mu_v S_v(t) - \frac{\beta \pi_v S_v(t) I_h(t)}{N_h(t)} - (\mu_v + u_2(t)) S_h(t) && (4.51)\\
\frac{dE_v}{dt} &= \frac{\beta \pi_v S_v(t) I_h(t)}{N_h(t)} - (\mu_v + \sigma_v + u_2(t)) E_v(t) && (4.52)\\
\frac{dI_v}{dt} &= \sigma_v E_v(t) - (\mu_v + u_2(t)) I_v(t) && (4.53)
\end{aligned}$$

which has basic reproductive number

$$R_0^2 = \frac{\beta^2 \pi_v \pi_h \sigma_v r_v (\epsilon_h + \mu_h) \mu_v}{\left(\mu_v + \sigma_v + u_2^0\right)\left(\mu_v + u_2^0\right)^2 \left(\mu_h + u_1^0\right)(\mu_h + \chi_h + \epsilon_h)}. \tag{4.54}$$

u_1^0, u_2^0 are constant vaccination and spraying rates which can be used to determine the threshold at which $R_0 = 1$. The relationship between the threshold at $R_0 = 1$ and u_1^0 and u_2^0 is shown in Figure (4-14). Increasing either u_1^0 or u_2^0 leads to a decrease in the value of the opposing control required for $R_0 < 1$. When either u_1^0 or u_2^0 equals zero, the minimum constant control rate required to prevent an epidemic is that of the corresponding one control problem.

In order to consider the physical and financial constraints of two controls we use optimal control theory with an objective function of the form:

$$J(u) = \int_0^T A_1 I_h(t) + B_1 u_1^2(t) + B_2 u_2^2(t)\, dt = A_1 \int_0^T I_h(t) + A_2 u_1^2(t) + A_3 u_2^2(t)\, dt \tag{4.55}$$

where $A_2 = \frac{B_1}{A_1} \geq 0$ is the cost of vaccination relative to the cost of infection and $A_3 = \frac{B_2}{A_1} \geq 0$ is the cost of spraying relative to the cost of infection. The number of susceptible hosts is excluded from the objective function in this case in order to compare results to those of both vaccination and spraying controls. We want to find $(u_1(t), u_2(t))$ such that

$$\min_{(u_1,u_2)} J(u_1, u_2) = J(u_1^*, u_2^*) \tag{4.56}$$

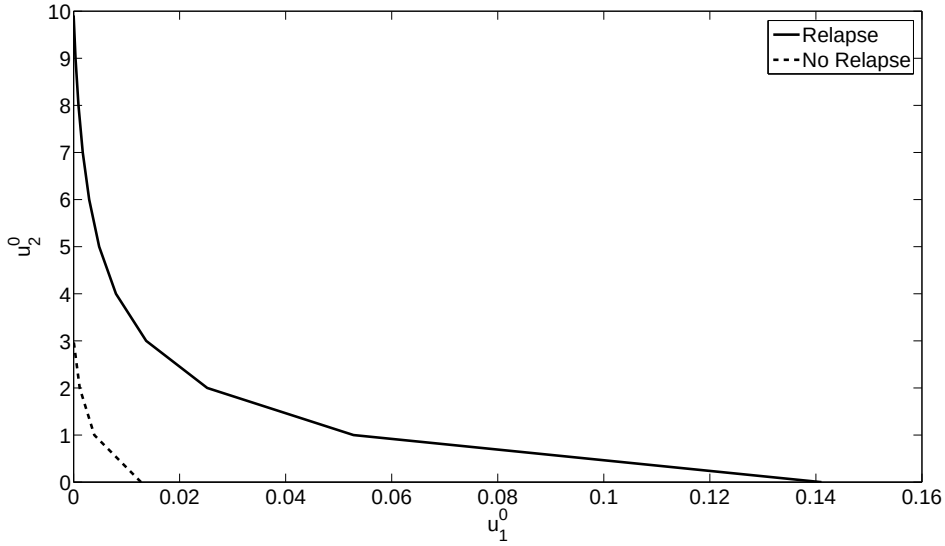

Figure 4-14: Threshold at which $R_0 = 1$ in terms of constant vaccination rate u_1^0 and constant spray rate u_2^0. One-host one-vector model (4.47)-(4.53) with vaccination and spraying. Non control parameters are fixed at the values given in Table (C.1).

under the control set:

$$U = \{(u_1(t), u_2(t)) : 0 \leq u_1(t) \leq 0.19, 0 \leq u_2(t) \leq 0.8, 0 \leq t \leq T\}. \tag{4.57}$$

To allow us to compare our findings to those of the one control cases, the control set (4.57) incorporates the upper bound for vaccination calculated in Section (4.2), and the low level spraying rate used for calculations in Section (4.4.1).

The existence of an optimal control can again be proved using the method outlined in Section (4.2). Following the arguments outlined in Section (4.2) it can be shown that the set of controls and state variables is non-empty, the control set is closed and convex, the state system is bounded by a linear function of the state and control variables, and the integrand of the objective functional is convex on the control set. Since two controls are present condition (5) is altered, and the integrand of the objective functional must be bounded below by a function $c_1\left(|u_1|^2 + |u_2|^2\right)^{\frac{\beta}{2}} - c_2$, where $c_1, c_2 > 0$ $\beta > 1$ are constants. Letting $c_1 = 1$, $c_2 = 5$, $\beta = 2$ we can satisfy condition 5 and prove an optimal control exists. Using the maximum principle we now obtain the Hamiltonian:

$$H = I_h(t) + A_2 u_1^2(t) + A_3 u_2^2(t) + \lambda_1(t)\frac{dS_h}{dt} + \lambda_2\frac{dI_h}{dt} + \lambda_3\frac{dR_h}{dt} + \lambda_4\frac{dV_h}{dt} + \lambda_5\frac{dS_v}{dt} + \lambda_6\frac{dE_v}{dt} + \lambda_7\frac{dI_v}{dt} \tag{4.58}$$

and costate equations:

$$\frac{d\lambda_1}{dt} = \lambda_1\left(\mu_h + u_1(t) + \frac{\beta\pi_h I_v(t)}{N_h(t)}\right) - \lambda_4 u_1(t) - \frac{\beta\pi_h I_v(t)\lambda_2}{N_h(t)} \quad (4.59)$$

$$\frac{d\lambda_2}{dt} = \lambda_2\left(\chi_h + \mu_h\right) - \chi_h\lambda_3 - A_1 + \frac{\beta\pi_v\lambda_5 S_v(t)}{N_h(t)} - \frac{\beta\lambda_6\pi_v S_v}{N_h(t)} \quad (4.60)$$

$$\frac{d\lambda_3}{dt} = \lambda_3\left(\epsilon_h + \mu_h\right) - \epsilon_h\lambda_2 \quad (4.61)$$

$$\frac{d\lambda_4}{dt} = \lambda_4\mu_h \quad (4.62)$$

$$\frac{d\lambda_5}{dt} = \lambda_5\left(\mu_v + u_2\left(t\right) + \frac{\beta\pi_v I_h(t)}{N_h(t)}\right) - \frac{\beta\pi_v I_h(t)\lambda_6}{N_h(t)} \quad (4.63)$$

$$\frac{d\lambda_6}{dt} = \lambda_6\left(\mu_v + \sigma_v + u_2(t)\right) - \lambda_7\sigma_v \quad (4.64)$$

$$\frac{d\lambda_7}{dt} = \lambda_7\left(\mu_v + u_2(t)\right) + \frac{\beta\pi_h\lambda_1 S_h}{N_h(t)} - \frac{\beta\pi_h S_h(t)\lambda_2}{N_h(t)} \quad (4.65)$$

with transversality conditions $\lambda_i(T) = 0\,\forall\, i \in (1,..,6)$. Solving $\frac{dH}{du_1} = 0$ for u_1^* and $\frac{dH}{du_2} = 0$ for u_2^*, the optimal control for the optimality system (4.47)-(4.53), (4.58), (4.59)-(4.65) is given by:

$$u_1^* = \min\left\{\max\left\{0, \frac{S_h\left(\lambda_1 - \lambda_4\right)}{2A_2}\right\}, 0.19\right\}, \quad (4.66)$$

$$u_2^* = \min\left\{\max\left\{0, \frac{E_v\lambda_6 + I_v\lambda_7 + S_v\lambda_5}{2A_3}\right\}, 0.8\right\}. \quad (4.67)$$

4.5.1 Optimal Control for the Two Control Problem

Using the numerical method outlined in Section (4.2.1) we now present a numerical solution for the optimality system (4.47)-(4.53), (4.58), (4.59)-(4.65). We compare the optimal rates of spraying and vaccination for the one and two control cases, and investigate the impact of increasing the cost of control relative to infection. Figures (4-15) and (4-16) show the optimal state solutions and corresponding optimal control strategies for relapsing and non-relapsing disease.

In Figures (4-15) and (4-16) we find that the epidemic peak for the two control problem occurs at approximately 9 months, when only 0.14% of the human population is infected. Disease relapse does not alter the timing and size of the epidemic peak; however it leads to a higher total proportion of vaccinated humans. The human disease dynamics are most similar to those for the one control problem with vaccination, as the majority of humans reside in the vaccinated class after $t = 10$ months. The vector

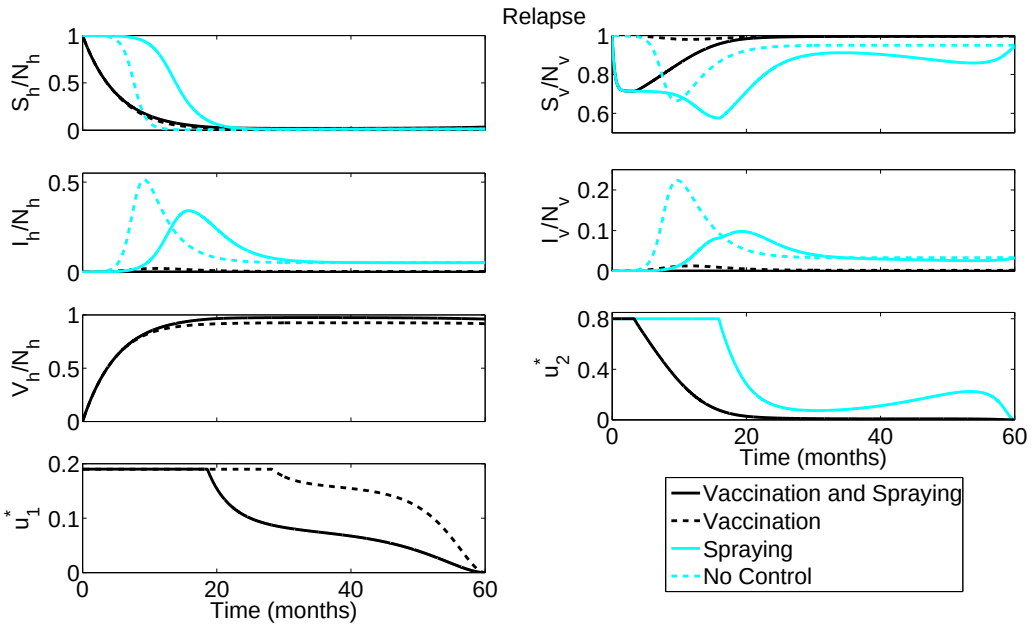

Figure 4-15: Optimal state solution and optimal control for the system (4.47)-(4.53) with both spraying and vaccination. $u_{1max} = 0.19$, $u_{2max} = 0.8$, $A_2 = A_3 = 20$ and human disease can relapse. Results are compared to those for the no control and one control cases. Disease parameters are fixed at the values given in Table (C.1).

disease dynamics are similar to those when spraying is the sole control. The application of both host and vector control greatly reduces the epidemic, and in all cases the epidemic was brought almost entirely under control.

In Figure (4-15) we find that when $t \leq 20$ the optimal vaccination strategy is identical for both the one and two control problems. Vaccination is employed at its maximum rate until the epidemic peaks in order to minimise the transmission rate of the disease, and reduce the number of individuals available to fuel the epidemic. Spraying is also employed at its maximum rate from $t = 0$ in the two control problem, but drops below this maximum level before the epidemic peaks. Since vaccination is the dominant and most efficient control, the rate of spraying in the two control problem is linked to the number of susceptible humans. Spraying drops below its maximum rate 14 months earlier in the two control problem, as there is no advantage to removing vectors from the system when there are no humans for them to infect. The rate of spraying is therefore high when a large proportion of humans are susceptible, and tends to zero as the proportion of susceptible humans tends to zero. The application of two simultaneous controls also reduces the time over which vaccination is applied at its maximum rate. The reduction in transmission and infection caused by the simultaneous application of both spraying and vaccination, coupled with the fact we now minimise

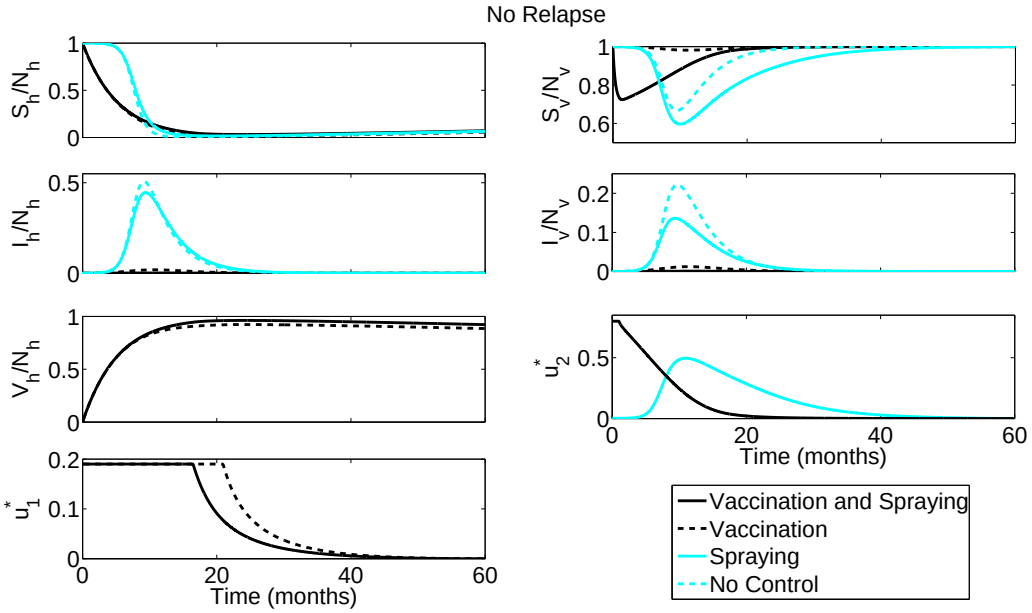

Figure 4-16: Optimal state solution and optimal control for the system (4.47)-(4.53) with both spraying and vaccination. $u_{1max} = 0.19$, $u_{2max} = 0.8$, $A_2 = A_3 = 20$ and human disease does not relapse. Results are compared to those for the no control and one control cases. Disease parameters are fixed at the values given in Table (C.1).

the costs of two controls leads to a reduction in the vaccination rate when $t > 20$.

In Figure (4-16) we find that when two controls are applied simultaneously the optimal vaccination strategy for non-relapsing disease is similar to that for the one control problem, however the optimal spraying strategy differs greatly. Since vaccination reduces the proportion of susceptible humans available to become infected, there is no longer a delay before spraying occurs and instead spraying begins at $t = 0$ when the number of susceptible hosts is at its highest. Results are similar to those obtained for relapsing disease in Figure (4-15). It is more advantageous to remove vectors when there are humans for them to infect and so the rate of spraying tends to zero as the proportion of susceptible humans tends to zero. In this case spraying increases the likelihood vaccination occurs before transmission.

The optimal vaccination strategy for the two control problem is also similar for both relapsing and non-relapsing infection. Vaccination is employed at its maximum level throughout the epidemic peak, then tails off to zero as the number of infections subsides. Vaccination is held at its maximum rate for a shorter duration when both vaccination and spraying are employed however, due to the reduction in infection prevalence and increased cost caused by applying two controls. The reduced cost of non-relapsing infection also reduces the time spent at maximum control compared to that for relapsing

infection in Figure (4-16).

We now investigate the impact of the cost of control relative to the cost of infection on the optimal control solution. We consider three cases; increasing the cost of spraying A_3 when the cost of vaccination $A_2 = 20$ is fixed, increasing the cost of vaccination A_2 when the cost of spraying $A_3 = 20$ is fixed, and increasing the cost of both vaccination A_2 and spraying A_3 simultaneously. When both costs are increased simultaneously, they are assigned the same value from a vector of increasing costs. Results are shown in Figure (4-17). Similar results can also be obtained for non-relapsing disease. The reduced cost of infection incurred by non-relapsing disease increases infection prevalence.

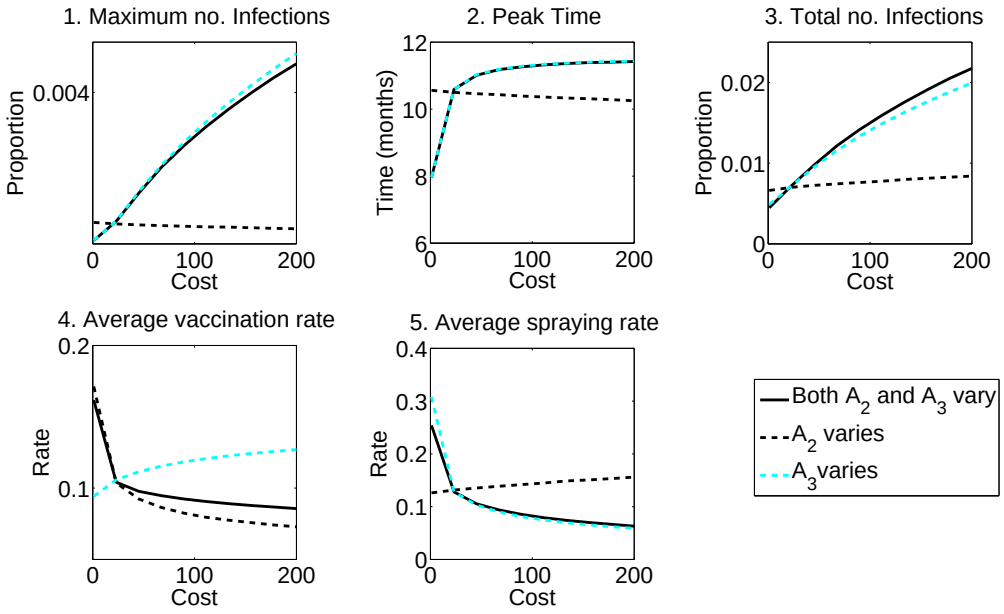

Figure 4-17: Relationship between the relative cost of vaccination A_2, spraying A_3 and: 1. The human epidemic peak. 2. Timing of the epidemic peak. 3. Total proportion of infected humans over the five year period. 4. The average rate of vaccination over the five year period and 5. The average rate of spraying over the five year period. $u_{1max} = 0.19$, $u_{2max} = 0.8$. Non-control parameters are fixed at the values given in Table (C.1). Disease relapse is present.

In Figure (4-17) we find that increasing the cost of both vaccination and spraying simultaneously leads to an increase in the number of infections, both at the epidemic peak and overall. The epidemic peak is also delayed. Increasing the cost of both controls decreases the average rates of spraying and vaccination, thus allowing more infection to occur. The lower the rate of the control the larger the susceptible population, and the greater the delay before the epidemic peak.

When the cost of vaccination is fixed and the cost of spraying A_3 varies, results for

panels 1-3 are similar to those for the case when both costs vary. Since vaccination is the dominant control, decreasing the rate of spraying by increasing its cost has little impact. Decreasing the rate of spraying does lead to a slight increase in the average vaccination rate however, as the optimal vaccination strategy is at maximum level u_{max} for longer to compensate for the increase in infections that would otherwise be prevented by spraying.

Increasing the cost of vaccination in the range $0 < A_2 < 200$ and fixing the cost of spraying $A_3 = 20$ leads to a slight reduction in the number of infections at epidemic peak, but increases the total number of human infections over the five year period. The time before the epidemic peak is also reduced. Increasing the cost of vaccination decreases the average rate of vaccination, but increases the average rate of spraying. Due to its inefficiency spraying is only applied at a higher level throughout the epidemic peak however, when the number of infections is high. This leads to a reduction in the number of infections at the peak, but does not prevent an overall increase in disease prevalence. The reduction in the level of vaccination caused by increased cost, coupled with the fact that increasing the rate of spraying does not prevent disease relapse leads to a higher proportion of human infections over the whole five year period. Increasing the cost of vaccination has a greater impact when two controls are applied since the cost of two treatments must be minimised.

4.5.2 Two Control Problem: Summary

The application of both host and vector control leads to a greater reduction in the number of human infections than when only one control is applied. Comparing human infection prevalence for both the no control and 2 control problems, we found that the simultaneous application of both spraying and vaccination led to a 99% reduction in human infection prevalence. This held true for both relapsing and non-relapsing infection. Vaccination led to a 96% reduction in infection prevalence, whereas spraying led to a 33% reduction for relapsing infection and a 13% reduction for non-relapsing infection. The optimal control strategy is again dependent on whether disease relapse is possible, with relapsing infection requiring a greater control effort. In both relapsing and non-relapsing infection the two controls are most effective when combined, particularly at the start of the infection and throughout the epidemic peak. This leads to a change in the shape of the optimal spraying strategy when relapse is absent, as there is no longer a delay before control is applied. Increasing the cost of spraying, or both controls simultaneously leads to an increase in the size of the epidemic peak, and delays the time at which it occurs.

4.6 Impact of Human Latency on Optimal Control

Although the duration of human latency had little impact on our equilibrium solutions in Chapter 2, it will influence time dependent solutions such as those used to calculate the optimal control. In order to investigate the potential impact of human latency on the optimal control we calculate example optimal control solutions for both one control and two control problems using our initial one-host one-vector model with latency (2.1)-(2.7) and the method outlined in Section (4.2.1). Results are displayed in Figures (4-18), (4-19) and (4-20).

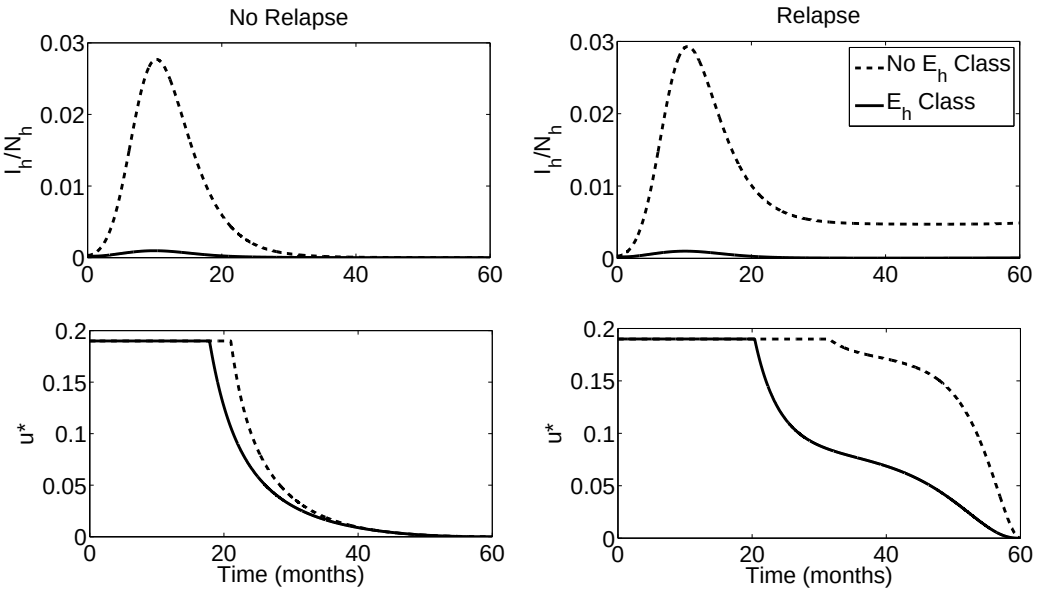

Figure 4-18: Optimal vaccination strategies for the one-host one-vector model (4.4)-(4.10) with and without human latency. Optimality condition (4.14), $u_{max} = 0.19$, $A = 20$. Non-control parameters are fixed at the values given in Table (C.1).Results are displayed for relapsing and non-relapsing disease.

In Figure (4-18) we compare the optimal vaccination strategy obtained for our one-host one-vector model without human latency to that obtained for our one-host one-vector model with human latency. We consider both relapsing and non-relapsing disease and find that in both cases the optimal control strategy is independent of latency for the first 20 months. After 20 months however, a lower level of control is applied when human latency is present. Human latency delays the time at which humans become infectious and allows a greater proportion of the susceptible population to be vaccinated before the epidemic arises. Decreasing the size of the susceptible population decreases the transmission rate of the disease, hence reducing both the size of the epidemic peak

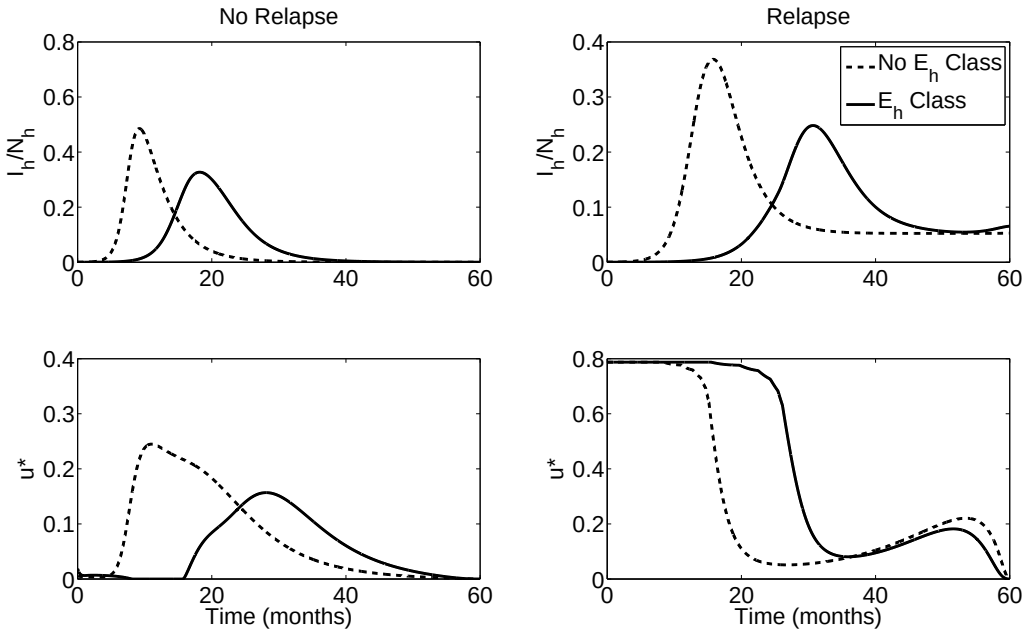

Figure 4-19: Optimal spraying strategies for the one-host one-vector model (4.30)-(4.35) with and without human latency. Optimality condition (4.37), $u_{max} = 0.8$, $A = 20$. Non-control parameters are fixed at the values given in Table (C.1). Results are displayed for relapsing and non-relapsing disease.

and the necessity of control. The greatest reduction in control occurs for relapsing disease. Decreasing the number of infectious individuals reduces the impact of relapse since fewer individuals are found in the recovered class. Consequently, the level of control drops. Human latency also leads to a slight reduction in the number of humans surviving to become infectious and so further decreases the number found in the I_h class.

In Figure (4-19) we compare optimal spraying strategies for our one-host one-vector model both with and without human latency. In the left hand column we find that the presence of human latency in non-relapsing disease increases the delay before control is applied, and also decreases the maximum level of control. Not all humans survive the latent period to become infectious and so the epidemic peak in humans is smaller in size. This leads to a reduction in the level of spraying applied. Since vector life expectancy is much shorter than that of humans, spraying is not employed before the epidemic peak. Human latency delays the epidemic peak hence increasing the delay before control is applied. In the case of relapsing disease we find that control is applied at a higher level for longer when a human latent class is present. Although human latency reduces the size of the epidemic peak, the additional delay before the epidemic

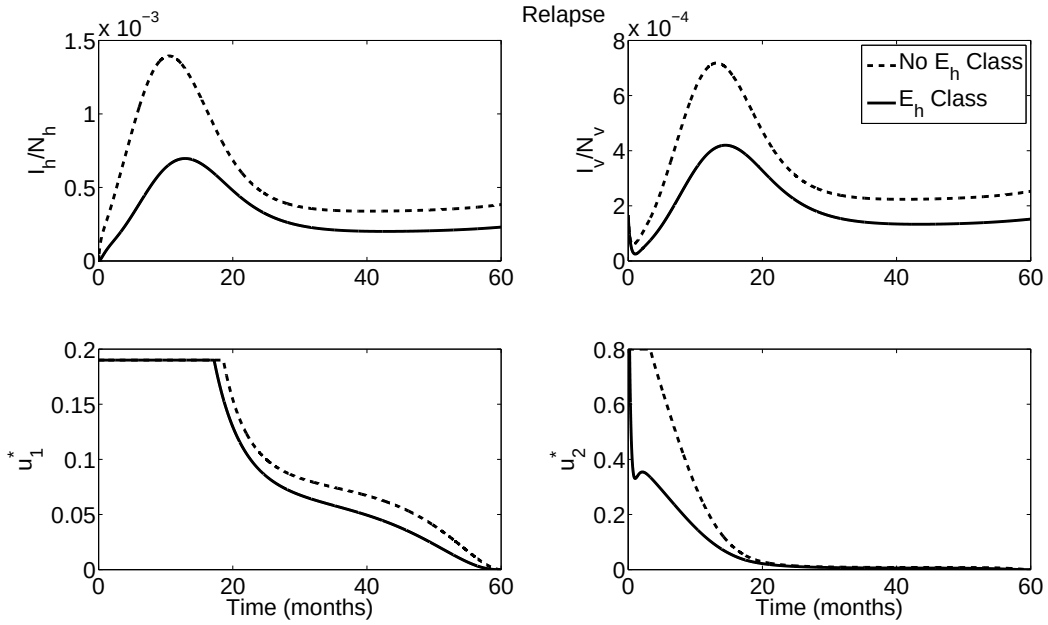

Figure 4-20: Optimal vaccination and spraying strategies for the one-host one-vector model (4.47)-(4.53) with and without human latency. $u_{1max} = 0.19$ $u_{2max} = 0.8$, $A_2 = A_3 = 20$. Disease parameters are fixed at the values given in Table (C.1). Relapse present.

peak increases the time over which control is applied at its maximum level. Applying control over this time reduces the detrimental impact of relapse by removing individuals who could otherwise become infected.

In Figure (4-20) we compute optimal vaccination and spraying strategies for the two control problem, both with and without human latency. The difference in the optimal vaccination strategy when latency is present is similar to that in Figure (4-18) for the one control problem. The delay before humans become infectious allows more susceptible humans to be removed from the system before transmission can occur, hence reducing the size of the epidemic peak and the control required after it subsides. Reducing the number of susceptible hosts also reduces the optimal spraying rate as the likelihood a vector infects a susceptible human is decreased and the benefit of reducing vector-host contacts is diminished. A similar plot can be produced for non-relapsing disease.

4.7 Conclusions

Results suggest that the largest reduction in Leishmania incidence is achieved by employing both host and vector control. Of the three controls considered in Chapter 4, the simultaneous application of both vaccination and spraying led to the largest drop

in the number of human infections, and greatly reduced the size of the epidemic peak. The most effective control began at its maximum rate, and did not reduce in level until after the epidemic peak had subsided. Increasing the cost of control reduced the level at which it was applied, and resulted in larger epidemics. In all cases considered the presence of disease relapse increased the level of control applied. The additional infections caused by relapsing hosts increase the cost of infection and hence the benefit of control. Relapsing infection is therefore more expensive to control.

When only one control was applied, vaccination proved most effective. If it were to become available, a human leishmaniasis vaccine could reduce both the size of the epidemic peak and the total number of human infections. The optimal control was again dependent on the cost of control. Decreasing the cost of control or increasing the maximum rate of control decreased the number of human infections. Spraying alone was not a beneficial control technique, even when its cost was relatively low. In order to be effective, spraying must occur at a much higher rate than vaccination. The benefits of reduced transmission caused by spraying are outweighed by the cost of the control. Since human life expectancy is much longer than that of the sandfly vector, the effects of vaccination last much longer than those of spraying. Vaccination can also be targetted at an easily identifiable and specific subpopulation, whereas the entire vector population must be targetted by spraying. The permanent removal of susceptible hosts via vaccination is particularly effective when disease can relapse. In this case vaccination prevents the relapsing infections which would otherwise maintain disease after the epidemic subsides.

The results of Chapter 4 can be used to suggest possible disease control techniques for vector-borne disease such as leishmaniasis. The application of any disease control technique can have negative evolutionary consequences however. The most common example is the evolution of antibiotic resistance. In many vector-borne diseases there is also an association between transmission and virulence [36]. Pathogens evolve heightened disease virulence in order to immobilise the host and increase the rate of vector transmission. The application of disease control which interrupts the transmission cycle may therefore lead to the fixation of highly virulent pathogen strains. In the next chapter we impose a trade-off between transmission and virulence in order to determine how the application of disease control impacts upon pathogen virulence.

Chapter 5

Evolutionary Consequences of Control

In previous chapters our models have been used to suggest control techniques for vector-borne diseases such as leishmaniasis. The application of some disease control techniques may not be beneficial in the long term however, as any perturbation to the system may have negative evolutionary consequences. In this chapter we use the theory of adaptive dynamics to investigate the evolution of virulence in vector-borne disease. We introduce a trade-off between transmission and virulence and assess the possibility a mutant pathogen strain can invade. Our aim is to identify control techniques that not only reduce disease spread and incidence, but also preclude the evolution of disease strains with heightened virulence. We begin by considering a trade-off between virulence in the host and the transmission rate from hosts to vectors. We investigate the relationship between disease virulence and individual model parameters in order to identify parameters for control. Using information from [71] we then introduce a new trade-off between virulence in the vector and the transmission rate from vectors to humans. Results are obtained for both the anthropontic and zoonotic models. We further our investigation by considering evolution in an amphixenotic model; a two-host one-vector model where both hosts are competent.

5.1 Adaptive Dynamics

Adaptive dynamics is a technique used to evaluate phenotypical evolution. Population dynamics are linked with an evolutionary analysis in order to determine the long-term effect of mutation upon a particular trait value [17].

It is first assumed that a resident population with trait value x has reached a

monomorphic equilibrium. A rare mutant with trait value y is then introduced and a fitness function is used to determine whether this rare mutant is able to invade the resident population. Letting $s_x(y)$ denote the fitness of some mutant phenotype y when invading a monomorphic resident population with phenotype x, equation (5.1) is a linear approximation for fitness:

$$s_x(y) = s_x(x) + D(x)(y - x) \tag{5.1}$$

where

$$D(x) = \left[\frac{\partial s_x(y)}{\partial y}\right]_{y=x} \tag{5.2}$$

is the local fitness gradient [31, 39].

The resident population at monomorphic equilibrium consists only of individuals with phenotype x, so the fitness of all individuals with phenotype x is $s_x(x) = k$. If $s_x(y) > k$ then the mutant can invade, and if $s_x(y) < k$ then the mutant will quickly die out. As such, the fate of the mutant strain can also be determined by considering the sign of $D(x)$. If $D(x) > 0$ mutants with $y > x$ can invade, and if $D(x) < 0$ mutants with $y < x$ can invade. It is assumed that an invading mutant excludes the resident strain and a new monomorphic equilibrium is attained before the next mutant appears. The trait value evolves in the direction of the local fitness gradient until it reaches an evolutionary singular strategy, or ESS, when $D(x) = 0$ [31, 39]. An ESS is a strategy that when adopted cannot be invaded by any other alternative strategy which is initially rare. In adaptive dynamics the invader strategy must also be nearby.

The evolutionary outcome of mutation can be visualised graphically using a pairwise invasion plot, or 'PIP'. By plotting the invasion fitness $s_x(y)$ against x and y, it allows us to determine which mutant trait values can invade, and to analyse any ESS which may occur. Plotting the invasion fitness for each possible combination of mutant and resident phenotypes reveals the shapes of zero contour lines at which $s_x(y) = k$, thus separating regions of invasion success $s_x(y) > k$ and failure $s_x(y) < k$. These regions can then be coloured, usually invasion $s_x(y) > k$ in black and no invasion $s_x(y) < k$ in white, to provide a picture of possible outcomes [31]. One zero contour is always $y = x$ since $s_x(x) = k$. Other information can also be obtained by considering a pairwise invasion plot (PIP). For example:

- Zero contours are termed neutral curves. ESS points occur at the intersections of neutral curves.
- If the vertical line through an ESS is (locally) entirely in the white region then the ESS is stable. This means that the ESS is an evolutionary trap and cannot

be invaded by other strategies.

- If the horizontal line through an ESS is (locally) entirely in the black region then the ESS is attainable. This means that the ESS can be attained via small evolutionary steps.

- If the line perpendicular to the leading diagonal at an ESS is (locally) entirely in the black region then mutual invisibility is possible close to the ESS i.e. two strains may co-exist close to the ESS. This is known as a dimorphism. If the ESS is unstable branching can occur, however if the ESS is stable dimorphism is transient.

5.1.1 Transmission-Virulence Trade-Off

In order to incorporate disease virulence into our model, we must first define it. According to [5], virulence is commonly defined by evolutionary biologists as the pathogen-induced host mortality. When virulence is independent of other disease parameters and processes, natural selection favours the evolution of minimum virulence. A reduction in host numbers caused by disease related death is not beneficial to pathogen survival, and so the pathogen evolves toward benignity. For many years it was believed that heightened virulence was a characteristic of novel infections which had not yet had time to evolve avirulence; however the introduction of the trade-off hypothesis in the early 1980s changed this line of thinking [5]. The trade-off hypothesis is based on the idea that pathogen virulence is a consequence of disease transmission [5]. It was suggested that a pathogen cannot increase transmission without incurring a cost, and so every value of transmission is associated with a virulence [5]. The trade-off between transmission and virulence is represented by a curve, the shape of which dictates the evolutionary outcome of the system. When the relationship between virulence and transmission is linear, the pathogen evolves to a state of heightened virulence. Increasing virulence will always increase transmission, and so potential disease spread is maximised. When the trade-off curve saturates, a finite optimal virulence exists. This is the ESS, described in Section (5.1). Empirical evidence supporting the existence of a transmission-virulence trade-off can be found in [6] and [36]. Examples of the implementation of transmission-virulence trade-offs can be found in [6], [30] and [48]. Although other virulence trade-offs exist, e.g. a recovery-virulence trade-off [5], we concentrate on a transmission-virulence trade-off in this work. Evidence for a transmission-virulence trade-off in vector-borne disease can be found in [6]. In [6] a within host model for malaria dynamics is used to show a saturating trade-off exists between host virulence and transmission. A convex trade-off is then used to asses the

potential impact of varying disease parameters on disease spread and control.

In the rest of this chapter we use adaptive dynamics to investigate the evolution of virulence in vector-borne disease when a saturating trade-off is in place between transmission and virulence. Defining virulence as the rate of pathogen induced mortality, we assume that transmission and virulence are linked due to their dependence on pathogen load. The higher the pathogen load, the greater the rate of disease induced mortality, but the higher the chance a sandfly will ingest a sufficient amount of the parasite for successful transmission to occur. Such increases in human pathogen load could be caused by a number of factors including an increased rate of pathogen multiplication, and the production of virulence factors which manipulate cell signalling pathways in such a manner that host immune defences are impaired.

We focus our investigation on virulence evolution in leishmaniasis. To our knowledge the evolution of virulence in leishmaniasis has not been previously studied in an adaptive dynamics framework. We begin by implementing a trade-off between virulence in the host, and the probability of transmission from host to vector. Phenotypes will be defined by their virulence, and virulence will vary continuously. We then investigate a new trade-off between virulence in the vector and the rate at which transmission occurs. We use our results to consider the evolutionary implications of control techniques such as those suggested in the elasticity analysis of Chapter 3. This will allow us to ensure that any control method employed will not favour the fixation of a disease strain with heightened virulence. It could perhaps be the case that the application of a particular control technique has short term benefits, but will lead to the fixation of a more virulent disease strain in the future.

In order to use adaptive dynamics we must first define a fitness function. Since the Leishmania protozoa grows in both host and vector simultaneously, $s_x(y)$ needs to be chosen in such a way that it takes into account growth rates in both species. To calculate the fitness gradient we use a quantity analogous to the basic reproductive number R_0 as a measure of overall pathogen growth. The invasion reproductive number R_x^y is the per generation multiplication number of the pathogen with virulence $\nu_h = y$, when invading a population at monomorphic equilibrium with $\nu_h = x$ and takes into account the growth of pathogen found in both host and vector populations. Since the resident population is at monomorphic equilibrium we know that the invasion reproductive number of strain x, is $R_x^x = 1$. This in turn means that $s_x(x) = 1$ and so if $R_x^y > 1$ the rare mutant strain y can invade, and if $R_x^y < 1$ the rare mutant cannot invade. Any ESS will occur when $R_x^y = 1$.

5.2 Virulence Evolution in the One Host Model

We begin by considering the one-host one-vector model (4.4)-(4.10), with humans as the sole host, sandflies as the vector and $u(t) = 0$. The evolution of virulence will be investigated when a concave trade-off of the form $\pi_v(\nu_h) = \frac{c\nu_h}{\nu_h+1}$, $0 < c < 1$ is imposed between the probability of transmission from host to vector π_v and the rate of human disease related death ν_h. Such a trade-off prevents the probability π_v taking values $\pi_v < 0$, or $\pi_v > 1$, and has not been previously considered. We multiply by some constant $0 < c < 1$ since factors such as limited nutrients and host immune responses limit the maximum attainable transmission probability.

Assuming a population at monomorphic equilibrium, where all individuals are infected with a resident strain with virulence x, we assess the possibility some rare mutant strain with virulence y can invade. The set of equations (4.4)-(4.10) is adapted to create the system (5.3)-(5.12) which includes both resident and mutant infections:

$$\begin{aligned}
\frac{dS_h}{dt} &= \mu_h N_h^0 - \frac{\beta\pi_h S_h(t)(I_{vx}(t) + I_{vy}(t))}{N_h(t)} - \mu_h S_h(t) && (5.3)\\
\frac{dI_{hx}}{dt} &= \frac{\beta\pi_h S_h(t) I_{vx}(t)}{N_h(t)} + \epsilon_h R_{hx}(t) - (\mu_h + \chi_h + x)\, I_{hx}(t) && (5.4)\\
\frac{dI_{hy}}{dt} &= \frac{\beta\pi_h S_h(t) I_{vy}(t)}{N_h(t)} + \epsilon_h R_{hy}(t) - (\mu_h + \chi_h + y)\, I_{hy}(t) && (5.5)\\
\frac{dR_{hx}}{dt} &= \chi_h I_{hx}(t) - (\epsilon_h + \mu_h)\, R_{hx}(t) && (5.6)\\
\frac{dR_{hy}}{dt} &= \chi_h I_{hy}(t) - (\epsilon_h + \mu_h)\, R_{hy}(t) && (5.7)\\
\frac{dS_v}{dt} &= \mu_v r_v N_h^0 - \frac{\beta S_v(t)(\pi_v(x) I_{hx}(t) + \pi_v(y) I_{hy})}{N_h(t)} - \mu_v S_v(t) && (5.8)\\
\frac{dE_{vx}}{dt} &= \frac{\beta\pi_v(x) S_v(t) I_{hx}(t)}{N_h(t)} - (\sigma_v + \mu_v) E_{vx}(t) && (5.9)\\
\frac{dE_{vy}}{dt} &= \frac{\beta\pi_v(y) S_v(t) I_{hy}(t)}{N_h(t)} - (\sigma_v + \mu_v) E_{vy}(t) && (5.10)\\
\frac{dI_{vx}}{dt} &= \sigma_v E_{vx}(t) - \mu_v I_{vx}(t) && (5.11)\\
\frac{dI_{vy}}{dt} &= \sigma_v E_{vy}(t) - \mu_v I_{vy}(t) && (5.12)
\end{aligned}$$

The subscript hp represents a host and vp a vector who has been or is infected with strain p, $p \in \{x, y\}$. When a mutant strain is present, the susceptible compartments must take into account infection caused by either of the two strains. Individuals infected

with strain x are considered separately from those infected with strain y, and additional disease compartments ensure the growth of the two different strains can be monitored. For simplicity, we assume that co-infection is not possible. The total population of hosts and vectors are represented by $N_h(t) = S_h(t) + I_{hx}(t) + I_{hy}(t) + R_{hx}(t) + R_{hy}(t)$ and $N_v(t) = S_v(t) + E_{vx}(t) + E_{vy}(t) + I_{vx}(t) + I_{vy}(t)$ respectively. In the absence of a mutant strain, system (5.3)-(5.12) simplifies to that of (4.4)-(4.10) without vaccination.

5.2.1 Methodology

With a system of equations in place, we now obtain the fitness of a rare mutant strain y when attempting to invade a monomorphic resident population infected with strain x. The single strain system represented by equations (4.4)-(4.10) is first solved to equilibrium with $\nu_h = x$ in order to extract the monomorphic endemic equilibrium for the resident strain. Setting $I_{hy} = R_{hy} = E_{vy} = I_{vy} = 0$, the set of equations (5.3)-(5.12) is then linearised about monomorphic equilibrium to construct the NGM in the case where a mutation has arisen and an individual infected with mutant strain y has been introduced to the system. The invasion reproductive number given by the spectral radius of this NGM will be our fitness function. In this case the fitness function $s_x(y) = R_x^y$ is the per generation multiplication number of the rare mutant y when invading a population infected only with resident strain x. For the one-host one-vector model:

$$R_x^y = \frac{\beta\sqrt{S_h^*(x)S_v^*(x)\pi_v(y)\pi_h\sigma_v\left(\epsilon_h+\mu_h\right)}}{N_h^*(x)\sqrt{\mu_v\left(\mu_v+\sigma_v\right)\left(\mu_h\left(\chi_h+\epsilon_h+y+\mu_h\right)+\epsilon_h y\right)}} \tag{5.13}$$

where $S_h^*(x)$, $S_v^*(x)$ and $N_h^*(x)$ represent the total number of susceptible humans, susceptible vectors and humans at strain x monomorphic equilibrium respectively. Differentiating R_x^y with respect to y, gives the local fitness gradient $D(x)$. Letting $y{=}x$ and solving $D(x) = 0$ for x we obtain the ESS virulence:

$$x^* = \sqrt{\frac{\mu_h\left(\mu_h+\epsilon_h+\chi_h\right)}{\mu_h+\epsilon_h}}. \tag{5.14}$$

We find that the ESS virulence (5.14) depends only on the parameters which govern the growth rate of the mutant strain y within the human population. The relapse rate ϵ_h, recovery rate χ_h and death rate μ_h govern the time hosts spend in the infectious class, and hence the time over which transmission and disease related death ν_h can occur. The dependence of the ESS on only three parameters means that control techniques aimed at any of the other parameters will not impact upon the virulence

of leishmaniasis infection. This means that under the assumptions made in this study, control techniques aimed at sandflies can be employed without having negative evolutionary impact on the disease related death rate in humans.

5.2.2 Pairwise Invasion Plot

Figure (5-1) shows an example of a PIP produced for the system (5.3)-(5.12). We plot the invasion fitness of a mutant strain y when invading a resident population of strain x. Regions where $R_x^y > 1$ and invasion is possible are shaded in black. Regions where $R_x^y < 1$ and invasion is not possible are shaded in white. In this example we use the parameter set given in Table (C.1), Appendix (C). Using the adaptive dynamics theory laid out in Section (5.1) we find that the ESS $x^* = 0.16$ is both attainable and convergent stable. Dimorphism is not possible.

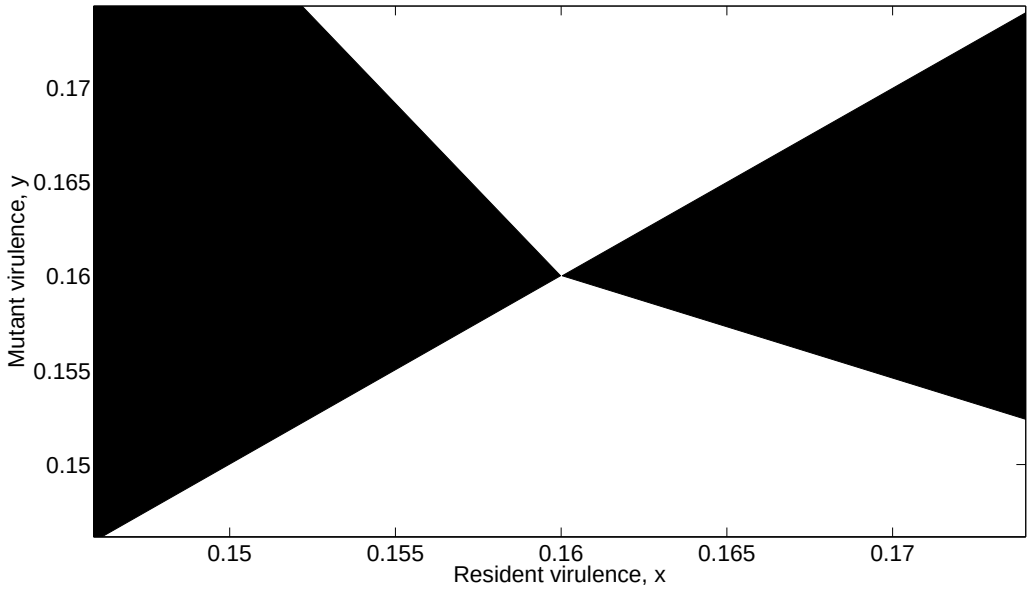

Figure 5-1: Example PIP for the one-host one-vector model (5.3)-(5.12) when host virulence is the evolving trait. A concave trade-off of the form $\pi_v(x) = \frac{cx}{x+1}$, $\pi_v(y) = \frac{cy}{y+1}$ is assumed between virulence in the host, and the probability of transmission from host to vector since both virulence and transmission depend on pathogen load. All other parameters are fixed at the values given in Table (C.1).

5.2.3 Investigating ESS Virulence

In order to examine the impact human disease control can have on disease virulence we use ESS virulence (5.14) to investigate the relationship between x^* and the three

parameters from which it is constructed. Results are displayed in Figure (5-2).

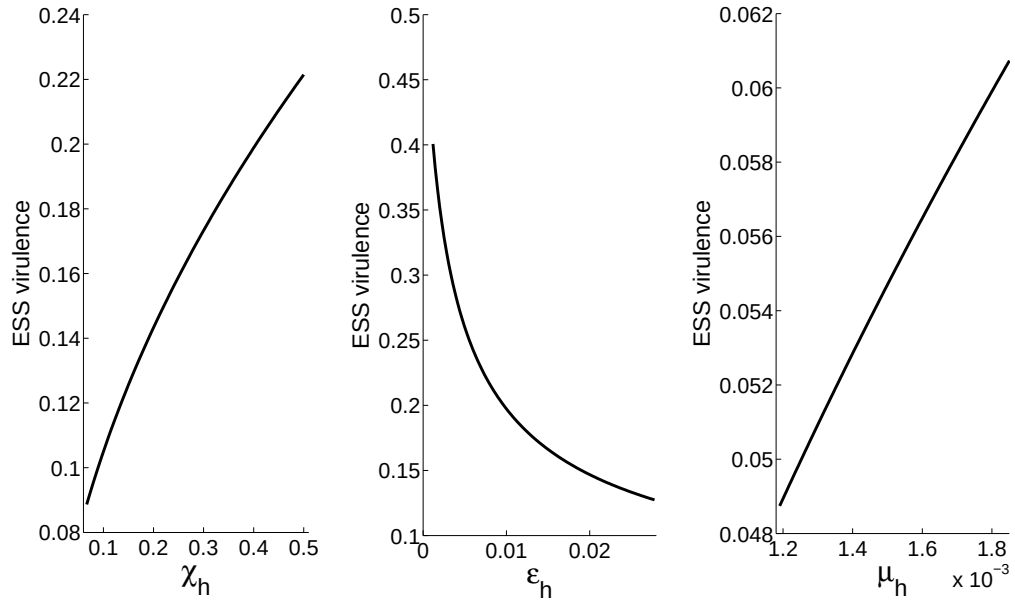

Figure 5-2: Relationship between the ESS virulence (5.14) for the one-host one-vector model (5.3)-(5.12), and the parameters from which it is constructed. A concave trade-off of the form $\pi_v(x) = \frac{cx}{x+1}$ is assumed between the probability of transmission π_v and human virulence x. Parameters that do not vary are fixed at the values given in Table (C.1).

Results in Figure (5-2) show that decreasing the duration of the infectious period in humans increases the ESS virulence. Increasing the recovery rate χ_h or the death rate μ_h increases the rate at which humans leave the infectious class, hence decreasing the time over which disease related death can occur. If virulence x remains constant, but acts for a shorter time period the total number of disease related deaths will be reduced. The relative impact of a fixed virulence x is reduced, and a higher virulence strain can be selected without increasing the effective probability of host mortality. Increasing the rate of relapse ϵ_h increases the expected duration of time spent in the infectious class over a whole lifetime and the exposure to disease related mortality. This leads to the selection of lower virulence pathogen strains.

The results in Figure (5-2) suggest that under the circumstances considered, control techniques aimed directly at the human population may not in fact be beneficial. Treatments aimed at reducing the relapse rate or increasing the recovery rate can lead to the fixation of Leishmania strains with heightened virulence. Control techniques aimed at targetting disease in the sandfly population should be employed to prevent the evolution of heightened virulence within the host.

5.3 Virulence in the Vector

In Section (5.2) we considered disease virulence within the host. One aspect of disease dynamics that is not often considered in vector-borne infections is virulence within the vector. Evidence presented in [71] suggests however that such a trade-off may in fact exist for some strains of Leishmania infection.

In [71], the authors discuss the results of several experiments aimed at investigating the behaviour of infected sandflies. Both uninfected and *L. infantum* and *L. mexicana* infected *Lu. longipalpis* were subjected to a number of tests designed to assess the impact of Leishmania infection upon fecundity, lifespan and different aspects of sandfly feeding. Although there was no significant difference in the reproductive ability of uninfected and infected flies, results of other tests suggest that the feeding behaviour of Leishmania infected sandflies is manipulated by the parasite in order to enhance its own transmission.

The first test looked at sandfly mortality rate. Measuring the lifespan of infected and uninfected flies under stressed and unstressed conditions, it was found that sandflies infected with Leishmania protozoa had significantly shorter lifespans than their uninfected counterparts. The median lifespan of infected flies under both stressed and unstressed conditions was 2 days less than that of uninfected flies; dropping from 7 days to 5 days in unstressed conditions and from 5 days to 3 days in stressed conditions.

Further tests were undertaken to investigate different aspects of feeding behaviour. It was determined that infected sandflies take 1.3-2.4 times longer to feed when compared to uninfected control flies, and are more likely to obtain a partial blood meal. Infected flies did not demonstrate increased probing, instead they often fed for longer until either full or discouraged. Furthermore, sandflies with an increased parasite load were found to have increased feeding persistence, as they made a significantly higher number of repeated feeding attempts when compared to control flies. Leishmania infection also promoted feeding on multiple hosts.

It was found that infection with Leishmania protozoa led to damage of the stomodeal valve, which is the valve that regulates blood intake during feeding. A plug of Leishmania protozoa forms to permanently hold the valve open, while distending the gut to cause blockages which limit the amount of blood that can be ingested when taking a blood meal. As a consequence, feeding persistence is positively correlated with the accumulation of the parasite, and infected individuals are more likely to take multiple feeds on multiple hosts.

In summary, the paper by Rogers and Bates, [71], provides experimental evidence that infection with Leishmania protozoa causes sandflies to alter their feeding behaviour

in a manner which enhances parasite transmission. Factors such as gut distension and stomodeal valve damage which cause this altered feeding behaviour, when coupled with the diversion of nutrient resources to parasite growth, reduce the lifespan of the infected sandfly vectors by increasing mortality above its natural rate.

5.4 Vector Virulence Trade-Off

To further our understanding of ESS virulence we incorporate the findings of Rogers and Bates [71] into our study. A disease related death term ν_v is introduced to the infectious sandfly compartments to allow us to consider the ESS virulence in the vector population. The previous trade-off between π_v and ν_h will be removed, and a new trade-off between the bite rate β and disease related death in the vector ν_v will be considered. Since we are considering the effect of altered feeding behaviour the bite rate β has been chosen for the trade-off rather than a transmission probability. Behavioural modifications such as increased feeding persistence and taking longer to feed will also affect both fly-human and human-fly transmission pathways. Once again, disease related mortality and transmission are dependent on parasite load.

We conjecture that the bite rate β increases concavely as virulence ν_v increases. As parasite load increases, the stomodeal block increases, and the size of blood meals taken decreases. This increases the rate of disease induced mortality. Reduced meal size also increases the bite rate as it leads to compensatory sandfly behaviour such as increased feeding persistence and an increased likelihood of feeding on multiple hosts. Due to physiological constraints such as the availability of hosts β levels out to a maximum level over time.

Incorporating a trade-off between β and virulence ν_v into a system with resident strain $\nu_v = x$ and mutant strain $\nu_v = y$, the system of equations (4.4)-(4.10) becomes:

$$\frac{dS_h}{dt} = \mu_h N_h^0 - \pi_h \left(\beta\left(x\right) I_{vx}(t) + \beta\left(y\right) I_{vy}(t)\right) \frac{S_h(t)}{N_h(t)} - \mu_h S_h(t) \tag{5.15}$$

$$\frac{dI_{hx}}{dt} = \beta\left(x\right) \pi_h I_{vx}(t) \frac{S_h(t)}{N_h(t)} - \left(\mu_h + \chi_h + \nu_h\right) I_{hx}(t) + \epsilon_h R_{hx}(t) \tag{5.16}$$

$$\frac{dI_{hy}}{dt} = \beta\left(y\right) \pi_h I_{vy}(t) \frac{S_h(t)}{N_h(t)} - \left(\mu_h + \chi_h + \nu_h\right) I_{hy}(t) + \epsilon_h R_{hy}(t) \tag{5.17}$$

$$\frac{dR_{hx}}{dt} = \chi_h I_{hx}(t) - \left(\mu_h + \epsilon_h\right) R_{hx}(t) \tag{5.18}$$

$$\frac{dR_{hy}}{dt} = \chi_h I_{hy}(t) - \left(\mu_h + \epsilon_h\right) R_{hy}(t) \tag{5.19}$$

$$\frac{dS_v}{dt} = \mu_v r_v N_h^0 - \pi_v S_v(t)\frac{(\beta(x)I_{hx}(t) + \beta(y)I_{hy}(t))}{N_h(t)} - \mu_v S_v(t) \tag{5.20}$$

$$\frac{dE_{vx}}{dt} = \beta(x)\,\pi_v S_v(t)\frac{I_{hx}(t)}{N_h(t)} - (\mu_v + \sigma_v)\,E_{vx}(t) \tag{5.21}$$

$$\frac{dE_{vy}}{dt} = \beta(y)\,\pi_v S_v(t)\frac{I_{hy}(t)}{N_h(t)} - (\mu_v + \sigma_v)\,E_{vy}(t) \tag{5.22}$$

$$\frac{dI_{vx}}{dt} = \sigma_v E_{vx}(t) - (\mu_v + x)\,I_{vx}(t) \tag{5.23}$$

$$\frac{dI_{vy}}{dt} = \sigma_v E_{vy}(t) - (\mu_v + y)\,I_{vy}(t) \tag{5.24}$$

where subscript hp once again represents a host and vp a vector who has been or is infected with strain p, $p \in \{x, y\}$. In the case of cutaneous leishmaniasis $\nu_h = 0$, and in visceral leishmaniasis $\nu_h > 0$.

Assuming the system of equations (5.15)-(5.24) has reached monomorphic equilibrium of resident strain x, and using the trade-off $\beta(x) = \dfrac{\hat{c}x}{x+1}$, $\hat{c} > 0$, we assess the possibility that a rare mutant strain with virulence y can invade. A reproductive number $R_x(y)$ is once again used as a measure of fitness and is calculated using the NGM created by linearising the system (5.15)-(5.24) about the monomorphic resident equilibrium when $I_{hy} = R_{hy} = E_{vy} = I_{vy} = 0$. The invasion fitness of the mutant is:

$$R_x^y = \frac{\hat{c}y\sqrt{S_h^*(x)S_v^*(x)\pi_v\pi_h\sigma_v\,(\epsilon_h + \mu_h)}}{(y+1)\,N_h^*(x)\sqrt{(\mu_v + \sigma_v)\,(\mu_v + y)\,(\mu_h\,(\chi_h + \epsilon_h + \nu_h + \mu_h) + \epsilon_h\nu_h)}}. \tag{5.25}$$

Differentiating the fitness function (5.25) with respect to y, gives the local fitness gradient $D(x)$. Setting $y{=}x$ and solving $D(x) = 0$ for x we obtain the ESS virulence:

$$x^* = \frac{1}{2}\left(1 + \sqrt{(8\mu_v + 1)}\right) \tag{5.26}$$

in both cutaneous and visceral cases.

Since vectors do not recover from infection, the duration of time in which disease related death can occur is governed by natural mortality μ_v alone. Figure (5-3) shows that increasing sandfly death rate, and thus reducing sandfly lifespan leads to the evolution of heightened virulence within the vector. Increasing the sandfly death rate μ_v reduces both the timespan over which disease transmission can occur, and the likelihood that latent sandflies survive to become infectious. As μ_v increases, a fixed value of ν_v causes fewer mortalities and as such heightened virulence can be selected. The selection of heightened virulence will also compensate for the drop in transmission

from flies to humans caused by reducing the duration of transmission.

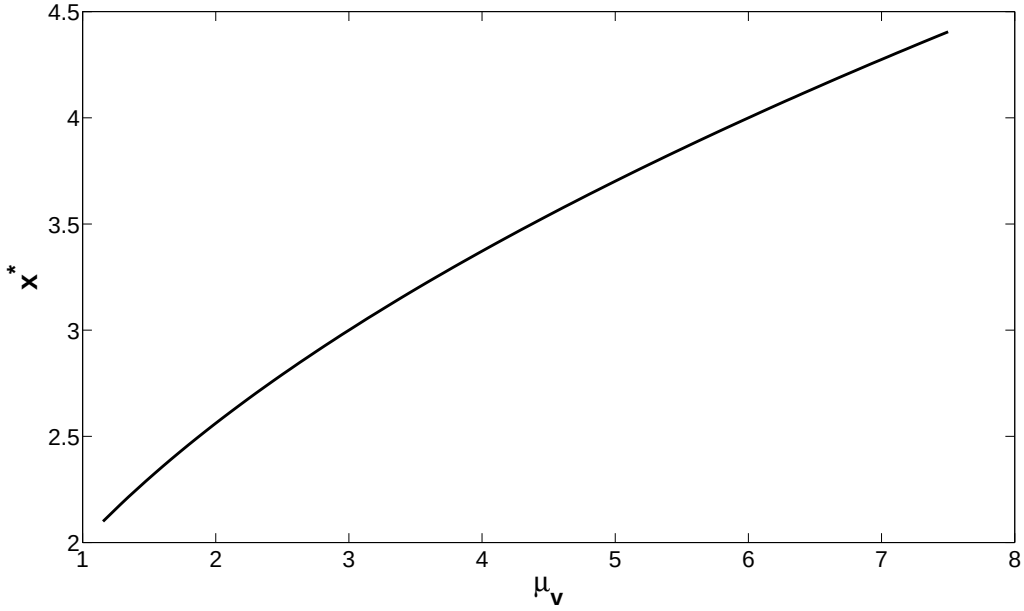

Figure 5-3: Relationship between the ESS virulence (5.26) and vector mortality μ_v for the one-host one-vector model (5.15)-(5.24). A concave trade-off of the form $\beta(x) = \frac{\hat{c}x}{x+1}$ is assumed between the bite rate β and vector virulence x. Parameters that do not vary are fixed at the values given in Table (C.1).

5.4.1 Consequences for Disease Control

In Chapter 4 we found that spraying must decrease sandfly life expectancy by at least 12.5 days to prevent an epidemic occurring in a one-host one-vector cutaneous leishmaniasis with relapse. A similar result can be calculated for visceral leishmaniasis with a trade-off between transmission and virulence (5.15)-(5.24). Including an additional death rate μ_s in all vector compartments (5.20)-(5.24) to represent spraying induced mortality, the basic reproductive number R_0 becomes:

$$R_0 = \frac{\hat{c}x\sqrt{r_v\mu_v\pi_h\pi_v\sigma_v\left(\epsilon_h+\mu_h\right)}}{\left(x+1\right)\sqrt{\left(\mu_s+\mu_v\right)\left(\mu_s+\mu_v+\sigma_v\right)\left(\mu_s+\mu_v+x\right)\left(\mu_h\left(\chi_h+\epsilon_h+\nu_h+\mu_h\right)+\epsilon_h\nu_h\right)}}. \tag{5.27}$$

Expression (5.27) for R_0 can then be maximised with respect to vector virulence x in order to obtain the ESS when a spraying regime is in place:

$$x^* = \frac{1}{2}\left(1+\sqrt{\left(8\left(\mu_v+\mu_s\right)+1\right)}\right). \tag{5.28}$$

The relationship between μ_s and x^* is similar to that between μ_v and x^* displayed in Figure (5-3). Since increasing μ_s increases the rate of vector mortality, increasing the rate of spraying induced mortality μ_s increases ESS virulence. Solving $R_0 = 1$ for μ_s we find that $\mu_s \geq 11.56$ is required in order for $R_0 < 1$ and an epidemic to be prevented. This equates to a 12 day reduction in vector life expectancy. The control effort required to prevent an epidemic is always highest when vector virulence is at ESS. A smaller control effort will therefore be required to obtain $R_0 < 1$ for sub-optimal virulences. We now asses the impact of increased vector virulence on human infection prevalence.

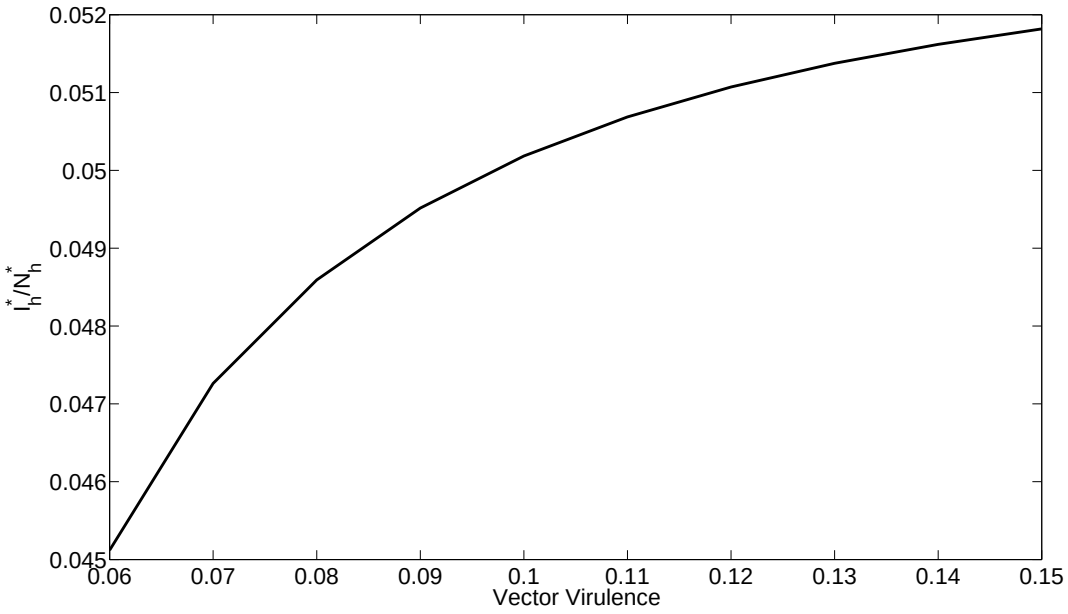

Figure 5-4: Relationship between vector virulence and human infection prevalence, one-host one-vector model (5.15)-(5.24). A concave trade-off of the form $\beta(x) = \frac{\hat{c}x}{x+1}$ is assumed between the bite rate β and vector virulence x. Parameters that do not vary are fixed at the values given in Table (C.1).

In Figure (5-4) we find that increasing the virulence in the vector leads to an increase in human infection prevalence. Results therefore suggest that when a concave trade-off is in place between the bite rate β and disease related death in flies ν_v, control techniques aimed at reducing sandfly life expectancy can in fact be counter productive. Techniques such as spraying must be maintained at a level which keeps R_0 below one for all time, else the application of control leads to the fixation of pathogen strains with heightened virulence and increases infection prevalence. In this case it may be more beneficial to target disease control techniques at the human population, as no human disease parameters influence the ESS virulence x^*. These results hold true

for both cutaneous and visceral anthroponotic leishmaniasis, since the ESS virulence takes the same form in both cases. The discrepancy between the control techniques suggested in Sections (5.2) and (5.4) highlights the need for further investigation into the transmission-virulence trade-off(s) governing the spread of vector-borne diseases such as leishmaniasis.

5.5 Finding ESS Virulence Using R_0 Maximisation

The ESS virulence obtained in Section (5.4) using the next generation matrix fitness function, may be verified using R_0 maximisation. Given that there is a trade-off between the bite rate β and disease related death ν_v in sandflies, the following expressions are obtained for the basic and effective reproductive numbers respectively:

$$R_0^y = \frac{\hat{c}y\sqrt{S_h^0 S_v^0 \pi_h \pi_v \sigma_v \left(\epsilon_h + \mu_h\right)}}{\left(y+1\right) N_h^0 \sqrt{\left(\mu_v + \sigma_v\right)\left(\mu_v + y\right)\left(\mu_h\left(\mu_h + \epsilon_h + \nu_h + \chi_h\right) + \epsilon_h \nu_h\right)}} \tag{5.29}$$

$$R_x^y = \frac{\hat{c}y\sqrt{S_h^*(x) S_v^*(x) \pi_h \pi_v \sigma_v \left(\epsilon_h + \mu_h\right)}}{\left(y+1\right) N_h^*(x) \sqrt{\left(\mu_v + \sigma_v\right)\left(\mu_v + y\right)\left(\mu_h\left(\mu_h + \epsilon_h + \nu_h + \chi_h\right) + \epsilon_h \nu_h\right)}} \tag{5.30}$$

where S_p^0 represents the total number of susceptible individuals of types $p \in \{h, v\}$ at disease free equilibrium, $S_p^*(x)$ represents the total number of susceptible individuals of types $p \in \{h, v\}$ at strain x monomorphic resident equilibrium, N_h^0 represents the total number of humans at disease free equilibrium, and $N_h^*(x)$ represents the total number of humans at strain x monomorphic equilibrium. Using the fact that $\mu_h, \hat{c}, \nu_h, \pi_h, \pi_v, \epsilon_h, \chi_h$ and σ_v are constant in both cutaneous and visceral cases, the above expressions can be simplified to give:

$$R_0^y = k\left(\frac{yS^0}{N_h^0\left(y+1\right)\sqrt{\mu_v + y}}\right) \tag{5.31}$$

and

$$R_x^y = k\left(\frac{yS_x^*}{N_h^*\left(y+1\right)\sqrt{\mu_v + y}}\right) \tag{5.32}$$

where

$$k = \frac{\hat{c}\sqrt{\pi_h \pi_v \sigma_v \left(\epsilon_h + \mu_h\right)}}{\sqrt{\left(\mu_v + \sigma_v\right)\left(\mu_h\left(\mu_h + \epsilon_h + \nu_h + \chi_h\right) + \epsilon_h \nu_h\right)}}, \tag{5.33}$$

$$S^0 = \sqrt{S_h^0 S_v^0} \tag{5.34}$$

and

$$S_x^* = \sqrt{S_h^*(x) S_v^*(x)} \tag{5.35}$$

Using the above equations we can prove that when there is a trade-off between the bite rate β and virulence ν_v the ESS virulence x^* can be obtained by maximising R_0^y with respect to the trait value y. The effective reproductive number R_x^y of the rare mutant strain when invading a monomorphic resident population with a susceptible population S_x^*, will only be above one if the basic reproductive number of the mutant strain is greater than the basic reproductive number of the resident strain.

Proposition: $R_x^y > 1 \Leftrightarrow R_0^y > R_0^x$.

Proof: We begin by noting that at monomorphic endemic equilibrium of strain x, $R_x^x = 1$, so that

$$R_x^y > 1 = R_x^x$$

Then:

$$\begin{array}{lccc} & R_x^y & > & R_x^x \\ \Leftrightarrow & \frac{kyS_x^*}{N_h^*(x)(y+1)\sqrt{\mu_v+y}} & > & \frac{kxS_x^*}{N_h^*(x)(x+1)\sqrt{\mu_v+x}} \\ \Leftrightarrow & \frac{y}{(y+1)\sqrt{\mu_v+y}} & > & \frac{x}{(x+1)\sqrt{\mu_v+x}} \\ \Leftrightarrow & \frac{kyS_x^0}{N_h^0(y+1)\sqrt{\mu_v+y}} & > & \frac{kxS_x^0}{N_h^0(x+1)\sqrt{\mu_v+x}} \\ \Leftrightarrow & R_0^y & > & R_0^x \end{array}$$

since $S_x^0, S_x^*, N_h^*, k > 0$.

Turning the inequality in $\frac{y}{(y+1)\sqrt{\mu_v+y}} > \frac{x}{(x+1)\sqrt{\mu_v+x}}$ into an equality, and solving for y in terms of x gives the neutral curves; the intersection of which occurs at the ESS virulence. Given that the size of the human population at disease free equilibrium is constant, expression (5.31) for R_0^y is the same in both cutaneous and visceral cases. Differentiating R_0^y with respect to y gives:

$$\frac{dR_0^y}{dy} = k\frac{\hat{c}\sqrt{N}}{2}\left(\frac{-y^3 + (2\mu_v + 1)\, y + 2\mu_v}{y^3 + y^2\,(\mu_v + 2) + y\,(2\mu_v + 1) + \mu_v}\right) \tag{5.36}$$

which may now be used to obtain the value of virulence that maximises R_0. Setting $\frac{dR_0^y}{dy} = 0$ and solving for y we obtain three solutions, only one of which is positive:

$$x^* = \frac{1}{2}\left(1 + \sqrt{8\mu_v + 1}\right) \tag{5.37}$$

This matches the ESS virulence obtained in Section (5.4). Given that $N_h(t) = N_h^*(0)$ at disease free equilibrium the same ESS values can be obtained by differentiating the expression for R_0^x with respect to x, setting to zero and solving for x.

5.6 Virulence Evolution in the Two Host model

We now consider the evolution of Leishmania virulence in the case of the two-host one-vector model, first presented in Chapter 2. Taking into account the results of the elasticity analysis in Chapter 3, the host latent classes are removed from (2.18)-(2.29) and we begin with the following system of equations:

$$\frac{dS_h}{dt} = \mu_h N_h^0 - \frac{\beta \pi_h S_h(t) I_v(t)}{N_h(t) + N_d(t)} - \mu_h S_h(t) \tag{5.38}$$

$$\frac{dI_h}{dt} = \frac{\beta \pi_h S_h(t) I_v(t)}{N_h(t) + N_d(t)} + \epsilon_h R_h(t) - (\mu_h + \chi_h + \nu_h) I_h(t) \tag{5.39}$$

$$\frac{dR_h}{dt} = \chi_h I_h(t) - (\mu_h + \epsilon_h) R_h(t) \tag{5.40}$$

$$\frac{dS_d}{dt} = \mu_d r_d N_h^0 - \frac{\beta \pi_d I_v(t) S_d(t)}{N_h(t) + N_d(t)} - \mu_d S_d(t) \tag{5.41}$$

$$\frac{dA_d}{dt} = (1 - \alpha_d) \frac{\beta \pi_d I_v(t) S_d(t)}{N_h(t) + N_d(t)} - \mu_d A_d(t) \tag{5.42}$$

$$\frac{dI_d}{dt} = \alpha_d \frac{\beta \pi_d I_v(t) S_d(t)}{N_h(t) + N_d(t)} + \epsilon_d R_d(t) - (\chi_d + \mu_d + \nu_d) I_d(t) \tag{5.43}$$

$$\frac{dR_d}{dt} = \chi_d I_d(t) - (\mu_d + \epsilon_d) R_d(t) \tag{5.44}$$

$$\frac{dS_v}{dt} = \mu_v r_v N_h^0 - \frac{\beta S_v(t)}{N_h(t) + N_d(t)} (\pi_d (I_d(t) + \omega_d A_d(t))) - \mu_v S_v(t) \tag{5.45}$$

$$\frac{dE_v}{dt} = \frac{\beta S_v(t)}{N_h(t) + N_d(t)} (\pi_d (I_d(t) + \omega_d A_d(t))) - (\mu_v + \sigma_v) E_v(t) \tag{5.46}$$

$$\frac{dI_v}{dt} = \sigma_v E_v(t) - \mu_v I_v(t) \tag{5.47}$$

As in the case of the one host model, the ability of a mutant strain to invade a monomorphic resident population will be analysed using adaptive dynamics. Trade-offs between virulence and transmission in both host and vector will be considered, but must now take into account the presence of multiple host species. We begin by considering a trade-off between virulence in the vector and the bite rate β.

5.6.1 Virulence in the Vector

When disease related death $\nu_v \in \{x, y\}$ is present in the sandfly population and a concave trade-off $\beta(\nu_v) = \frac{\hat{c}\nu_v}{\nu_v+1}$ is implemented, the ESS virulence can again be calculated using R_0 maximisation. Using a Next Generation Matrix to calculate R_0 for the resident system and solving $\dfrac{dR_0}{dx} = 0$ for x, we find that the ESS virulence is $x^* = \frac{1}{2}\left(1 + \sqrt{(8\mu_v + 1)}\right)$. The presence of an additional host species does not affect the evolution of virulence in the vector. The relationship between μ_v and x^* is the same as that shown in Figure (5-3), and no parameters other than the sandfly death rate μ_v change the ESS virulence. This holds true for any concave trade-off. As in Section (5.4), the reduction in the lifespan of the sandfly reduces both the likelihood that latent sandflies survive to become infectious and the time period over which ν_v can act. As μ_v increases a fixed value of ν_v leads to fewer mortalities as its impact is diluted. A heightened ν_v can therefore be selected as the point at which there is diminishing returns between the transmission and duration of infection is increased.

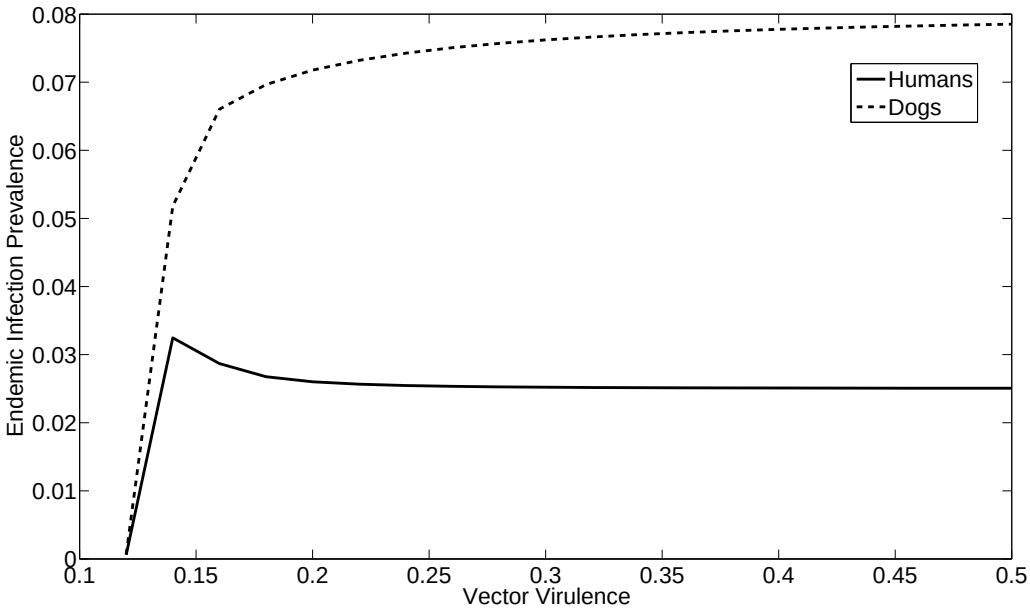

Figure 5-5: Relationship between virulence in the vector and the endemic infection prevalence in both humans and dogs. Two-host one-vector zoonosis model (5.48)-(5.64) under a concave trade-off of the form $\beta(x) = \frac{\hat{c}x}{x+1}$. All parameters that do not vary are fixed at the values given in Table (C.1).

In Figure (5-5) we see that increasing disease virulence in the vector leads to increased infection prevalence in the host species. This is similar to results for the anthroponotic model, and reduces the efficacy of vector control.

5.7 Virulence in the Host

We now investigate a trade-off between virulence in the hosts, ν_h and ν_d, and the probability of transmission from host to vector. We consider both the zoonotic model previously described in Section (5.6), and a model for amphixenotic disease. An amphixenosis is a disease where both human and non-human host are competent and have the ability to infect the vector species. In Morocco both humans and dogs are suspected reservoir hosts for *L.tropica* [79]. It is also stated in [4] that transmission can be partially anthroponotic, suggesting a situation where humans are not the sole competent host.

The two-host two strain model (5.38)-(5.47) must first be adapted to take into account the new transmission-virulence trade-off. Disease related death in the vector is removed, and the probability of transmission from infectious hosts to susceptible sandflies becomes dependent on host virulence. We introduce the parameters π_{vh} and π_{vd} to represent the probability of transmission to vectors by humans and dogs respectively. The new system can be represented by equations (5.48)-(5.64).

$$\frac{dS_h}{dt} = \mu_h N_h^0 - \frac{\pi_h S_h(t)\beta(I_{vx}(t) + I_{vy}(t))}{N_h(t) + N_d(t)} - \mu_h S_h(t) \tag{5.48}$$

$$\frac{dI_{hx}}{dt} = \frac{\beta\pi_h S_h(t) I_{vx}(t)}{N_h(t) + N_d(t)} + \epsilon_h R_{hx}(t) - (\mu_h + \chi_h + \nu_h(x))\, I_{hx}(t) \tag{5.49}$$

$$\frac{dI_{hy}}{dt} = \frac{\beta\pi_h S_h(t) I_{vy}(t)}{N_h(t) + N_d(t)} + \epsilon_h R_{hy}(t) - (\mu_h + \chi_h + \nu_h(y))\, I_{hy}(t) \tag{5.50}$$

$$\frac{dR_{hx}}{dt} = \chi_h I_{hx}(t) - (\mu_h + \epsilon_h)\, R_{hx}(t) \tag{5.51}$$

$$\frac{dR_{hy}}{dt} = \chi_h I_{hy}(t) - (\mu_h + \epsilon_h)\, R_{hy}(t) \tag{5.52}$$

$$\frac{dS_d}{dt} = \mu_d r_d N_h^0 - \frac{\pi_d(I_{vx}(t) + I_{vy}(t))\beta S_d(t)}{N_h(t) + N_d(t)} - \mu_d S_d(t) \tag{5.53}$$

$$\frac{dA_{dx}}{dt} = (1 - \alpha_d)\, \frac{\beta\pi_d I_{vx}(t) S_d(t)}{N_h(t) + N_d(t)} - \mu_d A_{dx}(t) \tag{5.54}$$

$$\frac{dA_{dy}}{dt} = (1 - \alpha_d)\, \frac{\beta\pi_d I_{vy}(t) S_d(t)}{N_h(t) + N_d(t)} - \mu_d A_{dy}(t) \tag{5.55}$$

$$\frac{dI_{dx}}{dt} = \alpha_d \frac{\beta\pi_d I_{vx}(t) S_d(t)}{N_h(t) + N_d(t)} + \epsilon_d R_{dx}(t) - (\chi_d + \mu_d + \nu_d(x))\, I_{dx}(t) \tag{5.56}$$

$$\frac{dI_{dy}}{dt} = \alpha_d \frac{\beta\pi_d I_{vy}(t) S_d(t)}{N_h(t) + N_d(t)} + \epsilon_d R_{dy}(t) - (\chi_d + \mu_d + \nu_d(y))\, I_{dy}(t) \tag{5.57}$$

$$\frac{dR_{dx}}{dt} = \chi_d I_{dx}(t) - (\mu_d + \epsilon_d)\, R_{dx}(t) \tag{5.58}$$

$$\frac{dR_{dy}}{dt} = \chi_d I_{dy}(t) - (\mu_d + \epsilon_d) R_{dy}(t) \tag{5.59}$$

$$\frac{dS_v}{dt} = \mu_v r_v N_h^0 - \frac{\beta S_v(t)}{N_h(t) + N_d(t)} (\pi_{vh}(x) I_{hx}(t) + (\pi_{vd}(x) I_{dx}(t) + \pi_d \omega_d A_{dx}(t))) - \frac{\beta S_v(t)}{N_h(t) + N_d(t)} (\pi_{vh}(y) I_{hy}(t) + (\pi_{vd}(y) I_{dy}(t) + \pi_d \omega_d A_{dx}(t))) - \mu_v S_v(t) \tag{5.60}$$

$$\frac{dE_{vx}}{dt} = \frac{\beta S_v(t)}{N_h(t) + N_d(t)} (\pi_{vh}(y) I_h(t) + (\pi_{vd}(y) I_d(t) + \pi_d \omega_d A_d(t))) - (\mu_v + \sigma_v) E_v(t) \tag{5.61}$$

$$\frac{dE_{vy}}{dt} = \frac{\beta S_v(t)}{N_h(t) + N_d(t)} (\pi_{vh} I_h(t) + (\pi_{vd}(y) I_d(t) + \pi_d \omega_d A_d(t))) - (\mu_v + \sigma_v) E_v(t) \tag{5.62}$$

$$\frac{dI_{vx}}{dt} = \sigma_v E_v(t) - \mu_v I_v(t) \tag{5.63}$$

$$\frac{dI_{vy}}{dt} = \sigma_v E_v(t) - \mu_v I_v(t) \tag{5.64}$$

We again consider a concave trade-off of the form $\pi = \frac{c\nu}{\nu+1}$; however the trade-off must now be implemented for both infected human and dog hosts. Transmission from asymptomatic dogs to sandflies is excluded from the trade-off, and the probability infection is passed from A_d to a sandfly is constant. We exclude the asymptomatic dogs on the basis that they have genetic immunity which prevents large increases in pathogen load; particularly when mutations are small. It is also observed in [1] that approximately 42% of infectious dogs showed symptoms of infection. This percentage could not be so high if virulence increased ad infinitum and quickly removed infected dogs.

When asymptomatic dogs are excluded from the transmission-virulence trade-off an ESS is obtained for a concave trade-off. When asymptomatic dogs are included in the trade-off and the terms $\omega_d A_{dx}(t)$ and $\omega_d A_{dy}(t)$ are multiplied by $\pi_{vd}(x)$ and $\pi_{vd}(y)$ respectively, there is no ESS. In this case the absence of a disease related death term in A_d means there is no negative consequence for the pathogen when replicating within A_d, yet there is still a transmission gain via π_{vd}. A heightened virulence will always be selected. Even if individuals in I_d and I_h are lost by increasing virulence, transmission can continue, and increase, via asymptomatic dogs. See Figure (5-6) for an example PIP. In this particular scenario, the culling of asymptomatic dogs would reduce pathogen virulence.

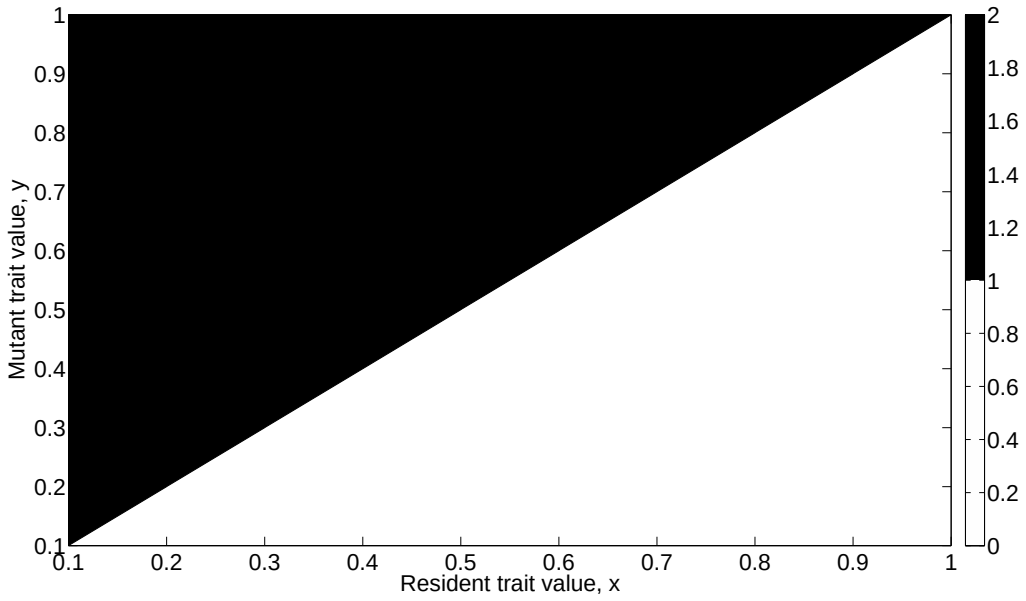

Figure 5-6: An example PIP showing the evolution of heightened virulence when A_d is included in the trade-off between host virulence and the probability of transmission from host to vector. Two-host one-vector zoonosis model (5.48)-(5.64). All parameters are fixed at the values given in Table (C.1).

5.7.1 Zoonotic Case

We begin by considering the two host model (5.48)-(5.64) when disease spread is zoonotic and humans are incidental hosts. In this case $\nu_d(x) = x$, $\nu_d(y) = y$, $\pi_{vd}(x) = \frac{cx}{x+1}$, $\pi_{vd}(y) = \frac{cy}{y+1}$, but $\nu_h = k$ and $\pi_{vh} = 0$, where $k \geq 0$ some constant. Since humans do not transmit infection they are excluded from the trade-off, and we only consider the evolution of virulence in the non-human host. Disease induced mortality in humans is present but constant to allow for visceral infection. The reproduction numbers R_0 and R_x for the zoonotic model are as follows:

$$R_0^y = \frac{\sqrt{S_v^0 S_d^0}}{\left(N_h^0 + N_d^0\right)} \sqrt{k_1 + \frac{k_2 y}{(y+1)\left(\mu_d\left(k_3 + y\right) + \epsilon_d y\right)}}$$

and

$$R_x^y = \frac{\sqrt{S_v^*(x) S_d^*(x)}}{\left(N_h^*(x) + N_d^*(x)\right)} \sqrt{k_1 + \frac{k_2 y}{(y+1)\left(\mu_d\left(k_3 + y\right) + \epsilon_d y\right)}}$$

where

$$k_1 = \frac{\beta^2 \pi_d^2 \omega_d \sigma_v (1-\alpha_d)}{\mu_d \mu_v (\mu_v + \sigma_v)}$$

$$k_2 = \frac{\beta^2 \pi_d c \alpha_d \sigma_v (\epsilon_d + \mu_d)}{\mu_v (\mu_v + \sigma_v)}$$

$$k_3 = \mu_d + \chi_d + \epsilon_d$$

As before, it is straightforward to show that $R_x^y > 1$ if and only if $R_0^y > R_0^x$. The ESS virulence can therefore be obtained by maximising R_0^x with respect to x. Solving $\frac{dR_0^x}{dx} = 0$ for x we obtain the following expression for the ESS for zoonotic leishmaniasis:

$$x^* = \frac{\sqrt{\mu_d (\epsilon_d + \mu_d)(\chi_d + \epsilon_d + \mu_d)}}{\epsilon_d + \mu_d} \tag{5.65}$$

As in the case of anthroponotic leishmaniasis with a trade-off between host virulence and transmission from host to vector, we see that the ESS depends only on the parameters which control the duration of the infectious period in the competent host. Further analysis can be found in Section (5.7.2). Figures (5-7), and (5-8) show the relationship between μ_d, χ_d, ϵ_d and ESS virulence x^*.

5.7.2 Amphixenotic Leishmaniasis

We now investigate the the impact of a transmission-virulence trade-off on ESS virulence in amphixenotic disease. In the case of amphixenotic leishmaniasis the virulence of the infection need not be equal in all host species. The pathogen may be better at evading the host immune responses of one particular species, at a cost to its ability of evading those of the other. To take this into account we again assume a concave trade-off of the form $\pi_{vh} = \frac{c\nu_h}{\nu_h+1}$, $\pi_{vd} = \frac{c\nu_d}{\nu_d+1}$, and introduce the parameter q which controls the ratio of human virulence to dog virulence. Three different cases will be considered:

- Amphixenotic transmission where virulence is equal in both host species i.e. $\nu_h = \nu_d = x$ is the disease related death rate in hosts infected with resident strain x.
- Amphixenotic transmission where virulence is greater in dogs than humans. $\nu_h = x$, $\nu_d = qx$ for some $q > 1$.
- Amphixenotic transmission where virulence is greater in humans than dogs. $\nu_h = x$, $\nu_d = qx$ for some $q < 1$.

5.7.3 Calculating ESS Virulence

Due to the complexity of the system (5.48)-(5.64), we are unable to obtain an analytic solution for the monomorphic resident equilibrium. In the case where we have a trade-off between host virulence and the probability of transmission from host to vector we are also unable to prove that R_0 maximisation can be used to calculate the ESS. The fitness function R_x^y is of the form:

$$R_x^y = \frac{\sqrt{S_v^*}}{N_h^* + N_d^*}\sqrt{\frac{k_1 S_h^* y}{(y+1)\,\mu_h\,(y+k_4) + \epsilon_h y} + \frac{k_3 S_d^* y}{(qy+1)\,\mu_d\,(qy+k_5) + \epsilon_d qy} + k_2 S_d^*} \tag{5.66}$$

where:

$$\begin{aligned}
k_1 &= \frac{\beta^2 c \pi_h \sigma_v\,(\epsilon_h + \mu_h)}{\mu_v\,(\mu_v + \sigma_v)} \\
k_2 &= \frac{\beta^2 \omega_d \pi_d^2 \sigma_v\,(1-\alpha_d)}{\mu_d \mu_v\,(\mu_v + \sigma_v)} \\
k_3 &= \frac{\beta^2 \alpha_d \pi_d \sigma_v c\,(\epsilon_d + \mu_d)\,q}{\mu_v\,(\mu_v + \sigma_v)} \\
k_4 &= \chi_h + \epsilon_h + \mu_h \\
k_5 &= \chi_d + \epsilon_d + \mu_d.
\end{aligned}$$

The mutant virulence y cannot be separated from the compartment sizes S_h^* etc. at monomorphic resident equilibrium, and as such a proof dependent on being able to divide through by $S_x^* > 0$ as in Sections (5.6.1) and (5.7.1) cannot be constructed. Instead, a numerical method to find ESS virulence is introduced in Section (5.7.4).

5.7.4 Numerical Method for Calculating ESS Virulence

The following pseudocode details the numerical method used to obtain estimates of ESS virulence:
A parameter of interest is chosen e.g. $\mu_h, \epsilon_d, \chi_d$ etc. and a vector of values is created for this parameter. For each entry of the vector the following is undertaken:

1. Input parameter values/intervals .
2. Linearise the resident only system about disease free equilibrium to obtain a next generation matrix. R_0^x is the largest eigenvalue of this matrix.
3. Differentiate R_0^x with respect to x.

4. Set $\frac{dR_0^x}{dx} = 0$ and solve for x. This gives $\hat{x}$, the value of x which maximises R_0.

5. Calculate the monomorphic equilibrium for a resident strain with virulence $x = \hat{x}$. We will use $\hat{x}$ as a starting point to find x^* in order to reduce computational time. If $\hat{x}$ cannot be calculated any starting value of $x = \hat{x}$ can be used.

6. Introduce a mutant strain y to the system. Linearise the mutant system about strain $\hat{x}$ monomorphic equilibrium, and use to obtain a next generation matrix. The largest eigenvalue of this matrix is $R_{\hat{x}}^y$.

7. Create a vector $y_i = [y_1, y_2, y_3] = [\hat{x} - \Delta x, \hat{x}, \hat{x} + \Delta x]$ of virulence values. In our case $\Delta x = 0.0005$.

8. Calculate $R_{\hat{x}}^{y_i}$ for each value of y contained within y_i.

9. If $R_{\hat{x}}^{y_1} > R_{\hat{x}}^{y_2}$ then $\hat{x}$ is not the ESS virulence. Repeat steps (5)-(8) for $\hat{x} = y_1$ until $R_{\hat{x}}^{y_1} < R_{\hat{x}}^{y_2=\hat{x}}$. $\hat{x}$ is our estimate for the ESS.

10. Alternatively if $R_{\hat{x}}^{y_3} > R_{\hat{x}}^{y_2}$ then $\hat{x}$ is not the ESS virulence. Repeat steps (5)-(8) for $\hat{x} = y_3$ until $R_{\hat{x}}^{y_3} < R_{\hat{x}}^{y_2=\hat{x}}$. $\hat{x}$ is our estimate for the ESS virulence.

The code is run through three times. Once for each of $q = 1$, $q = 0.5$, and $q = 3$.

5.8 ESS and Lower Level Parameters

Figures (5-7) and (5-8) show the relationship between ESS virulence x^* and the parameters from which it is constructed. The numerical method detailed in Section (5.7.4) was used to calculate the ESS virulence for both zoonotic and amphixenotic leishmaniasis when individual parameters were varied. The three types of amphixenotic leishmaniasis outlined in Section (5.7.2) were considered. When a parameter was not the subject of investigation it was fixed at the value given in Table (C.1).

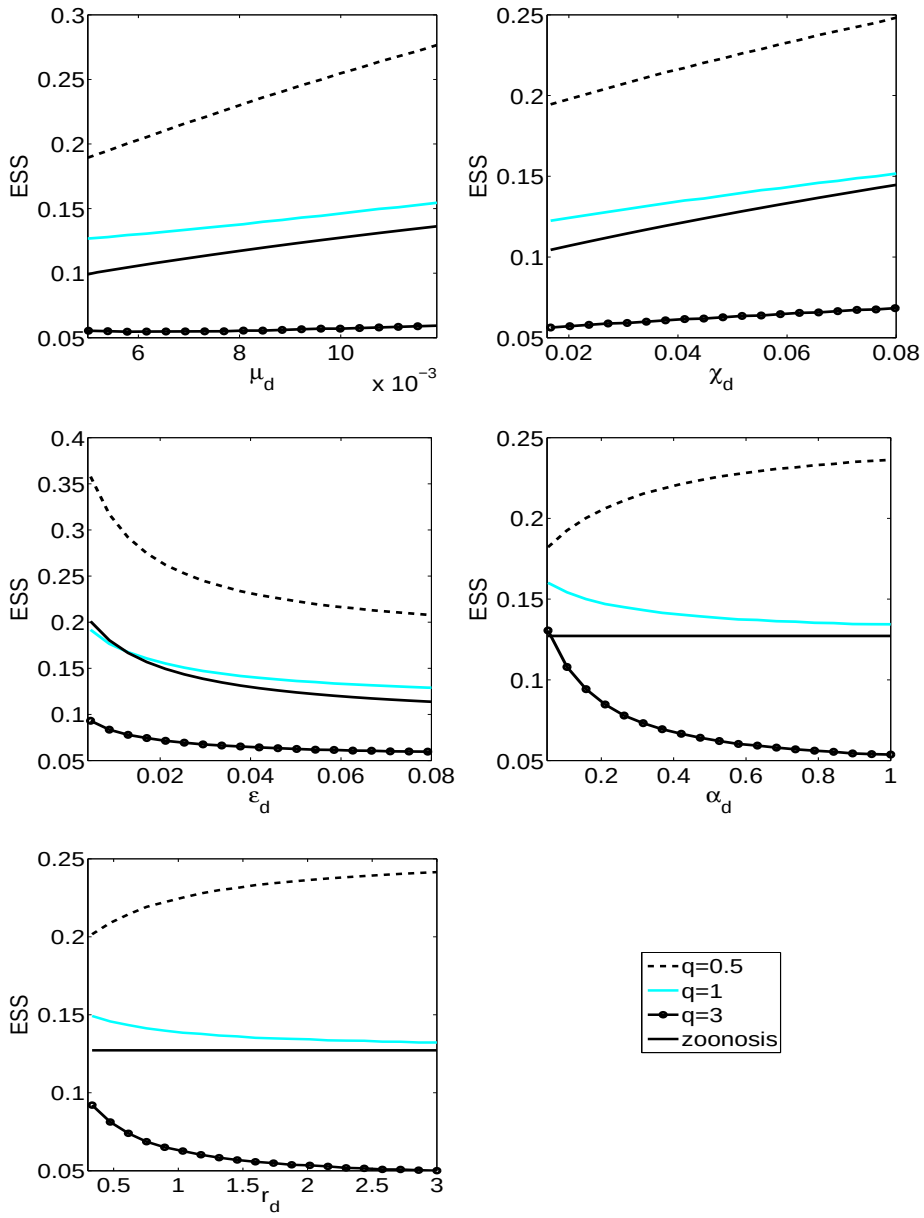

Figure 5-7: Relationship between the dog mortality rate μ_d, dog recovery rate χ_d, dog relapse rate ϵ_d, proportion of infected dogs that become infectious α_d, ratio of dogs to humans r_d, and the host ESS for the two-host one-vector model (5.48)-(5.64) when a concave trade-off of the form $\pi_v(x) = \frac{cx}{x+1}$ is in place between the virulence in the host and transmission from host to vector. Results are plotted for a zoonosis ($q = 0$), an infection best adapted to humans ($q = 0.5$), an infection best adapted to dogs ($q = 3$), and an infection which is equally virulent in both host species ($q = 1$). When a parameter is not varied it is fixed at the value given in Table (C.1).

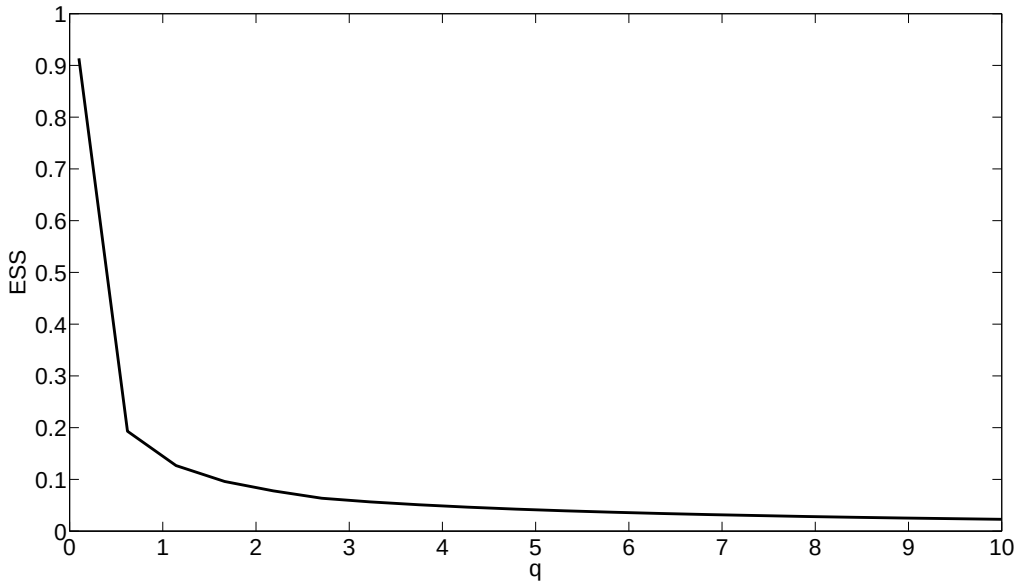

Figure 5-8: Relationship between virulence scaling factor q and the ESS for the amphixenotic two-host one-vector model (5.48)-(5.64) when a concave trade-off of the form $\pi_v(x) = \frac{cx}{x+1}$ is in place between the virulence in the host and transmission from host to vector. Transmission is amphixenotic. When a parameter is not varied it is fixed at the value given in Table (C.1).

In Figure (5-7) we again find that decreasing the duration of the infectious period in the competent host leads to the fixation of higher virulence pathogen strains. This matches the results obtained for the one-host one-vector model in Section (5.2.3). Increasing the recovery rate χ_d or death rate μ_d reduces the exposure of dogs to disease related death thus diluting the impact of virulence and reducing transmission. Increasing the relapse rate ϵ_d increases the number of visits the competent host makes to the infectious class and hence the exposure to disease related death. This leads to the fixation of lower virulence strains of infection. Similar plots are produced for human counterparts μ_h, χ_h and ϵ_h in the amphixenotic cases, when a trade-off between host virulence and transmission from host to vector is assumed. The point at which diminishing returns occurs and increasing virulence no longer increases disease transmission is altered when varying any of χ_h, χ_d, μ_h, μ_d, ϵ_h or ϵ_d.

The ESS virulence in the amphixenotic case is not only dependent upon the parameters which determine the duration of the infectious period in competent hosts, but also the proportion of competent hosts in the system. Figure (5-7) shows the relationship between ESS virulence x^* and the proportion of infected dogs that become symptomatically infectious α_d. We see that the shape of the curve is dependent upon the value of q. When $q > 1$ and infection is best adapted to dogs, increasing α_d de-

creases ESS virulence. When $q < 1$ and infection is best adapted to humans, increasing α_d increases ESS virulence. In both cases increasing α_d increases the proportion of symptomatic dogs and the exposure to disease related death. When $q > 1$ and disease related death in dogs is high, the duration of transmission is greatly reduced by this increased exposure and so reduced virulence is selected. When $q < 1$ the relative impact of a fixed virulence value is reduced. A higher virulence value can be selected in order to maximise transmission.

Figure (5-7) also shows the relationship between ESS virulence x^* and the ratio of dogs to humans r_d. Again we see that in the amphixenotic case the shape of the curve is dependent upon q. When $q < 1$ and human infection is most virulent, increasing r_d leads to an increase in ESS virulence. When $q > 1$, increasing r_d leads to a decrease in ESS virulence. Increasing the ratio of dogs to humans increases the likelihood a vector bites a dog. If more infection is in the dog population a high death rate reduces transmission and selects reduced virulence, whereas a low death rate reduces the impact of virulence and allows heightened virulence strains to be selected.

Figure (5-8) shows the relationship between q and the ESS virulence x^*. As shown in Figure (5-7), we see that increasing q decreases ESS virulence. Increasing q increases the virulence in dogs relative to humans, and reduces the duration of canine transmission. Reduced transmission leads to the selection of reduced ESS virulence. Reducing canine transmission also increases the importance of transmission from asymptomatic dogs and humans. Since humans and asymptomatic dogs have a longer life expectancy than symptomatic dogs a lower virulence infection is again selected.

5.9 Dimensions of ESS virulence x^*

Throughout this chapter the virulence parameter x represents a rate, however the dimensions of ESS virulence x^* are not consistent with this. For both host and vector transmission virulence trade-offs, $\pi_v(x), \beta(x) = \frac{cx}{x+1}$, the dimension of x^* is the square root of what is expected. A similar result is also obtained in Chapter 4 of [30], but is not commented upon. In Example 3, page 48 of [30] the ESS virulence x^* is calculated for the simple SI model:

$$\frac{dS}{dt} = b(S+I) - dS - \beta SI + \theta I \tag{5.67}$$

$$\frac{dI}{dt} = -(d+x)I + \beta SI - \theta I, \tag{5.68}$$

where b represents the per capita birth rate, d the per capita death rate, β the transmission rate, θ the recovery rate and x the rate of disease induced mortality. A trade-off

of the form $\beta(x) = \dfrac{x}{x+c}$ is assumed between transmission and virulence, $c \in \mathbb{R}$ some constant, and R_0 calculated. Maximising $R_0 = \dfrac{\beta S_0}{x+d+\theta}$ with respect to virulence the ESS $x^* = \sqrt{c\,(d+\theta)}$ is obtained. As we have found in our own work, the ESS does not have the dimensions of a rate. Example 4 on page 51 of [30] gives a similar result for a model with density-dependent natural mortality. Since these results are based on a different R_0 formulation to our own, we can assume that it is not our choice of fitness function that is producing the inconsistency in the dimension of x^*, but perhaps there is some problem with the method outlined in [30].

To investigate the consistency with which the method outlined in [30] produces an ESS with incorrect dimension, we calculated the ESS virulence x^* for our model using different trade-offs between transmission and virulence. Interestingly, we found that employing a different trade-off can change the dimensions of the ESS virulence obtained. For example, assuming a concave trade-off $\pi_v = c\sqrt{x}$ between the probability of transmission from host to vector π_v and host virulence x, we obtained the ESS virulence $x^* = \dfrac{\mu_h\,(\chi_h + \epsilon_h + \mu_h)}{(\epsilon_h + \mu_h)}$, which has the correct dimension for a rate. This suggests the dimension of the ESS is dependent on the choice of trade-off, and that further research into the method in [30] and suitable trade-offs is required. Results obtained using the method can still be used to determine parameters which influence ESS virulence however. For our model we found that no matter the trade-off, decreasing the duration of infection lead to the selection of higher virulence pathogen strains.

5.10 Conclusions

Under the conditions investigated, results suggest that treatment aimed at the competent host must be carefully considered when a trade-off is present between host virulence and the probability of transmission from host to vector. This holds true in both the zoonotic and anthroponotic cases, as decreasing the duration of the infectious period can lead to the fixation of higher virulence pathogen strains. In the case of amphixenotic spread, all host disease controls must be carefully considered. When disease is amphixenotic, the ESS virulence is dependent on which of the host species the pathogen is best adapted to. The adaptation of the pathogen to better evade host immune responses in one species can reduce the ESS, or even change the relationship between the ESS and lower level parameters. In the case of the ratio of dogs to humans r_d, the gradient of the curves which plot the parameter values against the corresponding ESS vary dependent on the species which infection is best adapted to. This means that the success of a control such as culling which aims to reduce the size of the dog popula-

tion, is dependent upon which species the pathogen is best adapted to. When infection is better adapted to humans, the culling of dogs will lead to the selection of strains of infection with lower virulence. When infection is better adapted to dogs, culling may be counter productive as any reduction in transmission leads to the selection of higher virulence pathogen strains. Under the conditions investigated, the best control techniques when a trade-off is present between host virulence and the probability of transmission from host to vector are those aimed at the vector population. This result is obtained for both the one and two host models. Since sandflies are independent of the host virulence trade-off they can be targetted, without affecting the ESS. This can be seen in the plots for varying sandfly parameters such as the natural death rate μ_v, which have no impact upon the ESS virulence in either host.

When a trade-off exists between vector virulence and the bite rate β we find that the ESS depends only on the fly life expectancy μ_v. In this case controls aimed at increasing vector mortality are counterproductive and lead to the fixation of highly virulent pathogen strains. Increasing virulence within the vector not only leads to the fixation of pathogen strains with high vector virulence, but also increases human infection prevalence. This suggests that virulence in the vector population should not be ignored.

When virulence is in the vector, control techniques aimed at either the host population, or reducing transmission via π_h or π_d may be more effective. Examples include the culling of infected dogs, and the administration of drugs to quicken host recovery, as none of the parameters controlling these processes impact upon the ESS virulence.

The difference in results for the two separate trade-offs highlights the need to further investigate and identify the host leishmaniasis is best adapted to, and their contributions to transmission before any control techniques are chosen. This will allow the most appropriate control techniques to be employed. The previously unconsidered vector virulence means that the implementation of typical control techniques such as the spraying of insecticide may in fact be counter productive and lead to increased infection prevalence in humans.

Our results so far assume all hosts and vectors are static, and coexist in one geographical space. The spread of infection and hence the evolution of virulence may also depend on the movement of host and vector species, and the habitats in which they live. In Chapter 6 we adapt our base model in order to consider a metapopulation model for the spread of vector-borne disease for infection with one-host and one-vector. We assess how land-use change affecting the sandfly natural habitat can impact on disease spread, and investigate the evolution of pathogen virulence in both host and vector when disease spread has spatial constraints.

Chapter 6

A Metapopulation Model for Leishmaniasis

The distribution of leishmaniasis is determined by that of the vector and the host species involved in transmission [10]. In recent years both the geographic range and incidence of the disease have increased, so that over 350 million people are now thought to be at risk of infection worldwide [79]. Between 1998 and 2001 leishmaniasis spread to all states of Brazil for instance, with the incidence of the infection increasing ten-fold [79]. One risk factor for the emergence of leishmaniasis is anthropogenic land-use change. Environmental changes such as deforestation, road construction, dam building, agricultural encroachment and urbanisation alter the proximity and contact between vector and host species and the distribution of vector natural habitat.

In this chapter we extend the compartmental model first introduced in Chapter 2 in order to investigate the role of spatial structure in vector-borne disease epidemiology. Using a metapopulation model we consider the impact of land-use change on the potential spread of disease, when vectors are free to move between human settlements. Using adaptive dynamics we then extend the investigations of Chapter 5 to consider the impact of land-use change and sandfly movement on the ESS virulence.

6.1 Land-Use Change and Leishmaniasis

Two types of land-use change that impact upon the spread of leishmaniasis are deforestation and urbanisation. Despite their name, sandflies have a natural habitat often located in and around forested areas. The removal of trees therefore alters the number of sandfly breeding sites in close proximity to human settlements, and impacts on the levels of transmission in peridomestic and domestic environments [29]. Smaller patches

of forest can also lead to a boom in the number of reservoir hosts such as rodents, as fewer large predators can be supported in a smaller ecosystem. According to Desjeux [29]:

> "Unprecedented widespread deforestation in recent decades was supposed to reduce zoonotic cutaneous leishmaniasis incidence but has in fact frequently led to a domestication of transmission throughout Latin America."

Also Patz et al. [66] state that:

> "Logging and road building in Latin America have increased the incidence of cutaneous and visceral leishmaniasis, which in some areas has resulted from an increase in fox reservoirs and sandfly vectors that have adapted to the peridomestic environment."

Evidence suggests that sandflies are also able to adapt to live in urban environments [74, 79]. Although information regarding sandfly population dynamics in urban areas is limited, the urbanisation of rural areas will alter the proximity and contact between sandflies and humans and impact on transmission rates. When times of upheaval lead to a large influx of susceptible migrants into cities where the residents have built up immunity to the disease, an epidemic can ensue. The building of shanty towns on the peripheries of cities can also lead to an increase in Leishmania transmission as poor sanitation and makeshift shelters create breeding sites for sandflies. According to [79], large epidemics of zoonotic visceral leishmaniasis have been known to occur in the fast growing peripheries of large cities in Latin American countries such as Brazil. It is also stated that:

> "Population migration has also resulted in outbreaks in newly arrived immigrants entering cutaneous leishmaniasis-endemic zones, for example, in lowland Bolivia"

6.2 Spatial Modelling Technique

In order to investigate the impact of land-use change on leishmaniasis we introduce a spatial aspect to disease transmission. We will adapt the compartmental differential equation models from Chapters 2 and 5 to consider a metapopulation model for the spread of leishmaniasis. According to the WHO technical report on the control of leishmaniasis [79]:

> "In most regions, leishmaniasis is characterised by a patchy distribution with discrete transmission foci".

A metapopulation model is one of the simplest forms of spatial model and is useful when modelling disease spread in naturally partitioned host species [51]. Host and vector populations are first divided into distinct subpopulations, where each subpopulation represents the number of individuals residing in a particular habitable site, or patch. Demographic and epidemiological parameters may vary between patches, but not within a patch. This allows each patch to be considered as a different local environment. Metapopulation models have been previously used to model the spatial spread of other vector borne diseases, including dengue [2] and bubonic plague [50].

With a patch structure in place, it may then be possible for some individuals to move between the different subpopulations. In the case of directly transmitted infections this movement can represent either immigrating, emigrating or commuting humans. In the case of a vector-borne disease either or both of the vector and host populations can move. In order to reduce complexity we will restrict movement in our model, so that only sandflies can travel between patches. This movement represents the foraging of female sandflies for blood meals, as they travel up to 2km a night in order to obtain the proteins necessary for egg maturation [52, 79]. Experimental evidence suggests that sandflies are drawn towards areas with a large number of hosts, particularly if the hosts themselves are also large [16, 67].

In order to construct our metapopulation model for leishmaniasis, we will adapt the compartmental differential equation model introduced in Chapter 2. We consider the simplest type of disease spread; an anthroponotic leishmaniasis with humans as the sole host species. Starting with the simplest case will allow us to better understand how processes such as movement can impact on the spread of leishmaniasis before additional layers of complexity are considered. The human and sandfly populations will be divided across a number of patches, that represent either an urban area or the sandfly natural habitat e.g. a forest. Humans will only reside in urban patches, whereas sandflies will reside in both urban and forest patches. Vectors will be free to move between the two types of patch, and we assume that sandflies in the forest take their blood meals from non-human blood sources which do not contribute to human disease transmission. Having two distinct patch types will allow us to investigate the impact of land-use change on disease prevalence, risk and evolution. Different scenarios may be represented by altering patch structure, size and number. For example, increasing the number of human hosts in the urban patch, or the total proportion of urban patches will allow us to consider the effects of urbanisation. Changing the number of forest patches and their proximity to urban patches will enable us to consider the effects of deforestation.

6.3 Two Patch Model, Humans in One Patch

We begin by considering the simplest case: A metapopulation model with two patches. Patch one represents the natural habitat of the sandfly, a section of forest for example. Humans do not reside in, or move into patch one. Patch two represents an urban area and contains both humans and sandflies. Sandflies are free to move between the two patches at rates c_{12} and c_{21}.

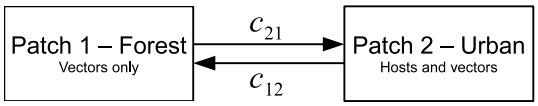

Figure 6-1: Diagram representing the patch structure of a two patch metapopulation model, humans reside only in patch 2.

Disease spread is based on the one host, one vector model introduced in Chapter 2, which has been adapted to take into account the movement of sandflies between patches. The set of model equations is as follows:

$$\frac{dS_{v1}}{dt} = \frac{\mu_v N_{v1}(t) r_v N_h^0}{N_{v1}(t)+N_{v2}(t)} - \mu_v S_{v1}(t) + c_{12}S_{v2}(t) - c_{21}S_{v1}(t) \quad (6.1)$$

$$\frac{dE_{v1}}{dt} = c_{12}E_{v2}(t) - c_{21}E_{v1}(t) - (\mu_v+\sigma_v)\,E_{v1}(t) \quad (6.2)$$

$$\frac{dI_{v1}}{dt} = \sigma_v E_{v1}(t) + c_{12}I_{v2}(t) - c_{21}I_{v1}(t) - \mu_v I_{v1}(t) \quad (6.3)$$

$$\frac{dS_{v2}}{dt} = \frac{\mu_v N_{v2}(t) r_v N_h^0}{N_{v2}(t)+N_{v1}(t)} - \frac{\beta\pi_v S_{v2}(t) I_{h2}(t)}{N_{h2}(t)} + c_{21}S_{v1}(t) - (\mu_v + c_{12})\,S_{v2}(t) \quad (6.4)$$

$$\frac{dE_{v2}}{dt} = \frac{\beta\pi_v S_{v2}(t) I_{h2}(t)}{N_{h2}(t)} - (\sigma_v+\mu_v)\,E_{v2}(t) + c_{21}E_{v1}(t) - c_{12}E_{v2}(t) \quad (6.5)$$

$$\frac{dI_{v2}}{dt} = \sigma_v E_{v2}(t) - \mu_v I_{v2}(t) + c_{21}I_{v1}(t) - c_{12}I_{v2}(t) \quad (6.6)$$

$$\frac{dS_{h2}}{dt} = \mu_h N_h^0 - \frac{\beta\pi_h S_{h2}(t) I_{v2}(t)}{N_{h2}(t)} - \mu_h S_{h2}(t) \quad (6.7)$$

$$\frac{dI_{h2}}{dt} = \frac{\beta\pi_h S_{h2}(t) I_{v2}(t)}{N_{h2}(t)} - (\mu_h+\chi_h)\,I_{h2}(t) + \epsilon_h R_{h2}(t) \quad (6.8)$$

$$\frac{dR_{h2}}{dt} = \chi_h I_{h2}(t) - (\epsilon_h+\mu_h)\,R_{h2}(t) \quad (6.9)$$

where c_{21} is the rate at which vectors move from the forest patch to the urban patch, c_{12} is the rate at which sandflies move from the urban patch to the forest and $N_{vz}(t)$ represents the number of vectors in patch z at time t. Once again we consider the ratio of vectors to humans r_v rather than explicit population sizes, however the vector birth

term is also dependent on the number of vectors which reside in each patch. A fraction $\frac{N_{v1}}{N_{v1}+N_{v2}}$ of the $\mu_v r_v N_h^0$ vector births occur in patch 1, and a fraction $\frac{N_{v2}}{N_{v1}+N_{v2}}$ of vector births occur in patch 2. $\frac{N_{v1}}{N_{v1}+N_{v2}} + \frac{N_{v2}}{N_{v1}+N_{v2}} = 1$.

In reality the rate of sandfly movement will not be constant, and will depend on factors such as the distance between patches and the number of blood sources that can be found there. To incorporate aspects of patch attractiveness into our model, the movement of sandflies from patch i to patch j will be represented by a gravity model term of the form:

$$c_{ji} = \frac{\theta n_i^{-p_\tau \tau} n_j^{\tau}}{d_{ij}^2}, \tag{6.10}$$

the parameters of which are detailed in Table 6.1.

Symbol	Definition
n_i	Total number of hosts in patch i.
θ	Proportionality constant.
d_{ij}	The distance between patch i and patch j.
p_τ	Measure of inertia. Increasing $p_\tau > 0$ decreases the likelihood Sandflies move away from the patch they currently reside in.
τ	Scaling factor for inertia.

Table 6.1: Table listing the variables and parameters used in the gravity term (6.10) for vector movement.

The gravity model originates from transportation theory where it allows flow to be governed by the sizes of donor and recipient communities, as well as the distance between them. In [75] a gravity term representing the movement of individuals between workplaces in the USA was incorporated into an SIR model for the spread of influenza. Comparing data from real epidemics to a simulation of the SIR model, the incorporation of a gravity term was found to be an effective way of capturing the impact of human movement on disease spread. Since highly populous areas are more attractive to commuters, epidemics starting in these areas were found to spread fastest and furthest. The regional spread of infection was also correlated with commuter movements, with individuals residing in sparsely populated areas those most likely to travel. A gravity term can therefore be used to quantify movement patterns both simply and realistically.

In our model we use the gravity term to represent the movement of sandflies between patches. The rate of movement between two patches is proportional to the attractiveness of the two patches in question, and the inverse of the distance between them. This means that sandflies are attracted to patches with a large number of blood sources,

provided they are not too far away. In forest patches that do not contain human hosts, the parameter p_n represents the ratio of blood sources in the forest compared to those found in the urban patch. In order to look at population ratios, rather than explicit numbers we set the total number of non-human blood sources in the forest N_f to be $N_f = p_n N_h^0$. If no blood meals can be obtained in a patch sandflies will not be attracted there. It is assumed that bites on non-human blood sources do not lead to infection, as anthroponotic Leishmania are adapted to cause infection in humans only. As such, there is no disease transmission in patches where humans are not present. Figures (6-2) and (6-3) show the relationship between the movement rates, and their constituent parameters. When a parameter is not the subject of investigation it is fixed at the value given in Table (C.1).

In Figure (6-2) we see that increasing the proportionality constant θ increases vector movement in both directions, whereas increasing the distance between the two patches d_{12} decreases vector movement in both directions. This holds true for all population ratios p_n and inertia measures p_τ. In Figure (6-3) we see that increasing the relative number of blood sources in the forest by increasing p_n increases movement to the forest via c_{12}, while reducing movement out of the forest via c_{21}. The larger the number of blood sources in the forest, the more attractive the patch is to sandflies and the greater the rate of movement into the forest. Increasing the attractiveness of the forest patch also reduces the likelihood sandflies will leave the forest, hence reducing the movement to the urban patch. The impact of increasing p_n is smallest when inertia is high and $p_\tau > 1$. The higher the inertia, the greater the likelihood a vector stays in its current patch. This can be seen when varying inertia via p_τ. As p_τ increases movement in both directions decreases. Movement occurs at a higher rate for longer when $p_n > 1$ and there are a larger number of blood sources in the forest. When inertia is high, a larger population of blood sources is required in an alternative patch before a vector will move.

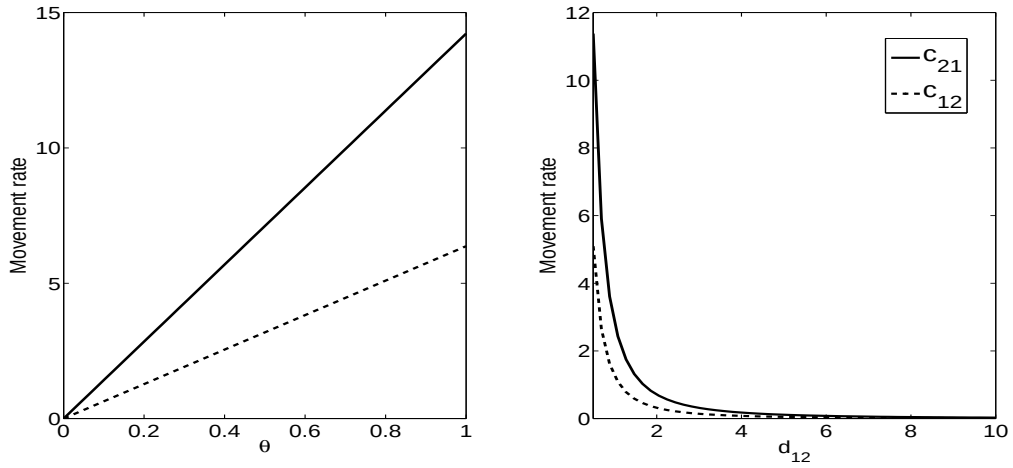

Figure 6-2: Relationship between the movement rates c_{12} and c_{21} for the two patch model (6.1)-(6.9), and: the scaling parameter θ (left-hand panel), the distance between the two patches d_{12} (right-hand panel). Movement rates are calculated using equation (6.10). All parameters that are not varied are fixed at the value given in Table (C.1).

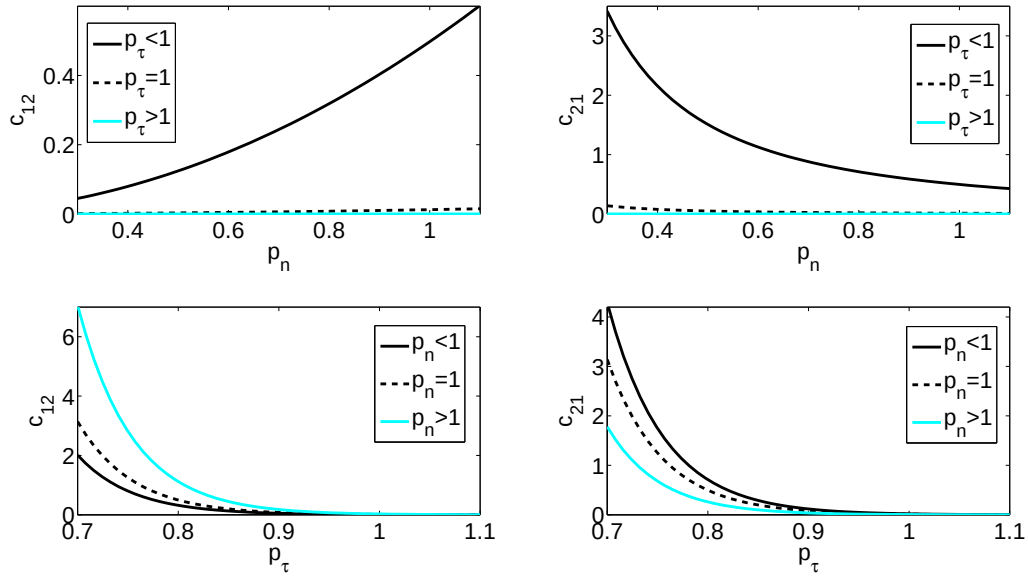

Figure 6-3: Parameter dependence of movement rates c_{12} and c_{21} for the two patch model (6.1)-(6.9). Top panels: Impact of the forest-urban blood source ratio p_n, in cases where inertia is low $p_\tau = 2$, inertia is high $p_\tau = 0.5$ and inertia is zero $p_\tau = 1$. Bottom panels: Impact of the inertia parameter p_τ, in cases where the number of blood sources in the forest is low $p_n = 0.5$, high $p_n = 2$ and equal to the number of blood sources in the city $p_n = 1$. Movement rates are calculated using equation (6.10). Parameters that are not varied are fixed at the value given in Table (C.1).

6.3.1 R_0

We now investigate the impact of vector movement on potential disease spread via the basic reproductive number R_0. R_0 can be calculated intuitively for the two patch model with humans in one patch. We first consider the human contribution to R_0. When one infected human is introduced to patch 2 they will infect:

$$\lambda_v = \frac{\pi_v}{\chi_h + \mu_h} \frac{\beta N_{v2}}{N_{h2}} \frac{S_{v2}}{N_{v2}} = \frac{\beta \pi_v S_{v2}}{N_{h2} (\chi_h + \mu_h)} \tag{6.11}$$

sandflies before recovery or death. A proportion $\frac{\chi_h}{\mu_h + \chi_h}$ of infectious hosts recover before dying, and a proportion $\frac{\epsilon_h}{\mu_h + \epsilon_h}$ of recovered hosts relapse before dying. The expected number of infections caused by a human on their first relapse is therefore $\lambda_v \left(\frac{\chi_h \epsilon_h}{(\chi_h + \mu_h)(\mu_h + \epsilon_h)} \right)$. The expected number of infections caused by their k^{th} relapse is $\lambda_v \left(\frac{\chi_h \epsilon_h}{(\chi_h + \mu_h)(\mu_h + \epsilon_h)} \right)^k$. The total number of expected sandfly infections is then:

$$R_{hv} = \lambda_v \sum_{k=0}^{\infty} \left(\frac{\chi_h \epsilon_h}{(\mu_h + \chi_h)(\mu_h + \epsilon_h)} \right)^k = \frac{\lambda_v}{1 - \frac{\chi_h \epsilon_h}{(\mu_h + \chi h)(\mu_h + \epsilon_h)}} = \frac{\beta \pi_v S_{v2} (\mu_h + \epsilon_h)}{\mu_h N_{h2} (\mu_h + \chi_h + \epsilon_h)}. \tag{6.12}$$

We now consider the vector contribution to R_0. Unlike humans, vectors can reside in either of the two patches and are free to move. Vectors become infected in patch 2, after which they enter a latent period of duration $\frac{1}{\sigma_v}$. Since vectors are free to move during all stages of infection, this means latent sandflies can enter the infectious state in either of the two patches. In order to calculate the vector contribution to R_0 we must therefore take into consideration infections in patch 1, infections in patch 2 and their corresponding transmission periods. Regardless of where a vector enters the infectious state, the force of infection it exerts on the human population while it is in patch 2 is $\lambda_h = \frac{\beta \pi_h S_{h2}}{N_{h2}}$.

We begin by considering the number of infections originating from individuals that become infectious in the urban patch, patch 2. First we calculate the total time spent in patch 2 by an individual that becomes infectious in patch 2. Let:

$v_2 = \frac{1}{\mu_v + c_{12}}$ represent the expected duration of a visit to patch 2,
$p_1 = \frac{c_{21}}{\mu_v + c_{21}}$ represent the probability a vector leaves patch 1 by moving, not death,
$p_2 = \frac{c_{12}}{\mu_v + c_{12}}$ represent the probability a vector leaves patch 2 by moving, not death.

Each visit to patch 2 is of duration v_2. The probability p_1p_2 is the probability a vector leaves and then returns to patch 2. The expected time spent in patch 2 by a vector that becomes infectious in patch 2, is therefore given by:

$$T_2 = v_2\left(1+\sum_{n=1}^{\infty}\left(p_1p_2\right)^n\right) = v_2\left(\sum_{n=0}^{\infty}\left(p_1p_2\right)^n\right) = \frac{v_2}{1-p_1p_2} = \frac{\mu_v + c_{21}}{\mu_v\left(\mu_v + c_{12} + c_{21}\right)}$$

We now calculate Σ_2, the probability that individuals in patch 2 survive the latent period to become infectious in patch 2. Let:

$$\begin{aligned}
l_1 &= \frac{\sigma_v}{\mu_v + \sigma_v + c_{12}} && \text{represent the probability a vector becomes infectious} \\
& && \text{in patch 1 (without leaving),} \\
l_2 &= \frac{\sigma_v}{\mu_v + \sigma_v + c_{21}} && \text{represent the probability a vector becomes infectious} \\
& && \text{in patch 2 (without leaving)} \\
p_{l1} &= \frac{c_{21}}{\mu_v + \sigma_v + c_{21}} && \text{represent the probability a vector leaves patch 1} \\
& && \text{while remaining latent} \\
p_{l2} &= \frac{c_{12}}{\mu_v + \sigma_v + c_{12}} && \text{represent the probability a vector leaves patch 2} \\
& && \text{while remaining latent}
\end{aligned}$$

The probability that a vector infected in patch 2 becomes infectious in patch 2 on their first visit is l_2. The probability that they become infectious on their second visit to patch 2 is $l_2p_{l1}p_{l2}$, and on their third visit is $l_2\left(p_{l1}p_{l2}\right)^2$. The probability of becoming infectious in patch two, having been infected in patch two is therefore:

$$\begin{aligned}
\Sigma_2 = l_2\left(1+\sum_{n=1}^{\infty}\left(p_{l1}p_{l2}\right)^n\right) &= l_2\left(\sum_{n=0}^{\infty}\left(p_{l1}p_{l2}\right)^n\right) \\
&= \frac{l_2}{1-p_{l1}p_{l2}} = \frac{\sigma_v\left(c_{21}+\mu_v+\sigma_v\right)}{\left(\mu_v+\sigma_v\right)\left(\mu_v+\sigma_v+c_{12}+c_{21}\right)}
\end{aligned}$$

The expected number of human infections caused by a sandfly that becomes infectious in patch 2 is:

$$\Sigma_2\lambda_hT_2 = \frac{\beta\pi_hS_{h2}\sigma_v\left(\mu_v+c_{21}\right)\left(\mu_v+\sigma_v+c_{21}\right)}{N_{h2}\mu_v\left(\mu_v+c_{12}+c_{21}\right)\left(\mu_v+\sigma_v\right)\left(\mu_v+\sigma_v+c_{12}+c_{21}\right)}.$$

We now consider the human infections arising from sandflies who become infectious in patch 1. A vector visits patch 2 with probability p_1. A second visit occurs with probability $p_1^2 p_2$, and a third with probability $p_1^3 p_2^2$. Each visit has duration v_2, so the expected time spent in patch 2 is therefore:

$$T_1 = p_1 v_2 \left(1 + \sum_{n=1}^{\infty} (p_1 p_2)^n\right) = p_1 v_2 \left(\sum_{n=0}^{\infty} (p_1 p_2)^n\right) = \frac{p_1 v_2}{1 - p_1 p_2} = \frac{c_{21}}{\mu_v (\mu_v + c_{12} + c_{21})}.$$

The probability a sandfly becomes infectious in patch 1, given that they were infected in patch 2 is:

$$\begin{aligned}\Sigma_1 = l_1 p_{l2} \left(1 + \sum_{n=1}^{\infty} (p_{l1} p_{l2})^n\right) &= l_1 p_{l2} \left(\sum_{n=0}^{\infty} (p_{l1} p_{l2})^n\right) \\ &= \frac{p_{l2} l_1}{1 - p_{l1} p_{l2}} = \frac{c_{12} \sigma_v}{(\mu_v + \sigma_v)(\mu_v + \sigma_v + c_{12} + c_{21})}.\end{aligned}$$

So the expected number of infections in humans caused by sandflies that become infected in patch 2, but become infectious in patch 1 is:

$$\Sigma_1 T_1 \lambda_h = \frac{\beta \pi_h S_{h2} \sigma_v c_{12} c_{21}}{N_{h2} \mu_v (\mu_v + c_{12} + c_{21})(\mu_v + \sigma_v)(\mu_v + \sigma_v + c_{12} + c_{21})}.$$

The total number of human infections caused by sandflies is therefore:

$$R_{vh} = \lambda_h (\Sigma_1 T_1 + \Sigma_2 T_2) = \frac{\beta \pi_h S_{h2} \sigma_v (c_{12} c_{21} + (\mu_v + c_{21})(c_{21} + \mu_v + \sigma_v))}{N_{h2} \mu_v (\mu_v + \sigma_v)(\mu_v + c_{21} + c_{12})(\mu_v + \sigma_v + c_{12} + c_{21})} \tag{6.13}$$

In order to obtain the pathogen growth rate in one generation, $R_0 = \sqrt{R_{hv} R_{vh}}$. This result can be verified using the next generation matrix method.

6.4 R_0 and Lower Level Parameters

Once again, we find that parameters which increase the rate or duration of transmission increase R_0. The relationships between R_0 and the parameters β, π_h, π_v, r_v, σ_v, ϵ_h, μ_h, μ_v and χ_h are the same as in previous sections and will not be discussed further. Instead, we focus our investigation on the two movement parameters which have the greatest impact on R_0; the measure of inertia p_τ and the ratio of blood meals in the forest p_n. The uppermost plots of Figures (6-4) and (6-5) show how R_0 varies with p_n and p_τ respectively. In order to better understand the relationship between R_0 and these two movement parameters we also consider the split of the vector population at disease free equilibrium, and the total duration of transmission in the forest patch, urban patch and both patches combined.

In the top panel of Figure (6-4) we see that increasing the forest-urban blood source ratio p_n decreases R_0. The greater the value of p_n, the greater the attractiveness of the forest to the vector. This increases the likelihood that vectors leave the transmission patch, hence decreasing the transmission and potential spread of infection. The presence of a non-human blood source which cannot transmit infection causes a dilution effect, similar to that of dead-end humans in the zoonotic model from Chapter 2. The greater the number of non-human blood sources the less likely the vector takes a blood meal from a competent host, thus transmission and potential disease spread decrease.

Patch attractiveness is not only governed by p_n, but also the inertia p_τ. High inertia implies that vectors are unlikely to move from the patch in which they reside, particularly if a large number of blood sources are found there. The higher the inertia the longer the duration of a visit to the transmission patch, and the longer the duration of transmission. When $p_n < 1$ the majority of vectors reside in the transmission patch at disease free equilibrium, see panels 2 and 3 of Figure (6-4). In this case, high inertia leads to the greatest values of R_0 as vectors are likely to remain in the transmission patch for the duration of the infectious period. There is no transmission from patch 1 vectors as they do not move to become infected, see panel 4. Decreasing inertia decreases R_0 by increasing the number of vectors found in the forest, and decreasing the duration of time over which patch 2 infections can be transmitted. Sandflies becoming infectious in patch 2 account for the majority of transmission and the overall duration of transmission decreases. See panels 4, 5 and 6.

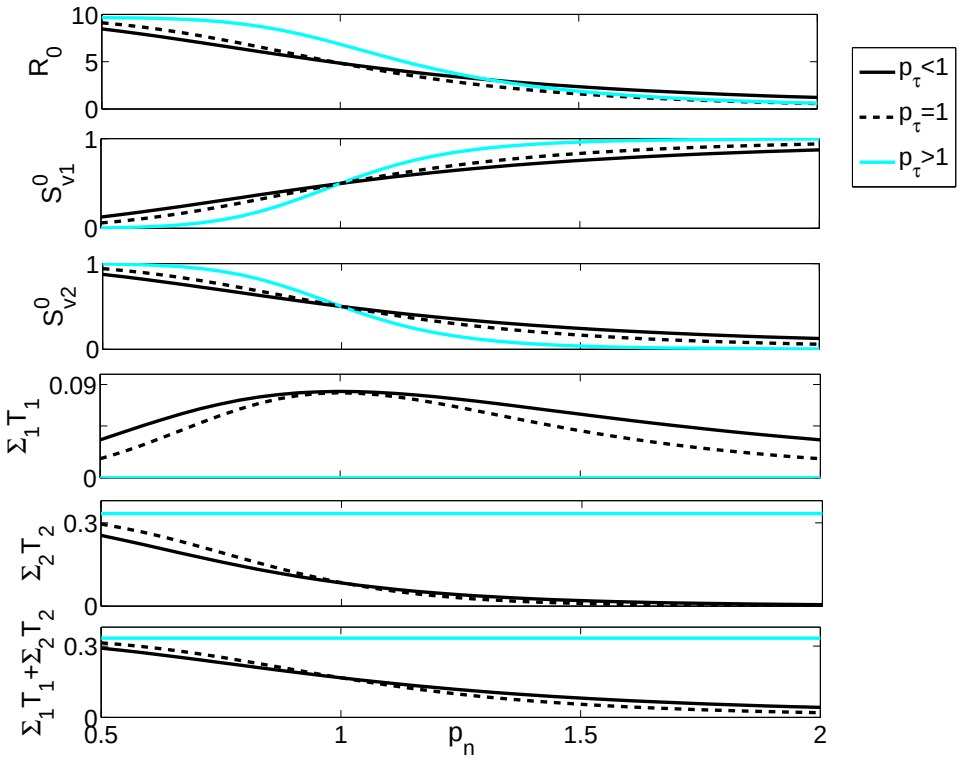

Figure 6-4: The relationship between forest-urban blood source ratio p_n and, Top panel: the basic reproductive number R_0, Second panel: The number of susceptible vectors in the forest patch 1 at DFE, Third panel: The number of susceptible vectors in the urban patch 2 at DFE, Fourth panel: The duration of transmission for vectors becoming infectious in the forest patch 1, Fifth panel: The duration of transmission for vectors becoming infectious in the urban patch 2, and Sixth panel. The total duration of vector transmission for the two patch model with humans in one patch (6.1)-(6.9). Results are displayed for cases where inertia is low $p_\tau = 2$, inertia is high $p_\tau = 0.5$ and inertia is zero $p_\tau = 1$. Parameters that are not varied are fixed at the values given in Table (C.1).

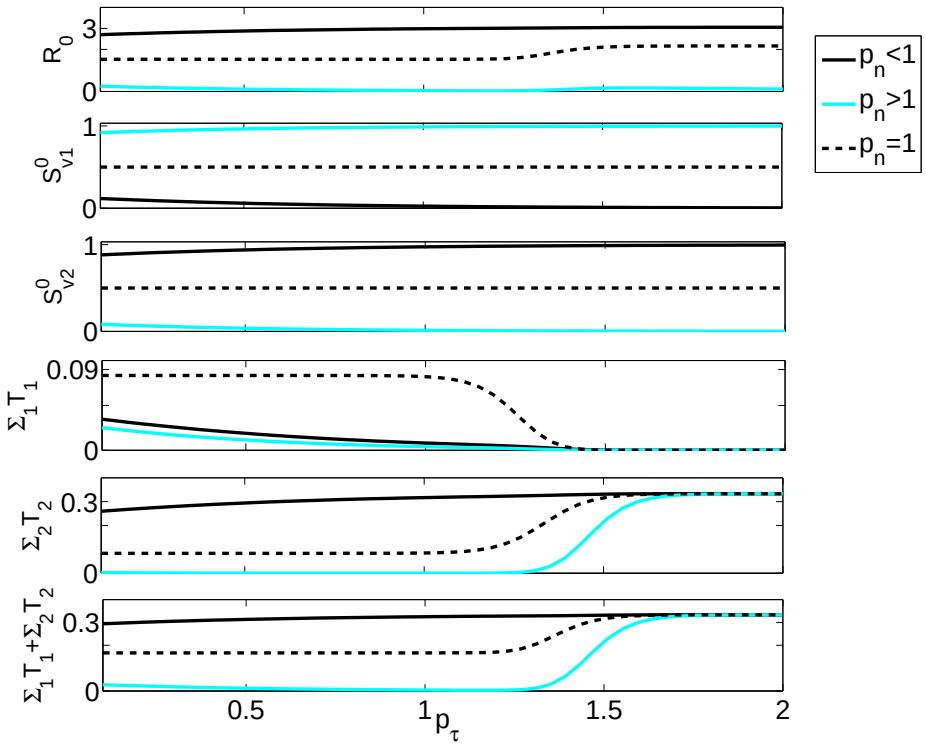

Figure 6-5: The relationship between the inertia parameter p_τ and, Top panel: the basic reproductive number R_0, Second panel: The number of susceptible vectors in the forest patch 1 at DFE, Third panel: The number of susceptible vectors in the urban patch 2 at DFE, Fourth panel: The duration of transmission for vectors becoming infectious in the forest patch 1, Fifth panel: The duration of transmission for vectors becoming infectious in the urban patch 2, and Sixth panel: The total duration of vector transmission for the two patch model with humans in one patch (6.1)-(6.9). Results are displayed for cases where the number of blood sources in the forest is low $p_n = 0.5$, high $p_n = 2$ and equal to the number of humans $p_n = 1$. Parameters that are not varied are fixed at the values given in Table (C.1).

When $p_n > 1$ the majority of hosts and vectors reside in the forest patch. For $1 < p_n < 1.5$, R_0 is lowest when $p_\tau = 1$ and inertia is equal in both directions. The vector population in the transmission patch depletes at a faster rate than when inertia is low, and the duration of time over which patch 2 infections can be transmitted is decreased. See panels 2, 3 and 5. Increasing the attractiveness of the forest patch by increasing p_n also decreases the rate of movement between patches. This reduces the likelihood infectious vectors are found in patch 1, and so the duration of transmission for vectors becoming infectious in patch 1 is reduced. R_0 remains highest for $p_\tau > 1$ in the interval $1 < p_n < 1.25$ as high inertia increases the average duration of a visit to the transmission patch.

The dependence of R_0 on patch attractiveness is also investigated in Figure (6-5). We find that increasing inertia p_τ for a fixed forest-urban blood source ratio p_n has little impact on R_0. Increasing inertia does not greatly alter the total duration of vector transmission, only the duration of time spent in a patch. See panels 4, 5 and 6. When $p_\tau < 1.4$, vectors that become infectious in either patch transmit infection in patch 2. Inertia is low enough for vectors to move between patches, and so any vector can become infectious. When $p_\tau > 1.4$, only vectors becoming infectious in patch 2 transmit infection. Vectors in patch 1 at DFE are unlikely to leave and become infectious, whereas vectors in patch 2 at DFE are most likely to remain in the transmission patch for the entire infectious period. Increasing the inertia p_τ has the greatest impact on R_0 when $p_n = 1$ and there are the same number of blood sources in both forest and urban patches. In this case inertia alone governs patch attractiveness. R_0 is lowest when the majority of blood sources are found in the forest, as transmission cannot occur in this patch.

6.5 Evolution of Virulence

We now investigate the evolution of virulence in our two patch metapopulation model, with humans in one patch. This will allow us to identify the impact of vector movement on ESS virulence. As in previous sections, two separate trade-offs between virulence and transmission will be considered. In the first instance, a disease related death rate $\nu_h = x$ will be incorporated into the infectious human compartment. A trade-off between the virulence of the disease within humans and the probability of transmission from humans to flies will be assumed, and the ESS virulence calculated. In the second case, a disease related death rate $\nu_v = x$ will be incorporated into the infectious fly compartments. A trade-off between the virulence of the disease within sandflies and the sandfly bite rate will be assumed, and the ESS virulence calculated.

6.5.1 Virulence in the Host

We begin by incorporating the rate of disease related mortality in the host, x, into equation (6.8) to obtain:

$$\frac{dI_{h2}}{dt} = \frac{\beta \pi_h S_{h2} I_{v2}}{N_{h2}} - (\mu_h + \chi_h + x) I_{h2} + \epsilon_h R_{h2}. \tag{6.14}$$

A concave trade-off between x, and the probability of transmission from humans to sandflies $\pi_v = \frac{cx}{x+1}$ is assumed. The ESS virulence can then be obtained using the numerical method detailed in Section (5.7.4).

For all patch structures considered both in this, and subsequent sections we found that ESS virulence in the host depends only on the rates of host mortality μ_h, host recovery χ_h and host relapse ϵ_h. Since the duration of infection in humans is independent of sandfly movement, results match those in Figure (5-2) for the non-spatial model. We therefore focus all further investigation on the evolution of virulence in the vector.

6.5.2 Virulence in the Vector

In order to investigate the evolution of virulence in the vector we now introduce a concave trade-off $\beta(x) = \frac{\hat{c}x}{x+1}$ between the vector bite rate and vector virulence. More information about this trade-off can be found in Section (5.3). Disease related death in humans is removed, and disease related death x is instead incorporated into the infectious sandfly compartments:

$$\frac{dI_{v1}}{dt} = \sigma_v E_{v1} + c_{12} I_{v2} - c_{21} I_{v1} - (\mu_v + x) I_{v1} \tag{6.15}$$

$$\frac{dI_{v2}}{dt} = \sigma_v E_{v2} - (\mu_v + x) I_{v2} + c_{21} I_{v1} - c_{12} I_{v2} \tag{6.16}$$

The next generation matrix is obtained for the altered system of equations and used to obtain R_0. The ESS virulence x^* can then be calculated using R_0 maximisation.

In our non-spatial model the ESS virulence under the trade-off $\beta(x) = \frac{\hat{c}x}{x+1}$ was only dependent on the duration of infection $\frac{1}{\mu_v}$. In the spatial model we find that the ESS not only depends on the parameters governing the duration of infection, but also the movement parameters which govern the duration of time spent in the transmission patch. Figures (6-6)-(6-8) show the relationship between ESS virulence x^* and the lower level parameters from which it is constructed.

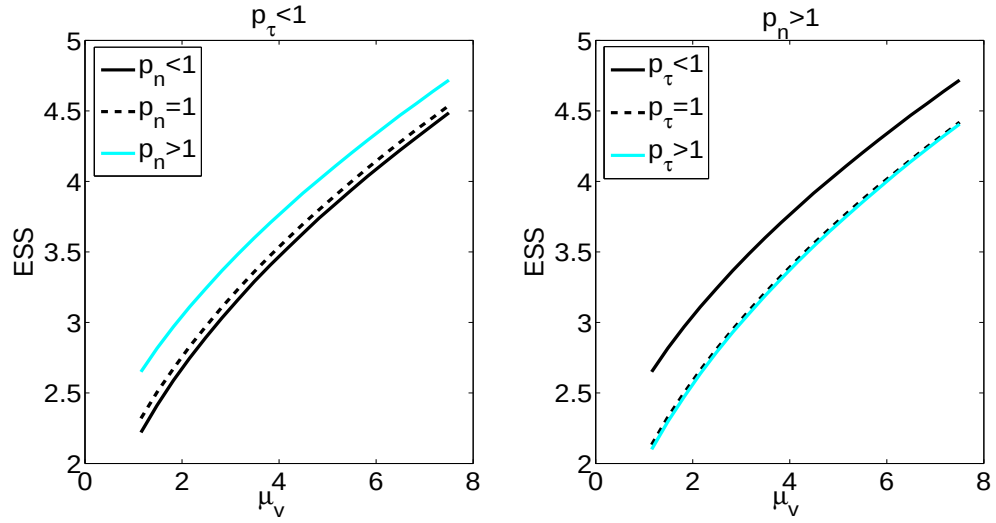

Figure 6-6: Relationship between ESS virulence in the vector and vector mortality rate μ_v for the two patch model, humans in one patch, when $\beta = \frac{\hat{c}x}{(x+1)}$. In the left hand panel results are displayed for cases where the number of blood sources in the forest is low $p_n = 0.5$, high $p_n = 2$ and equal to the number of humans $p_n = 1$. In the right hand panel results are displayed for cases where inertia is low $p_\tau = 2$, high $p_\tau = 0.5$ and zero $p_\tau = 1$. Parameters that are not varied are fixed at the values given in Table (C.1).

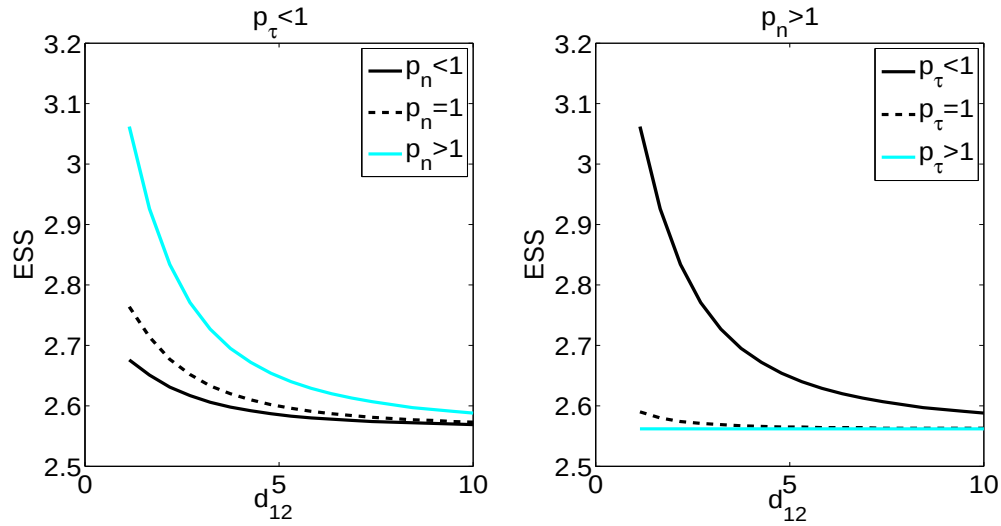

Figure 6-7: Relationship between ESS virulence in the vector and the distance between patches d_{12} for the two patch model, humans in one patch, when $\beta = \frac{\hat{c}x}{(x+1)}$. In the left hand panel results are displayed for cases where the number of blood sources in the forest is low $p_n = 0.5$, high $p_n = 2$ and equal to the number of humans $p_n = 1$. In the right hand panel results are displayed for cases where inertia is low $p_\tau = 2$, high $p_\tau = 0.5$ and zero $p_\tau = 1$. Parameters that are not varied are fixed at the values given in Table (C.1).

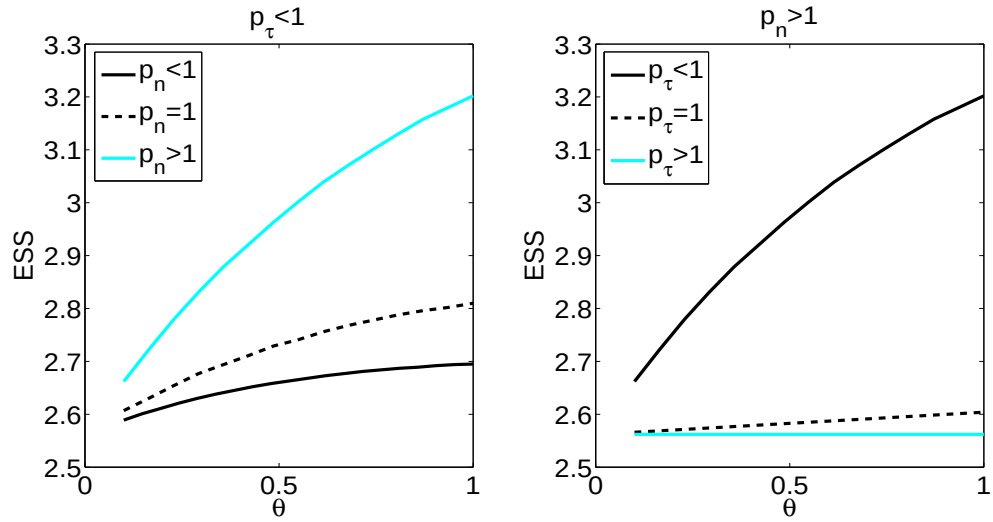

Figure 6-8: Relationship between ESS virulence in the vector and the movement scaling parameter θ for the two patch model, humans in one patch, when $\beta = \frac{\hat{c}x}{(x+1)}$. In the left hand panel results are displayed for cases where the number of blood sources in the forest is low $p_n = 0.5$, high $p_n = 2$ and equal to the number of humans $p_n = 1$. In the right hand panel results are displayed for cases where inertia is low $p_\tau = 2$, high $p_\tau = 0.5$ and zero $p_\tau = 1$. Parameters that are not varied are fixed at the values given in Table (C.1).

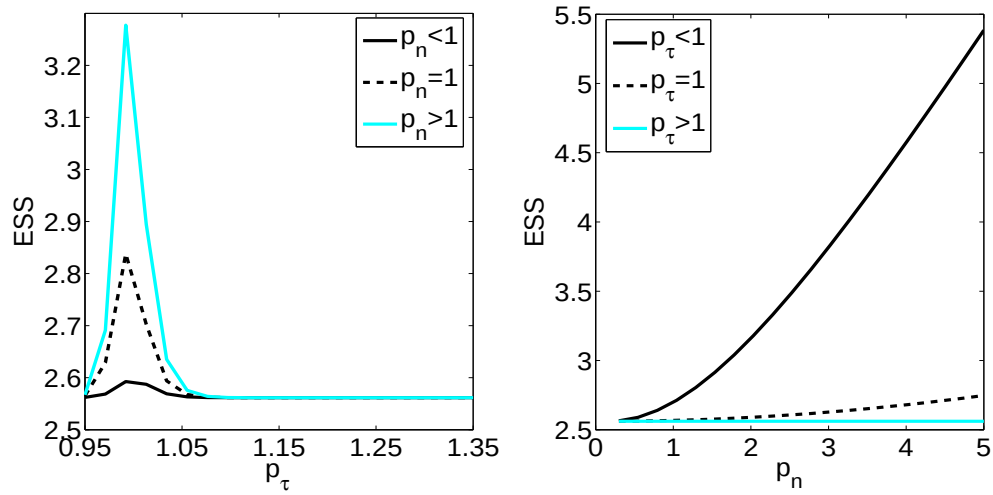

Figure 6-9: Left hand panel: Relationship between ESS virulence in the vector and inertia p_τ. Results are displayed for cases where the number of blood sources in the forest is low $p_n = 0.5 < 1$, high $p_n = 2 > 1$ and equal to the number of humans $p_n = 1$. Right hand panel: Relationship between ESS virulence in the vector and the forest-urban blood source ratio p_n. Results are displayed for cases where inertia is low $p_\tau = 2$, high $p_\tau = 0.5$ and zero $p_\tau = 1$. All results are for the two patch model, humans in one patch, when $\beta = \frac{\hat{c}x}{(x+1)}$. Parameters that are not varied are fixed at the values given in Table (C.1).

In Figure (6-6) we see that increasing the vector mortality rate μ_v increases the ESS virulence. This holds true for all combinations of patch attractivity measures p_n and p_τ. As in the non-spatial model, increasing μ_v decreases the time over which disease related death can occur, thus reducing the negative impact of a fixed virulence and allowing a heightened virulence pathogen strain to be selected. The increase in ESS virulence caused by varying μ_v is highest when $p_n > 1$ and the majority of blood sources are found in the forest. As p_n increases, fewer vectors are attracted to the transmission patch. Transmission is reduced, and a heightened virulence pathogen strain is selected.

In Figure (6-7) we find that increasing the distance between the urban and forest patch decreases ESS virulence. Increasing the distance between the two patches decreases the rate at which movement occurs, and so individuals are more likely to stay in the patch in which they initially reside. Once again, increasing the duration of time spent in the transmission patch increases the likelihood transmission occurs and leads to the selection of a lower virulence pathogen strain. In Figure (6-8) we find that increasing movement by increasing the scaling parameter θ leads to an increase in ESS virulence. Increasing the rate of movement decreases the duration of each visit to the transmission patch, thus decreasing the overall level of transmission and increasing virulence.

The impact of increasing patch attractiveness is further investigated in Figure (6-9). Increasing the forest-urban blood source ratio p_n increases the ESS virulence. Increasing the number of blood sources in the forest increases the attractiveness of the forest patch. The dilution effect is strengthened, fewer sandflies are attracted to the urban patch, transmission is reduced and ESS virulence increases. Increasing p_n has the smallest impact when inertia is low. In this case the rate of vector movement is high, and vectors are likely to move even when blood sources are concentrated in one patch. More vectors therefore visit patch 2, and the rate of transmission is not so greatly decreased. When p_n and p_τ are high, vectors do not move from patch one, transmission is reduced and virulence increased.

In Figure (6-9) we find that inertia p_τ has the greatest impact on ESS virulence at approximately $p_\tau \approx 1$. When $p_\tau < 1$ the rate of movement is high. Increasing p_τ increases the likelihood vectors remain in the forest patch, and so transmission decreases and the ESS increases. When $p_\tau > 1$, the rate of movement is low and vectors are unlikely to leave the patch they were in at DFE. Those who start in the transmission patch remain in the transmission patch and are exposed to transmission for a longer time period. This leads to a decrease in the ESS virulence. ESS virulence is highest when the majority of blood sources are found in the forest patch, as this further reduces the likelihood of movement into the transmission patch.

Increasing inertia p_τ decreases the ESS virulence obtained when μ_v is varied. As inertia increases, vectors residing in the transmission patch are less likely to leave. Increasing the duration of time spent in the transmission patch increases the likelihood transmission occurs and leads to the selection of a lower virulence pathogen strain. The ESS virulence also increases with p_n and decreases with p_τ in Figures (6-7) and (6-8).

6.5.3 Impact of Land-Use Change: Two Patch Model, One Human Patch

Results for the two patch model, with humans in one patch, suggest that urbanisation can increase the potential spread of vector-borne diseases such as leishmaniasis. Increasing the proximity of humans to vector natural habitat, or decreasing the forest-urban blood source ratio leads to an increase in R_0. The magnitude of the increase in R_0 is governed by patch attractivity measures, including inertia and the ratio of blood sources in the two patches. The greater the number of people in the urban patch, the greater the impact of inertia and the higher the levels of vector transmission.

When a trade-off is present between virulence in the host and the probability of host transmission, we find that ESS virulence depends only on the duration of infection in the host. The same result was obtained for the non-spatial anthroponotic model in Chapter 5. When a trade-off is present between the vector bite rate and the virulence within the vector, we find that the ESS depends on both the duration of infection in the vector and the rate of vector movement. Since transmission is only possible in one patch, the duration of transmission is not only governed by vector mortality but by the duration and number of sandfly visits to the urban environment. We find that increasing the forest-urban blood source ratio increases ESS virulence. This therefore implies that deforestation which increases the density of non-human blood sources and hence p_n can increase ESS virulence. Land-use change which decreases the distance between forest and urban patches will also increase ESS virulence. Decreasing the rate of vector movement, or altering inertia can also impact on ESS virulence.

The relationship between virulence in the vector and endemic infection prevalence is explored in Figure (6-10). Results show that increasing virulence in the vector increases the proportion of humans infected at endemic equilibrium. This suggests that any increase in vector virulence caused by urbanisation will not only increase the potential spread of disease, but also increase the human infection prevalence. Reducing the distance between urban and forest environments via deforestation and urbanisation will therefore increase ESS virulence and lead to a higher infection prevalence in humans. Although the proportion of infected humans levels off as virulence increases, we find that this is due to the exhaustion of the susceptible human population. If human

immigration led to an influx of susceptible hosts, disease prevalence would further increase.

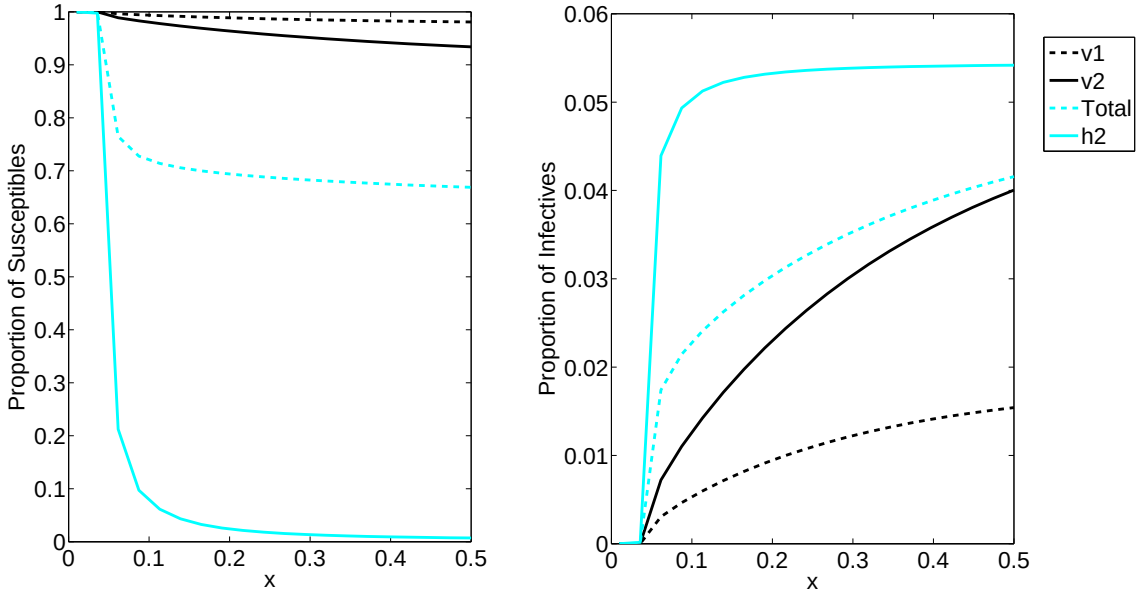

Figure 6-10: Relationship between virulence in the vector and the number of susceptible and infected individuals of all types. Two patch model, humans in one patch (6.1)-(6.9), no trait evolution. Parameters that are not varied are fixed at the values given in Table (C.1).

6.6 Two Patch Model, Humans in Both Patches

We now consider a two patch model where humans are the sole blood source. Humans reside in either of two urban patches, and do not move. Vectors also reside in both patches, but move between the two at a rate governed by the gravity term (6.10). The total human population is split between the patches so $N_{h2} = p_h N_h^*$ and $N_{h1} = (1 - p_h)N_h^*$ at DFE. This will allow us to investigate the impact of the human distribution on potential disease spread in a spatial model. We will also consider the impact of vector movement, and its relationship with the ESS virulence.

We adapt the system of equations (6.1)-(6.9) to include human compartments for patch one, and to allow for disease transmission in both patches. The basic reproductive number R_0 was calculated using the next generation matrix in order to assess the impact varying lower level parameters have on potential disease spread. With the exception of the new parameter p_h, the results for the two patch model with humans in two patches are the same as those for the two patch model with humans in one patch. Parameters which increase the rate or duration of transmission increase R_0. The relationship

between the parameter p_h, which governs the host distribution, and R_0 is shown in Figure (6-11). Since the human disease parameters are the same in both patches, p_h need only be considered in the range $0 \leq p_h \leq 0.5$ to account for all possible host distributions.

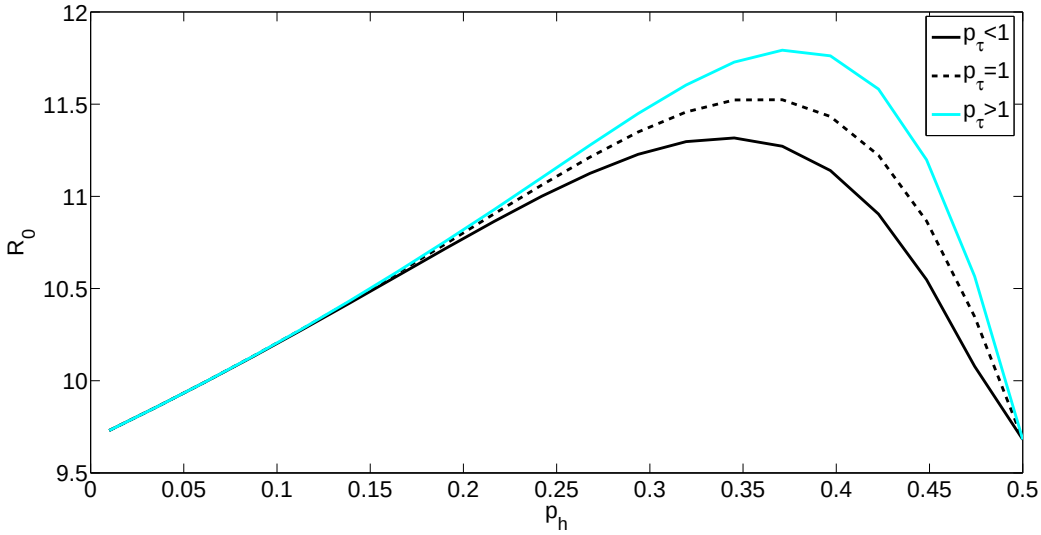

Figure 6-11: Relationship between R_0 and the host distribution p_h for the two patch model, humans in both patches. Parameters that are not varied are held at the values given in Table (C.1).

We find that R_0 is at its highest when $p_h \approx 0.35$. A complex dilution effect caused by splitting human blood sources between patches, coupled with the impact of inertia, leads to a skew in the value of p_h for which R_0 is maximised. Increasing p_h increases the number of human blood sources in patch 2, while decreasing the number of blood sources in patch 1. This increases the attractiveness of patch 2 to the vector, while decreasing the attractiveness of patch 1. The number of vectors in patch 2 therefore increases, while the number of vectors in patch 1 decreases. Increasing the number of vectors in patch 2 leads to an increase in the rate of transmission to vectors which feeds back into R_0, see Figure (6-12). Decreasing the number of humans in patch 1 also leads to an initial increase in the rate of transmission to vectors in patch 1, see Figure (6-12). When $p_h < 0.35$, inertia prevents patch 2 becoming attractive enough to move a large number of vectors away from the majority of blood sources in patch 1. Reducing the number of humans N_{h1} therefore results in an increase in the transmission rate $\frac{S_{v1}I_{h1}}{N_{h1}}$ which also feeds back into R_0. As patch 2 becomes more attractive, the rate at which susceptible vectors leave patch 1 increases. This leads to a reduction in the rate of transmission to vectors in patch 1. R_0 is therefore at its maximum before the rate of

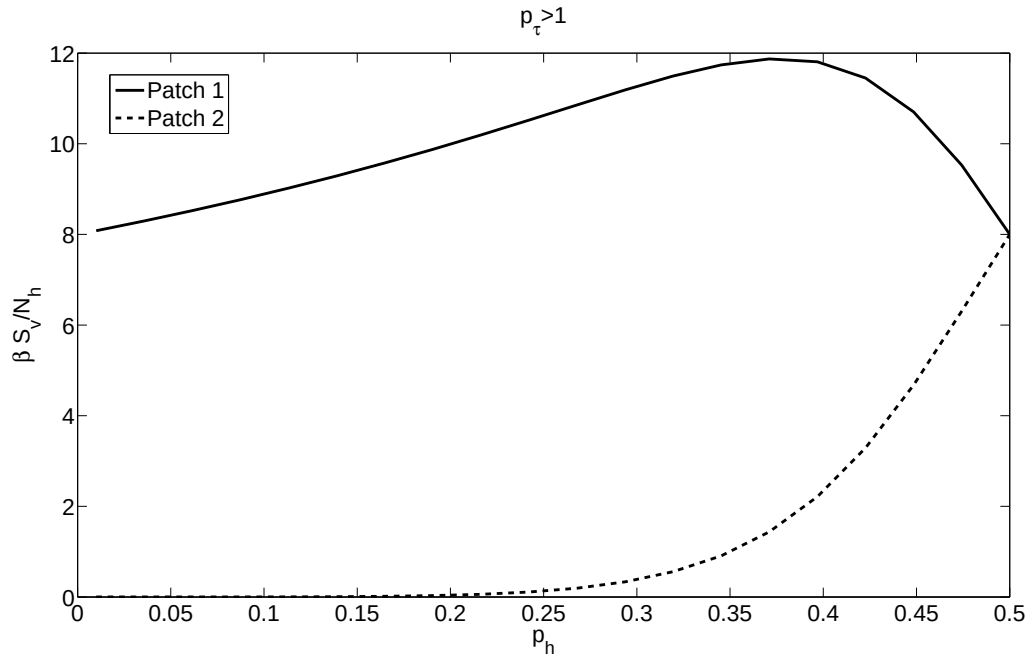

Figure 6-12: Relationship between the host distribution parameter p_h and the rate of transmission to the vector population $\frac{\beta S_v}{N_h}$ in each patch when one infected host is introduced. Two patch model, humans reside in both patches. Parameters that are not varied are held at the values given in Table (C.1).

transmission subsides in either patch. R_0 is also higher when inertia is high and $p_\tau > 1$ as this increases the duration of time over which transmission to vectors in patch 1 increases.

6.6.1 Evolution of Virulence in the Vector

When a concave trade-off is imposed between the bite rate β and virulence in the vector, we find that the ESS virulence is only dependent upon the sandfly mortality rate μ_v. Since the duration of transmission is no longer limited by the parameters in the gravity term, vector movement no longer influences the ESS virulence. A similar result can be obtained for a three patch model with humans in three patches. In Figure (6-13) we see that increasing vector mortality increases ESS virulence. This result is similar to that for the anthroponotic non-spatial model.

In Figure (6-13) we compare the results for the two patch model with humans in one and two patches. We find that the ESS virulence is lower when humans reside in both patches. Since transmission can now occur in both patches the duration of transmission has increased and the ESS virulence is reduced. As in Figure (6-10) for the one urban patch model it can be shown that increasing virulence in the vector leads

to an increase in human infection prevalence at endemic equilibrium.

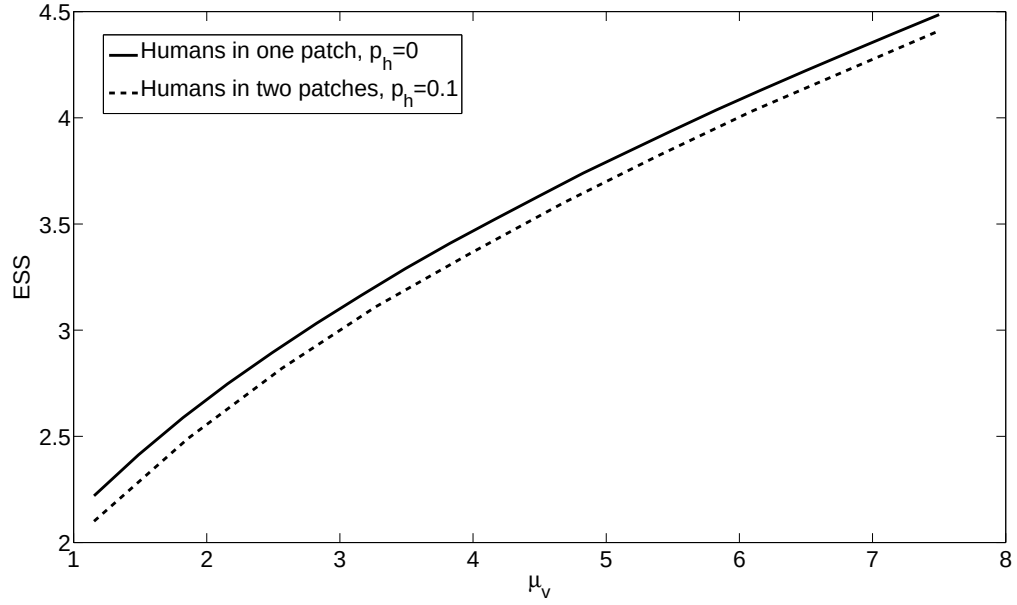

Figure 6-13: Relationship between vector mortality μ_v and the ESS vector virulence. The black line represents the ESS for the two patch model with humans in one patch, the grey line represents the ESS for the two patch model with humans in both patches. In each case $N_h^0 = 3000$. Parameters that are not varied are held at the values given in Table (C.1).

6.7 Three Patch Model, Humans in One Patch

In order to further investigate how patch structure and host distribution impact upon disease spread and virulence, we now consider a metapopulation model with three patches. Patches will again be divided into two types: urban and forest. Humans reside only in urban patches, whereas sandfly vectors can reside in either urban or forest environments. Once again we incorporate vector movement governed by a gravity term to see how patch attractivity and vector movement affects disease spread. We begin by considering a three patch metapopulation model with two forest patches and one

urban patch. Disease dynamics are described using the following system of ODEs:

$$\frac{dS_{v1}}{dt} = \frac{\mu_v N_{v1} r_v N_h^0}{N_{v1}+N_{v2}+N_{v3}} - \mu_v S_{v1} - (c_{31}+c_{21})\, S_{v1} + c_{13} S_{v3} + c_{12} S_{v2} \quad (6.17)$$

$$\frac{dE_{v1}}{dt} = c_{13} E_{v3} + c_{12} E_{v2} - (c_{31}+c_{21})\, E_{v1} - (\mu_v+\sigma_v)\, E_{v1} \quad (6.18)$$

$$\frac{dI_{v1}}{dt} = \sigma_v E_{v1} + c_{13} I_{v3} + c_{12} I_{v2} - (c_{31}+c_{21})\, I_{v1} - \mu_v I_{v1} \quad (6.19)$$

$$\frac{dS_{v2}}{dt} = \frac{\mu_v N_{v2} r_v N_h^0}{N_{v1}+N_{v2}+N_{v3}} - \mu_v S_{v2} - (c_{12}+c_{32})\, S_{v2} + c_{23} S_{v3} + c_{21} S_{v1} \quad (6.20)$$

$$- \frac{\beta \pi_v S_{v2} I_{h2}}{N_{h2}} \quad (6.21)$$

$$\frac{dE_{v2}}{dt} = \frac{\beta \pi_v S_{v2} I_{h2}}{N_{h2}} + c_{23} E_{v3} + c_{21} E_{v1} - (c_{12}+c_{32})\, E_{v2} - (\mu_v+\sigma_v)\, E_{v2} \quad (6.22)$$

$$\frac{dI_{v2}}{dt} = \sigma_v E_{v2} + c_{23} I_{v3} + c_{21} I_{v1} - (c_{12}+c_{32})\, I_{v2} - \mu_v I_{v2} \quad (6.23)$$

$$\frac{dS_{v3}}{dt} = \frac{\mu_v N_{v3} r_v N_h^0}{N_{v1}+N_{v2}+N_{v3}} - \mu_v S_{v3} - (c_{13}+c_{23})\, S_{v3} + c_{32} S_{v2} + c_{31} S_{v1} \quad (6.24)$$

$$\frac{dE_{v3}}{dt} = c_{32} E_{v2} + c_{31} E_{v1} - (c_{13}+c_{23})\, E_{v3} - (\mu_v+\sigma_v)\, E_{v3} \quad (6.25)$$

$$\frac{dI_{v3}}{dt} = \sigma_v E_{v3} + c_{32} I_{v2} + c_{31} I_{v1} - (c_{13}+c_{23})\, I_{v3} - \mu_v I_{v3} \quad (6.26)$$

$$\frac{dS_{h2}}{dt} = \mu_h N_h^0 - \mu_h S_{h2} - \frac{\beta \pi_h S_{h2} I_{v2}}{N_{h2}} \quad (6.27)$$

$$\frac{dI_{h2}}{dt} = \frac{\beta \pi_h I_{v2} S_{h2}}{N_{h2}} - (\chi_h+\mu_h)\, I_{h2} + \epsilon_h R_{h2} \quad (6.28)$$

$$\frac{dR_{h2}}{dt} = \chi_h I_{h2} - (\epsilon_h+\mu_h)\, R_{h2} \quad (6.29)$$

where

$$c_{12} = \frac{\theta N_{f1}^{\tau} N_{h2}^{-p_\tau \tau}}{d_{12}^2}, c_{21} = \frac{\theta N_{f1}^{-p_\tau \tau} N_{h2}^{\tau}}{d_{12}^2}, c_{13} = \frac{\theta N_{f1}^{\tau} N_{f3}^{-p_\tau \tau_2}}{d_{13}^2}$$
$$c_{31} = \frac{\theta N_{f3}^{\tau} N_{f1}^{-p_\tau \tau}}{d_{13}^2}, c_{23} = \frac{\theta N_{h2}^{\tau} N_{f3}^{-p_\tau \tau}}{d_{23}^2}, c_{32} = \frac{\theta N_{h2}^{-p_\tau \tau} N_{f3}^{\tau}}{d_{23}^2}.$$

$N_{f1} = p_f p_n N_h^0$ is the total number of non-human blood sources in forest patch 1, $N_{f3} = (1-p_f) p_n N_h^0$ is the total number of non-human blood sources in forest patch 3 and the proportion p_f, $0 \le p_f \le 0.5$ controls their distribution.

In order to explore how alternative patch structures affect disease spread, we consider three arrangements of the three patches. Diagrams representing the three ar-

rangements under consideration can be found in Figure (6-14). In the first and second arrangements, the three patches represent an isosceles triangle. In the first arrangement the edge with shortest distance is between the two forest patches, in the second arrangement the edge with shortest distance is between the urban patch and a forest patch. In the third arrangement the three patches represent the corners of an equilateral triangle.

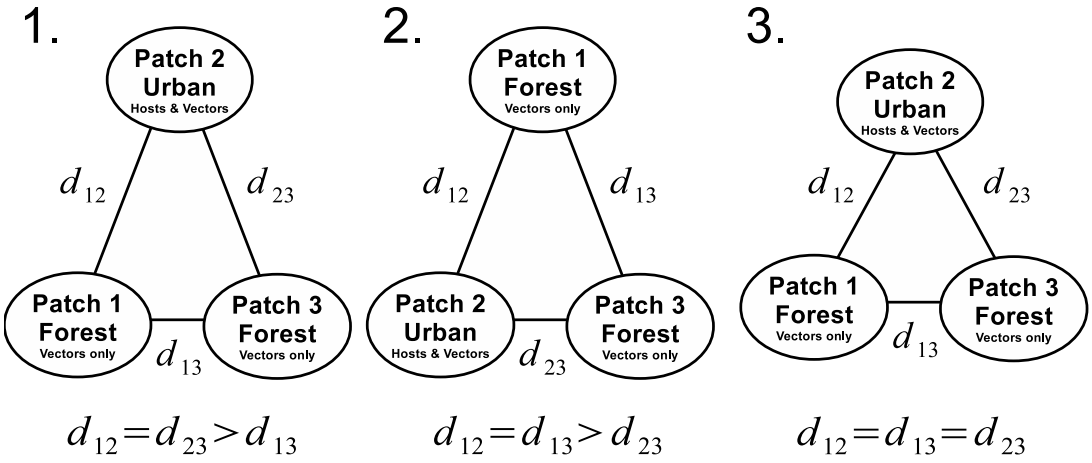

Figure 6-14: Schematic of the three patch arrangements considered for the three patch model, with humans in one patch. Arrangement 1 is an isosceles triangle with the shortest edge between two forest patches. Arrangement 2 is an isosceles triangle with the shortest edge between the urban patch and a forest patch. Arrangement 3 is an equilateral triangle.

The basic reproductive number R_0 was calculated for the system (6.17)-(6.29) from a Next Generation Matrix, and used to investigate the relationship between potential disease spread and model parameters. We found that R_0 was negligibly different for the 3 patch arrangements in Figure (6-14), and we therefore focus our investigation on the impact of vector movement and host distribution on R_0.

In Figure (6-15) we find that increasing the number of non-human blood sources decreases R_0. This holds true for all inertia measures p_τ. Results are similar to those in Figure (6-4) for the two patch model with humans in one patch. Increasing the number of hosts in the forest decreases the number of vectors in the transmission patch and reduces the potential spread of infection. Since the number of non-human blood sources is split between two forest patches, a greater proportion of vectors reside in the transmission patch and the reduction in R_0 is less than for the two patch model.

The relationship between R_0 and inertia p_τ depends on the forest-urban blood source ratio p_n. When $p_n < 1$ and $p_n = 1$, increasing inertia increases R_0. In this case the higher number of blood sources in the urban patch make it most attractive to

sandflies. Increasing inertia increases the likelihood vectors remain in the transmission patch and so transmission and R_0 increase. When $p_n > 1$ and the forest patch is most attractive, increasing inertia decreases ESS. Increasing p_τ increases the likelihood vectors do not enter the urban patch, and so transmission and R_0 decrease. R_0 always increases when $p_\tau < 1$ and inertia is low, as decreasing the rate of movement increases the duration of a visit to the transmission patch. Since non-human blood sources are distributed between two patches, the urban patch is more attractive in the three patch model than in the two patch model. This increases the impact of inertia when comparing Figures (6-5) and (6-15).

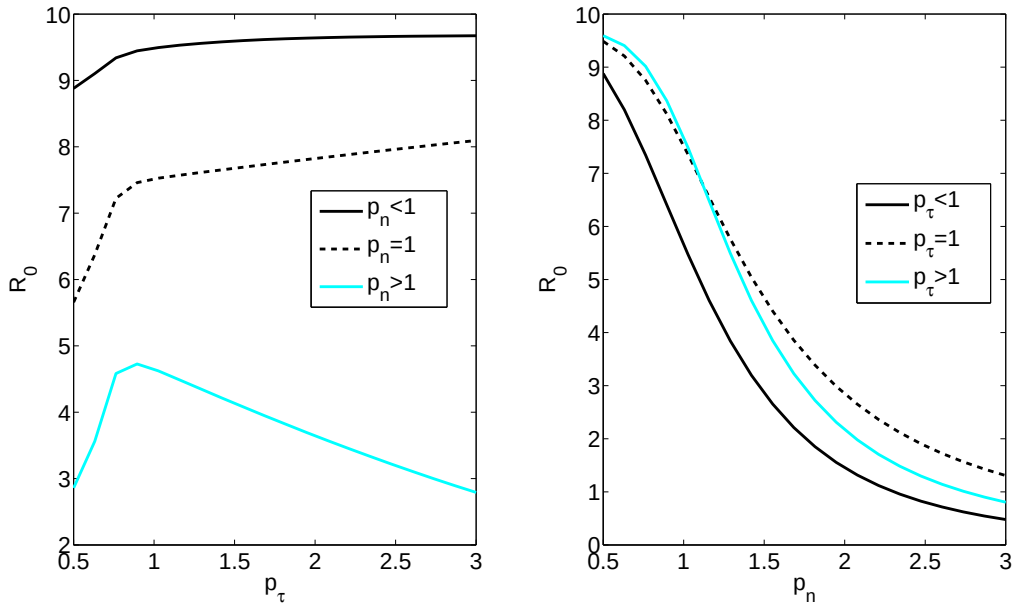

Figure 6-15: Relationship between R_0, inertia p_τ and the ration of non-human blood sources p_n. Three patch model, humans in one patch (6.17)-(6.29). Results are shown for patch arrangement 1. Parameters that do not vary are fixed at the values given in Table (C.1).

In Figure (6-16) we see that R_0 is at its highest when non-human blood sources are split equally between the two forest patches. As p_f increases, the proportion of blood sources in the urban patch becomes greater than that in either of the two forest patches. Vectors are more likely to move to and stay in the urban patch where transmission can occur. The duration of transmission and hence R_0 are increased. The value of R_0 is highest when patches are arranged in isosceles triangle 1, from Figure (6-14). In this case the transmission patch is isolated from the forest patches, and so vectors are less likely to move away. Again, this increases the duration of transmission and R_0.

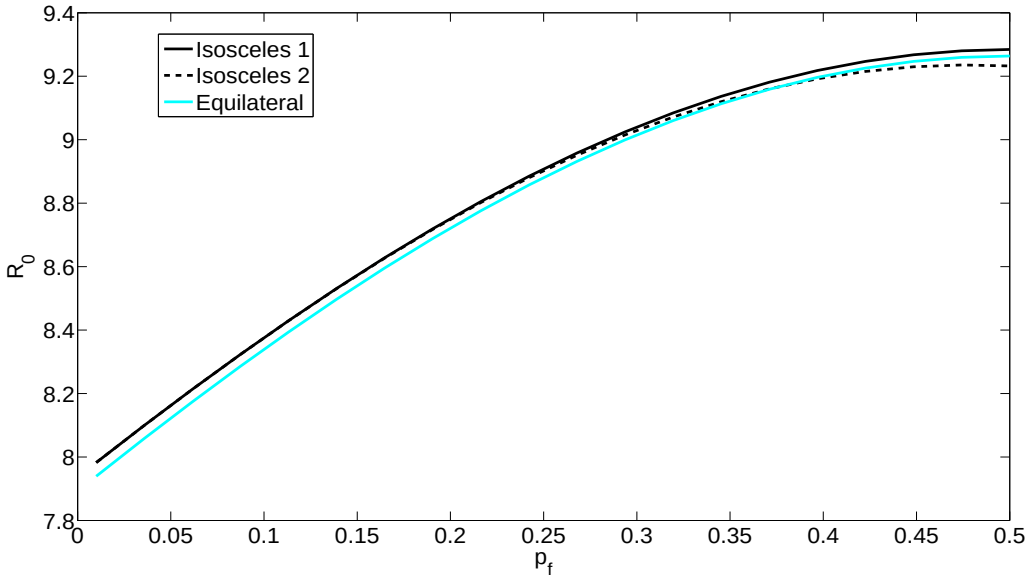

Figure 6-16: Relationship between R_0 and non-human blood source distribution p_f. Three patch model, humans in one patch (6.17)-(6.29). Results are shown for each of the three patch arrangements given in Figure (6-14). Parameters that do not vary are fixed at the values given in Table (C.1).

6.7.1 Virulence in the Vector

A concave trade-off of the form $\beta = \frac{\hat{c}x}{x+1}$ will now be assumed between the bite rate β and virulence in the vector for the three patch model with humans in one patch. We find that the ESS virulence is dependent on the same parameters as in the two patch model with humans in one patch. The vector mortality rate μ_v, the forest-urban blood source ratio p_n, scaling factor θ and inertia parameter p_τ all influence ESS virulence. In the three patch model with humans in one patch, the patch arrangement and host distribution also impact upon ESS virulence. The relationship between ESS virulence and the parameters from which it is constructed is shown in Figure (6-17), (6-18), (6-19) and (6-20).

In Figures (6-17)-(6-20) we find that parameters have similar relationships with the ESS virulence as in the two host model with humans in one patch and a trade-off between β and x. Parameters which increase either the duration of infection or the rate of movement increase the ESS virulence. For the three patch model, we also find that for the majority of parameters the ESS virulence also depends on the patch structure and host distribution. The only exception is the vector mortality rate μ_v.

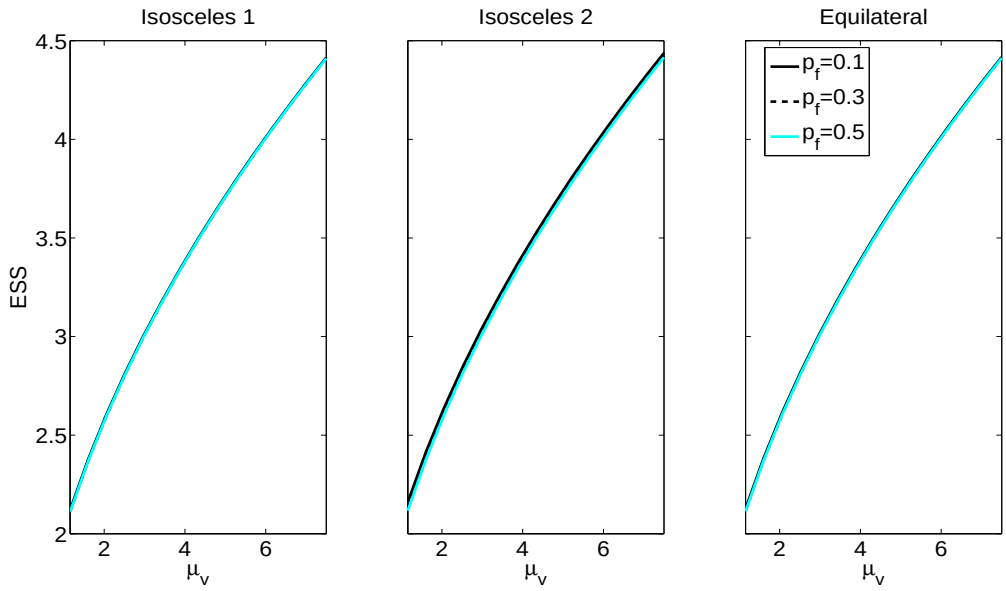

Figure 6-17: Relationship between ESS virulence in the vector and vector mortality μ_v, three patch model humans in one patch (6.17)-(6.17) with $\beta = \frac{\hat{c}x}{x+1}$. Each panel represents the ESS virulence when patches are laid out in one of the structures given in Figure (6-14). For each patch structure the ESS virulence is displayed for three distributions of non-human blood sources. Parameters which are not varied are fixed at the values in Table (C.1).

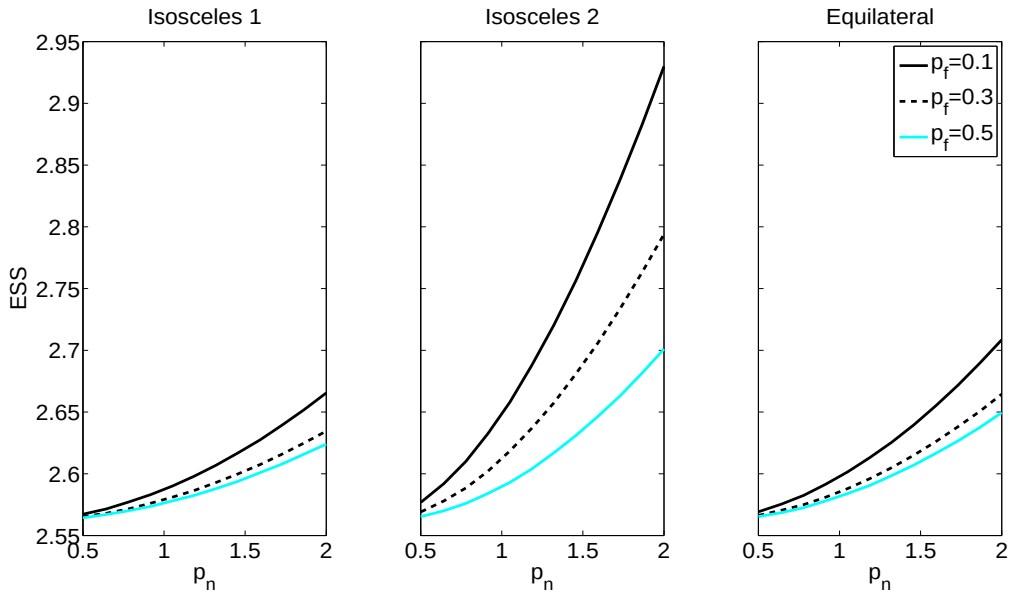

Figure 6-18: Relationship between ESS virulence in the vector and the forest-urban blood source ratio p_n, three patch model humans in one patch (6.17)-(6.17) with $\beta = \frac{\hat{c}x}{x+1}$. Each panel represents the ESS virulence when patches are laid out in one of the structures given in Figure (6-14). For each patch structure the ESS virulence is displayed for three distributions of non-human blood sources. Parameters which are not varied are fixed at the values in Table (C.1).

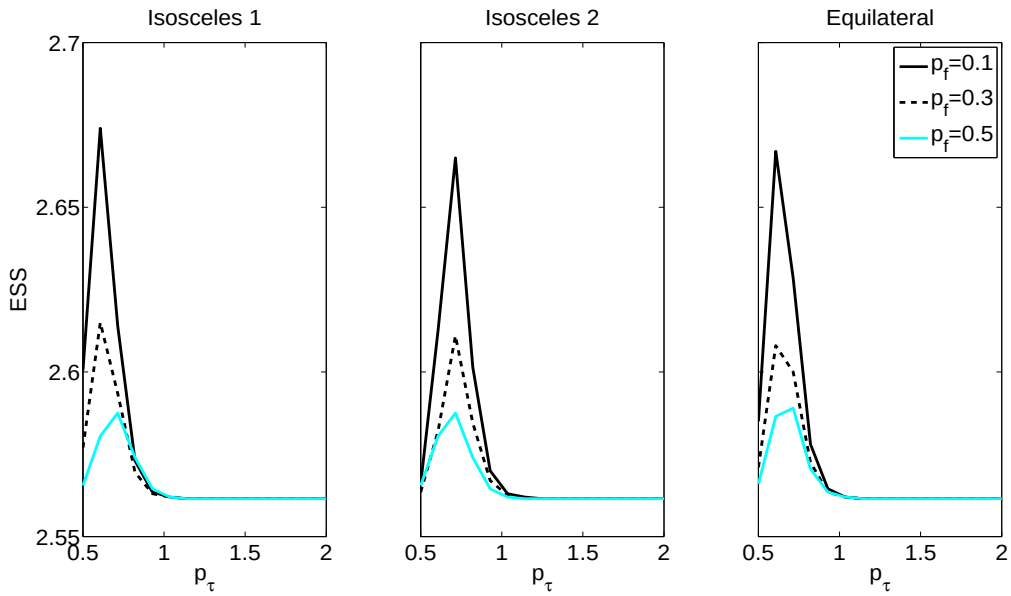

Figure 6-19: Relationship between ESS virulence in the vector and inertia p_τ, three patch model humans in one patch (6.17)-(6.17) with $\beta = \frac{\hat{c}x}{x+1}$. Each panel represents the ESS virulence when patches are laid out in one of the structures given in Figure (6-14). For each patch structure the ESS virulence is displayed for three distributions of non-human blood sources. Parameters which are not varied are fixed at the values in Table (C.1).

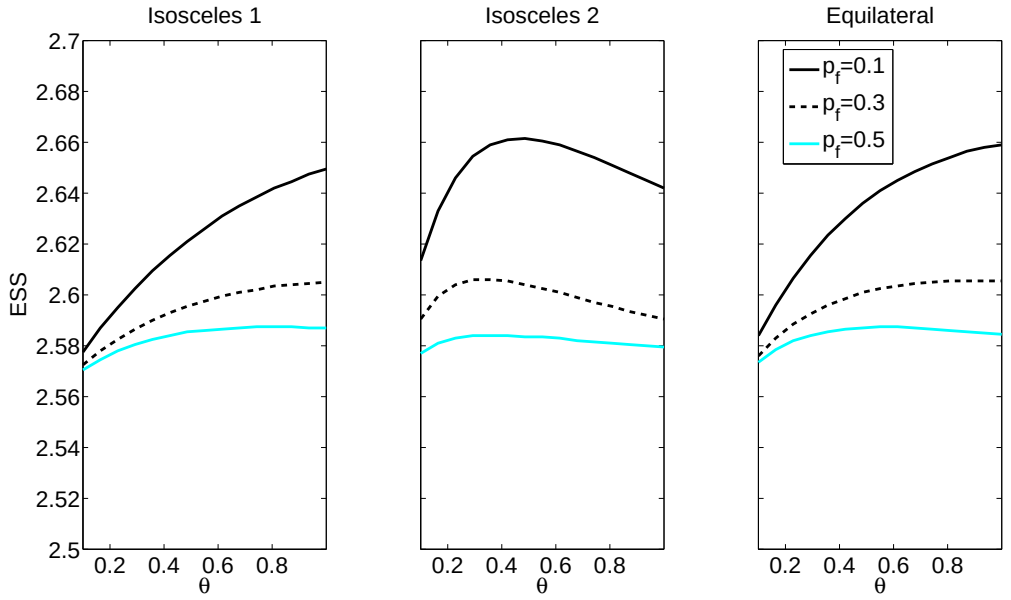

Figure 6-20: Relationship between ESS virulence in the vector and the scaling parameter θ, three patch model humans in one patch (6.17)-(6.17) with $\beta = \frac{\hat{c}x}{x+1}$. Each panel represents the ESS virulence when patches are laid out in one of the structures given in Figure (6-14). For each patch structure the ESS virulence is displayed for three distributions of non-human blood sources. Parameters which are not varied are fixed at the values in Table (C.1).

In Figure (6-17) we find that patch structure and host distribution have a negligible impact on the relationship between the ESS virulence and μ_v. The duration of infection is unaffected by parameters which govern movement and patch attractivity. For all other parameters, the ESS virulence is lowest when $p_f = 0.5$ and non-human blood sources are equally distributed between the two forest patches. In this case the transmission patch is the most attractive patch to the vector and so the duration and frequency of visits to the transmission patch is high. Increasing the duration of transmission leads to a decrease in ESS virulence. We compare the relationship between μ_v and ESS virulence for different models in Figure (6-26).

In Figure (6-18) we find that increasing the forest-urban blood source ratio p_n increases ESS virulence. The greater the attractiveness of the non-urban patches, the shorter the duration of transmission and the higher the ESS virulence. The ESS virulence is highest when patches are arranged in an isosceles triangle with the shortest edge between an urban and forest patch. The greater the number of non-human blood sources the more attractive the forest patches become. If a forest patch is both attractive and close by, a vector is unlikely to move to or stay in the urban patch. This reduces the duration of transmission and increases the ESS. The ESS virulence is therefore smallest when the transmission patch is isolated from the forest patches in isosceles triangle 1. The additional distance between the urban and forest patches reduces the likelihood of movement away from the transmission patch.

In Figure (6-19) we find that the relationship between inertia p_τ and ESS vector virulence is similar to that in Figure (6-9) for the two patch model with humans in one patch. The ESS virulence is slightly higher when one of the transmission patches is isolated, as vectors are less likely to move into one of the transmission patches and transmission is reduced.

In Figure (6-20) we find that the relationship between the scaling parameter θ and ESS virulence is dependent on patch structure. When patches are arranged in either an equilateral triangle or an isosceles triangle with an isolated transmission patch, increasing the scaling parameter θ increases the ESS virulence. When patches are arranged in an isosceles triangle with the shortest edge between a forest and urban patch, increasing θ first increases, then decreases the ESS. As in the two host model with humans in one patch, increasing θ increases movement and decreases the duration of each visit to the transmission patch. The close proximity of the urban patch and a forest patch in arrangement 2 increases movement into the urban patch, thus the duration of transmission is not so greatly decreased. This is exaggerated by the fact that there are more human than non-human blood sources for the value of p_n used.

Results show that the ESS virulence is dependent on the distribution of blood

sources between the forest patches. Increasing p_f in the interval $0 \leq p_f \leq 0.5$ increases the proportion of non-human blood sources residing in patch 1 and decreases the ESS virulence. Dividing the non-human blood sources equally between two patches decreases the attractiveness of the forest relative to the urban patches. The dilution effect caused by the non-human blood source is at a minimum so transmission increases and the ESS decreases. Deforestation which reduces the number of forest patches and causes an increase in non-human blood source numbers will therefore increase disease virulence in the vector.

In some cases the ESS virulence also depends on patch arrangement. Increasing the forest-urban blood source ratio p_n increases the ESS virulence in the vector; however the magnitude of the increase depends on the patch structure. For all non-human blood source distributions p_f the ESS virulence is highest for isosceles triangle 2, when the urban patch is close to a forest patch. The closer the urban patch to the forest patch the greater the rates of movement between the two patches. As p_n increases, vectors are more likely to move into forest patch 3 and stay there. This decreases both the number of vectors in the urban patch, the rate of transmission is reduced and the ESS virulence increases. This suggests that deforestation and urbanisation reducing the distance between the urban and forest patches can increase disease virulence within the vector population. As in Section (6.5.3) it can be shown that increasing vector virulence increases endemic infection prevalence in humans. This holds for all patch arrangements considered. Land-use change can therefore increase infection prevalence in humans.

6.8 Three Patch Model, Humans in Two Patches

We extend our investigation of the three patch model by considering a three patch model with two urban patches and one forest patch. This will allow us to investigate the impact of patch structure and host distribution when more than one patch contains a competent host. We extend the system of equations (6.17)-(6.29) to include human dynamics in patch 1:

$$\frac{dS_{h1}}{dt} = \mu_h N_{h1} - \mu_h S_{h1} - \frac{\beta \pi_h S_{h1} I_{v1}}{N_{h1}} \tag{6.30}$$

$$\frac{dI_{h1}}{dt} = \frac{\beta \pi_h I_{v1} S_{h1}}{N_{h1}} - (\chi_h + \mu_h) I_{h1} + \epsilon_h R_{h1} \tag{6.31}$$

$$\frac{dR_{h1}}{dt} = \chi_h I_{h1} - (\epsilon_h + \mu_h) R_{h1} \tag{6.32}$$

and alter equations (6.17) and (6.18) for susceptible and latent vectors in order to incorporate infection:

$$\frac{dS_{v1}}{dt} = \frac{\mu_v N_{v1} r_v N_h^0}{N_{v1}+N_{v2}+N_{v3}} - \mu_v S_{v1} - (c_{31}+c_{21})\, S_{v1} + c_{13}S_{v3} + c_{12}S_{v2} \quad (6.33)$$

$$- \frac{\beta \pi_v S_{v1} I_{h1}}{n_{h1}} \quad (6.34)$$

$$\frac{dE_{v1}}{dt} = \frac{\beta \pi_v S_{v1} I_{h1}}{N_{h1}} + c_{13}E_{v3} + c_{12}E_{v2} - (c_{31}+c_{21})\, E_{v1} - (\mu_v + \sigma_v)\, E_{v1}. \quad (6.35)$$

We consider three arrangements of the three patches, all of which are illustrated in Figure (6-21). Humans are split between the two urban patches such that $N_{h1} = (1-p_h)N_h$ and $N_{h2} = p_h N_h$ to allow us to consider different host distributions.

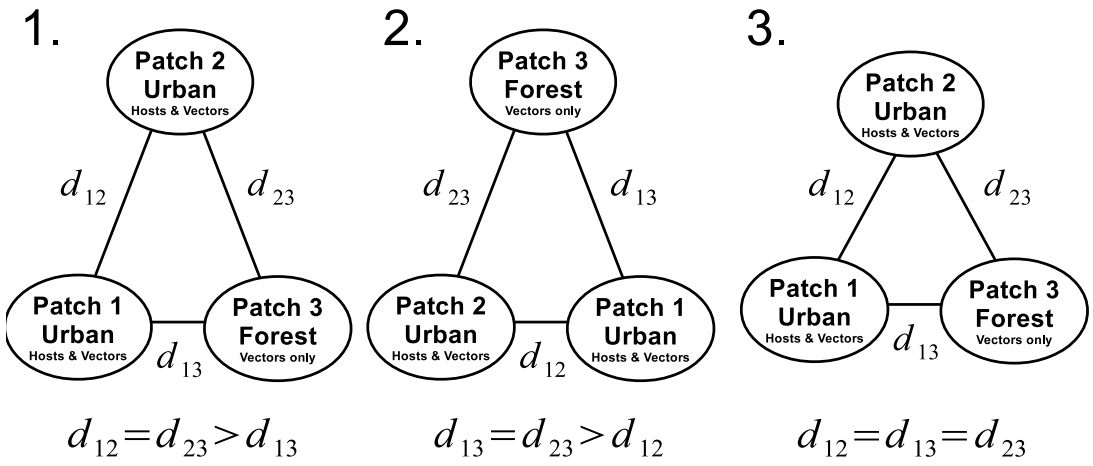

Figure 6-21: Schematic of the three patch arrangements considered for the three patch model, with humans in two patches. Arrangement 1 is an isosceles triangle with the shortest edge between an urban and forest patch. Arrangement 2 is an isosceles triangle with the shortest edge between two urban patches. Arrangement 3 is an equilateral triangle.

The basic reproductive number was calculated using a Next Generation Matrix and used to investigate the relationship between R_0 and lower level parameters. Figure (6-22) shows the impact of varying the host distribution on potential disease spread. We find that for all patch arrangements, R_0 is at its lowest when humans are split equally between the two urban patches. The likelihood of transmission, and hence R_0, is maximised when all human hosts are in one patch. In this case, a large proportion of hosts are available for blood meals and the patch is highly attractive to vectors. A large human population counteracts the dilution effect caused by the non-human blood source, and transmission is maximised.

Potential disease spread also depends upon the patch arrangement. In Figure (6-22), R_0 is highest when the patches are arranged in isosceles triangle one and one of the two urban patches is isolated. Vectors are first attracted to the isolated urban patch since it contains a large number of blood sources. Since the distance between urban patch 2 and the other urban and forest patches is high, vectors are then unlikely to to leave patch 2 and the duration of transmission is increased.

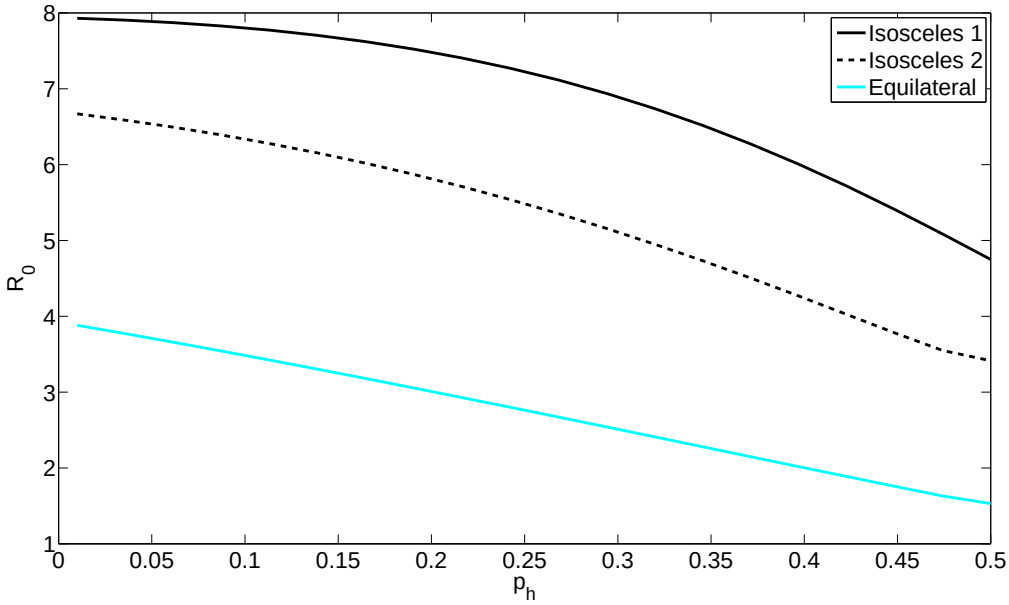

Figure 6-22: Relationship between R_0 and the host distribution parameter p_h, three patch model with humans in two patches. Results are displayed for each of the three patch arrangements given in Figure (6-21). All other parameters are fixed at the values given in Table (C.1).

6.8.1 Virulence in the Vector

We now impose a trade-off of the form $\beta = \frac{\hat{c}x}{x+1}$ between the bite rate β and virulence in the vector x. We find that the ESS virulence depends on the movement parameters θ, p_n and p_τ and the vector mortality rate μ_v. We concentrate our investigation on the forest-urban blood source ratio p_n, inertia p_τ and mortality μ_v which have the greatest impact on ESS virulence. Figures (6-23) and (6-24) show how the forest-urban blood source ratio p_n and inertia p_τ impact on ESS virulence for the three patch model with humans in two patches. Figure (6-26) shows the relationship between ESS virulence and vector mortality μ_v.

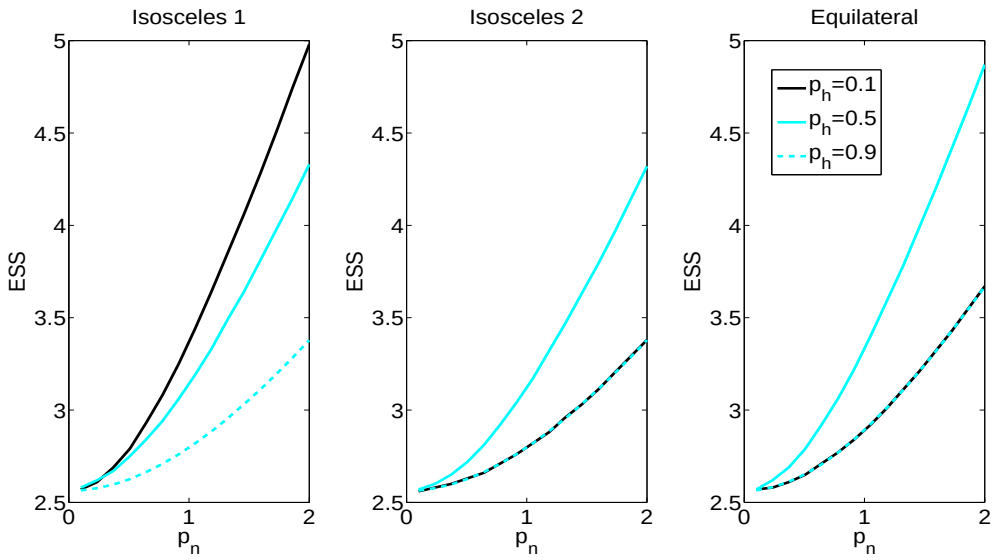

Figure 6-23: Relationship between ESS virulence in the vector and the ratio of non-human blood sources p_n, three patch model humans in two patches with $\beta = \frac{\hat{c}x}{x+1}$. Each panel represents the ESS virulence when patches are laid out in one of the structures given in Figure (6-21). For each patch structure the ESS virulence is displayed for three host distributions. Parameters which are not varied are fixed at the values in Table (C.1).

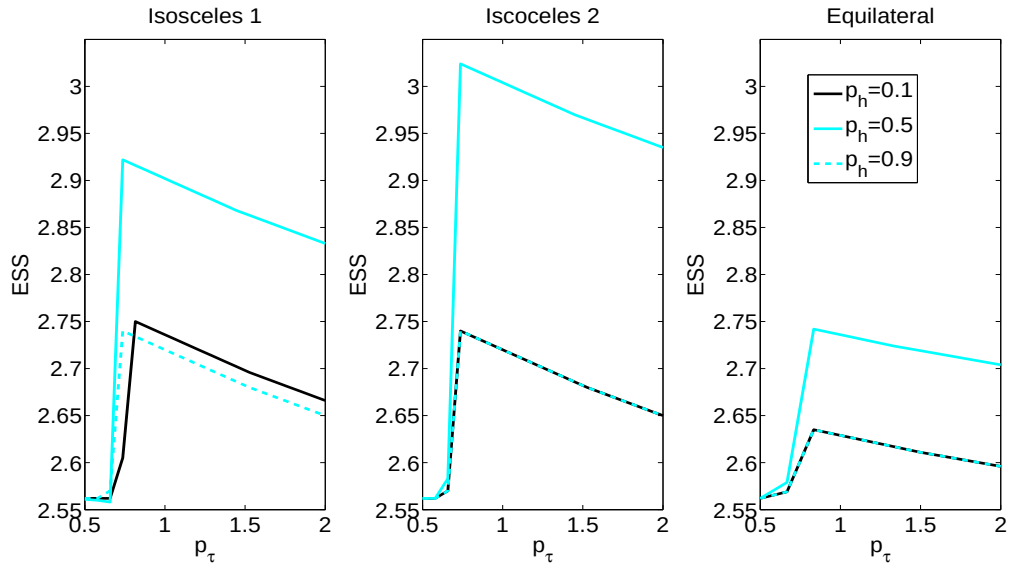

Figure 6-24: Relationship between ESS virulence in the vector and inertia p_τ, three patch model humans in two patches with $\beta = \frac{\hat{c}x}{x+1}$. Each panel represents the ESS virulence when patches are laid out in one of the structures given in Figure (6-21). For each patch structure the ESS virulence is displayed for three host distributions. Parameters which are not varied are fixed at the values in Table (C.1).

In Figure (6-23) we find that increasing the ratio of non-human blood sources p_n increases ESS virulence. The same result was obtained for both the two and three patch models with one human patch. In the case of the three patch model with humans in two patches, we also find that the ESS depends on the patch arrangement and host distribution. When both transmission patches are the same distance from the forest patch, the ESS virulence is highest when $p_h = 0.5$ and humans are equally split between the two urban patches. When humans are evenly spread out and forest hosts are concentrated, movement into the forest is at its highest. This increased rate of movement decreases the time available for transmission and so the ESS virulence increases. When patches are arranged in isosceles triangle 1 and one urban patch is isolated, the ESS virulence is lowest when the majority of humans are found in the isolated patch. Increasing the number of hosts in the isolated patch reduces the ESS virulence as vectors are less likely to move to the forest patch, and transmission increases. Comparing results for all three patch arrangements we find that the ESS is lowest when the forest patch is isolated (patch arrangement 2). In this case movement to the forest is reduced, and a greater increase in p_n is required for vectors to leave the urban patches.

In Figure (6-24) we find that inertia p_τ has a greater impact on ESS virulence in the three patch model with humans in two patches than in Figures (6-9) and (6-19) for the two and three patch models with humans in one patch. Splitting the human population between two patches strengthens the dilution effect of the non-human blood source and increases the attractiveness of the forest. The reduction in ESS virulence for $p_\tau > 1$ is therefore slower than in Figures (6-9) and (6-19) as fewer vectors are attracted to the transmission patches. When humans reside in two of three patches, the ESS virulence is always highest when humans are equally split between the two urban patches. In this case the concentrated population of non-human blood sources in the forest make the forest patch the most attractive of the three. The duration of transmission is decreased and ESS increases. When one urban patch is isolated, increasing inertia leads to the biggest decrease in ESS virulence. Vectors are more likely to stay in the isolated patch, both due to its isolation and increased inertia. The duration of transmission is increased and the ESS decreases.

When the human population is split between two patches we find that the potential spread of infection is reduced. This suggests that urbanisation which increases the number of human blood sources in a patch will increase disease transmission. Although this leads to a reduction in ESS vector virulence in some cases, the splitting of the human population leads to a patch arrangement having a greater impact on transmission and ESS virulence.

In Figure (6-25) we find that increasing the ESS virulence for the three patch model with humans in two patches increases the number of human infections. In the example shown ($p_h = 0.1$) and the majority of humans reside in a non-isolated urban patch. The dependence of the ESS on patch arrangement can also be seen in the infection prevalence. The greatest increase in human infection prevalence occurs when patches are arranged in isosceles triangle 2. In this case the forest patch is isolated and vectors are more likely to reside in and stay in a transmission patch.

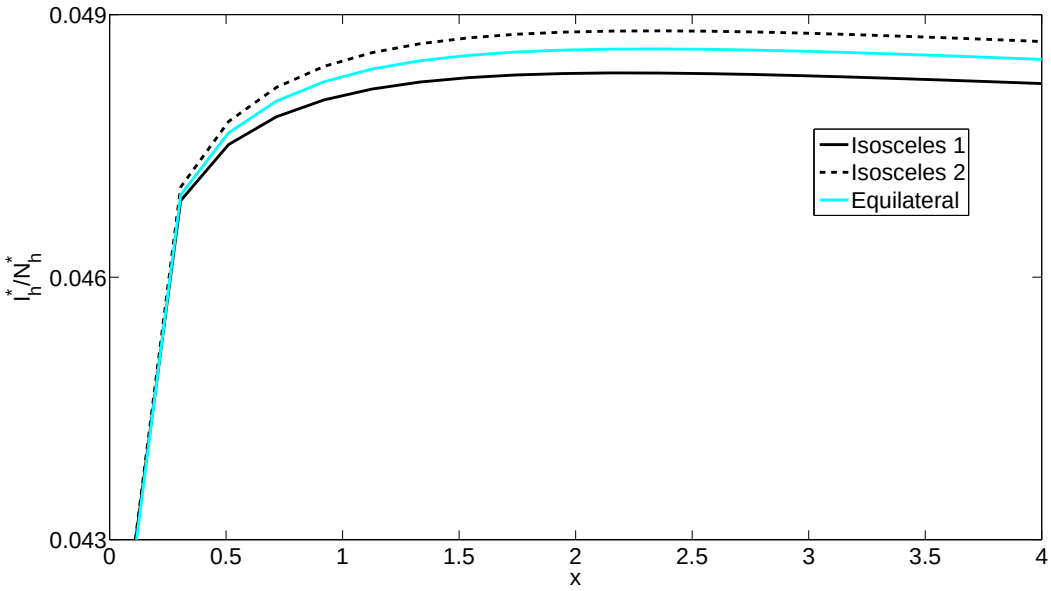

Figure 6-25: Relationship between endemic infection prevalence in humans and virulence in the vector when a trade-off of the form $\beta = \frac{\hat{c}x}{x+1}$ is in place between vector virulence and bite rate. Three patch model, humans in two patches. Results are displayed for the three patch structures given in Figure (6-21). Parameters that do not vary are fixed at the values given in Table (C.1). $p_h = 0.1$.

6.9 Comparing Model Results

To review the impact of land-use change on ESS virulence we compare the relationship between vector mortality μ_v and ESS vector virulence for all the metapopulation models considered in detail in Chapter 6. We compare results for the vector mortality rate μ_v as this is the only parameter that affects the ESS for all model variants. Results are shown in Figure (6-26).

We find that ESS virulence is higher for the two patch model with humans in one patch than for either of the three patch models. Concentrating the non-human blood sources in one patch strengthens the dilution effect and increases the likelihood

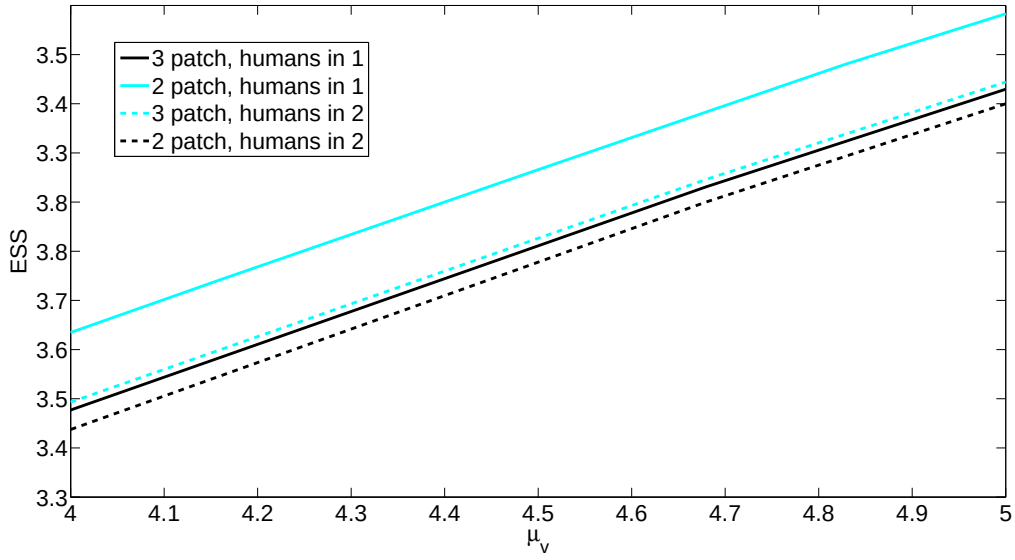

Figure 6-26: Relationship between ESS virulence in the vector and the vector mortality rate μ_v for the two patch model with humans in one or two patches and the three patch model with humans in one or two patches when a trade-off of the form $\beta = \frac{\hat{c}x}{x+1}$ is in place between vector virulence and bite rate. Parameters that do not vary are fixed at the values given in Table (C.1).

vectors will move to and stay in the forest. This reduces transmission in the urban patch and increases ESS virulence. When the non-human blood source population is split between two patches in the three patch model the ESS is reduced. Splitting up the human population leads to a slight increase in ESS virulence, since it reduces the number of susceptible hosts in one of the urban patches. The ESS virulence is lowest when humans reside in all patches. In this case the duration of transmission is maximised as it is independent of vector movement. Results therefore suggest that urbanisation which decreases the number of urban patches or increases host density increases both ESS virulence and human infection prevalence. The removal of forest patches via deforestation can also increase ESS virulence in the vector and hence human infection prevalence.

6.10 Conclusions

Our results show that urbanisation and deforestation can increase not only the rate of vector-borne disease transmission but also disease virulence within the vector population. Removing the sandfly natural habitat via deforestation, or reducing the distance

between human and vector natural habitat via urbanisation increases the likelihood of urban transmission and can lead to increases in human infection prevalence. Increasing the number of human hosts in an urban patch also increases the attractiveness of urban patches and causes vectors to abandon their natural habitat. Control aimed at reducing the number of non-human blood sources would therefore be counterproductive. The presence of a non-human blood source which cannot transmit infection causes a dilution effect, similar to that of dead-end human hosts in the zoonotic model of Chapter 2. The force of infection on the human population is reduced, as some vectors are attracted to forest patches where transmission cannot occur. Assuming vectors can be supported in urban environments, reducing the number of blood sources in the forest will therefore encourage urban transmission. This suggests that deforestation which decreases the number of non-human blood sources in a patch by splitting them between patches will increase the rate at which vectors move to the urban patch and lead to increased disease transmission.

When transmission is not possible in all model patches, we find that the ESS virulence in the vector is dependent on the rate of vector movement. The use of a gravity term to model the movement of vectors has also allowed us to assess the impact of patch attractiveness on both ESS vector virulence and human infection prevalence. Increasing inertia can increase ESS virulence, which in turn increases human infection prevalence. Decreasing the number of non-human blood sources in the forest decreases ESS virulence, but only due to an increase in disease transmission. Disease control which impacts on the rate of vector movement will therefore need to be carefully considered before it is employed. The ESS virulence in the human population was unaffected by vector movement, and results are the same for both non-spatial and metapopulation models.

Chapter 7

Conclusions

In this thesis we investigate the epidemiology and evolution of vector-borne disease. We suggest suitable strategies for disease control and prevention, and assess their evolutionary implications.

In Chapter 2 we construct a mathematical model for leishmaniasis which includes disease relapse in the host. We find that the rate and duration of disease transmission are key factors in determining potential disease spread; however human relapse is the driving force behind anthroponotic disease at endemic equilibrium. When disease is zoonotic and humans are dead-end hosts, asymptomatic dogs are integral for both the spread and maintenance of leishmaniasis. This is confirmed by an elasticity analysis in Chapter 3. Comparing the elasticities of R_0 and I^* to disease parameters we also find that in the absence of evolution, the most effective control for both anthroponotic and zoonotic leishmaniasis is to reduce the rate of vector transmission. Results can easily be obtained for other vector-borne diseases by considering alternative parameterisations.

In Chapter 4 we use optimal control theory to determine optimal vaccination and spraying strategies for an anthroponotic vector-borne disease. We find that vaccination is more effective than spraying and can greatly reduce the size of the epidemic peak. The impact of vaccination can be increased by simultaneously spraying throughout the epidemic peak, however the application of spraying as a sole control proves to be ineffective. The reduction in infection prevalence caused by spraying alone is outweighed by its cost. Host relapse exhibited by leishmaniasis increased the average rate of control for both the one and two control problems. Including the total size of the population to be vaccinated in the objective function also increases the average rate at which control is applied.

In Chapter 5 we investigate the evolution of virulence in both the host and vector species. Results are used to determine the evolutionary impact of disease control.

When a trade-off is in place between transmission from a species and virulence within the same species, we find that increasing the duration of transmission leads to the fixation of heightened virulence pathogen strains. We also find that any increase in ESS virulence leads to an increase in human infection prevalence. When virulence is in the host, control techniques which increase the rate of host recovery can therefore be counterproductive and lead to an increase in human infection prevalence. When virulence is in the vector, we find that controls which reduce vector life expectancy are counterproductive and lead to an increase in human infection prevalence. We suggest this is an explanation for why the spraying of insecticide has failed to prevent the continued spread and emergence of leishmaniasis, and may warrant further investigation.

In Chapter 6 we extend the evolutionary investigations of Chapter 5 to a metapopulation model with vector movement. We find that land-use change such as urbanisation and deforestation has the potential to increase both disease transmission and ESS virulence. Reducing the distance between forest and urban patches increases both the attractiveness of the human habitat and the likelihood of urban transmission. When transmission is not possible in all model patches, we find that the ESS virulence in the vector is dependent on the rate of vector movement. Using a gravity term to represent vector movement we find that both the number of blood sources in the forest and inertia can increase ESS virulence. Patch arrangement and the distribution of human hosts can also impact on transmission and virulence. If a large proportion of human hosts are isolated from the forest, the ESS virulence decreases, whereas isolating a small proportion of human hosts increases ESS virulence.

This thesis provides a thorough examination of a base model for leishmaniasis; however our results will also be of use when considering the control and prevention of other vector-borne diseases. Not only can the one-host one-vector model introduced in Chapter 2 be easily adapted for other vector-borne diseases, but many of the results discussed in later chapters can be directly applied. One such result is contained within Chapter 4, where we find that spraying alone is an inefficient control technique. Since this result is independent of both host relapse and the cost of control it will hold true for other vector-borne diseases which infer the immunity assumed by our model. One example is the mosquito borne disease dengue, an anthroponotic viral disease whose control depends solely on vector control measures [81]. Although dengue infections vary in severity, lifelong immunity from a strain is obtained after infection, and the disease can be modelled in a similar way to leishmaniasis. Spraying has been implemented against dengue for many years in countries such as Singapore, however the disease continues to spread [2]. Such experimental evidence supports the findings of Chapter 4 and suggests that other control techniques are necessary. The inefficiency of spraying

when relapse increases the cost of infection also suggests that spraying may not be the best control for vector-borne diseases such as malaria and African trypanosomiasis, which do not infer permanent immunity. Although this differs from the optimal control work in [3] which suggests that spraying can lead to a large reduction in malaria prevalence, the authors only consider control targeted at a small proportion of the vector population and not the population as a whole. The continued emergence of malaria despite the application of many spraying regimes also suggests that spraying may not be the most efficient control.

The adaptive dynamics work in Chapters 5 and 6 can also be related to other vector-borne diseases. For our anthroponotic, zoonotic and amphixenotic models we find that when a trade-off is assumed between transmission and virulence the ESS within a species depends on the parameters governing the duration of transmission. This will hold true for other vector-borne diseases, even if the parameters governing the duration of transmission differ from that of leishmaniasis. For example, West Nile virus is a zoonotic mosquito borne infection with a primary reservoir in birds [80]. Unlike leishmaniasis West Nile virus does not relapse, and so the ESS virulence within the host will depend only on the rates of host recovery and mortality. Control aimed at the host is potentially counterproductive and can lead to the fixation of higher virulence pathogen strains. We expect a similar result for malaria. This matches the findings of MacKinnon and Read in [56] who find that immunity promotes virulence evolution in malaria.

Although the host ESS will need to be adjusted for different diseases, the vector ESS is independent of host disease dynamics. We therefore conjecture that the expressions calculated in Chapters 5 and 6 can be used directly for other vector-borne diseases. This suggests that the application of spraying to reduce vector life expectancy will not only increase the virulence of leishmaniasis, but also that of other vector-borne diseases. In addition to increasing vector virulence, we have also found that reducing the duration of vector transmission can lead to increased infection prevalence. Control techniques aimed at reducing the duration of vector transmission may therefore be counterproductive for a range of vector-borne diseases. Further experimental studies such as [71] for leishmaniasis and [24] for West Nile Virus are therefore required to identify those diseases for which vector transmission-virulence trade-offs exist.

For many vector-borne diseases no efficient treatment or vaccination is available and so prevention methods are very important. The spraying of insecticide is a commonly used preventative method; however it has achieved mixed results in the past [2]. Not only have we shown in Chapter 4 that spraying can be inefficient, but in Chapters 5 and 6 we find that spraying can be counterproductive and result in increased human infec-

tion prevalence. Since parameters controlling the duration of transmission also govern the virulence and prevalence of a disease we therefore suggest the implementation of control aimed at reducing the vector transmission rate. One such control is the use of bed nets to reduce the vector bite rate. In Chapter 3 we show that control targeted at the bite rate has the potential to produce consistent results. The use of bed nets will also have limited impact on virulence evolution as they interrupt the transmission cycle without altering the epidemiology of the disease within the host or vector. Bed nets are both affordable and attainable and can be used to protect against bites from a range of insect vectors.

In order to further investigate the use of bed nets as a control technique the optimal control work in Chapter 4 could be extended to consider a control reducing the bite rate β. Furthermore, optimal control could be considered for the zoonotic and amphixenotic models, for both one and multiple control problems. The adaptive dynamics framework used in Chapters 5 and 6 could also be extended to consider multiple trait evolution. This would allow us to assess the impact of different control techniques in a system where both host and vector virulence can evolve.

When considering our model for the spread of leishmaniasis, control could also be investigated for more specific strains of infection. For example, evidence in [79] suggests that in some cases asymptomatic humans exist as well as asymptomatic dogs. A further compartment could therefore be added to the model to represent humans that do not show obvious signs of infection and remain asymptomatic after the latent period. Our research has shown that asymptomatic and relapsing hosts must be included in future model systems as they can greatly increase the rate of control required to prevent an epidemic from occurring. It is also suggested in [79] that sandflies are more active at certain times of the year. The optimal control problems and evolution of virulence work could therefore be repeated for a model with seasonal transmission. Likewise, calculations for the metapopulation model in Chapter 6 could be furthered by including both host and vector movement. This would allow us to assess the impact of human commuting patterns on disease spread and virulence evolution; however, considering the results in Chapter 6 we suggest that human movement will only affect the ESS within the host population. It is therefore questionable whether including human movement into the metapopulation model would provide novel results.

Although many studies focus upon the impact of pathogen resistance on disease control they do not consider the effects of pathogen virulence. This is particularly true for vector-borne diseases. In this thesis we have found that many control and prevention techniques for vector-borne diseases not only lead to the fixation of higher virulence pathogen strains in both host and vector populations, but can increase the

human infection prevalence. The ability of heightened vector virulence to increase human infection prevalence provides a novel explanation as to why control techniques such as spraying have not prevented the emergence of vector-borne diseases such as leishmaniasis. Future work to determine control strategies for vector-borne diseases should therefore include virulence within the vector species to obtain a more accurate result. Our research indicates that the use of bed nets may be a more effective control technique for all vector-borne diseases. Not only are bed nets affordable and available, they can be used to disrupt the transmission cycle without altering the duration of transmission or pathogen virulence.

Appendix A

Steady States for the One-Host One-Vector Model

By setting model equations (2.1)-(2.7) to zero and solving for each variable, two steady states are obtained for the one-host one-vector model. The first is the trivial disease free steady state:
$\left(S_h^0, E_h^0, I_h^0, R_h^0, S_v^0, E_v^0, I_v^0\right) = \left(N_h^0, 0, 0, 0, r_v N_h^0, 0, 0\right)$.
The second is a non-trivial steady state which can be found in table A.

Variable	Value at Steady State
S_h^*	$\frac{\lambda_2}{\sigma_h\left(\epsilon_h+\mu_h\right)\kappa_1}$
E_h^*	$\frac{\mu_h\lambda_1}{\sigma_h\left(\epsilon_h+\mu_h\right)\left(\mu_h+\sigma_h\right)\kappa_1}$
I_h^*	$\frac{\mu_h\lambda_1}{\left(\mu_h+\sigma_h\right)\left(\left(\mu_h+\epsilon_h\right)\left(\mu_h+\chi_h+\nu_h\right)-\epsilon_h\chi_h\right)\kappa_1}$
R_h^*	$\frac{\chi_h\mu_h\lambda_1}{\left(\mu_h+\sigma_h\right)\left(\epsilon_h+\mu_h\right)\left(\left(\mu_h+\epsilon_h\right)\left(\mu_h+\chi_h+\nu_h\right)-\epsilon_h\chi_h\right)\kappa_1}$
S_v^*	$\frac{\mu_v N_h^*\left(\mu_h+\sigma_h\right)\left(\left(\mu_h+\epsilon_h\right)\left(\mu_h+\chi_h+\nu_h\right)-\epsilon_h\chi_h\right)\kappa_1}{\sigma_v\beta\pi_v\kappa_2}$
E_v^*	$\frac{\mu_h\mu_v\lambda_1}{\left(\sigma_v+\mu_v\right)\sigma_v\kappa_2}$
I_v^*	$\frac{\mu_h\lambda_1}{\left(\sigma_v+\mu_v\right)\kappa_2}$

Where:

$$
\begin{aligned}
\lambda_1 &= r_v\beta^2\left(N_h^0\right)^2\pi_h\pi_v\sigma_h\sigma_v\left(\epsilon_h+\mu_h\right)-\mu_v\left(N_h^*\right)^2\left(\mu_v+\sigma_v\right)\mu_h^3 \\
&- \mu_v\left(N_h^*\right)^2\left(\mu_v+\sigma_v\right)\left(\left(\chi_h+\epsilon_h+\nu_h+\sigma_h\right)\mu_h^2+\left(\epsilon_h\nu_h+\sigma_h\left(\chi_h+\epsilon_h+\nu_h\right)\right)\mu_h\right) \\
&- \mu_v\left(N_h^*\right)^2\left(\mu_v+\sigma_v\right)\left(\epsilon_h\nu_h\sigma_h\right) \\
\lambda_2 &= \mu_v N_h^*\left(\mu_v+\sigma_v\right)\left(\mu_h^3+\mu_h^2\left(\chi_h+\epsilon_h+\nu_h+\sigma_h\right)\right) \\
&+ \mu_v N_h^*\left(\mu_v+\sigma_v\right)\left(\mu_h\left(\epsilon_h\nu_h+\sigma_h\left(\chi_h+\epsilon_h+\nu_h\right)\right)+\epsilon_h\nu_h\sigma_h\right) \\
&+ N_h^*\left(\mu_v+\sigma_v\right)\left(\beta N_h^0\pi_v\sigma_h\mu_h\left(\epsilon_h+\mu_h\right)\right) \\
\kappa_1 &= \beta\pi_v\left(\mu_h N_h^*\left(\mu_v+\sigma_v\right)+r_v\beta N_h^0\pi_h\sigma_v\right) \\
\kappa_2 &= \beta\pi_h\mu_v N_h^*\left(\mu_h^3+\mu_h^2\left(\chi_h+\epsilon_h+\nu_h+\sigma_h\right)\right) \\
&+ \beta\pi_h\mu_v N_h^*\left(\mu_h\left(\epsilon_h\nu_h+\sigma_h\left(\chi_h+\epsilon_h+\nu_h\right)\right)+\epsilon_h\nu_h\sigma_h\right) \\
&+ \beta\pi_h\left(\beta\mu_h N_h^0\pi_v\sigma_h\left(\mu_h+\epsilon_h\right)\right)
\end{aligned}
$$

The endemic infection prevalence is given by $I^* = I_h^* + I_v^*$.

Appendix B

Sensitivity Analysis for a 2 by 2 Matrix

Consider the NGM in its general form, i.e.

$$K = \begin{pmatrix} k_{11} & k_{12} \\ k_{21} & k_{22} \end{pmatrix}$$

R_0 is the spectral radius of this matrix, which can be calculated using the formula:

$$R_0 = \rho(K) = \frac{1}{2}\left(\text{trace}(K) + \sqrt{(\text{trace}(K))^2 + 4\det(K)}\right)$$

so

$$R_0 = \frac{1}{2}(k_{11} + k_{22}) + \frac{1}{2}\sqrt{k_{11}^2 - 2k_{11}k_{22} + k_{22}^2 + 4k_{21}k_{12}}$$

Which gives rise to the sensitivities for a next generation matrix whose elements are assumed to be independent of one another:

$$\frac{\partial R_0}{\partial k_{11}} = \frac{1}{2} + \frac{1}{4}\frac{2k_{11} - 2k_{22}}{\sqrt{k_{11}^2 - 2k_{11}k_{22} + k_{22}^2 + 4k_{12}k_{21}}} \tag{B.1}$$

$$\frac{\partial R_0}{\partial k_{12}} = \frac{k_{21}}{\sqrt{k_{11}^2 - 2k_{11}k_{22} + k_{22}^2 + 4k_{12}k_{21}}} \tag{B.2}$$

$$\frac{\partial R_0}{\partial k_{21}} = \frac{k_{12}}{\sqrt{k_{11}^2 - 2k_{11}k_{22} + k_{22}^2 + 4k_{12}k_{21}}} \tag{B.3}$$

$$\frac{\partial R_0}{\partial k_{22}} = \frac{1}{2} + \frac{1}{4}\frac{2k_{22} - 2k_{11}}{\sqrt{k_{11}^2 - 2k_{11}k_{22} + k_{22}^2 + 4k_{12}k_{21}}} \tag{B.4}$$

Appendix C

Parameter Values

The following table details the parameter ranges and sets used in this work:

Parameter	Description	Parameter Range	Value	Source(s)
β	Vector bite rate	$1 < \beta < 8$	4	[37],[64],[71]
π_h	Transmission probability	$0 < \pi_h < 1$	0.5	-
π_v	Transmission probability	$0 < \pi_v < 1$	0.5	-
π_d	Transmission probability	$0 < \pi_d < 1$	0.5	-
μ_h	Human natural mortality rate	$\frac{1}{840} < \mu_h < \frac{1}{540}$	0.0015	[21]
μ_v	Vector natural mortality rate	$\frac{15}{13} < \mu_v < \frac{15}{2}$	2	[37],[49]
μ_d	Dog natural mortality rate	$\frac{1}{216} < \mu_d < \frac{1}{84}$	0.0083	[62]
σ_h	Rate latent hosts become infectious	$\frac{1}{12} < \sigma_h < 1$	0.54	[22],[73]
σ_v	Rate latent vectors become infectious	$\frac{6}{5} < \sigma_v < \frac{15}{2}$	4	[79]
σ_d	Rate latent dogs become infectious	$\frac{1}{8} < \sigma_d < \frac{1}{2}$	0.3125	[12],[63]
r_v	Vector:human ratio	$\frac{1}{3} < r_v < 3$	2	-
r_d	Dog:human ratio	$\frac{1}{3} < r_d < 3$	1	-
N_h^0	Humans at DFE	$1000 < N_h^0 < 10000$	3000	-
χh	Human recovery rate	$\frac{1}{15} < \chi_h < \frac{1}{2}$	0.28	[26]
χ_d	Dog recovery rate	$\frac{1}{60} < \chi_d < \frac{1}{12}$	0.05	[57]
ϵ_h	Human relapse rate	$\frac{1}{841} < \epsilon_h < \frac{1}{36}$	0.014	-
ϵ_d	Dog relapse rate	$\frac{1}{217} < \epsilon_d < \frac{1}{12}$	0.044	[63]

Parameter	Description	Parameter Range	Value	Source(s)
ν_h	Rate of disease induced mortality, humans	$\frac{1}{36}\nu_h < \frac{1}{24}$	0.0347	[79]
ν_d	Rate of disease induced mortality, dogs	$\frac{217}{7811} < \nu_d < \frac{84}{2015}$	0.0347	[63]
α_d	Proportion of infected dogs becoming infectious	$0 < \alpha_d < 1$	0.5	-
ω_d	Proportional reduction in infectiousness, A_d class	$0 < \omega_d < 1$	0.5	-
θ	Movement scaling param.	$0 < \theta < 1$	0.1	-
p_τ	Inertia parameter	$0.5 < p_\tau < 3$	0.8	-
p_n	Forest-urban blood source ratio	$0.5 < p_n < 3$	0.8	-
p_f	Fly distribution param.	$0 < p_f < 1$	0.1	-
p_h	Host distribution param.	$0 < p_h < 1$	0.1	-
c	Trade-off scaling param.	$0 < c < 1$	0.9	-
$\hat{c}$	Trade-off scaling param.	$0 < \hat{c} < 10$	9	-

Table C.1: Table listing the base parameter values used in this thesis.

Bibliography

[1] P. Abranches, M. C. D. Silva-Pereira, F. M. Conceio-Silva, G. M. Santos-Gomes, and J. G. Janz. Canine leishmaniasis: Pathological and ecological factors influencing transmission of infection. *The Journal of Parasitology*, 77(4):557–561, 1991.

[2] B. Adams and D. D. Kapan. Man Bites Mosquito:Understanding the Contribution of Human Movement to Vector-Borne Disease Dynamics. *PLoS One*, 8(4):e6763.

[3] F. B. Agusto, N. Marcus, and K. O. Okosun. Application of Optimal Control to the Epidemiology of Malaria. *Electronic Journal of Differential Equations*, 2012(81):1–22, 2012.

[4] B. Alexander and M. Maroli. Control of Phlebotomine Sandflies. *Medical and Veterinary Entomology*, 17(1):1–8, 2003.

[5] S. Alizon, A. Hurford, N. Mideo, and M. van Baalen. Virulence evolution and the trade-off hypothesis: history, current state of affairs and the future. *Journal of Evolutionary Biology*, 22(2):245–259, 2009.

[6] S. Alizon and M. van Baalen. Transmision-virulence trade-offs in vector-borne disease. *Theoretical Population Biology*, 74(1):6–15, 2008.

[7] R. M. Anderson, editor. *The Population Dynamics of Infectious Diseases: Theory and Applications*. Chapman and Hall, 1982.

[8] R. M. Anderson and R. M. May. *Infectious diseases of humans: dynamics and control*. Oxford University Press, 1992.

[9] Armed Forces Health Surveillance Center, Department of Defense USA. Msmr - medical surveillance monthly report, 2009.

[10] R. W. Ashford. The leishmaniases as emerging and reemerging zoonoses. *International Journal of Parasitology*, 30:1269–81, 2000.

[11] G. Baneth, A. F. Koutinas, L. Solano-Gallego, P. Bourdeau, and L. Ferrer. Canine leishmaniosis - new concepts and insights on an expanding zoonosis: part one. *Trends in parasitology*, 24(7):324–330, 2008.

[12] Bayer AG, Canine vector borne diseases website. http://www.cvbd.org, Accessed April 2010.

[13] H. Behncke. Optimal Control of Deterministic Epidemics. *Optimal Control Applications and Methods*, 21:269–285, 2000.

[14] K. Blayneh. Optimal Control of Vector-Borne Diseases: Treatment and Prevention. *Discrete and Continuous Dynamical Systems Series B*, 11(3):1–31, 2009.

[15] S. M. Blower and H. Dowlatabadi. Sensitivity and Uncertainty Analysis of Complex Models of Disease Transmission: an HIV model, as an Example. *International Statistical Review*, 62(2):229–243, 1994.

[16] G. Bonjiorno, A. Habluetzel, C. Khoury, and M. Maroli. Host preferences of phlebotomine sandflies at a hypoendemic focus of canine leishmaniasis in central Italy. *Acta Tropica*, 88(2):109–16, 2003.

[17] A. Brannstrom and N. V. Festenberg. The Hitchhikers guide to Adaptive Dynamics. http://urn.kb.se/resolve?urn=urn:nbn:se:umu:diva-80169, 2007.

[18] V. L. Brown and K. A. J. White. The role of optimal control in assessing the most cost-effective implementation of a vaccination programme: HPV as a case study. *Mathematical Biosciences*, 231:126–134, 2011.

[19] H. Caswell. *Matrix Population Models: Construction, Analysis and Interpretation*. Sinauer Associates Inc. U.S., 2nd revised edition edition, November 2000.

[20] Centers for Disease Control and Prevention. http://www.cdc.gov, Accessed June 2010.

[21] Central Intelligence Agency. CIA - The World Factbook. https://www.cia.gov/library/publications/the-world-factbook/, Accessed May 2010.

[22] F. Chappuis, S. Sundar, A. Hailu, H. Ghalib, S. Rijal, R. W. Peeling, J. Alvar, and M. Boelaert. Visceral leishmaniasis: what are the needs for diagnosis, treatment and control? *Nature Reviews Microbiology*, 5(11):873–882, 2007.

[23] L. F. Chaves and M. J. Hernandez. Mathematical modelling of American Cutaneous Leishmaniasis: incidental hosts and threshold conditions for infection persistence. *Acta Tropica*, 92(3):245–252, November 2004.

[24] A.T Ciota, D. J. Ehrbar, A. C. Matacchiero, G. A. Van Slyke, and L. D. Kramer. The evolution of virulence of west nile virus in a mosquito vector: implications for arbovirus adaptation and evolution. *BMC Evolutionary Biology*, 13(71):1–12, 2013.

[25] N. F. Crum, N. E. Aronson, E. R. Lederman, J. M. Rusnak, and J. H. Cross. History of US military contributions to the study of parasitic diseases. *Military medicine*, 170(Supplement 1):17–29, 2005.

[26] C. V. David and N. Craft. Cutaneous and mucocutaneous leishmaniasis. *Dermatologic Therapy*, 22(6):491–502, 2009.

[27] H. de Kroon, A. Plaisier, J. van Groenendael, and H. Caswell. Elasticity: The Relative Contribution of Demographic Parameters to Population Growth Rate. *Ecology*, 67(5):1427–1431, October 1986.

[28] P. Van den Driessche and J. Watmough. Reproduction numbers and sub-threshold endemic equilibria for compartmental models of disease transmission. *Mathematical Biosciences*, 180(1):29–48, 2002.

[29] P. Desjeux. The increase in risk factors for leishmaniasis worldwide. *Transactions of the Royal Society of Tropical Medicine and Hygiene*, (3):239–43, 2001.

[30] U. Dieckman, J.A.J Metz, M.W. Sabelis, and K. Sigmund. *Adaptive Dynamics of Infectious Diseases: In Pursuit of Virulence Management*. Cambridge University Press, 2002.

[31] O. Diekmann. A Beginners Guide to Adaptive Dynamics. *Mathematical modelling of population dynamics*, 63:47–86, 2004.

[32] O. Diekmann and J. A. P. Heesterbeek. *Mathematical epidemiology of infectious diseases: Model building, analysis, and interpretation*. Wiley, 2000.

[33] O. Diekmann, J. A. P. Heesterbeek, and M. G. Roberts. The construction of next-generation matrices for compartmental epidemic models. *Journal of The Royal Society Interface*, 7(47):873–885, 2010.

[34] C. Dye, R. Killick-Kendrick, M. M. Vitutia, R. Walton, M. Killick-Kendrick, A. E. Harith, M. W. Guy, M. C. Canavate, and G. Hasibeder. Epidemiology of canine

leishmaniasis: prevalence, incidence and basic reproduction number calculated from a cross-sectional serological survey on the island of Gozo, Malta. *Parasitology*, 105(01):35–41, 1992.

[35] I. M. Elmojtaba, J. Y. T. Mugisha, and M. H. A. Hashim. Vaccination model for visceral leishmaniasis with infective immigrants. *Mathematical Methods in the Applied Sciences*, 36:216–226, 2012.

[36] P. Ewald. Evolution of Virulence. *Infectious Disease Clinics of North America*, 18:1–15, 2004.

[37] C. Ferro, E. Cárdenas, D. Corredor, A. Morales, and L. E. Munstermann. Life cycle and fecundity analysis of Lutzomyia shannoni (Dyar)(Diptera: psychodidae). *Memórias do Instituto Oswaldo Cruz*, 93(2):195–199, 1998.

[38] W. H. Fleming and R. W. Rishel. *Deterministic and stochastic optimal control*. Springer-Verlag, 1975.

[39] S. A. H. Geritz, E. Kisdi, G. Meszena, and J. A. J. Metz. Evolutionary Singular Strategies and the Adaptive Growth and Branching of the Evolutionary Tree. *Evolutionary Ecology*, 12:35–57, 1998.

[40] H. A. Hanafi, D. J. Fryauff, G. B. Modi, M. O. Ibrahim, and A. J. Main. Bionomics of phlebotomine sandflies at a peacekeeping duty site in the north of Sinai, Egypt. *Acta tropica*, 101(2):106–114, 2007.

[41] E. Handman. Leishmaniasis: current status of vaccine development. *Clinical microbiology reviews*, 14(2):229, 2001.

[42] N. A. Hartemink, S. E. Randolph, S. A. Davis, and J. A. P. Heesterbeek. The Basic Reproduction Number for Complex Disease Systems: Defining R_0 for Tick-Borne Infections. *The American naturalist*, 171(6):743–754, 2008.

[43] G. Hasibeder, C. Dye, and J. Carpenter. Mathematical Modelling and theory for estimating the basic reproductive number of canine Leishmaniasis. *Parasitology*, 105(01):43–53, 1992.

[44] J. A. P. Heesterbeek and M. G. Roberts. The type-reproduction number T in models for infectious disease control. *Mathematical biosciences*, 206(1):3–10, 2007.

[45] P. J. Hotez and A. Kamath. Neglected tropical diseases in sub-Saharan Africa: review of their prevalence, distribution, and disease burden. *PLoS Neglected Tropical Diseases*, 3:e412:1–10, 2009.

[46] K. C. Hyams, J. Riddle, D. H. Trump, and J. T. Graham. Endemic infectious diseases and biological warfare during the Gulf War: a decade of analysis and final concerns. *The American journal of tropical medicine and hygiene*, 65(5):664, 2001.

[47] H. M. Joshi, S. Lenhart, M. Y. Li, and L. Wang. Optimal control methods applied to disease models. *Contemporary Mathematics*, 410:1–18, 2006.

[48] M. Kamo, A.Sasaki, and M. Boots. The role of trade-off shapes in the evolution of parasites in spatial host populations: an approximate analytical approach. *Journal of Theoretical Biology*, 244(4):558–596, 2007.

[49] O. E. Kasap and B. Alten. Comparative demography of the sand fly Phlebotomus papatasi (Diptera: psychodidae) at constant temperatures. *Journal of Vector Ecology*, 31(2):378–385, 2006.

[50] M. J. Keeling and C. A. Gilligan. Metapopulation Dynamics of bubonic plague. *Nature*, 407:903–906, 2000.

[51] M. J. Keeling and P. Rohani. *Modeling Infectious diseases in Humans and Animals*. Princeton University Press, 2007.

[52] R. Killick-Kendrick. Phlebotomine vectors of the leishmaniases: a review. *Medical and Vetinary Entomology*, 4:1–24, 1990.

[53] R. Killick-Kendrick. The biology and control of phlebotomine sand flies. *Clinics in dermatology*, 17(3):279–289, 1999.

[54] S. Lenhart and J. T. Workman. *Optimal Control Applied to Biological Models*. Chapman and Hall/CRC, 2007.

[55] D. L. Lukes. *Differential Equations:Classical to Controlled*. Academic Press Inc., 1982.

[56] M. J. MacKinnon and A. F. Read. Immunity promotes virulence evolution in malaria. *PLOS Biology*, 2(9):1286–1292, 2004.

[57] J. Madany, S. Winiarczyk, J. L. Gundlach, W. Lopuszynski, and Z. Gradzki. Canine subclinical leishmaniosis-a study report. *Medycyna Wererynaryjna*, 60(10):1071–1074, 2004.

[58] D. Mahajan, M. L. Bhat, J. B. Singh, and D. Hans. Visceral leishmaniasis in a native kashmiri boy. *JK Science*, 11(3):152–153, 2009.

[59] H. C. Maltezou. Drug resistance in visceral leishmaniasis. *Journal of Biomedicine and Biotechnology*, 2010:1–8, 2010.

[60] A. Matser, N. Hartemink, H. Heesterbeek, A. Galvani, and S. Davis. Elasticity analysis in epidemiology: an application to tick-borne infections. *Ecology Letters*, 12(12):1298–1305, 2009.

[61] M. D. Mckay, R. J. Beckman, and W.J. Conover. A Comparison of Three Methods for Selecting Values of Input Variables in the Analysis of Output from a Computer Code. *Technometrics*, 21(2):239–245, 1979.

[62] A. R. Michell. Longevity of British breeds of dog and its relationships with-sex, size, cardiovascular variables and disease. *Veterinary Record*, 145(22):625–629, November 1999.

[63] J. Moreno and J. Alvar. Canine leishmaniasis: epidemiological risk and the experimental model. *TRENDS in Parasitology*, 18(9):399–405, 2002.

[64] G. R. Mullen, G. Mullen, and L. Durden. *Medical and veterinary entomology*. Academic Press Inc., 2009.

[65] C. B. Palatnik-de-Sousa, W. R. dos Santos, J. C. Franca-Silva, R. T. da Costa, A. B. Reis, M. Palatnik, W. Mayrink, and O. Genaro. Impact of canine control on the epidemiology of canine and human visceral leishmaniasis in Brazil. *The American journal of tropical medicine and hygiene*, 65(5):510, 2001.

[66] J. A. Patz, P. Daszak, G. M. Tabor, A. A. Aguirre, M. Pearl, J. Epstein, N. D. Wolfe, A. M. Kilpatrick, J. Foufopoulos, D. Molyneux, and D. J. Bradley. Unhealthy Landscapes: Policy Recommendations on Land Use Change and Infectious Disease Emergence. *Environmental Health Perspectives*, 112(10):1092–1098, 2004.

[67] R. J. Quinnell, C. Dye, and J. J. Shaw. Host preferences of the phlebotomine sandfly Lutzomyia longipalpis in Amazonian Brazil. *Medical and Vetinary Entomology*, 6:195–200, 1992.

[68] J. E. Rabinovich and M. Feliciangeli. Parameters of Leishmania braziliensis transmission by indoor Lutzomyia ovallesi in Venezuela. *The American journal of tropical medicine and hygiene*, 70(4):373–382, 2004.

[69] P. D. Ready. Leishmaniasis emergence and climate change. *Revue scientifique et technique (International Office of Epizootics)*, 27(2):399–412, 2008.

[70] M. G. Roberts and J. A. P. Heesterbeek. A new method for estimating the effort required to control an infectious disease. *Proceedings of the Royal Society of London. Series B: Biological Sciences*, 270(1522):1359–1364, 2003.

[71] M. E. Rogers and P. A. Bates. Leishmania manipulation of sand fly feeding behavior results in enhanced transmission. *PLOS Pathogens*, 3:818–825, 2007.

[72] M. A. Sanchez and S. M. Blower. Uncertainty and sensitivity analysis of the basic reproductive rate: Tuberculosis as an example. *American journal of epidemiology*, 145(12):1127–1137, 1997.

[73] W. Takken, B. G. J. Knols, A. Van Gompel, and W. Van Bortel. *Emerging pests and vector-borne diseases in Europe*. Wageningen Academic Publishers, 2007.

[74] V. D. Tarallo, F. Dantas-Torres, R. P. Lia, and D. Otranto. Phlebotomine sand fly population dynamics in a leishmaniasis endemic peri-urban area in Southern Italy. *Acta Tropica*, 116:227–234, 2010.

[75] C. Viboud, O. N. Bjørnstad, D. L. Smith, and L. Simonsen. Synchrony, Waves, and Spatial Hierarchies in the Spread of Influenza. *Science*, 312:447–451, 2006.

[76] Natural History Museum Website. http://www.nhm.ac.uk, Accessed May 2010.

[77] P. J. Weina, R. C. Neafie, G. Wortmann, M. Polhemus, and N. E. Aronson. Old world leishmaniasis: an emerging infection among deployed US military and civilian workers. *Clinical infectious diseases*, 39(11):1674–1680, 2004.

[78] World Health Organisation. Control of Leishmaniasis - Report by the Secretariat, 2007.

[79] World Health Organisation. WHO Technical Report Series on the control of the leishmaniases - TRS No. 949, 2010/1, Accessed June 2013.

[80] World Health Organisation. WHO Factsheet No. 354: West Nile virus , July 2011, Accessed October 2013.

[81] World Health Organisation. WHO Factsheet No. 117: Dengue and severe dengue, September 2013, Accessed October 2013.